AN INVESTIGATION OF SEISMIC RESPONSE OF CONNECTIONS IN PRECAST CONCRETE DOUBLE-TEES

by

Hashem Shariatmadar

Department of Civil Engineering and Applied Mechanics

McGill University

Montreal, Canada

November 1992

A THESIS SUBMITTED TO THE FACULTY OF GRADUATE STUDIES
AND RESEARCH IN PARTIAL FULFILMENT OF THE REQUIREMENTS
FOR THE DEGREE OF MASTER OF ENGINEERING

© Copyright 1992 by Hashem Shariatmadar

SEISMIC RESPONSE OF CONNECTIONS IN DOUBLE-TEES

In the Name of Allah

The Beneficent, The Merciful

Abstract

An experimental study of typical connections commonly used in precast concrete buildings subjected to reversed cyclic loads is presented, along with an analytical study of the linear behaviour of these specimens subjected to monotonically increasing loads.

Five precast connection specimens were constructed and tested under reversed cyclic loads to determine their seismic responses. The specimens represent a series of connections between double-tee flanges or between a double-tee flange and a lateral load resisting element in a typical roof of a precast concrete structure.

The analytical study consisted of two parts: linear finite element analysis of the connection to determine the test specimen geometry and to define its boundary conditions, and non-linear finite element analysis, using the NONLACS program, to predict the complete responses of the connections subjected to monotonically increasing loads.

The experimental results were compared with the predictions made using theoretical calculations, the CPCI design method and non-linear finite element analysis.

It is noted that the CPCI design method gives conservative predictions for the ultimate strength of the connection reinforced with a bent deformed bar anchor and a 90° hook, and the one with two deformed bars oriented at 45° and headed studs, both welded to a steel plate. The predicted ultimate strength of the connection with a bent deformed bar anchor welded to a steel plate and one with two straight deformed bars oriented at 90° and welded to an embedded steel angle, are close to the experimental results. The ultimate strength of the connection with the headed studs welded to a steel plate predicted by CPCI method is overestimated. Design guidelines to increase the strength of the connections and to improve the displacement ductility are presented.

Sommaire

L'auteur présente les résultats d'une étude expérimentale du comportement sous charges cycliques de connexions types utilisées avec les éléments préfabriqués de bâtiments en béton armé. L'étude s'accompagne de la modélisation par éléments finis de ces connexions sujettes à un chargement monotonique afin d'en estimer la résistance ultime

Cinq connexions différentes ont été construites et mises à l'essai sous charges cycliques afin d'en simuler le comportement sous effets sismiques. Ces connexions représentent une série de connexions horizontales entre les semelles de doubles Tés, ou entre une semelle de double Té et un élément de résistance latérale typique d'un tout préfabriqué.

L'analyse numérique par éléments finis compte deux volets: une analyse linéaire de la connexion afin de déterminer la géométrie et les conditions frontières des prototypes à mettre à l'essai, et une analyse non linéaire utilisant le logiciel NONLACS, pour simuler la réponse des connexions sous charges monotoniques croissantes jusqu'à la rupture.

Les résultats expérimentaux sont comparés aux prédictions des modèles numériques non linéaires, aux calculs théoriques, et aux prédictions de la méthode du code de l'Institut Canadien du Béton Précontraint (CPCI).

L'étude indique que la méthode de conception du CPCI sous-estime la résistance ultime de la connexion avec armature d'ancrage pliée avec crochet à 90° ainsi que celle avec deux barres à 45° avec goujons, l'ensemble étant soudé à une plaque en acier. Par contre, pour la connexion avec barre d'ancrage pliée soudée à une plaque en acier et pour la connexion avec deux barres droites orientées à 90° l'une de l'autre et soudées à une cornière en acier encastrée dans l'élément de béton préfabriqué, les prédictions sont proches des résultats d'essais. D'autre part, la méthode du CPCI surestime la résistance de la connexion avec goujons soudés à une plaque en acier.

Des recommandations pour le dimensionnement sont également suggérées, visant à augmenter la résistance ultime des connexions et à en améliorer la ductilité en déplacement.

Acknowledgements

The author wishes to express his sincere appreciation and gratitude to Professor. M. S. Mirza for his invaluable guidance and advice throughout the development and execution of this research program, and for interacting with him at all times including holidays, early mornings and late evenings.

The author is grateful to the Ministry of Culture and Higher Education of the Islamic Republic of Iran for providing him a fellowship

The author wishes to thank Mr Salem Bouhairie for his volunteer assistance during the experimental work.

The advice and technical assistance offered by Mr. N. A. Huszar, Consulting Engineer, is gratefully acknowledged

The experimental research was carried out in the Jamieson Structure Laboratory at McGill University. The author is grateful for the assistance provided by Messrs.M. Przykorski, J. Barteczak and R. Sheppard.

The author would like to extend sincere thanks to Professor G. McClure for excellent French translation of the abstract despite her busy schedule.

The author would like to thank the staff of McGill University Computing Centre for their valuable assistance and for the computer funds provided.

The author would like to express his heartfelt thanks to his parents whose love, perseverance, and incessant support enabled him to endure and persevere all through his life.

Table of Contents

Abstract i
Sommaire ii
Acknowledgements iii
Table of Contents iv
List of Figures vii
List of Tables xi
List of Symbols xii

1 Introduction 1
1.1 Introduction 1
1.2 Summary of Previous Investigations 4
1.2.1 Design Concept and Models 4
1.2.2 Experimental Investigations 5
1.2.2.1 Connection with Headed Studs 7
1.2.2.2 Connection with Embedded Reinforcing Bar . . . 11
1.3 Current Design Approach 27
1.3.1 Lateral Seismic Force 27
1.3.2 Connections 29
1.3.2.1 Deformed Bar Anchors Connection 29
1.3.2.2 Connection with Welded Headed Studs 34
1.3.2.2.1 Studs in tension 34
1.3.2.2.2 Studs in shear 38
1.3.2.2.3 Combined shear and tension 40
1.4 Objectives 40

2 Experimental Program 42
2.1 Introduction 42
2.2 Design of Prototype Building 44
2.2.1 Single - Storey Precast Structure 44
2.3 Choice of Test Specimen Size and Boundary Conditions 52
2.3.1 Analysis of Partial Flange with Three Connections 52
2.3.2 Test Specimen and Boundary Conditions 56
2.4 Design and Description of Test Specimens 59
2.4.1 Test Specimen S1 61
2.4.2 Test Specimen S2 61
2.4.3 Test Specimen S3 64
2.4.4 Test Specimen S4 64

2.4.5 Test Specimen S5 64
2.5 Construction Sequence 68
2.6 Material Properties 73
2.7 Test Set-Up 75
2.8 Loading History 78
2.9 Instrumentation 79

3 NONlinear Analysis of Connection Responses 82
3.1 Finite Element Program - NONLACS Program 82
3.1.1 Finite Element Modelling 82
3.1.2 Nonlinear Analysis Method 85
3.1.3 Procedure of Analysis 89
3.2 NONLACS Program- Application and Results 90
3.2.1 Finite Element Idealization 90
3.2.2 Discussion of Analytical Results 93
3.2.2.1 Load-Deflection Characteristics and Ultimate Strength 93
3.2.2.2 Response of Steel Bar Anchor in Connections 100
3.2.2.3 Cracking and Crack Propagation 105

4 Experimental Results 111
4.1 Introduction 111
4.2 Test Specimen S1 115
4.3 Test Specimen S2 127
4.4 Test Specimen S3 142
4.5 Test Specimen S4 154
4.6 Test Specimen S5 162
4.7 Discussion and Comparison of Experimental Results . . . 177

5 Evaluation of Analytical and Experimental Results . . . 181
5.1 Specimen S1 182
5.2 Specimen S2 184
5.3 Specimen S3 187
5.4 Specimen S4 190
5.5 Specimen S5 190

6 Design Recommendations and Conclusions 194

References 198

A Design and Analysis of Test Specimens 201
A.1 Specimen S1 201

A.2 Specimen S2 204
A.3 Specimen S3 206
A.4 Specimen S4 207
A.5 Specimen S5 208

List of Figures

1.1 Framing system for a single-story precast concrete wall panel industrial building . . . 3
1.2 Typical connections between double-tee elements . . . 3
1.3 Dry shear connectors . . . 6
1.4 Typical headed studs connection demonstrating two common stud configurations . . . 8
1.5 Details of the test connections . . . 9
1.6 Load deflection curves for connections shown in Figure 1.5 . . . 9-11
1.7 Connection with embedded reinforcing bar . . . 12
1.8 Details of connections and test results reported by Aswad . . . 15-16
1.9 Behaviour of connections subjected to reversed cyclic loads as reported by Spencer . . . 17-20
1.10 Cyclic test on embedded bar connection reported by Kaltros . . . 21-26
1.11 Seismic response factors in the 1990 NBCC . . . 28
1.12 Analogous beam design of diaphragm . . . 30
1.13 Typical flange welded plate details . . . 33
1.14 Assumed failure surface for headed studs . . . 36
1.15 Effective stress area for welded headed studs . . . 36
1.16 Development of welded headed studs . . . 37
1.17 Stress area reduction for limited depth . . . 37
1.18 Edge distance effect for welded headed studs . . . 39

2.1 Details of connections investigated in this research program . . . 43
2.2 Details of single-story precast wall panel building . . . 45
2.3 Specified forces acting on roof and walls . . . 47
2.4 Reinforcing details of double-tee flange . . . 49
2.5 Connections between the flanges of double-tees . . . 51
2.6 Distributed shear on diaphragm with 10% eccentricity . . . 51
2.7 Boundary conditions along the web of double-tee . . . 53
2.8 Finite element idealization for partial flange . . . 54
2.9 Distribution of principal stresses around the middle connection of partial flange . . . 55
2.10 Force distribution along the anchor in the middle connection of partial flange . . . 56
2.11 Finite element idealization for the test specimen . . . 57
2.12 Distribution of principal stresses in the test specimen . . . 58
2.13 Force distribution along the anchor in the test specimen . . . 59
2.14 Details of Specimen S1 . . . 62

2.15 Details of Specimen S2 63
2.16 Details of Specimen S3 65
2.17 Details of Specimen S4 66
2.18 Details of Specimen S5 67
2.19 Formwork for casting specimens 69-71
2.20 Stress-strain curves for concrete and steel 74
2.21 Test set-up 76-77
2.22 Typical loading history 78
2.23 Instrumentation for Specimen S1 79
2.24 Instrumentation for Specimen S2 80
2.25 Instrumentation for Specimen S3 80
2.26 Instrumentation for Specimen S4 81
2.27 Instrumentation for Specimen S5 81

3.1 Some typical finite elements in NONLACS program 83
3.2 Layered element used in the analysis 84
3.3 Stress-strain relationships for concrete and reinforcing steel 87-88
3.4 Material constitutive model for concrete 88
3.5 Finite element idealization for the specimens used in NONLACS program 92
3.6 Load-deflection response for Connection S1 94
3.7 Load-deflection response for Connection S2 96
3.8 Load-deflection response for Connection S3 97
3.9 Load-deflection response for Connection S5 99
3.10 Load-strain curve for Connection S1 100
3.11 Load-strain curve for Connection S2 102
3.12 Load-strain curve for Connection S3 103
3.13 Load-strain curve for Connection S5 105
3.14 Cracked elements for Connection S1 107
3.15 Cracked elements for Connection S2 109
3.16 Cracked elements for Connection S3 111
3.17 Cracked elements for Connection S5 113

4.1 Hysteresis response of Specimen S1 117
4.2 Measured strains along the length of reinforcing bar anchor for Specimen S1 118-119
4.3 Maximum principal strain distribution in the slab for Specimen S1 . . . 121
4.4 Photographs of Specimen S1 122-123
4.5 Load vs. vertical displacement for Specimen S1 124
4.6 Strain vs. distance along the length of reinforcing bar prior to failure for Specimen S1 124
4.7 Peak loads vs maximum crack width for Specimen S1 126

4.8 Load vs. deflection of steel frame as modelled for Specimen S1 126
4.9 Hysteresis response of Specimen S2 129
4.10 Measured strains along the length of reinforcing bar anchor for Specimen S2 131-132
4.11 Maximum principal strain distribution in the slab for Specimen S2 ... 133
4.12 Photographs of Specimen S2 136-137,139
4.13 Load vs. vertical displacement for Specimen S2 138
4.14 Strain vs. distance along the length of reinforcing bar prior to failure for Specimen S2 138
4.15 Peak loads vs. maximum crack width for Specimen S2 141
4.16 Load vs. deflection of steel frame as modelled for Specimen S2 141
4.17 Hysteresis response of Specimen S3 144
4.18 Measured strains along the length of reinforcing bar anchor for Specimen S3 145-146
4.19 Maximum principal strain distribution in the slab for Specimen S3 ... 147
4.20 Photographs of Specimen S3 149-150
4.21 Load vs. vertical displacement for Specimen S3 151
4.22 Strain vs. distance along the length of reinforcing bar prior to failure for Specimen S3 152
4.23 Peak loads vs. maximum crack width for Specimen S3 153
4.24 Load vs. deflection of steel frame as modelled for Specimen S3 153
4.25 Hysteresis response of Specimen S4 156
4.26 Measured strains in headed studs for Specimen S4 157
4.27 Photographs of Specimen S4 158-159
4.28 Maximum principal strain distribution in the slab for Specimen S4 ... 160
4.29 Load vs. vertical displacement for Specimen S4 161
4.30 Peak loads vs. maximum crack width for Specimen S4 161
4.31 Load vs. deflection of steel frame as modelled for Specimen S4 162
4.32 Hysteresis response of Specimen S5 164
4.33 Measured strains along the length of reinforcing bar anchor for Specimen S5 165-166
4.34 Maximum principal strain distribution in the slab for Specimen S5 ... 168
4.35 Photographs of Specimen S5 170-172
4.36 Load vs. vertical displacement for Specimen S5 173
4.37 Strain vs. distance along the length of reinforcing bar prior to failure for Specimen S5 174
4.38 Peak loads vs. maximum crack width for Specimen S5 175
4.39 Load vs. deflection of steel frame as modelled for Specimen S5 176
4.40 Envelopes of responses 178
4.41 Energy dissipated by specimens reinforced with bar anchors 180

5.1 Comparison of analytical and experimental load-deflection responses

for Specimen S1 183
5.2 Comparison of analytical and experimental load-steel strain responses at Location 1 for Specimen S1 184
5.3 Comparison of analytical and experimental load-deflection responses for Specimen S2 186
5.4 Comparison of analytical and experimental load-steel strain responses at Location 1 for Specimen S2 187
5.5 Comparison of analytical and experimental load-deflection responses for Specimen S3 188
5.6 Comparison of analytical and experimental load-steel strain responses at Location 1 for Specimen S3 189
5.7 Comparison of analytical and experimental load-deflection responses for Specimen S5 191
5.8 Comparison of analytical and experimental load-steel strain responses at Location 1 for Specimen S5 192

List of Tables

1.1 Force modification factors 29
1.2 Values of modification factor k_2 for development length 32

2.1 Mix design for 35 MPa concrete 72
2.2 Summary of concrete properties 73
2.3 Summary of reinforcing steel properties 74

4.1 Summary of loading history for Specimen S1 116
4.2 Summary of loading history for Specimen S2 128
4.3 Summary of loading history for Specimen S3 143
4.4 Summary of loading history for Specimen S4 155
4.5 Summary of loading history for Specimen S5 163

5.1 Comparison of analytical and experimental ultimate strengths 193

6.1 Design requirements and values of β 197

List of Symbols

A	effective stress area
A_{cv}	area of concrete section resisting shear transfer
A_h	total area of anchor
A_s	area of reinforcement
A_{vf}	area of shear-friction reinforcing steel
B_ϕ	factored bearing resistance
b_n	net thickness of concrete panel
C	average concrete cover thickness
C_1	cover thickness to the edge
C_r	factored resistance in compression reinforcing steel
C_u	ultimate compression strength in the compression reinforcing steel
d_b	diameter of steel bar or headed stud
d_{max}	measured crack width
e	distance between centre of mass and centre of rigidity
E_c	tangent modulus of elasticity of concrete
E_s	modulus of elasticity of steel
E'_s	strain-hardening modulus
F	foundation factor
f'_c	measured concrete compressive strength
f_t	splitting tensile strength of concrete
f_s	strength of reinforcing steel
f_{sty}	specified yield strength for headed stud steel
f_{ult}	measured ultimate strength of reinforcing steel
f_y	measured yield strength of reinforcing steel
I	importance factor of structure
k_1	modification factor to account for clear concrete cover thickness
l_d	anchorage length
l_{dbpo}	development length to prevent pull-out failure
l_{dbsp}	development length to prevent splitting failure
l_e	embedded length for studs
l_{hb}	basic anchorage length in hook anchorage
l_{hd}	straight lead of hook anchorage
n	number of bars in one layer of reinforcement
P	experimental applied load
P_ϕ	factored tensile capacity of a connection
P_{ult}	ultimate static design load of connection
R	force modification factor
R_{ba}	inside bent radius

S seismic response factor
s_1 spacing between connections in double-tee flanges
S_{max} maximum principal stress
T fundamental period of vibration of the structure
T_r factored resistance in tensile reinforcing steel
T_u ultimate tensile strength in the tension reinforcing steel
u,w translational degrees of freedom
U calibration factor
V zone velocity ratio
V_{do} ultimate dowel strength
V_e equivalent elastic base shear
V_r design shear force for the connection
V_{ult} ultimate shear strength of connection
$V_{ult(bar)}$ contribution of ultimate strength of steel bar to Specimen S5 strength
$V_{ult(stud)}$ contribution of ultimate strength of studs to Specimen S5 strength
W dead load of the structure
Z_a acceleration-related seismic zone
Z_v velocity-related seismic zone
ε strain
ε'_c concrete strain at stress f'_c
ε_{cu} strain at peak stress
ε_t concrete strain at stress f'_t
ε_{ult} ultimate strain of reinforcing steel
ε_y yield strain of reinforcing steel
Δ_y measured displacement of connection at yielding of reinforcing steel
λ coefficient for use with low density concrete
μ shear-friction coefficient
ρ ratio of reinforcement
ϕ_c resistance factor for concrete
ϕ_m member resistance factor
ϕ_s resistance factor for reinforcing steel
Θ_z Θ_x Θ_y rotational degrees of freedom

Chapter 1

Introduction

1.1 Introduction

A large number of prefabricated structures have been built all over the world during recent years. Large panel construction is used mainly for residential buildings, while prefabricated structures made principally of linear elements are used for one to three storey industrial buildings.

The connections between precast members normally constitute the weakest link in the structure. Therefore the satisfactory performance and economy of precast concrete structures depends to a great extent on the proper selection and design of the connections. Test results on full scale structures have shown that the connections start yielding even when steel in the precast panels is in the elastic range. This is because the strength of a connection is much less than that of the surrounding panel, and this strength can decrease with cyclic loading. The philosophy for the design of connections is:

-to remain elastic for small earthquakes

-to be able to undergo inelastic deformations without structural collapse.

Connections can be used to dissipate energy if they show stable elasto-plastic behaviour.

Some of the floor and roof slabs in early projects consisted of double-tees, single-tees, solid flat slabs, and many variations of these shapes. However, double tees have proved to be the most economical for spans of 9 to 21 m and have become standardized for industrial applications. Figure 1.1 indicates the components of a single - storey precast concrete wall panel industrial building. It is essential to ensure adequate connection between the elements forming the roof diaphragm (usually double - tees with thin flanges) and between these elements and the lateral load resisting systems. During earthquakes, horizontal connections in the floor system are

subjected to cyclic shear and direct loads. Figure 1.2 illustrates the details of a typical connection between the double-tee elements. Due to lack of sufficient data on the shear resistance of connections between prefabricated elements, the designers make appropriate assumptions concerning the failure criteria, which may lead to uneconomical or unsafe designs. The design of these connections based solely on their static strengths is thus inappropriate. Some recorded data [1] from the response of prefabricated structures subjected to earthquake show that the most common failure mode occurs at the connection of the roof diaphragm with the boundary elements, which consist of reinforcing bars embedded in the thin flange by pullout of a bar from one of the flanges. This emphasizes the importance of adequate cover and embedment length for proper connection behaviour. Another common area of distress occurs at the connection of exterior precast panels (wall panels) to the diaphragm system. The welded embedded anchors exhibit little ductility, and failure often occurs in a brittle manner by pull out or fracture of the weld between the reinforcing bar and the steel plate.

There is considerable lack of experimental and analytical data on the resistance of such connections subjected to shear and normal forces (monotonically increasing or reversed cyclic loads). The objective of this research program is to study the seismic response of typical connections representing the connection between the double tee flanges in the diaphragm system as well as between double tee flange and the lateral load resisting elements such as wall panels.

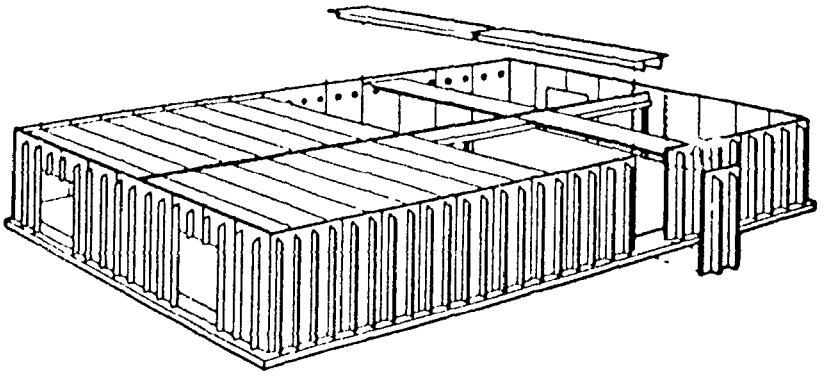

Figure 1.1 Framing system for a single-storey precast concrete wall panel industrial building

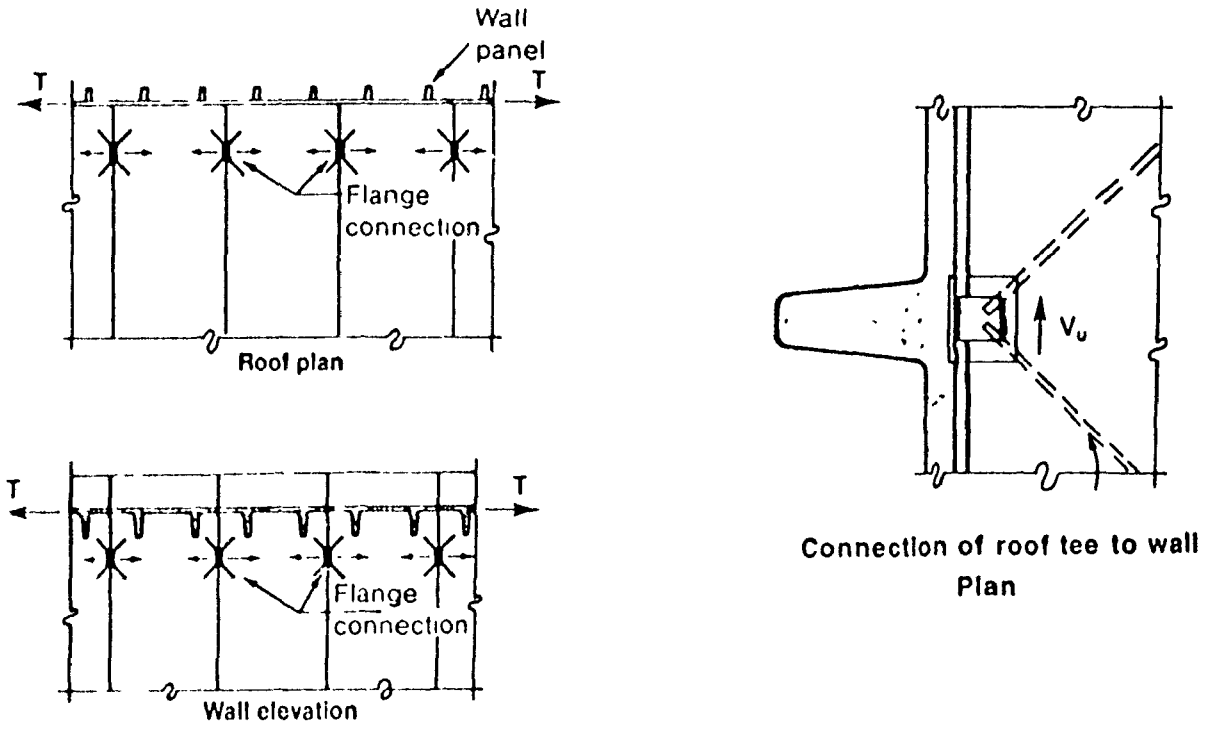

Figure 1.2 Typical connections between double-tee elements

1.2 Summary of Previous Investigations

Previous studies on typical connections in precast concrete structures are summarized in this section

1.2.1 Design Concept and Models

Analysis for the design of connections requires analytical models, which should be simple but should still reveal the essential features of behaviour. Truss, or strut and-tie models appear to be well suited and they have been developed for most connections. They are useful because they allow a designer to identify easily the functions performed by each element of the connection and to obtain the approximate magnitude of the forces.

In 1978, Hawkins [2,3] reviewed the seismic performance of precast concrete buildings. He noted the following areas necessary to be investigated: determine the design force levels; design of elements; design of connections, understand the contribution of floor systems; and means of providing structural integrity

In 1981, Becker and Sheppard [4] classified the types of connections by dividing the connection in precast concrete elements into three groups as follows:

i) Strong connection - Under the ultimate seismic load, the connection does not exceed the elastic limit.

ii) Ductile connection - The connection is designed based on the loading beyond the elastic range into the inelastic range to absorb energy, to achieve ductility or to limit load transmission to other elements in the structural system.

iii) Guided connection - It permits displacement under the lateral loads (earthquake or wind) and adapts to changes due to creep, shrinkage and temperature variations.

In 1986 Stanton et al. [5] suggested that due to the lack of special seismic design criteria and details, one of the following procedures may be used. (i) design the structure to remain in the elastic range; (ii) design the connection to be stronger than the precast member; (iii) design the structure so that the connections are located outside of potential inelastic zones.

The models proposed for typical horizontal connections are summarized in the following:

Aswad [6] used panels in combination as a horizontal joint which were modeled as an elasto-plastic model. It seems that the elasto - plasto model without any strength or stiffness degradation can be used to model this connection.

Neille [7] modelled the behaviour of welded headed stud connections by combining a trilinear load - deformation model with a stress - strain model for concrete adopted from the work of Karson and Jirsa[8]. Neille obtained very good agreement between the calculated behaviour of his analytical model and the measured cyclic behaviour.

Shricken and Powell [9] used a variety of load - displacement relationships for the connection elements using a finite element approach. The shear friction element was developed for modelling the dry connection to capture the pinched hysteresis loops, stiffness at the end of each cycle and the degradation of stiffness and strength with an increasing number of load cycles.

1.2.2 Experimental Investigations

In this section, a brief review of the cyclic experimental investigation of response of some common connections between precast elements is presented. In spite of the concern and recognized need for information on the cyclic loading response of precast connections, only a few tests have been conducted to study the behaviour of these connections when subjected to reversed cyclic loads representing design earthquake forces. Again, there is very little data on energy absorption and ductility characteristics of connections commonly used in precast construction. For convenience, connections are classified into two general categories according to the material used: dry and wet connections. This report focuses on the description of the response of "dry" connections (using headed studs or embedded reinforcing bars).

Dry Connections

These connections utilize mechanical anchors such as welded headed studs and embedded reinforcing bars welded to a plate to transmit the shear forces between the precast elements such as double - tees and wall panels. The most common type of dry shear connections are composed of embedded steel shapes anchored into the precast members by studs or reinforcing bars. The connection is completed by bolting or welding a third element to the embedded steel shape. Figure 1.3 details some of the most commonly used dry connections.

Shear force is transferred across the connection in a variety of mechanisms. Depending on the details of the connection, shear is transferred through bearing of the steel shapes, shear of the connecting elements, shear of the welds or bolts, or through the friction between bolted plates. Many tests have been conducted to determine on the ultimate strength of dry connections under static or monotonic increasing loading, however only a few tests have been carried out under reversed cyclic load.

The research on cyclic behaviour of different types of welded connections is described briefly for: i) headed stud connections; ii) embedded reinforcing bar connections

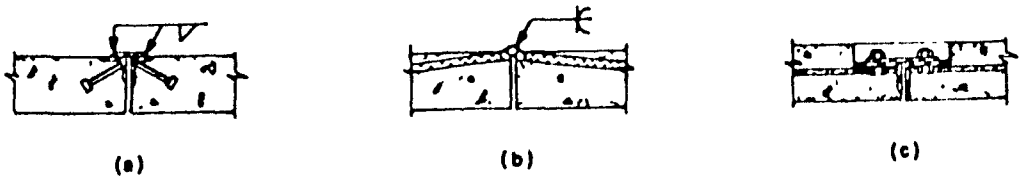

Figure 1.3 Dry shear connectors[25]

1.2.2.1 Connection with Headed Studs

A typical headed stud connection is presented in Figure 1.4 [7]. The strength of the headed stud may be limited by either concrete or stud failure. Spencer and Neille[10] have conducted tests on the behaviour of six welded headed stud connections subjected to cyclic loading. Each connection angle was cast in a 2 ft x 4 ft x 8 in concrete panel. Details of the test connections are shown in Figure 1.5. Five of the test specimens were subjected to cyclic loading. Connection A1 was subjected to monotonically increasing load until failure. Reversed cyclic shear forces were applied to all other specimens at distance of 7/8 inch (22 mm) from the face of the connection angle in the longitudinal direction (see Figure 1.5). Load-deflection curves for these connections are presented in Figure 1.6 [10]. Test results for connection A1 exhibited considerable ductility under monotonically increasing load (see Figure 1.6a). The yield strength of the connection was greater than the design strength predicted by the equation in the PCI Design Handbook [11,12]. The test results for Connections A subjected to reversed cyclic loads illustrates the change in the behaviour of the specimen when subjected to monotonically increasing and reversed cyclic loading for the same connection. The connection was loaded to yield after several initial cycles in the elastic range, and then subjected to steadily increasing deflections. The results show a decrease in stiffness and strength with cycling. The failure of the connection was preceded by progressive crushing and spalling of the concrete above and below the angle. They also observed progressive tension cracking parallel to, but several inches away from the angle. Connections A1 and B1 failed when a large block of concrete surrounding the studs broke away while other connections failed when one of the studs broke close to the weld. Spencer and Neille[10] concluded as follows:

1. The PCI procedures for calculating the ultimate design strength of these connections under static loading give conservative results.
2. The strength of the connections in the first cycles of loading up to yield is approximately the same as the strength under monotonically increasing loads.
3. If the cyclic loading is continued above the stability limit [see Figure 1.6(b) for

definition], the strength of the connections decrease with an increasing number of cycles and the yield strength envelop extends to approach the stability limit.

4. The deflections reached before failure were from seven to twenty-four times the theoretical elastic deflection corresponding to the designed ultimate strength.

5. These connections if properly designed and detailed, appear to be suitable for use in earthquake-resistant buildings designed as box - type systems.

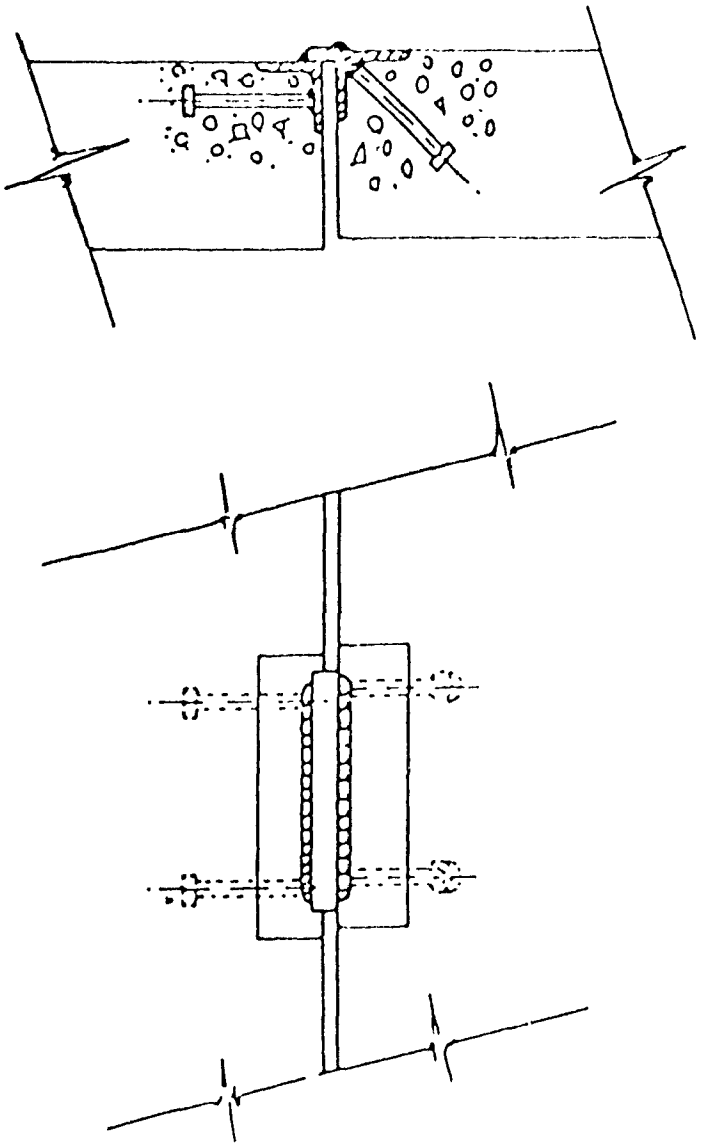

Figure 1.4 Typical headed studs connection demonstrating two common stud configurations and the ease with which minor imperfections and misalignments may be accommodated[7]

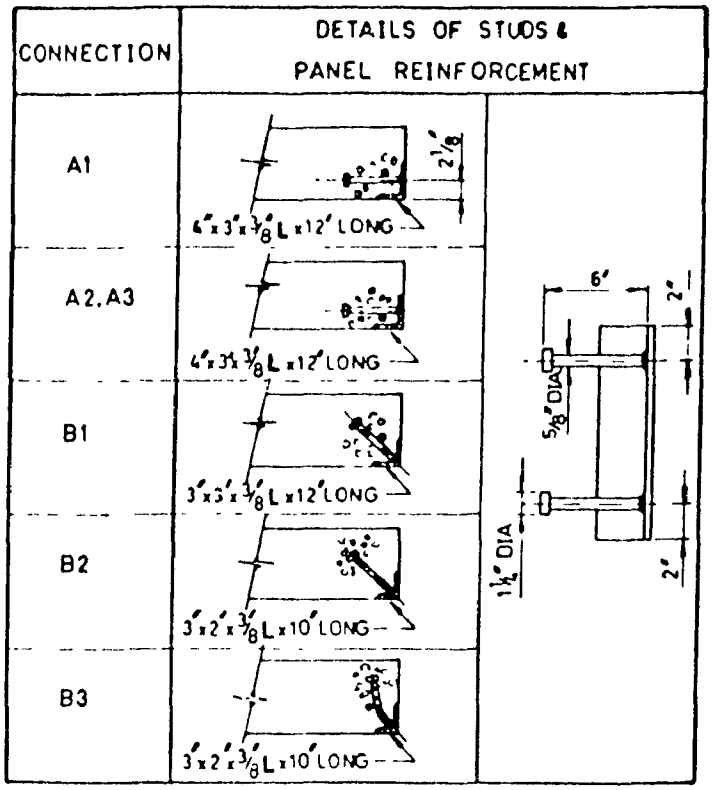

Figure 1.5 Details of test connections[10]

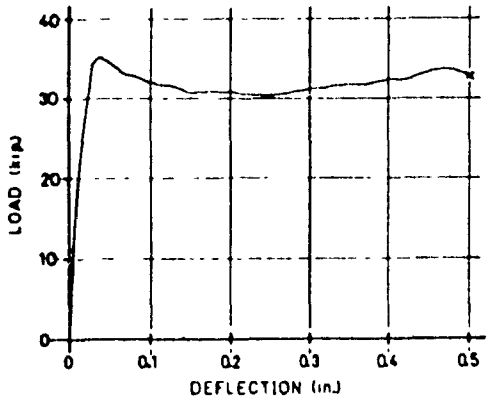

(a) Load-deflection curve (connection A1) for monotonic loading to failure

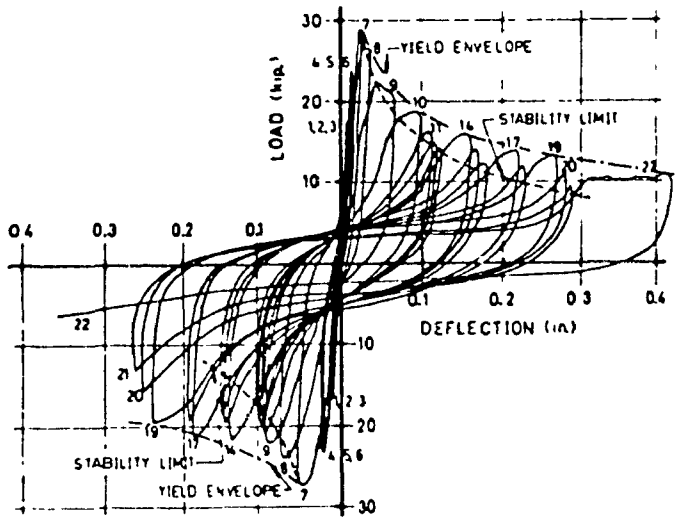

(b) Load-deflection loops (connection A3)

Figure 1.6 Load-deflection curves for the connections shown in Figure 1.5[10]

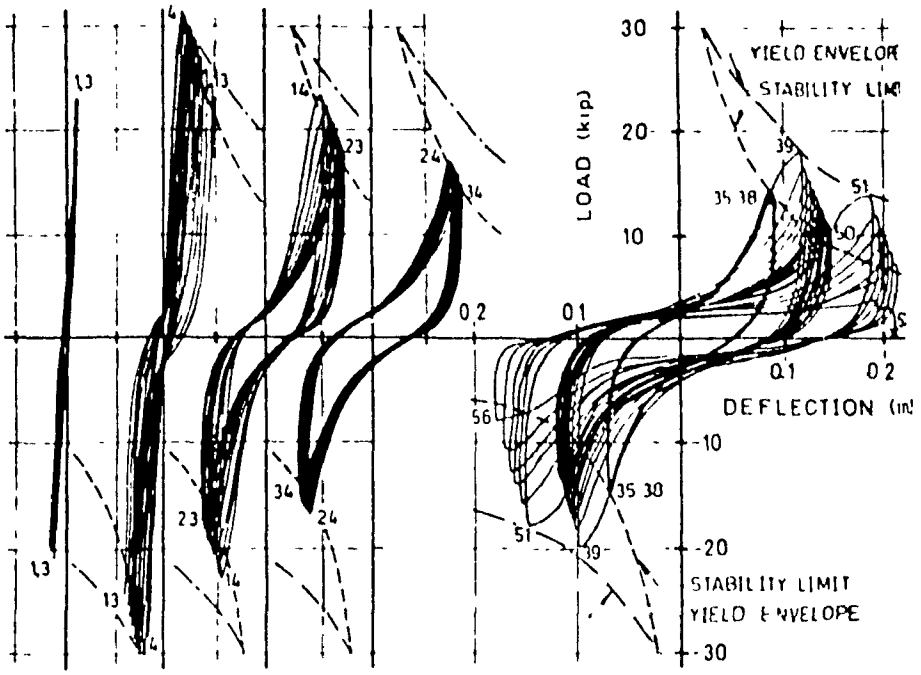

(c) Load-deflection loops (connection A2). showing stable behaviour after 36th cycle. Groups of curves have been separated for greater clarity.

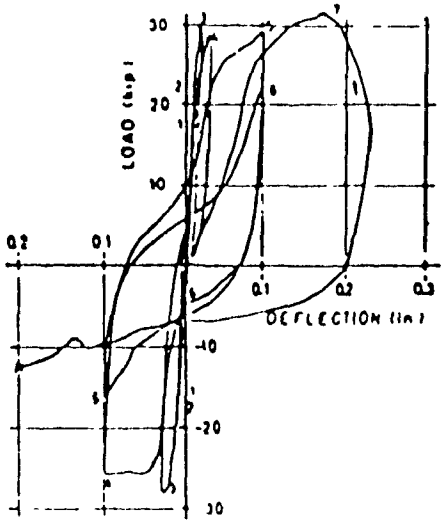

(d) Load-deflection loops (connection B1). Rapid increase in the applied deflection led to failure after a relatively few cycles

Figure 1.6 (Continued) Load-deflection curves for the connections in Figure 1.5[10]

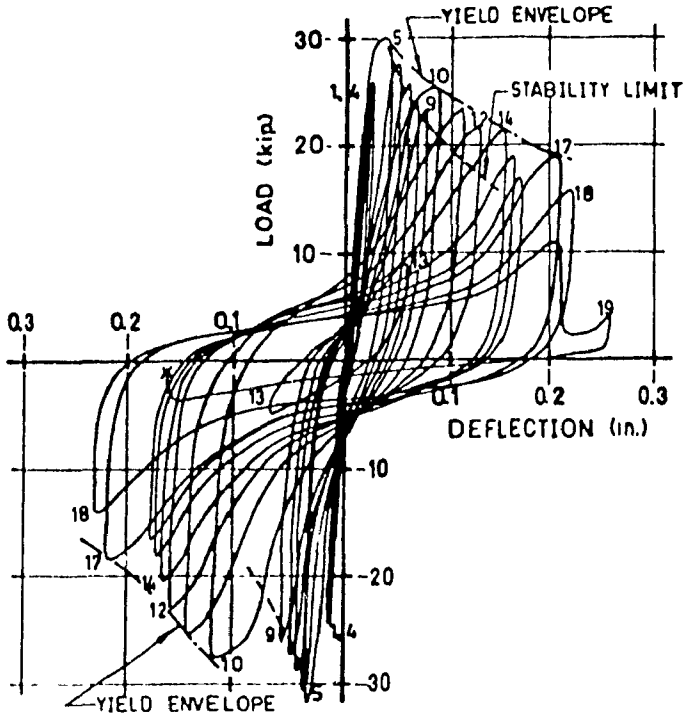

(e) Load-deflection loops (Connection B2). The stud failure can be seen in Cycle 19

Figure 1.6 (Continued) Load-deflection curve for the connection in Figure 1.5[10]

1.2.2.2 Connection with Embedded Reinforcing Bar

An alternate method for embedding steel sections in precast members is to replace the headed studs with welded reinforcing bars, as shown in Figure 1.7. Deformed bar anchors are anchored in the concrete by bond. Although sufficient seismic test data is not available, there are several advantages to this type of connection. The first advantage is the large surface area available for welding the reinforcing bars to the angle, which reduces the chance of brittle weld failure because of lower weld stresses. The second advantage of this connection is the larger development length of the bars into the precast member. This allows for lower bond stresses and reduces the chance of pullout and splitting failure of the connection.

In general, dry connections should be designed conservatively for earthquake resistant construction. Longer weld lengths, additional anchorage lengths for reinforcing bars and lower allowable stresses are justified for earthquake loading especially in the presence of forces normal to the shear connection.

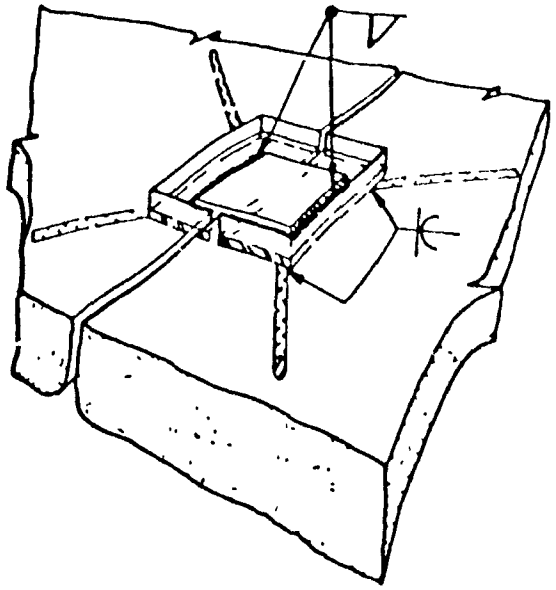

Figure 1.7 Connection with embedded reinforcing bar

A brief summary of the response of connections with anchored reinforcing bar subjected to reversed cyclic loads follows:

Aswad [6] conducted a series of low cyclic tests on connections using full scale double tees and wall panel (21' x 8' or 6.4 m x 2.4 m panels). Two types of connections for double tee (2" or 50 mm flange thickness) and connections for precast wall panels (6" or 150 mm thick) were tested. The experiment did not cover a wide range of cyclic tests because the main objective was to find out the failure strengths of the connections and to measure the relative displacements between the adjacent precast double tees. In a majority of cases, the specimens were subjected to three cycles of reversed loadings between $\pm P_o$, where P_o is a value smaller than the ultimate strength and the connection was then brought to failure. However, the cyclic tests were not carried far enough to present the actual cyclic response of the connections. Details of the connections and the respective load - displacement curves are shown in Figure 1.8. Connections D-34, D-36 and D-40 present the tests on the double tees (2" or 50 mm flange thickness), while P-9 presents the tests on the precast wall (6" or 150 mm thick) connection. As can be seen from Figure 1.8, the stiffness and strength did not deteriorate considerably since the reversed cyclic loads remained essentially in the elastic range. The following conclusions were reported by Aswad[6]:

1. When forces applied to the plate were simple shear, failure strengths were greater than the ones expected.
2. The embedded length of the reinforcing bars were sufficient to develop the ultimate capacity.
3. A pull out force normal to a connection reduced its ultimate shear capacity.

Spencer [13] carried out some cyclic shear tests on connections with reinforcing bars anchored into typical 4'x 2'x 5.5" (1220 x 610 x 140 mm) concrete panels. The hysteresis response curves for the tests are presented in Figure 1.9. The following dynamic characteristics were observed by Spencer:
1. The strength of the connection does not reduce during loading cycles in the elastic range.
2. The nominal strength of the connections can be determined using the truss analogy.
3. The strength of the connection with the anchor bar running into the connection at 45 degrees and at 90 degrees falls to about 50% and less than 50% of their nominal strengths, respectively.
4. The connection with a recess in the panel edge and straight embedded bars at 45 degrees appears to perform best under simulated earthquake loading.
5. Panel thickness and concrete strength influence the behaviour of connection.

Other tests on six different types of connections with embedded bar in thin panels were conducted by Kallros[14]. All specimens were loaded into the elastic range and then the loading continued until the connection failed. The modes of failure occurred either by bar fracture or by spalling of the concrete. When bar failure occurred, the related measured deflection was very small. In the case of spalling failures, when the connections started cracking, the stiffness gradually decreased with an increased number of cycles into the inelastic range and larger load-deflection loops were observed. Connections with an angle and reversed angle welded directly to the reinforcing mesh did not respond well in comparison with the other connections. The details of connections and the load - deflection curves are presented in Figure 1.10. Kallros stated the following conclusions:

1. Good quality control is necessary with the use of the reinforcing bar and the angle.
2. A thicker flange with a larger concrete cover thickness behaves better under cyclic loading.
3. The connections should be designed for 50% of the expected monotonic capacity of the connections.
4. The strength of connections does not seem to reduce in the elastic range.
5. Connections with 45 degree embedded bar appear to perform best under simulated earthquake loading.

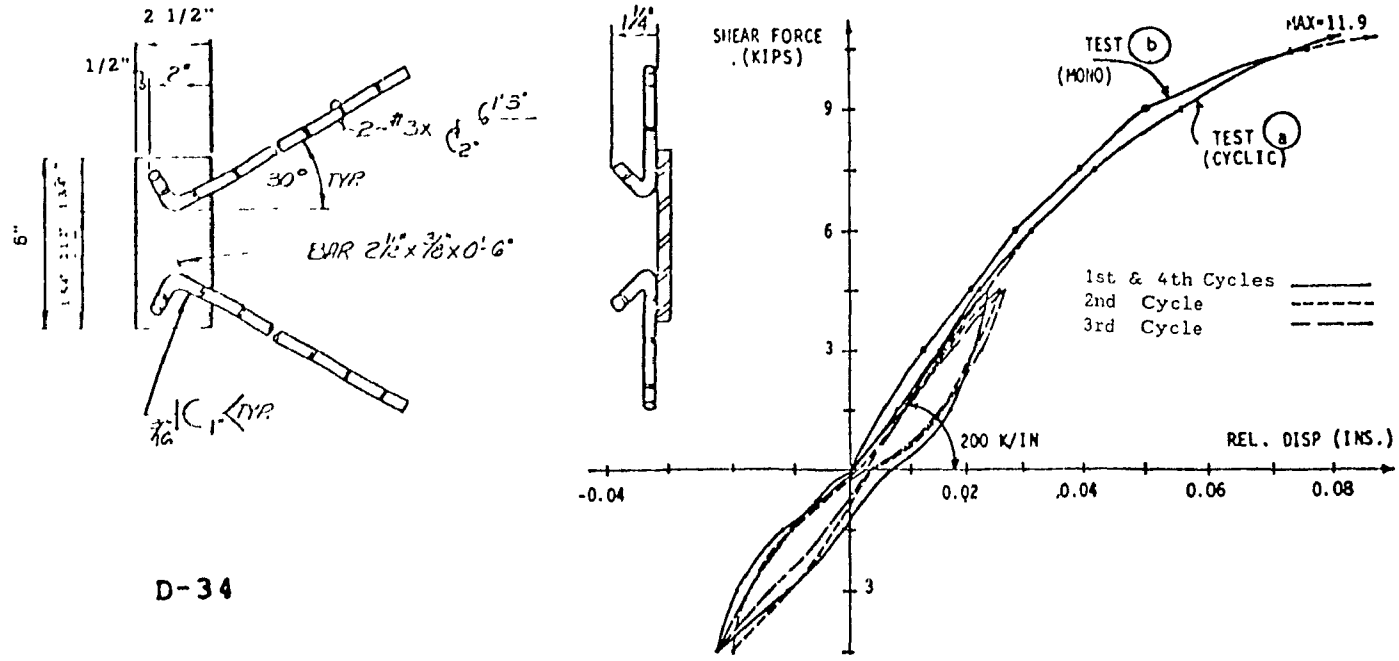

(a) Shear force vs. relative slip for Specimen D-34

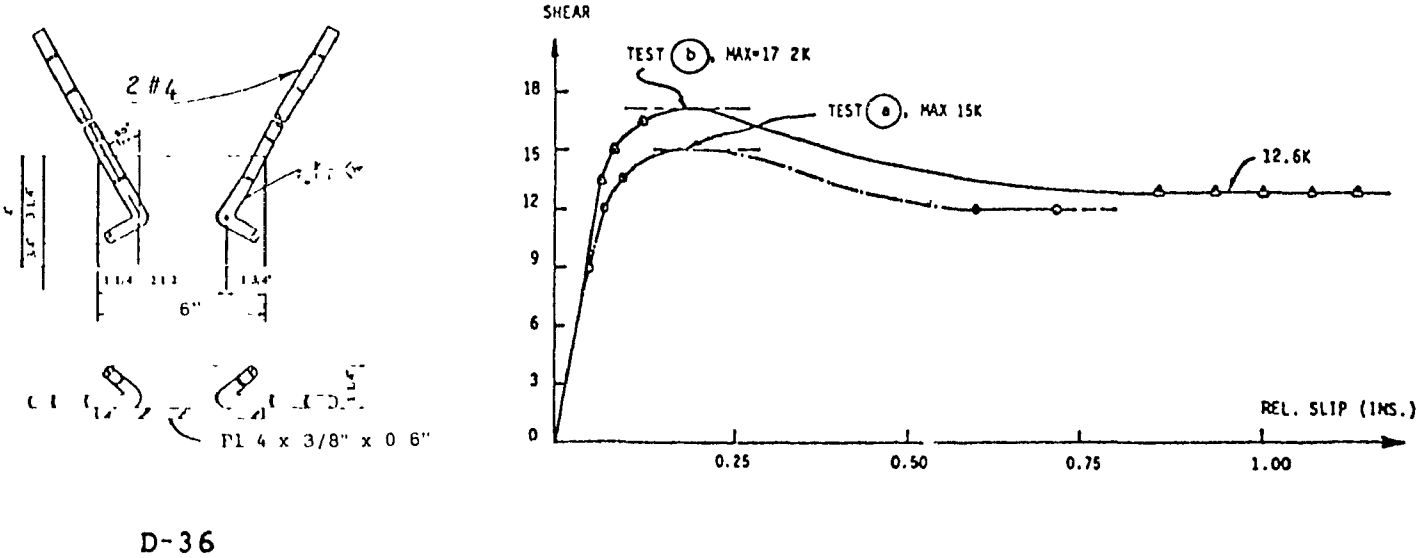

(b) Shear force vs. relative slip for Specimen D-36

Figure 1.8 Details of connections and test results reported by Aswad [6]

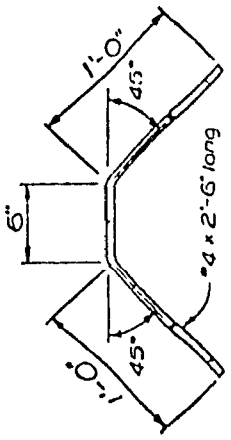

D-40

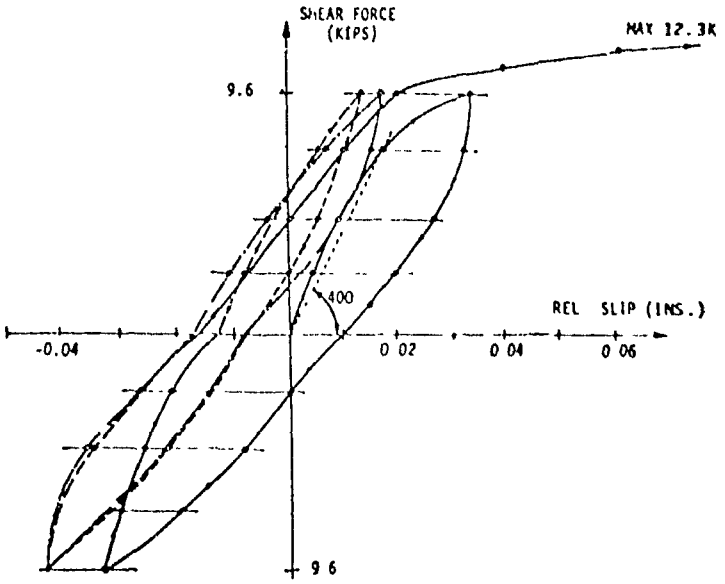

(c) Shear force vs. relative slip for Specimen D-40

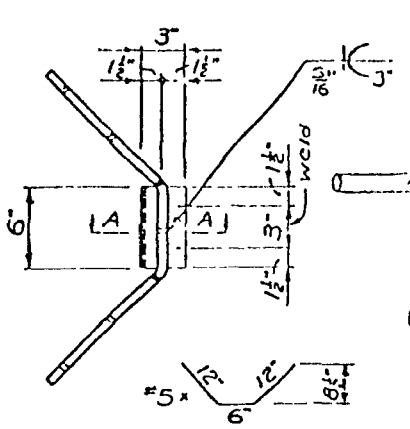

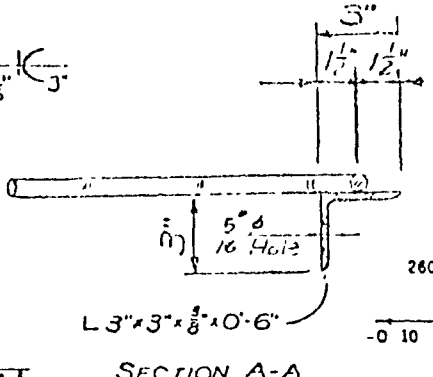

P-9

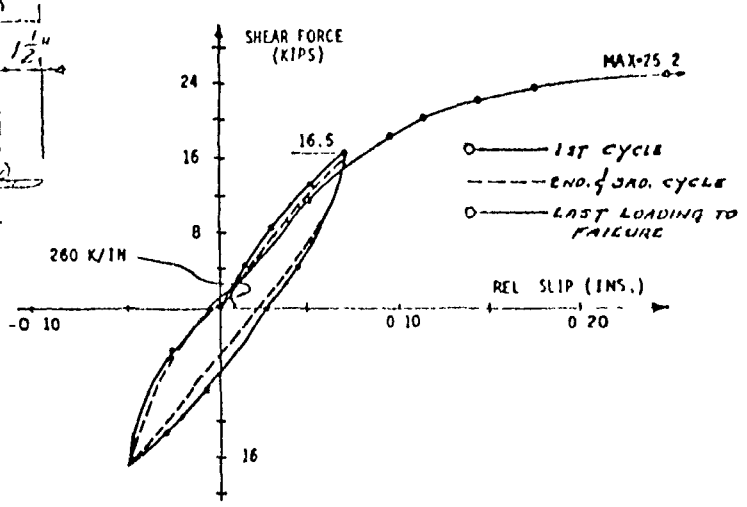

(d) Shear force vs. relative slip for Specimen P-9
(connection previously loaded in shear to 15 kips)

Figure 1.8 (Continued) Connection Details and test results reported by Aswad[6]

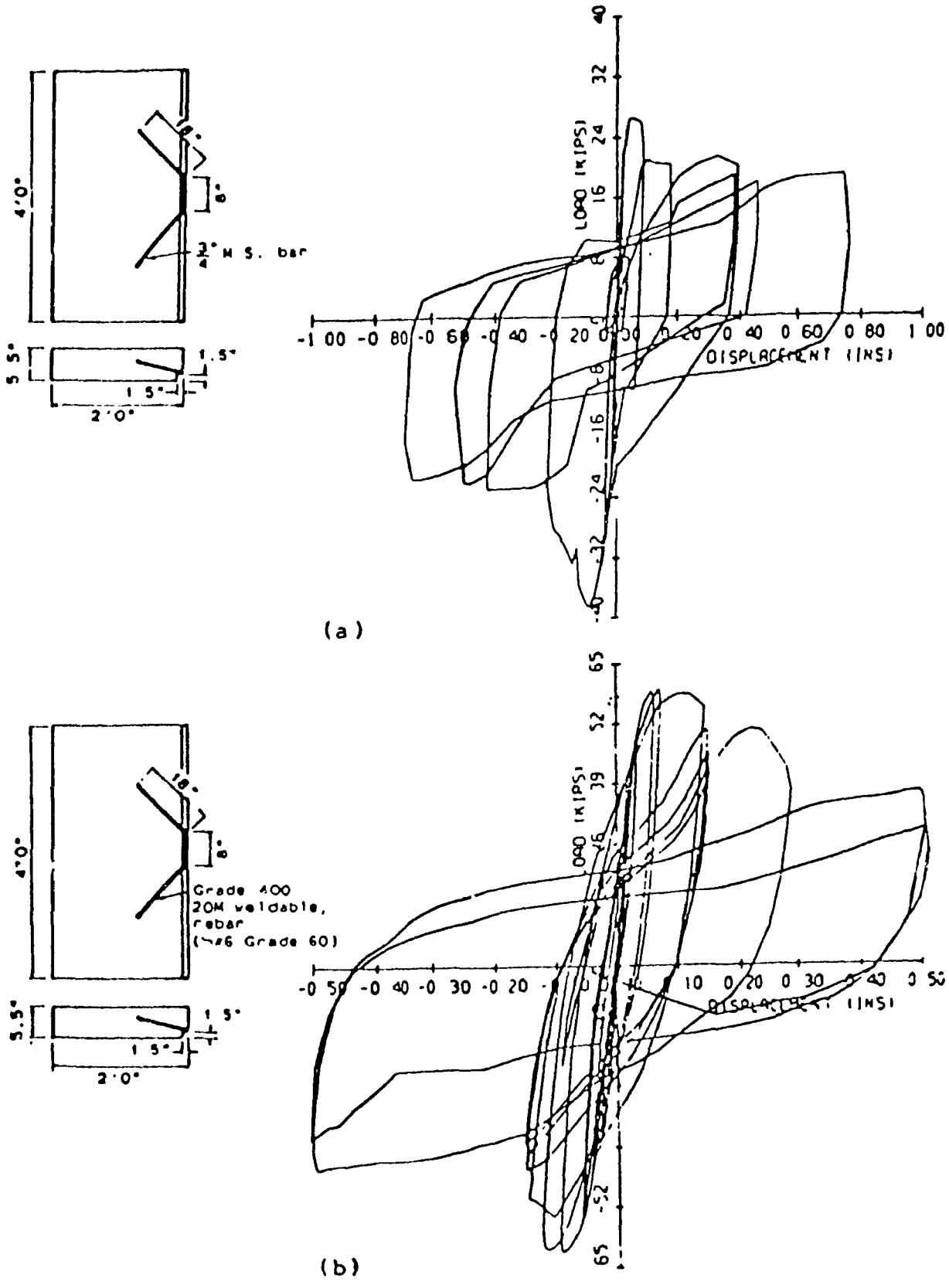

Figure 1.9 Behaviour of connections subjected to reversed cyclic loads as reported by Spencer[13]

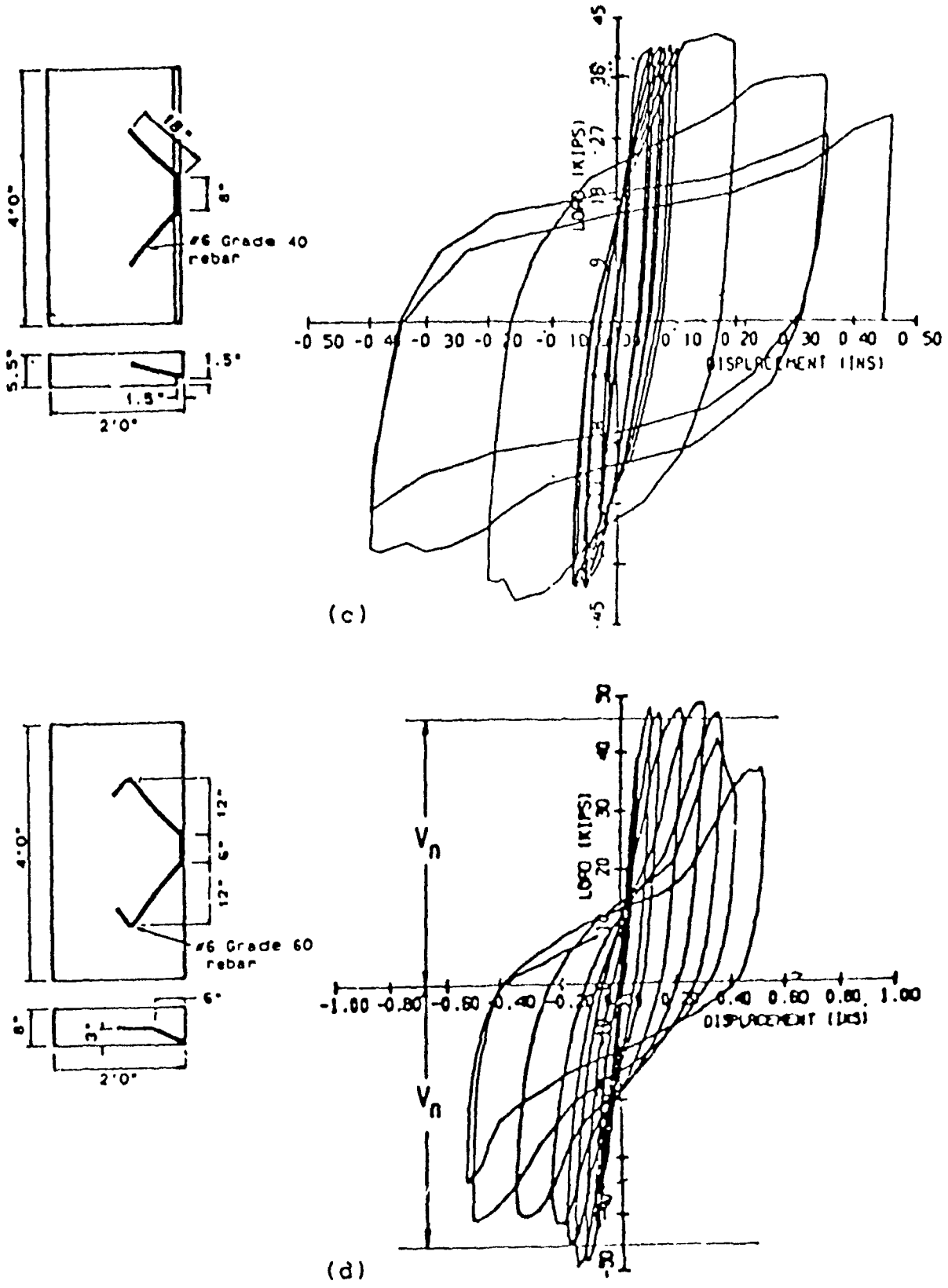

Figure 1.9 (Continued) Behaviour of connections subjected to reversed cyclic loads as reported by Spencer[13]

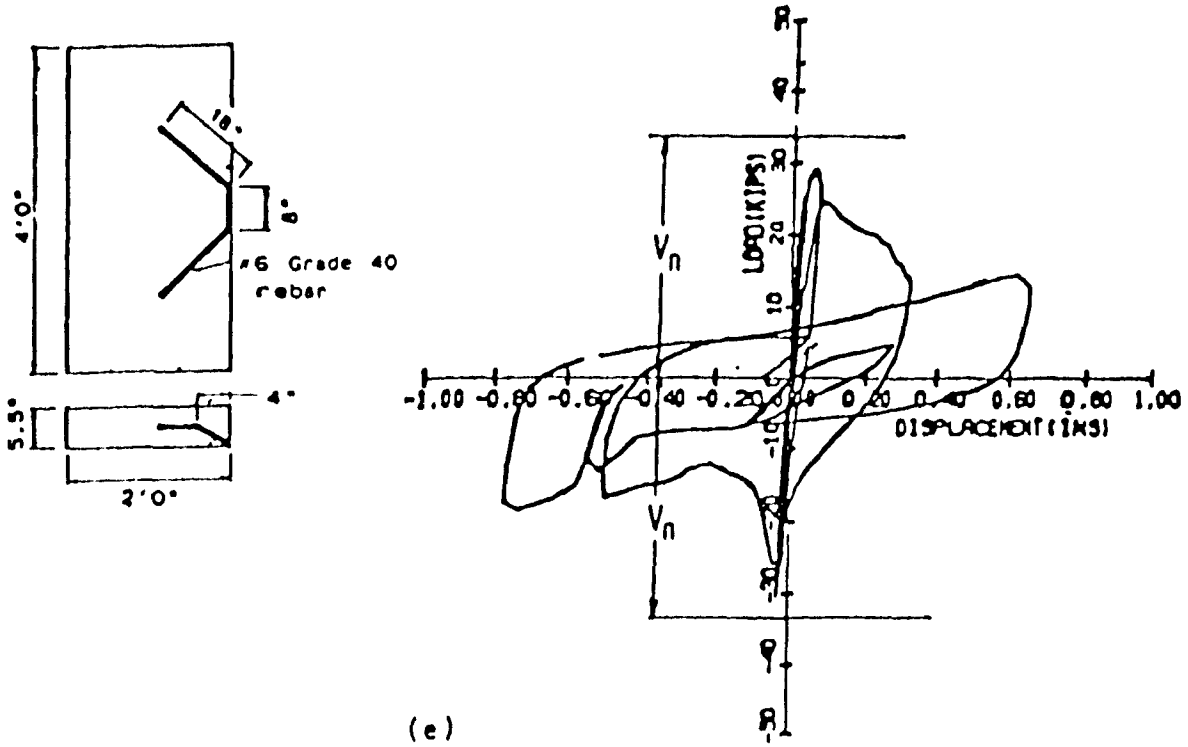

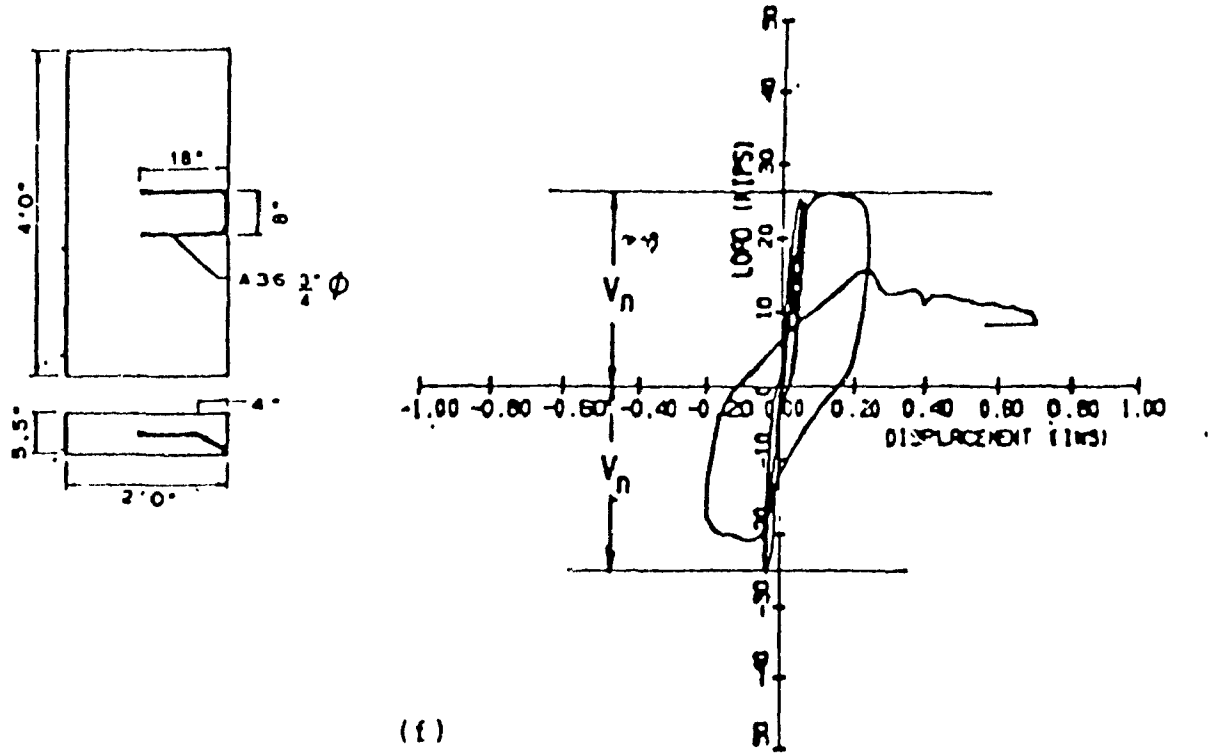

Figure 1.9 (Continued) Behaviour of connections subjected to reversed cyclic loads as reported by Spencer[13]

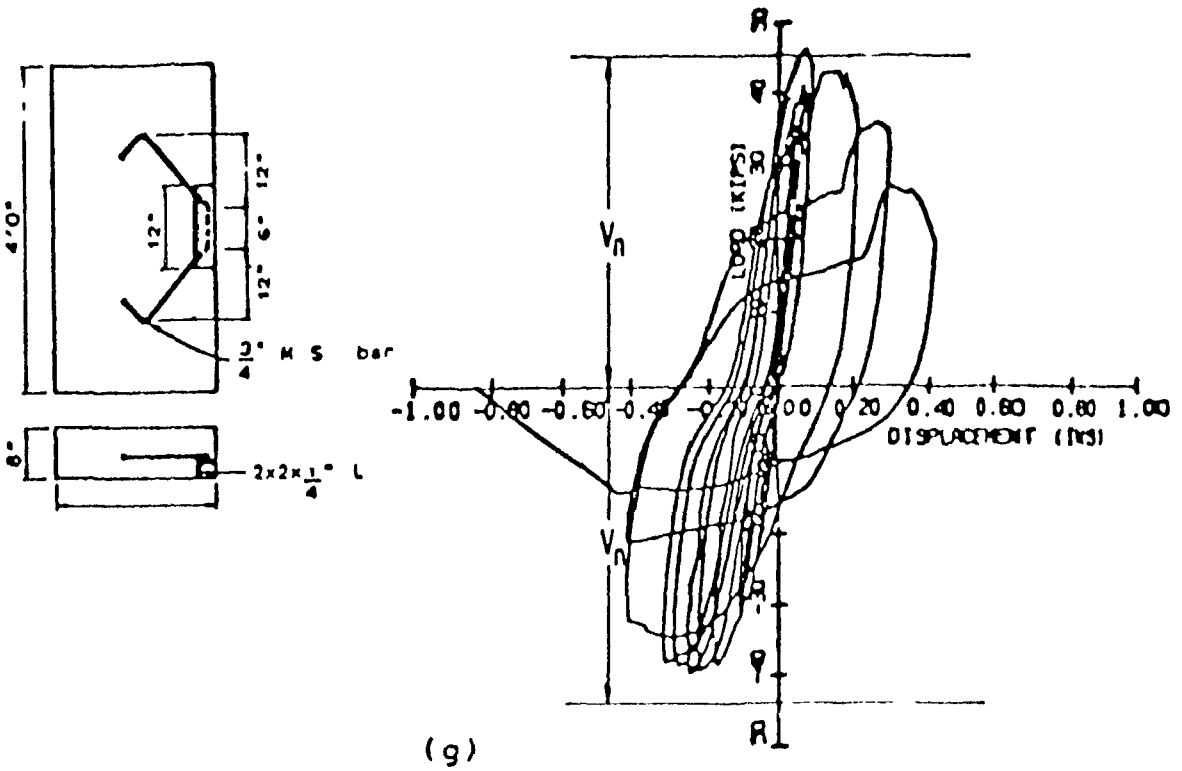

(g)

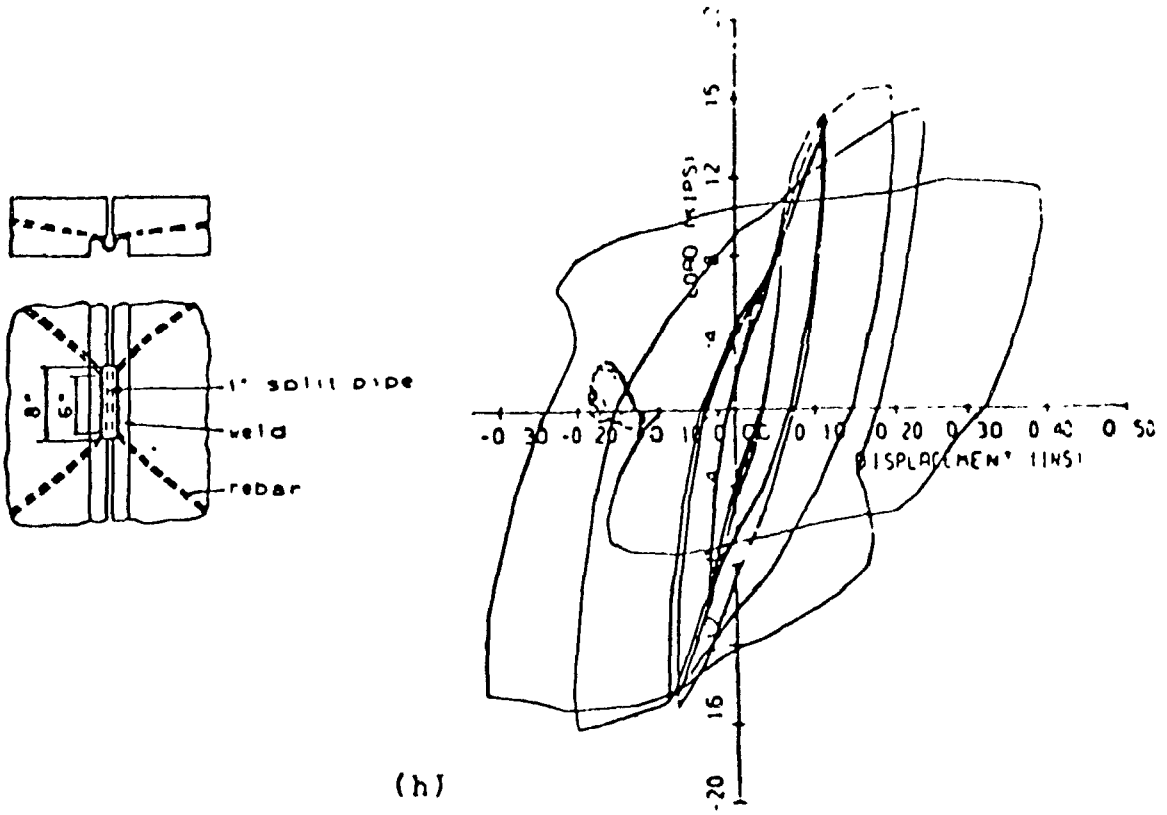

(h)

Figure 1.9 (Continued) Behaviour of connections subjected to reversed cyclic loads as reported by Spencer[13]

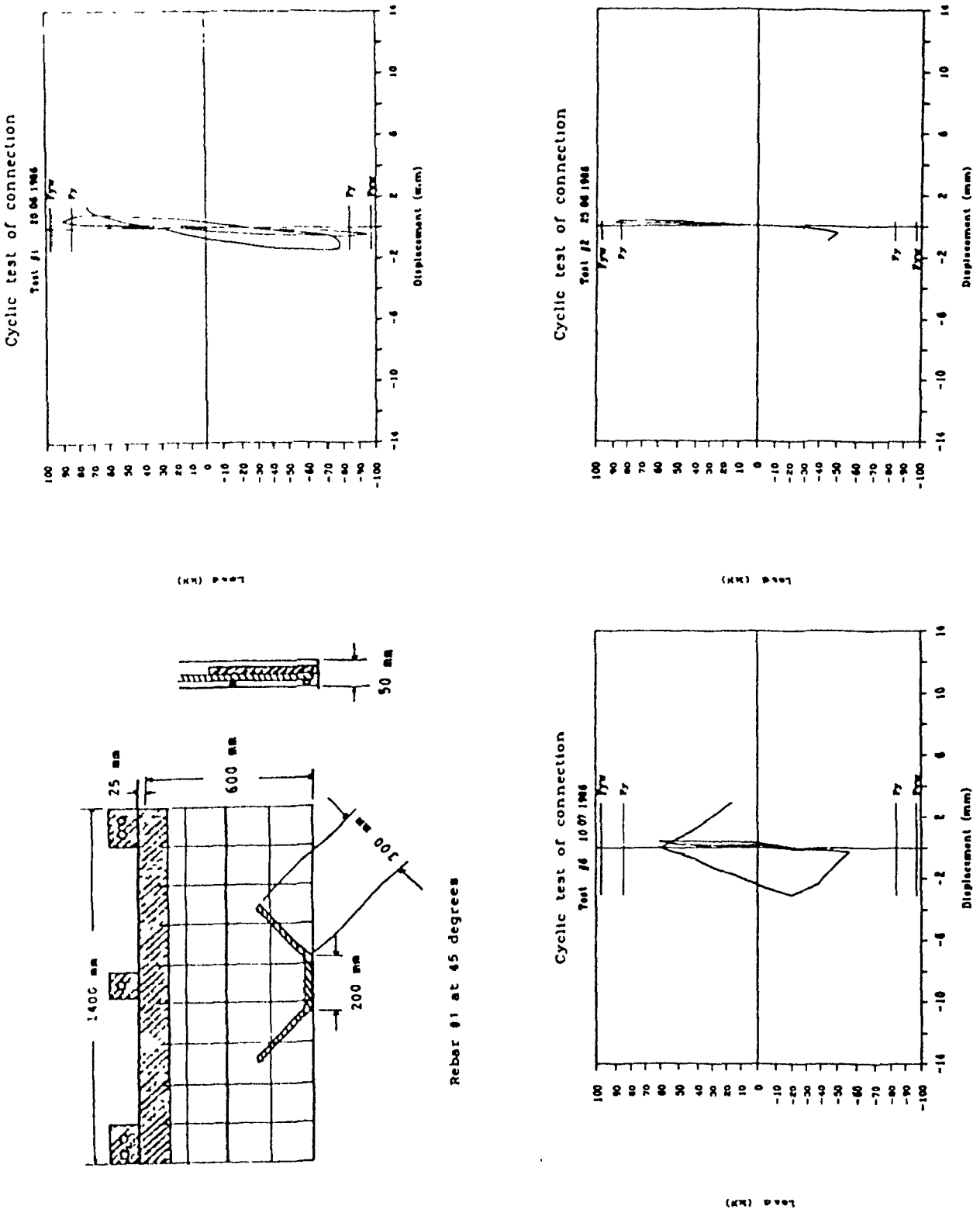

Figure 1.10 Cyclic test on thin panel embedded bar connection reported by Kallros[14]

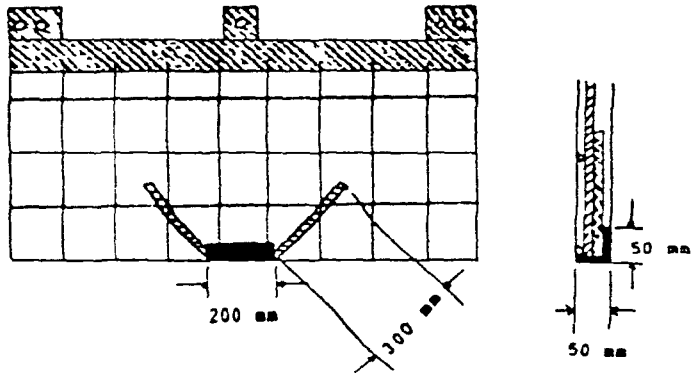

Rebar #1 at 45 degrees welded to angle

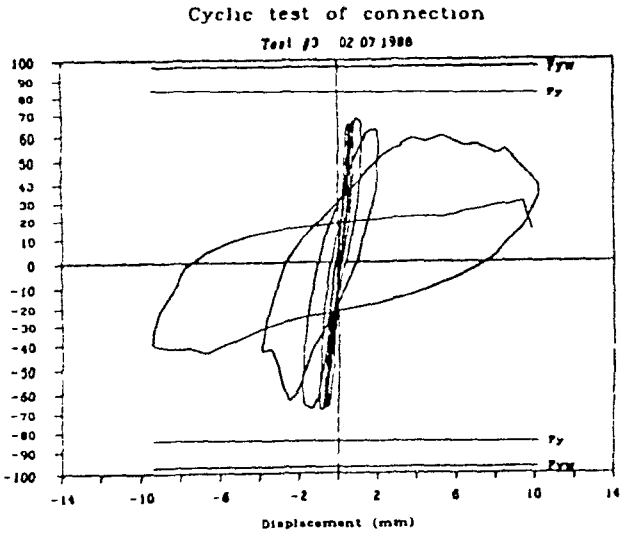

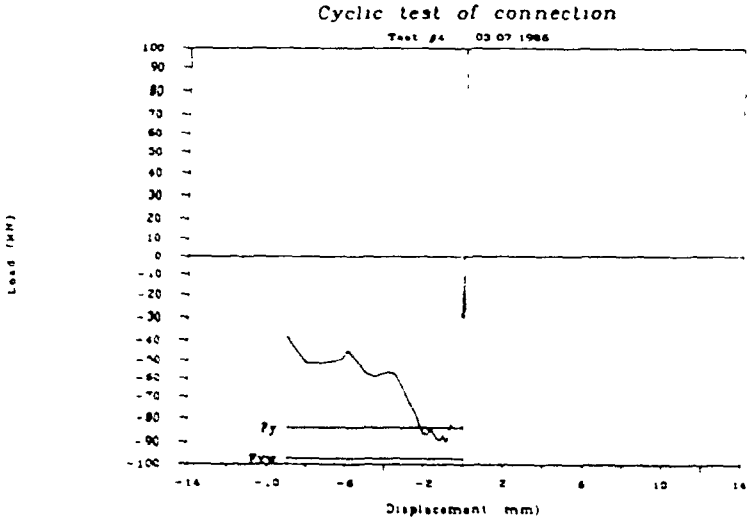

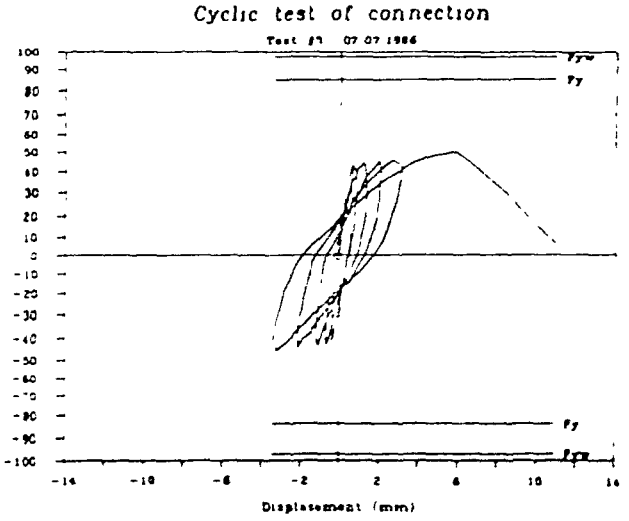

Figure 1.10 (Continued)

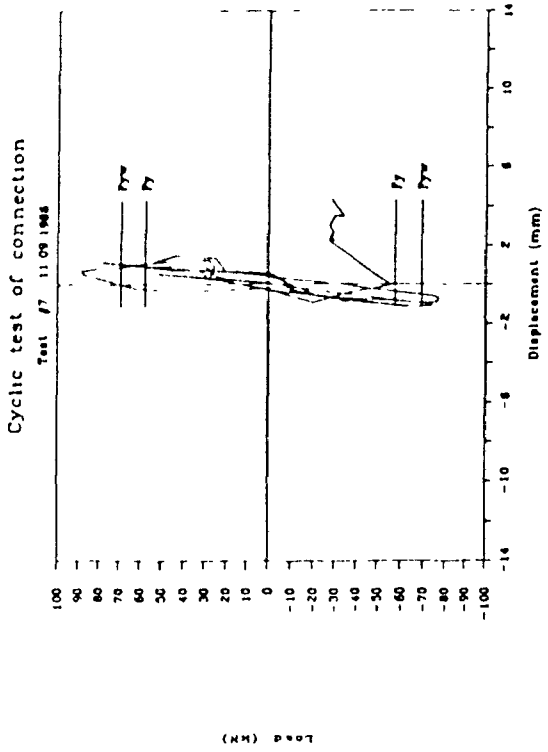

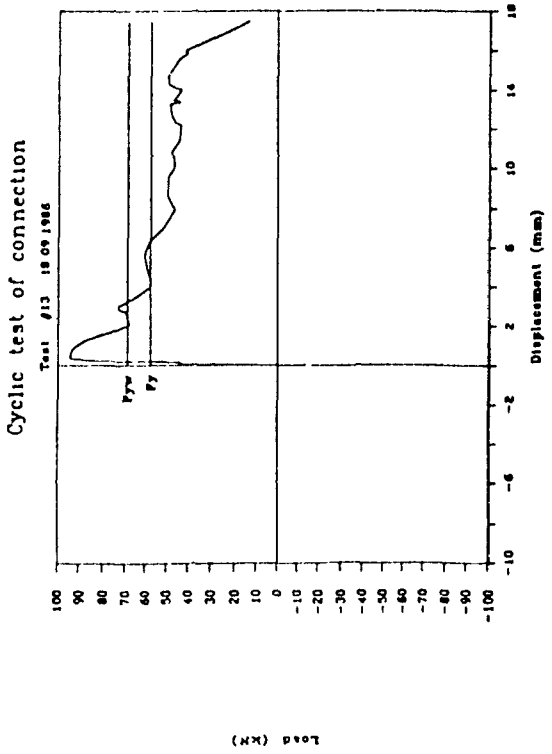

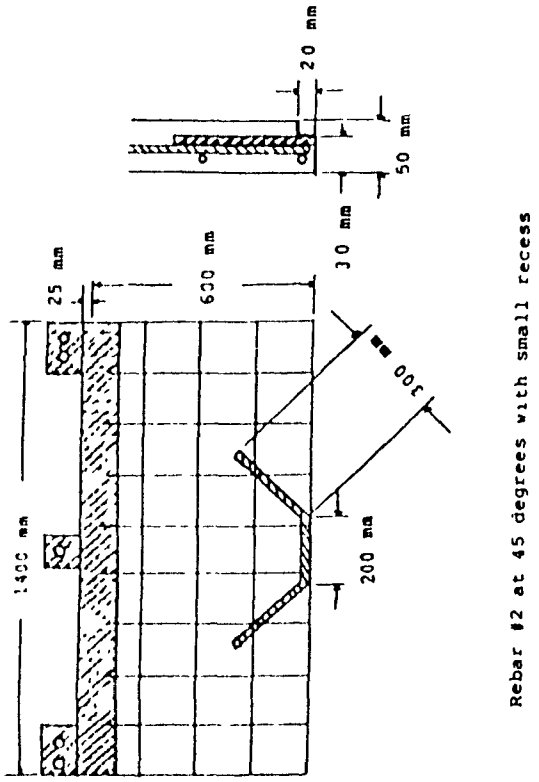

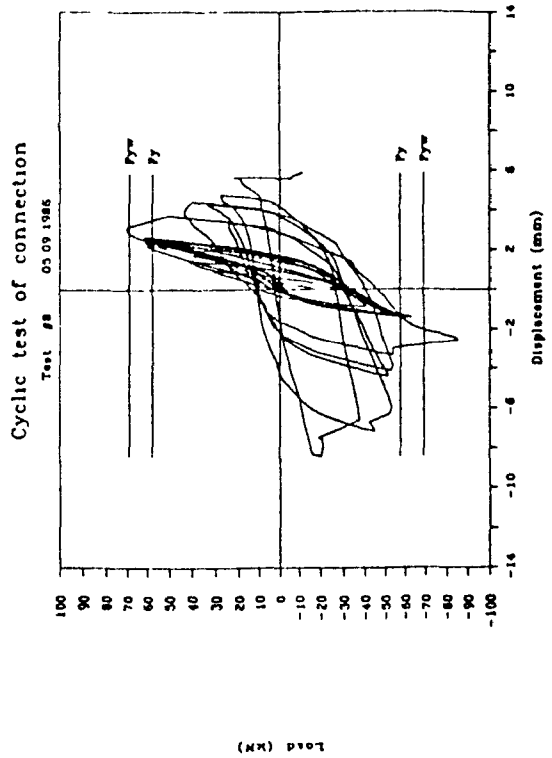

Figure 1.10 (Continued)

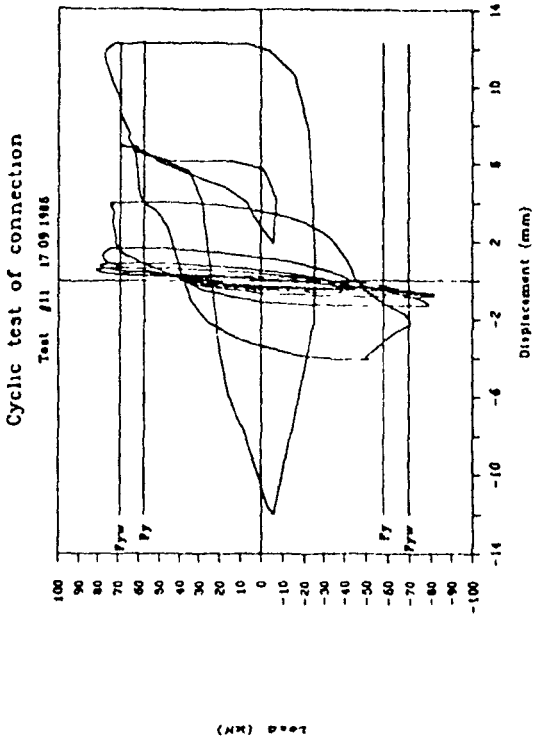

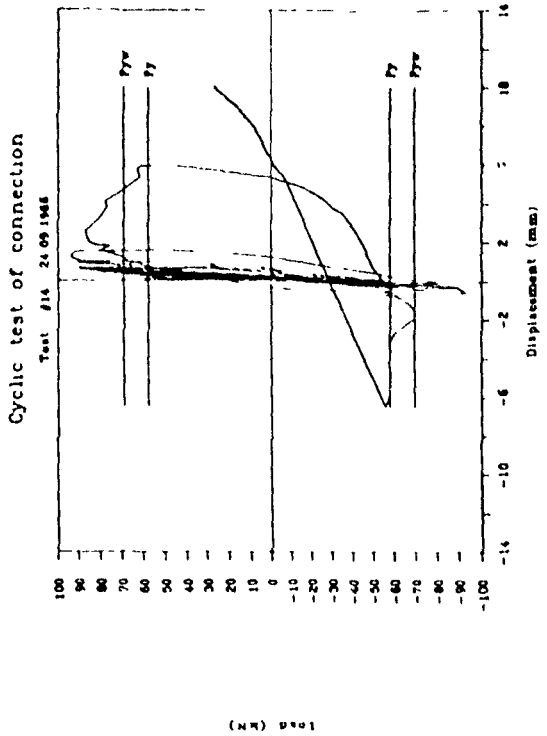

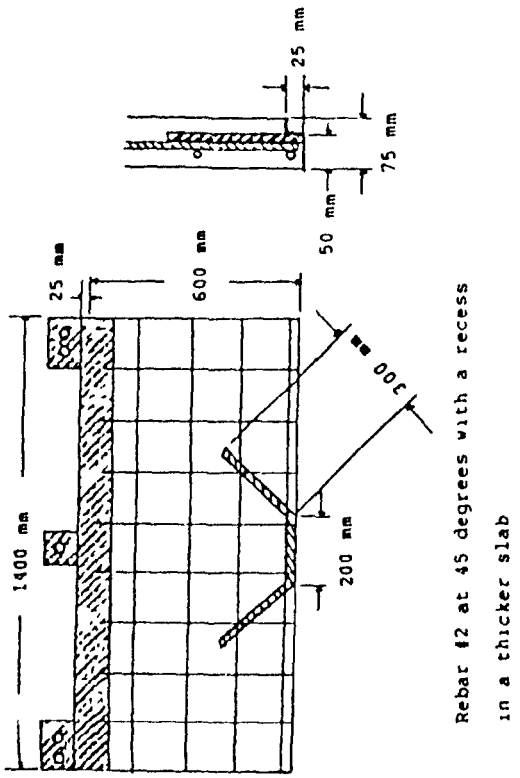

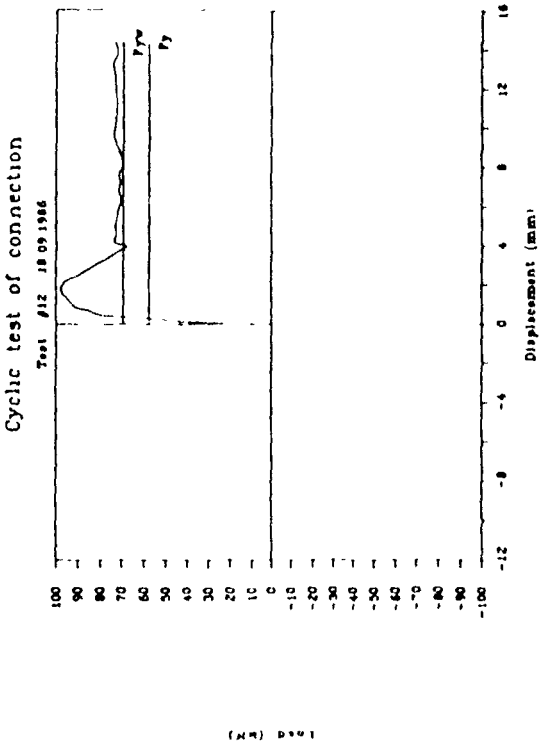

Figure 1.10 (Continued)

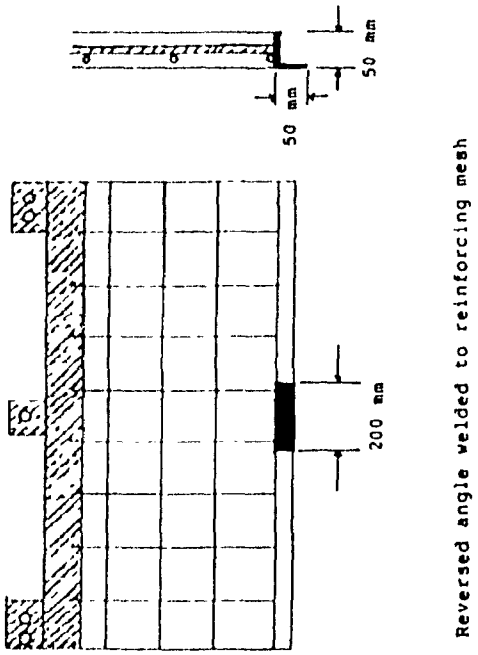

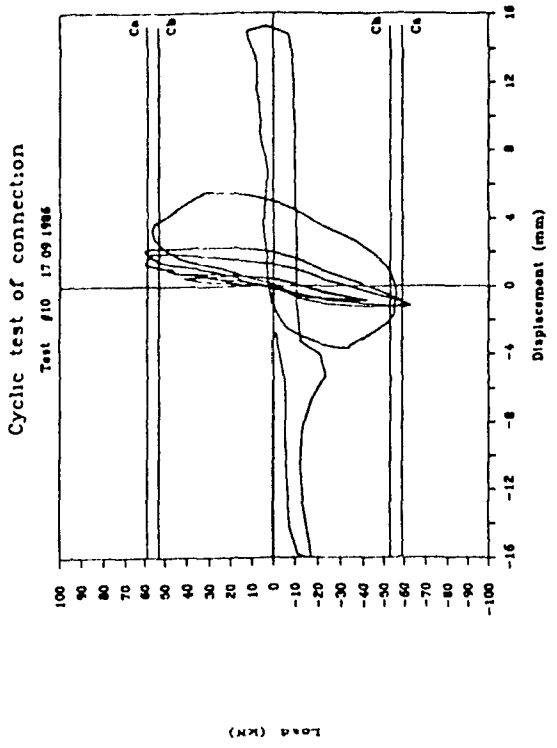

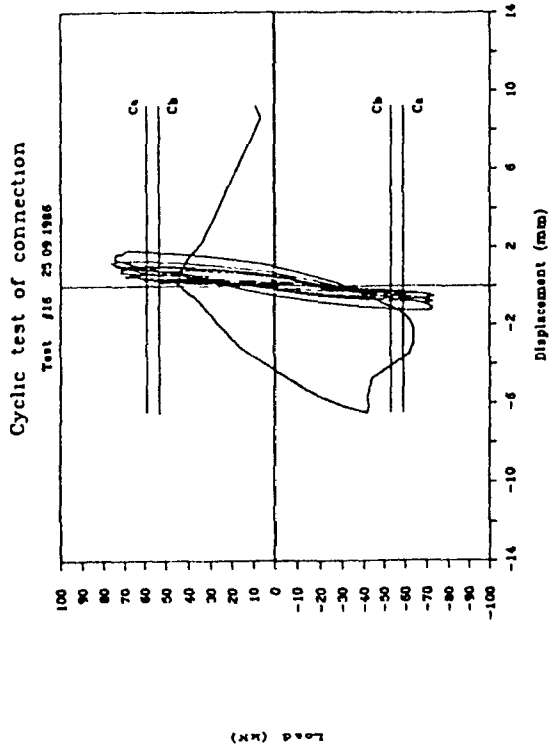

Figure 1.10 (Continued)

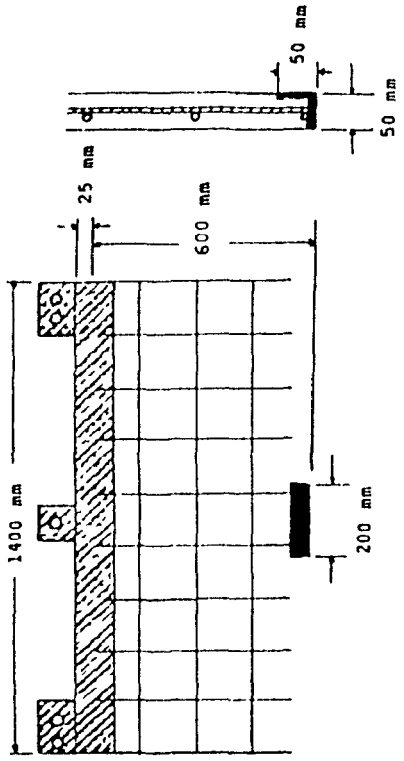

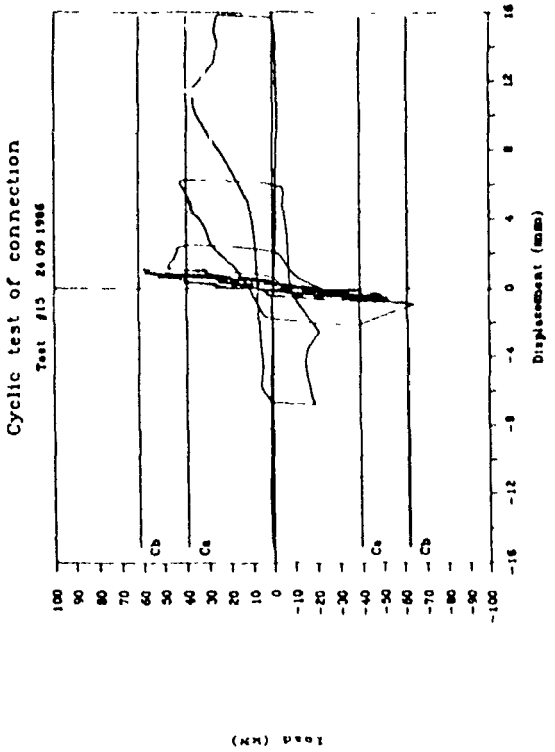

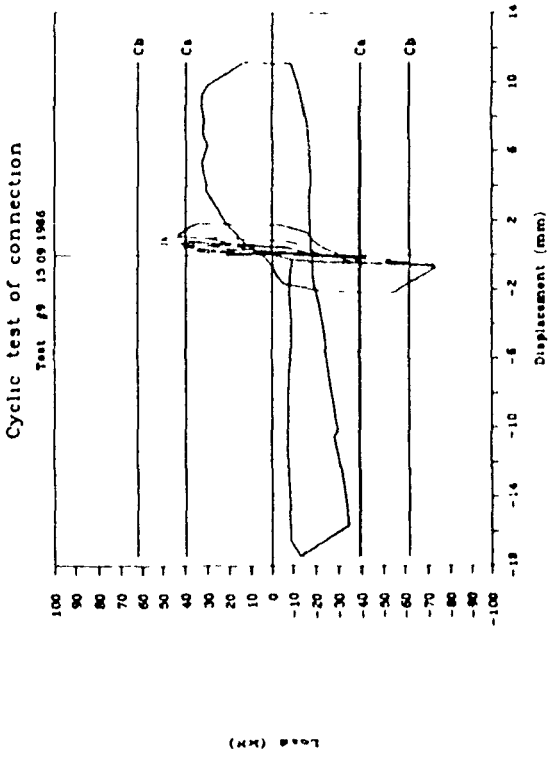

Figure 1.10 (Continued)

1.3 Current Design Approach

1.3.1 Lateral Seismic Force

The National Building Code of Canada (N.B.C.C. 1990)[15] specifies two approaches for the evaluation of the design earthquake load on a building as follows:

(i) Quasi-static seismic analysis

(ii) Dynamic analysis, using either average response spectra or step - by - step calculation in the time domain of the response of the structure subjected to a particular disturbance.

The quasi-static approach is usually quite satisfactory using the quasi-static seismic analysis. The equivalent elastic base shear, V_e, to determine the minimum lateral seismic force, according to NBCC 1990, is given by:

$$V_e = VSIFW \qquad (1\text{-}1)$$

where V = zone velocity ratio

S = Seismic response factor (see Figure 1.11)

Z_a = Acceleration-related seismic zone factor

Z_v = Velocity-related seismic zone factor

T = Fundamental period of vibration of the structure (in seconds)

= 0.1N for moment - resisting frames (N = number of storeys)

= $0.09h_n/\sqrt{D_s}$ for other structures (h_n and D_s are the height and length of the lateral load resisting system, respectively)

I = importance factor of the structures.

= 1.5 for post disaster building, 1.3 for schools and 1.0 for all other buildings

F = Foundation factor (ranging from 1.0 for rock to 2.0 for soft deep soil)

W = Dead load of the structure plus 25% of the design snow load.

The minimum lateral seismic force, V, for which the structure has to be designed is:

$$V = (V_e / R)U \qquad (1\text{-}2)$$

where R = force modification factor that depends on the capability of the structure to absorb energy during inelastic response (see Table 1.1).

U = 0.6 (calibration factor to adjust level of protection)

It must be mentioned that precast concrete buildings are not listed in Table 1.1, nor does the CSA Standard A23.3-M84 (Code for the Design of Concrete Structures and Buildings [16] give specific seismic design guidance for precast construction.

In addition to the lateral seismic forces, a building must also be designed for horizontal torsional moments. The largest design eccentricity, e_n, is given by:

$$e_n = 1.5e + 0.10D_n$$

or

$$e_n = 0.5e - 0.10D_n$$

where e = distance between the centre of mass and centre of rigidity

D_n = plan dimension of the building in the direction of the computed eccentricity.

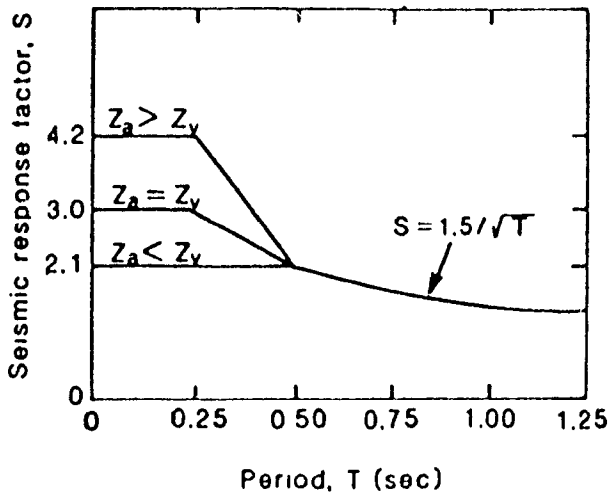

Figure 1.11 Seismic response factor in the 1990 National Building Code of Canada

Table 1.1 Force modification factors for reinforced concrete structures designed and detailed according to CAN3-A23.3 [15]

Type of lateral load resisting system	R
-Ductile moment-resisting space frame	4.0
-Ductile flexural shear wall	3.5
-Moment-resisting space frame with nominal ductility	2.0
-Wall with nominal ductility	2.0
-Other lateral force resisting systems	1.5

1.3.2 Connections

Horizontal loads from wind or earthquakes are usually transmitted to shear walls or moment resisting frames through the roof and floors acting as horizontal diaphragms. It is assumed that a diaphragm acts as a deep horizontal beam as presented in Figure 1.12 [17]. It is analogous to plate girders or I-beams. The shear walls or frames are considered as supports of this analogous beam. Therefore the support reactions are induced by the lateral force resultant from the earthquake loading. The tension and compression chords forces are induced in the diaphragm by assuming bending of the diaphragm in its own plane. The precast concrete double-tees which span parallel to the supporting walls or frames must be designed to transfer shear between the adjacent elements and also to the supporting elements. Thus the design of a diaphragm is essentially a connection design problem.

1.3.2.1 Deformed Bar Anchor Connection

This section presents the data and methodology for designing typical flange connections between double-tee flanges. Deformed bars are anchored in the concrete by bond. The required embedded length can be calculated in the same fashion as the development length for the normal reinforcing bars. The CPCI Metric Design Manual[18] suggests the following equations for development length of deformed reinforcing bar anchors:

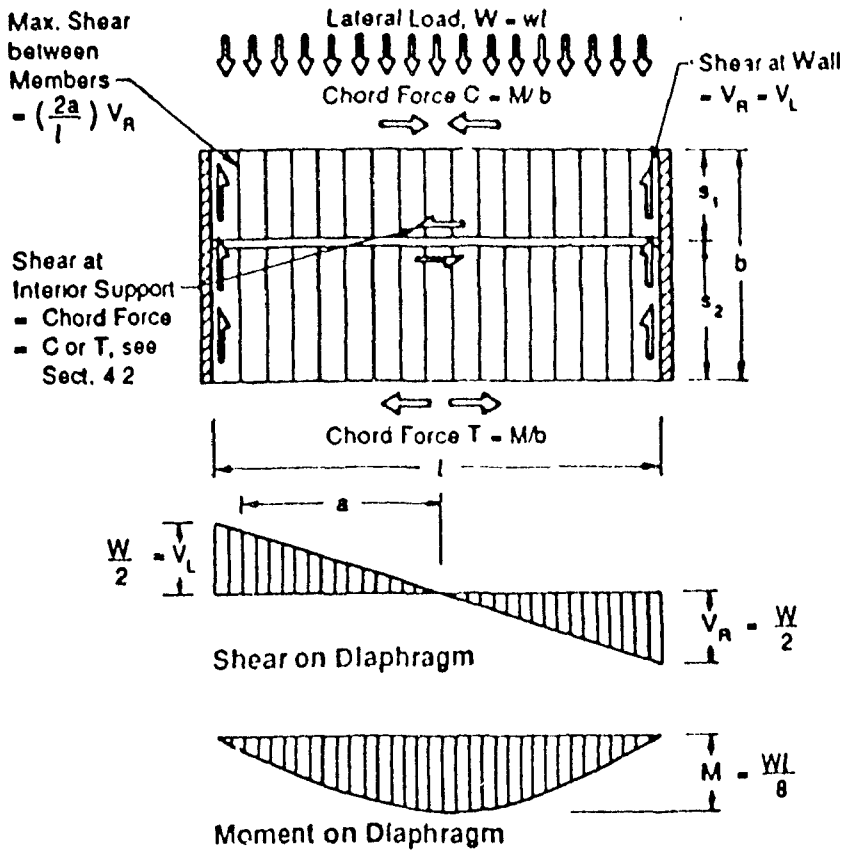

Figure 1.12 Analogous beam design of diaphragm[17]

For No. 35 reinforcing bars or smaller, in tension:

$$l_d = 0.019A_s f_y/\sqrt{f'_c} \quad (1\text{-}3)$$

which has to be greater than the minimum of $0.058\ f_y d_b$ or 300 mm

For No. 45 bars, $l_d = 26f_y/\sqrt{f'_c}$ (1-4)

and for No. 55 bars, $l_d = 34f_y/\sqrt{f'_c}$ (1-5)

while compression development length is given by :

$$l_d = 0.24d_b f_y/\sqrt{f'_c} \quad (1\text{-}6)$$

where A_s = area of the reinforcing bar (mm^2)

d_b = diameter of bar (mm)

All modification factors currently in the code would apply.

The ACI Code [19] , ACI committee 318, assumes that the basic development length required to prevent splitting failures, $l_{db\,sp}$, is a function of the cross-sectional

area of the bar, while the length required to prevent pullout, $l_{db\ po}$, is a function of the diameter of the bar. The equations to determine basic development length are as follows:

For No. 35 bars and smaller:

$$l_{dp\ sp} = 0.02A_s f_y/\sqrt{f'_c} \quad \text{(mm, MPa)} \tag{1-7}$$

$$l_{dp\ po} = 0.375d_b f_y/\sqrt{f'_c} \tag{1-8}$$

The ACI code requires that the basic development length to prevent splitting failure given by equation (1 - 7) be multiplied by a modification factor "k_1" to account for the clear cover thickness. Both development lengths to prevent splitting and pull-out must be multiplied by factor "k_2" to account for the parameters listed in Table 1.2. Therefore, the development lengths to prevent splitting and pull-out failures, respectively, are the following:

$$l_{d\ sp} = k_1 k_2 l_{db\ sp} \tag{1-9}$$

$$l_{d\ po} = k_2 l_{db\ po} \tag{1-10}$$

where $k_1 = 2.0$ for $c \leq d_b$

$k_1 = 1.4$ for $d_b < c < 2d_b$

$k_1 = 1.0$ for $c \geq 2d_b$

$k_1 = 0.8$ for $c_1 \geq 2.5d_b$ in addition to the factors listed below

c = Clear cover thickness

c_1 = Clear cover thickness to the edge

k_2 = factors listed in Table 1.2

Finally, the development length, l_d, required by the ACI Code is the larger of the two lengths calculated by equations (1-9) and (1-10) but must not be less than 300 mm. Although the ACI Committee 408 has not explicitly recommended an anchorage length (development length) under cyclic loading, it is likely that the committee would adopt proposals such as those presented by the researchers at the University of Texas at Austin and Cornell University[20]. The results are summarized as follows:

1) For straight anchorages with a cover of at least 1.5 d_b:

$$l_d = (1860 \times d_b)/\sqrt{f'_c} > 30\ d_b \quad \text{(Imperial units)} \tag{1-11}$$

$$l_d = (154.5 \times d_b)/\sqrt{f'_c} > 30\ d_b \quad \text{(S. I. units)} \tag{1-12}$$

ii) For hooked bar anchors:

$$l_{hd} = (1800 \times d_b)/\sqrt{f'_c} \quad \text{(Imperial units)} \qquad (1\text{-}13)$$

$$l_{hd} = (149.5 \times d_b)/\sqrt{f'_c} \quad \text{(S. I. units)} \qquad (1\text{-}14)$$

All modification factors currently in the code would apply. It must be mentioned that in this study the equations for the evaluation of developments lengths for reinforcing bar subjected to cyclic loading are used (Equations 1-12 and 1-14).

Table 1.2 Values of modification factor k_2 for development length[19]

(a) Top reinforcement - horizontal reinforcement with more than 300 mm of fresh concrete cast below the reinforcement	1.3
(b) Lightweight aggregate concrete, or, if f_{ct} is specified	1.3 $0.556\sqrt{f'_c}/f_{ct}$
(c) Excess reinforcement	(A_s required/A_s provided)

The CPCI Metric Design Manual[18] suggests that this connection should be designed to resist only the shear forces. Since earthquake loading is induced into the diaphragm in any direction, the connections must be designed for the most critical load combination. For convenience, the ATC (Applied Technology Council)[7] requires that 100% of the forces for one principal axis plus 30% of the force for the perpendicular axis be used for design of these connections. In design and analysis, this combination is considered for both principal directions and requires the maximum component strength to be used.

The current method for design of connections utilizes the development length provisions as described above and analysis based on truss analogy model, as presented by CPCI[18] and PCI[11,12] Handbook. A typical detail for double - tee flange connections is presented in Figure 1.13.

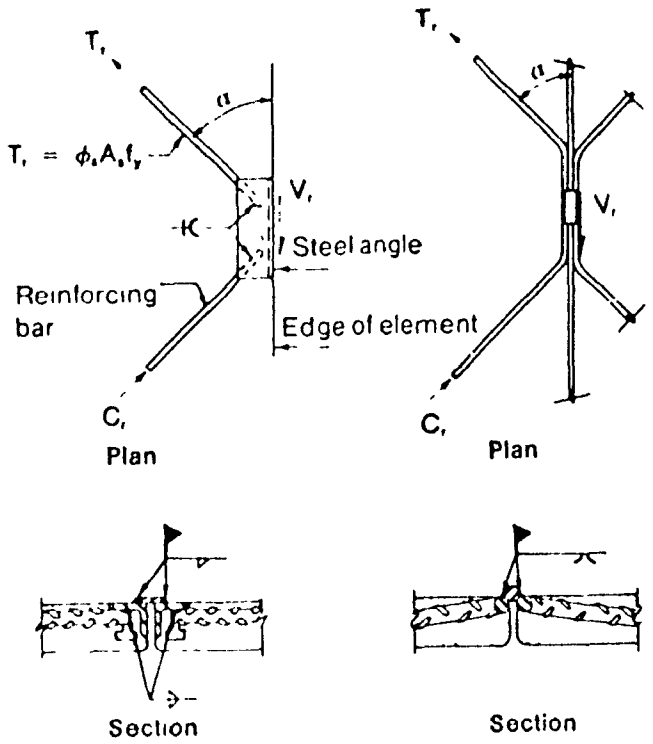

Notes: (a) Unless ends of elements are prevented from translating sideways, this connection cannot be used for earthquake connection as rotation will occur under high loads

(b) Design of welds and weld details in accordance with CSA-W186[22]

Figure 1.13 Typical flange weld plate details[18]

In using the truss analogy, it is assumed that for a given shear force, the forces resulting in the tension and compression legs of the anchorage reinforcing are equal (see Figure 1.13). Therefore, the design shear force for the connection is determined by nodal equilibrium for the truss members as follows:

$$V_r = 2T_r \text{ Cos } \alpha = 2C_r \text{ Cos } \alpha \qquad (1\text{-}15)$$

Therefore,

$$V_r = 2\phi_s A_s f_y \text{ Cos } \alpha \qquad (1\text{-}16)$$

In a typical connection, the angle α is equal to 45 degrees, consequently, for a typical connection, the design factored shear is resistance given by:

$$V_r = \sqrt{2}\phi_s A_s f_y \qquad (1\text{-}17)$$

where $\phi_s = 0.85$

A_s = Area of the reinforcing bar cross section (mm^2)

f_s = Yield strength of the steel bar

In the case when force is applied normal to the connection, the factored capacity of the connection is determined by:

$$V_r = \sqrt{2}\phi_s A_s f_y \qquad (1\text{-}18)$$

1.3.2.2 Connection with Welded Headed Studs

Welded headed studs are designed to transfer shear, tension or a combination of the two from one element to the adjacent one through the connection. The designs are based on either strength of the steel or of the concrete, and both must be checked to find the critical capacity of the joint. It is preferred to design the embedded steel anchor to ensure that a tensile failure in the anchor governs. The current design and analysis method are summarized in the following sections for design of connections with headed studs, which are previously welded to a steel plate and embedded in unconfined concrete. With confining of concrete, the critical capacity increases, as expected. The thickness of the plates to which studs are attached, should be at least 2/3 of the diameter of the studs[11].

1.3.2.2.1 Studs in tension

Studs depend on the head to engage a concrete area that causes a cone-type pullout failure. The method in the CPCI Metric Design Manual[13] assumes a shearing surface and applies a unit shearing strength to that surface area (see Figure 1.14). The factored tensile capacity of the concrete surrounding a headed stud,for failure by a cone-type pullout, is given by:

$$P_\phi = 0.30\lambda\phi_c\sqrt{f'_c}A \qquad (1\text{-}19)$$

where $\phi_c = 0.6$

A = Effective stress Area

λ = factor defined in Clause 11.2.3. of CAN3 - A23.3

The effective stress area is the projected area of a 45 degree pyramid from the

bearing edge of the anchor (see Figure 1.15). In the case of a stud group, the area of the heads of studs or the area involved in overlapping stress areas of studs must not be included. Also if the thickness of concrete is not sufficient to develop the full projection area, a reduction in the effective stress area must be considered.

Since the cone type pullout failure occurs in practice, a reduction factor equal to 0.3 is included in the above formulas to account for the difference between the assumed pyramidal and the conical failure surfaces. The effective stress area for a single headed stud (Figure 1.15) is given by

$$A = (2l_e + 1.58d_b^2) - 2.5\ d_b^2 \qquad (1\text{-}20)$$

where l_e = embedded length of the stud

d_b = stud anchor diameter

If a stud is located near a free edge of a member, a bursting type of failure can be expected. In this respect the minimum cover (mm) from the anchor head to any free edge is given by:

$$m = d_b \sqrt{\frac{f_u}{6\sqrt{f_c}}} \geq 50mm \qquad (1\text{-}21)$$

where f_u = ultimate tensile stress of the anchor

The minimum concrete thickness for full development of a stud group is:

$$h_{min} = l_e + b/2 \quad \text{(see Figure 1.16)} \qquad (1\text{-}22)$$

If the above criteria are not satisfied, special procedures are necessary to include a reduction factor. Referring to Figure 1.17, the effective stress area (A) is given by:

$$A = h(2a + 8l_e + 2b - 4h) - A_h \qquad (1\text{-}23)$$

where A_h = total area of the anchor heads. Other symbols are shown in Figure 1.16.

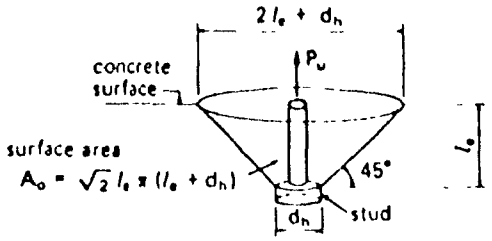

Figure 1.14 Assumed failure surface for headed studs[25]

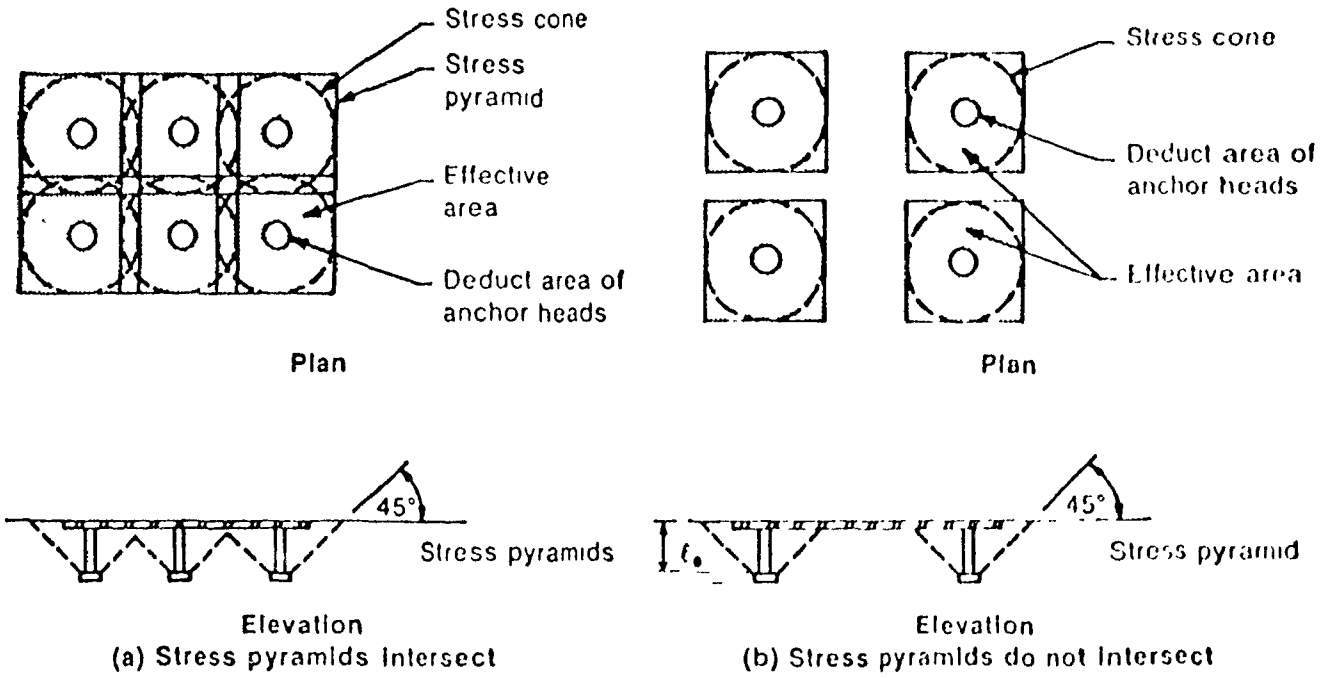

Figure 1.15 Effective stress area for welded headed studs[18]

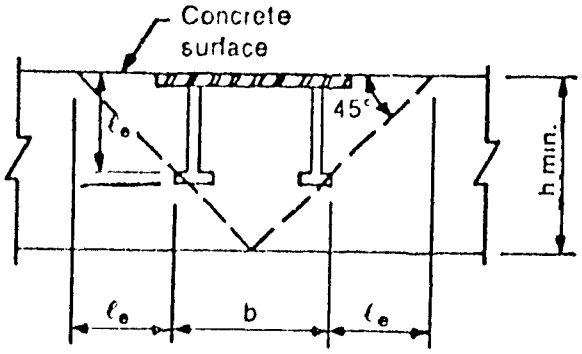

Figure 1.16 Development of welded headed studs[18]

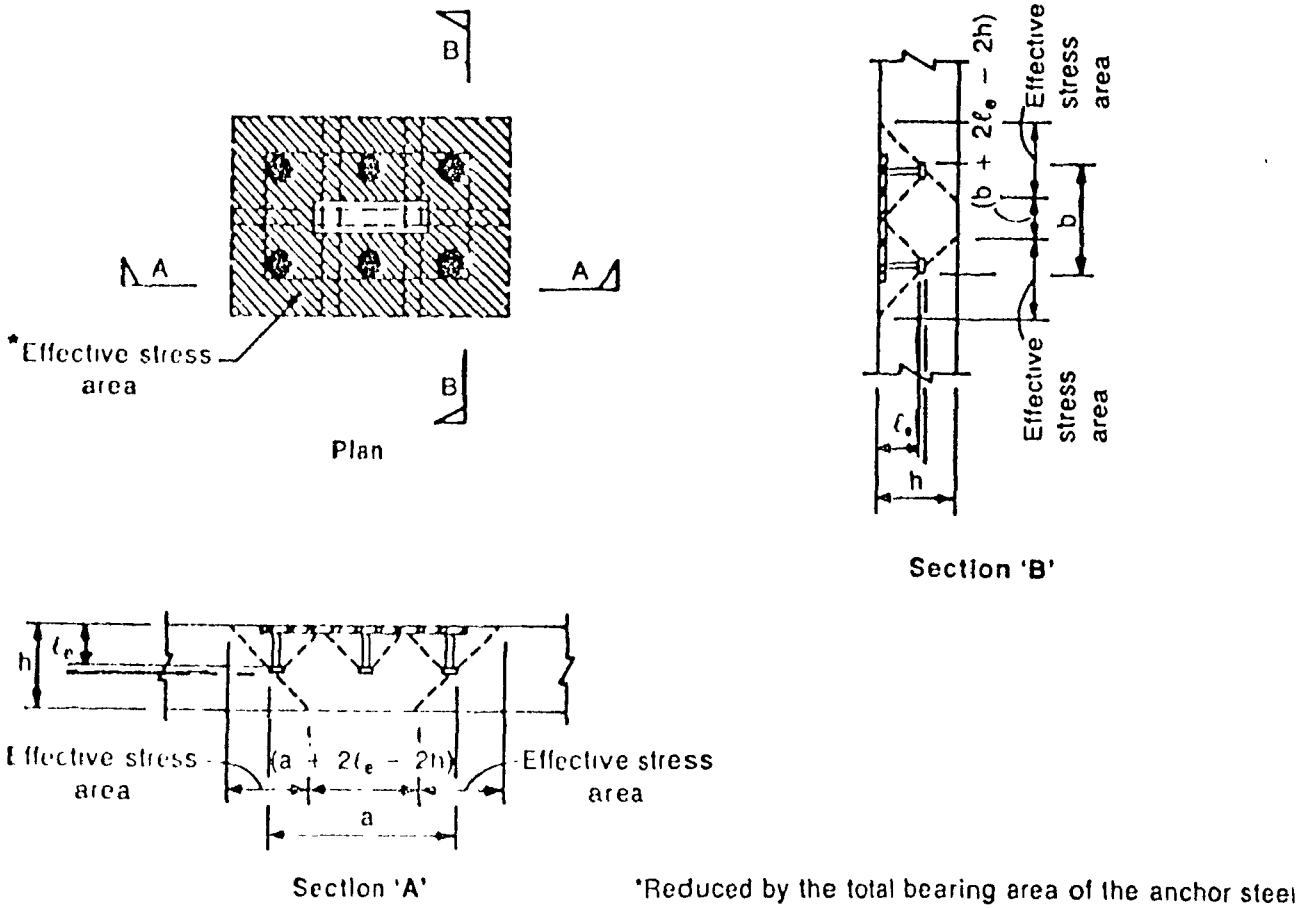

Figure 1.17 Stress area reduction for limited depth A_r[18]

When the tensile strength of steel governs, the factored resistance of a headed stud is given by:

$$P_\phi = A_b \phi_s f_u \qquad (1\text{-}24)$$

where A_b = area of stud anchor

$\phi_s = 0.85$

f_u = ultimate tensile stress

A value of 400 MPa is recommended for the ultimate tensile strength of the headed stud steel. As mentioned previously, to achieve ductile behaviour, the factored resistance of the connection derived based on steel strength, should not be less than the factored resistance of the connection, derived based on the pullout failure of the headed stud (concrete cone-type failure).

1.3.2.2.2 Studs in shear

Studs are frequently subjected to shearing forces in precast element connections. The concrete strength for studs not located near a free edge can be calculated using either the lateral bearing of the stud or by the shear friction concept. The factored bearing resistance of a single headed stud subjected to shear can be determined using the equation:

$$B_\phi = 1.4 \phi_c A f'_c \qquad (1\text{-}26)$$

where $\phi_c = 0.6$ and A = projected bearing area of the stud ($d \times l_c$)

The factored shear resistance calculated using the shear friction principle for studs which are welded to a plate is given by:

$$V_\phi = \phi_s A_{vf} f_y \mu \qquad (1\text{-}27)$$

where $\phi_s = 0.85$

A_{vf} = cross sectional area of the studs

f_y = yield strength of the stud

$\mu = 0.6\lambda$ for the contact plane coincidental with the concrete surface

$\mu = 0.8\lambda$ for the contact plane a full plate thickness below the concrete

surface

The above value of V_ϕ must be smaller than the value the values calculated using Equations 11.31 and 11.32 and provision of Section 11.7 of the CSA Standard A 23.3-M84[16]. When the shear load is in the direction of a free edge, the shear strength of concrete becomes more critical. The factored shear resistance specified by the CPCI [18] can be calculated using the equation:

$$V_\phi = 0.30\lambda\phi_c\sqrt{f'_c}A \qquad (1\text{-}28)$$

where A = effective stress area.

For the stud group in the connection, the effective stress area is equal to the area of projected 45 degree plane from a line parallel to the free edge through the middle of the contact surface and from the edge of the contact surface to the free edges (see Figure 1.18).

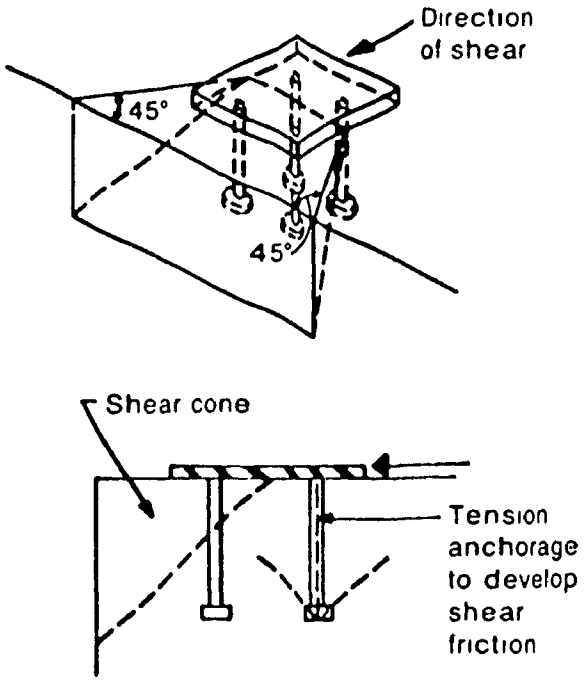

Figure 1.18 Edge distance effect for welded headed studs[18]

1.3.2.2.3 Combined shear and tension

Most of the embedded steel devices in precast concrete connections are normally subjected to a combination of shear and tensile forces. For design purposes an interaction equation can be used. For concrete, this interaction equation is:

$$\frac{1}{\phi_1}[(\frac{P_u}{P_c})^2+(\frac{V_u}{V_c})^2] \leq 1.0 \qquad (1\text{-}29)$$

where $\phi_1 = 0.85$

P_u = factored tension loads

V_u = factored shear loads

P_c = tensile strength of connection governed by concrete failure

V_c = shear strength of connection governed by concrete failure

For steel, the interaction equation is:

$$\frac{1}{\phi_2}[(\frac{P_u}{P_s})^2+(\frac{V_u}{V_s})^2] \leq 1.0 \qquad (1\text{-}30)$$

where $\phi_2 = 1.0$

P_s = tensile strength of connection governed by steel failure

V_s = shear strength of connection governed by steel failure

It must be noted that in the current method for design of connections between double-tee flanges under lateral loading, design is based only on the shear acting on the connection.

1.4 Objectives

The overall objectives of this research program are to study the behaviour of typical connections between flanges of double-tees or between a double-tee flange and the lateral load resisting element in a typical roof of a precast structure under simulated seismic loading. The research program consists of the following:

1. Analysis of a part of a double-tee roof flange with three connections subjected to

lateral loads to develop the boundary conditions for the test specimen with one connection using the SAP90 Program.

2. Nonlinear analysis of the complete behaviour of the connections selected for the experimental work along with the boundary conditions worked out in Objective 1 above, using the NONLACS (NONLinear Analysis of Concrete and Steel Structure) Program.

3. Experimental study of the complete behaviour until failure of selected connections subjected to reversed cyclic loads.

4. Comparison of the experimental response of the connection subjected to reversed cyclic loads with the analytical response of the same connections subjected to monotonically increasing loads, and development of practice-oriented recommendations for design of these connections.

Chapter 2

Experimental Program

2.1 Introduction

Five typical types of connections between double tee flanges commonly used in the precast industry, were investigated in this research program. The connection details are shown in Figure 2.1; the connection details were selected for their simplicity and ease of construction. A total of five precast concrete connections in concrete panels of a size 1300 mm x 800 mm, were constructed and tested in the Jamieson Structures Laboratory at McGill University.

The connections details are defined as follows:

1) Specimen S1: Connection with a bent deformed bar anchor welded to a steel plate

2) Specimen S2: Connection with a bent deformed bar anchor and a 90° hook welded to steel plate

3) Specimen S3: Connection with straight deformed bar anchors, oriented at 90° and welded to an embedded angle

4) Specimen S4: Connection with headed studs welded to a steel plate

5) Specimen S5: Connection with a deformed bar oriented at 45° and headed studs both welded to an angle

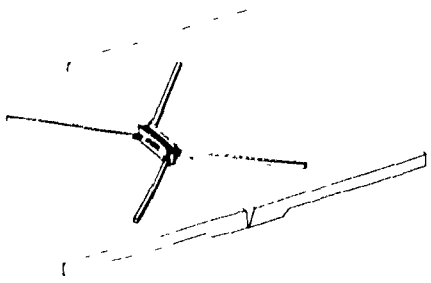

a) Connection S1

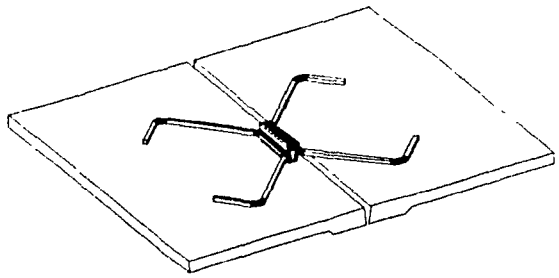

(b) Connection S2

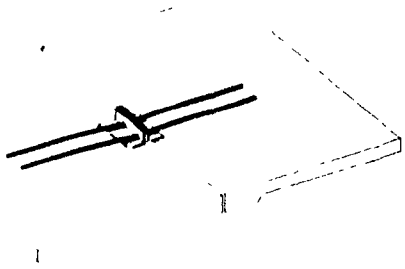

(c) Connection S3

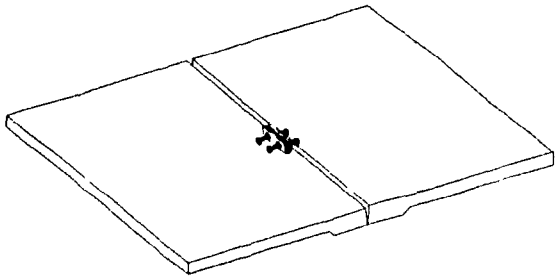

(d) Connection S4

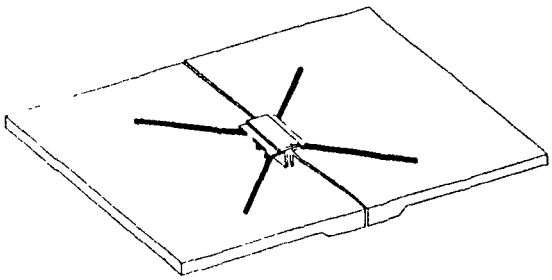

(e) Connection S5

Figure 2.1 Details of connections investigated in this research program

2.2 Design of Prototype Building

To understand the importance of connections between the flanges of double-tee slabs and between the flange and lateral load resisting elements and the loads transmitted by these connections the design of a single story precast structure with a precast double-tee roof and precast wall panels is reviewed in the following sections.

2.2.1 Single - Storey Precast Structure

Figure 2.2 shows the plan and elevation of a prototype single - storey precast concrete structure. This example of the prototype structure is selected from the CPCI Metric Design Manual[18].

The precast building shown in Figure 2.2 is 38.4 m by 48 m in plan and has 4.8 m clear height inside. The walls are composed of 400 mm deep double - tees and the roof assemblage of 600 mm deep double tees. The double tees are 2400 mm wide with stems 1200 mm on centres. The flanges of the roof tees are 50 mm thick, while the wall tees are 100 mm thick.

The seismic design of the prototype structure was performed in the North South direction, and it was assumed that the building was located in Montreal. The dead and live loads conform to the 1990 National Building Code of Canada and are

Wall Panels:

Unit weight of wall panel = 3.3 kN/m^2

Height of wall panel = 6150 mm

North or South Wall:

Total length of one wall = 48.0 m

Weight above mid - height = (3.45)(48.0)(3.3) = 545 kN

Weight of complete wall = (6.15)(48.0)(3.3) = 971 kN

East and West Wall:

Total length of one wall = 38.4 m

Weight above mid - height = (3.45)(38.4)(3.3) = 436 kN

Weight of the complete wall = (6.15)(38.4)(3.3) = 770 kN

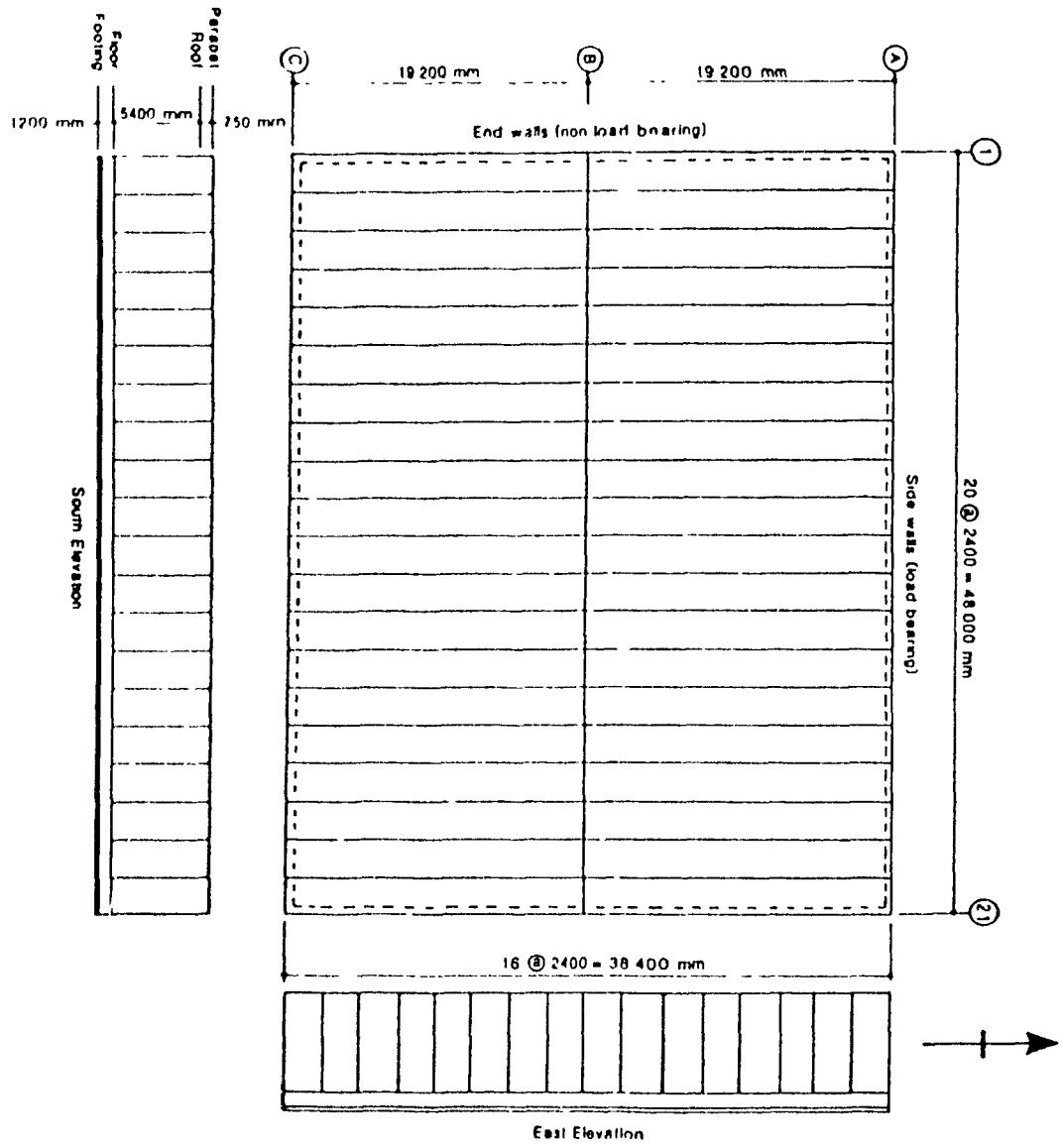

Figure 2.2 Details of single-storey precast wall panel building

Roof:

Weight of a roof panel (with water proofing membrane) = 2.8 kN/m²

Weight of roof = (48.0)(38.4)(2.8) = 5179 kN

Weight of building (roof + all walls) = 8675 kN

Snow Load:

25% of design snow load,S, is taken into consideration.

For the structure under consideration, the snow load was calculated to be:

$S = 2.64\ kN/m^2$

Total snow load = (0.25)(38.4)(48.0)(2.64)=1216 kN

Total lumped weights:

- Roof + N-S walls + Snow = 8926 kN

_ Roof + N-S wall + E-W walls + Snow = 9933 kN

Specified lateral seismic force

The minimum lateral seismic force, acting at the top of the panels is given:

V = (v s I F W)(U) / (R)

where the seismic factors are:

v = 0.1 for Montreal

T = 0.1 N, for one storey building N=1, therefore, T= 0.1 s

S = 4.2 for T<0.25 s

I = 1.0

F = 1.0

W = weight of the roof, N-S walls, and 25% of design snow load = 8926 kN

U = 0.6

R= force modification factor = 2.0

Therefore,

V = (0.1 x 4.2 x 1.0 x 1.0 x 8926 x 0.6) /(2.0) = 1125 kN

The design earthquake load, V, is applied to the roof diaphragm as indicated in Section 1.3.1. To guard against accidental torsional effects, a minimum eccentricity equal to 10% of the lateral dimension must be assumed between the centroid of resistance and the centre of mass as shown in Figure 2.3. Therefore, the design forces on the roof diaphragm are:

Maximum shear force, V_w, assumed to act on each of the east and west walls at roof level is : $V_w = 0.6\ V = 0.6 \times 1125 = 675$ kN

Average shear intensity , $v_0 = 675/38.4 = 17.6$ kN/m

Maximum bending moment, $M_w = (Vw\ L)/8 = (1125 \times 48)/8 = 6750$ kN.m

Maximum chord forces, $C_w = T_w = M_w/d = 6750 / 38.4 = 176$ kN

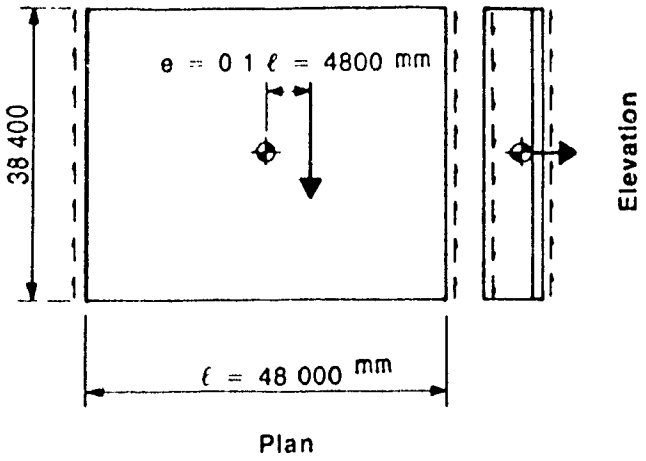

Figure 2.3 Specified forces acting on roof and walls

Resistance analysis

Analysis of the structure is undertaken in two parts. The first part deals with design and detailing of the roof diaphragm and its connections, while the second part deals with the design of the wall panels. Because this thesis focuses on the behaviour of connection between the flanges of the double-tees which constitute the roof diaphragm and between the flange and lateral load resisting elements, focus is placed on the design of connections.

The diaphragm is required to resist the shear forces induced by the earthquake load. The maximum factored shear intensity in double tee flanges adjacent to the wall panel is :

$$v_u = 1.5\ V_w = 1.5 \times 17.6 = 39.6\ \text{kN/m}$$

where the v_u is shear force per unit length

The design shear strength of the concrete per unit length in the double tee flanges along the web is:

$$v_c = 0.2\ \phi_c \sqrt{f'_c}\ d \times 1000$$

$$= 0.2 \times 0.6\ \sqrt{35} \times 50 \times 1000 = 35.5\ \text{kN/m}$$

which is less than the v_u, therefore the flanges need reinforcement, normally using

welded wire fabric (WWF). The principles of shear friction are used to design the diaphragm shear reinforcement. The steel area required to resist the v_u is determined as follows:

$$v_r = \mu \phi_s f_y A_s$$

where μ=1.25, for concrete cast monolithically [CSA A23.3-M84, sec. 11.7.4.3(a)]

A_s= area of reinforcement per unit length normal to the web, and

f_y= 350 MPa (assumed)

Substitution of values in the above equation gives:

$$A_s = (v_u) / (\mu \phi_s f_y) = (39.6) / (1.25 \times 0.85 \times 350) = 106 \text{ mm}^2/\text{m}$$

Therefore, the double-tee flanges are reinforced with WWF 100 x 100 MW 13.3 / MW 13.3 which provides a steel area, A_s = 133 mm^2/m in each direction. Therefore, the shear resistance of the double tee flanges is adequate. Figure 2.4 shows the reinforcement details of flange.

Design of Connections

The roof and the wall to roof connections must now be designed for applied loads along the east and west edges. The factored design shear force, $V_u = v_u \times 38.4$ = 39.6 x 38.4 = 1520 kN

A typical connection to be used in this design is shown in Figure 1.13. The material resistance factor for reinforcing steel, ϕ_s=0.85 is used to find the force in the reinforcing bar. According to the Standard, CAN3-A23.3-M84, Section 21.2.3.2 , if these connections are intended to yield during an earthquake, an allowance is made for the loss of strength during the cycles of inelastic loading by using an additional member resistance factor, ϕ_m=0.7 . In this study, the most critical case is considered, since the purpose of research program is to investigate the strength of the connection in the inelastic range subjected to reversed cyclic loads.

Conventionally, the minimum size of steel bar used as anchors for the connection is

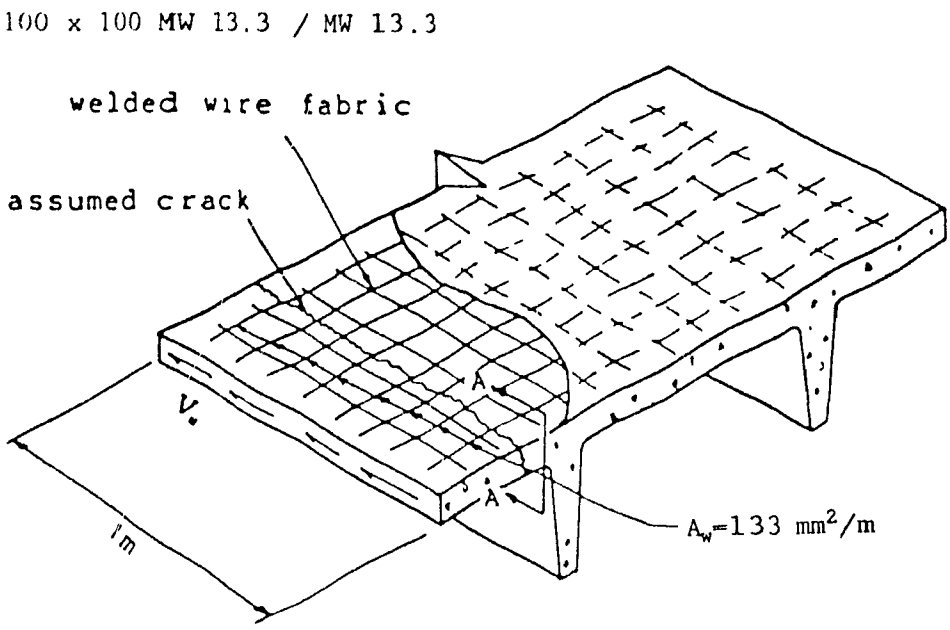

(a)

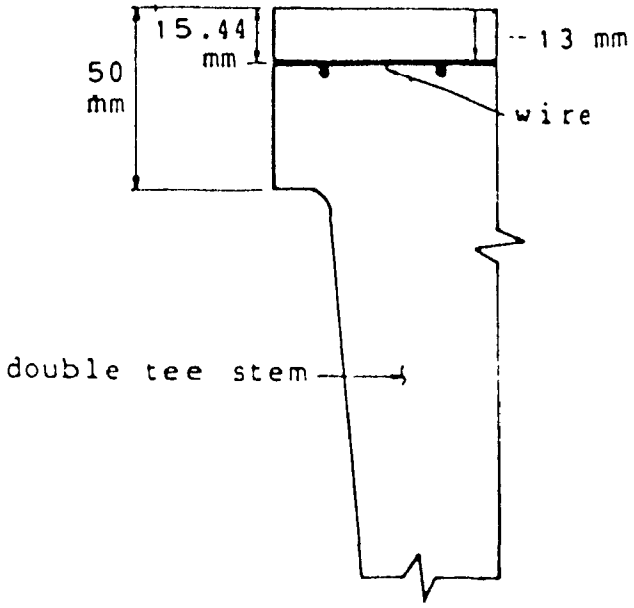

(b) Section AA

Figure 2.4 Reinforcement details of double-tee flange

M15 deformed steel bar.

The factored resistance, V_{rc}, of the connection can then be calculated as follows. The maximum compression force, Cr, in the compression leg and the maximum tensile force, Tr, in the tensile leg are given by:

$$Cr = Tr = \phi_m \phi_s f_y A_s = 0.7 \times 0.85 \times 400 \times 200 \times 10^{-3} = 47.6 \text{ kN}$$

And, using the truss analogy, the value of V_{rc} is computed by:

$$V_{rc} = (Cr + Tr) \cos 45° = 67.3 \text{ kN}$$

Connection between double-tee flange and wall panels

The connection to the east and west walls (Fig. 2.2) must be designed for factored design load induced at the top of the walls. Hence the spacing between these connections must not exceed:

$$s = V_{rc}/v_u = 67.3/39.6 = 1.70\text{m}$$

A suitable spacing between connections would be 1500 mm on centres. The connection details are shown in Figure 2.5.

Connections between double-tee flanges

The double tee flanges must also be connected to each other along their edges using a connection similar to that between the double-tee flange and the wall. The number of connections required is proportional to the shear force which decreases towards the middle of the diaphragm.

During an earthquake, one wall panel may yield while others are still in the elastic range due to the result of torsion and other effects. Therefore, as recommended in the CPCI Metric Design Manual[18], the resultant shear force on the diaphragm is assumed to act with a minimum eccentricity of 10% relative to the centre. The shear force will therefore have zero value at 0.6L, (= 0.6x4800 = 28800 mm) as shown in Figure 2.6.

Using the shear force distribution shown in Figure 2.6, the spacing of the connection along the interior flange of the first double tee can be calculated as follows:
The shear force acting on the interior flange:

$$V_I = (1520)(28800 - 2400) / (28800) = 1393 \text{ kN}$$

Therefore, the spacing of the connection at the interior flange is given by:

$$s_I = (1520 \times S)/(1393) = (1520 \times 1.7)/(1393) = 1.85 \text{ m}$$

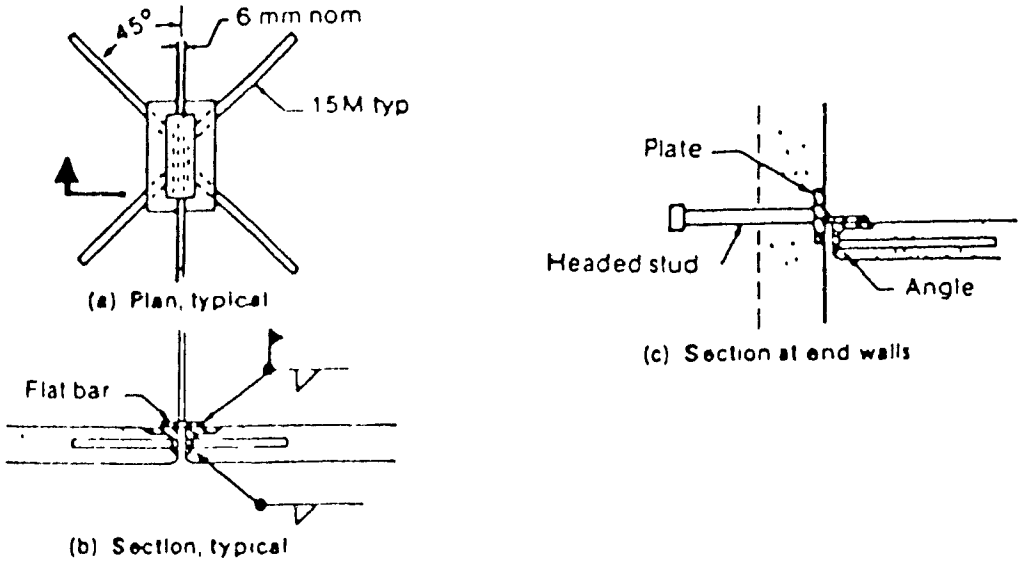

Figure 2.5 Connections between the flanges of double- tees

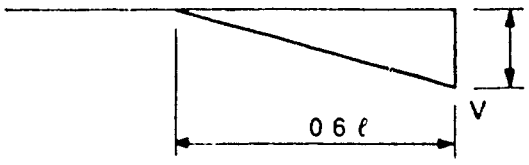

Figure 2.6 Distributed shear on diaphragm with 10% eccentricity

2.3 Choice of Test Specimen Size and Boundary Conditions

To study the connection between the flanges of the double-tees, the ideal solution would be to have a specimen consisting of two connected double-tees and apply the shearing force to the system to investigate the behaviour of the connections. However, tests of this kind are extremely cumbersome and expensive. Therefore, it was decided to study the behaviour of a single connection in an effective part of the flange resistante to the shear force applied at the connection. To determine the size of such an effective flange part and its boundary conditions, for simplicity a part of a double-tee flange with three connection was isolated and analyzed using the SAP90 program[23]. This would ensure that the stresses in the vicinity of the central connection are reasonably close to those in a full double-tee flange, as the connections further away do not have any significant effect on the central connection.

2.3.1 Analysis of Partial Flange with Three Connections

The forces acting at the connection are transmitted in the plane of the diaphragm which has a large in-plane rigidity at the flange-web connection, the resistance of the connection can be resolved into two components one parallel to the span of the double-tee and the other perpendicular to it. The resistance to the moments caused by the connection shear force arises from the rigid flange-web connection. To account for these conditions, and for simplicity, the finite element model shown in Figure 2.7, with hinges at each node along the line AB, was adopted.

The analysis of the selected partial flange was made using the computer program SAP90[23], which employs the stiffness method of analysis. The static analysis of a structure involves the solution of a system of linear equations represented by

$$K\,U = R$$

where K is the stiffness matrix, U is the vector of resulting displacements and R is the vector of applied loads.

The concrete in the selected partial flange is modeled with 1248 three dimensional 4-node membrane shell elements (Figure 2.8). This membrane is an isoparametric formulation including two in-plane translational degrees of freedom (w and u) and

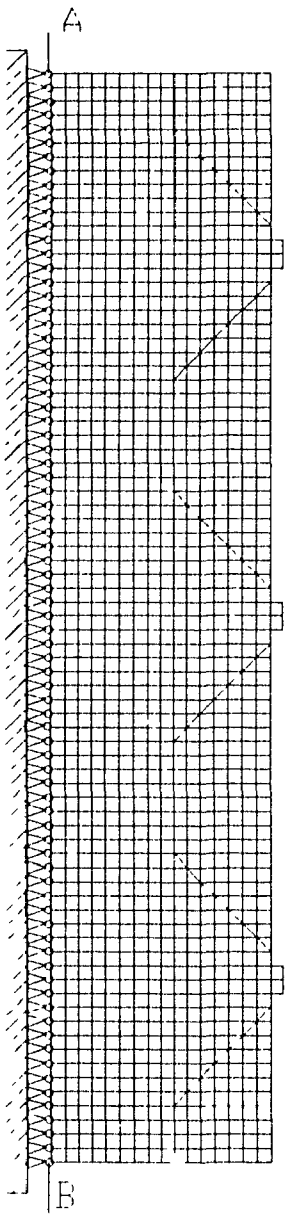

Figure 2.7 Boundary conditions for partial double-tee flange

a rotational component in the direction normal to the plane of the element (Θ_z). Six shell elements are used to model the welded steel plate, while 54 beam elements model the steel anchor. The 1352 nodes are numbered in an efficient way to get an optimum stiffness matrix with a minimum band width. The ratio of smallest length to thickness for the flange is 800/50 = 16, therefore using the shell element represents an appropriate choice. Also, these membrane elements can model the behaviour of slab adequately since the applied loads are only in the plane of the

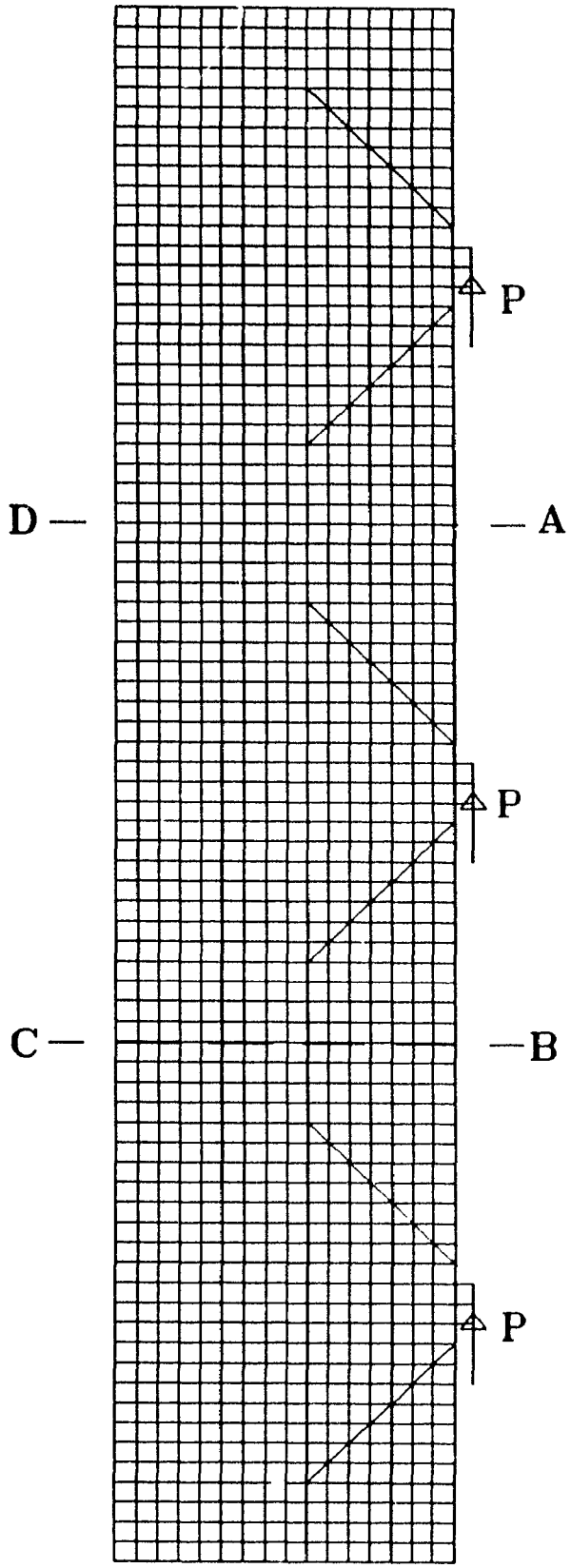

Figure 2.8 Finite element idealization for partial double-tee flange

flange. The beam element can model the axial and dowel behaviour of the steel anchor. The applied load is 200 kN which is about 1.3 times the ultimate strength of the connection.

The results for principal stresses for the area around the middle connection (region ABCD in Figure 2.8) are shown in Figure 2.9. The resulting axial forces in the steel anchors are presented in Figure 2.10.

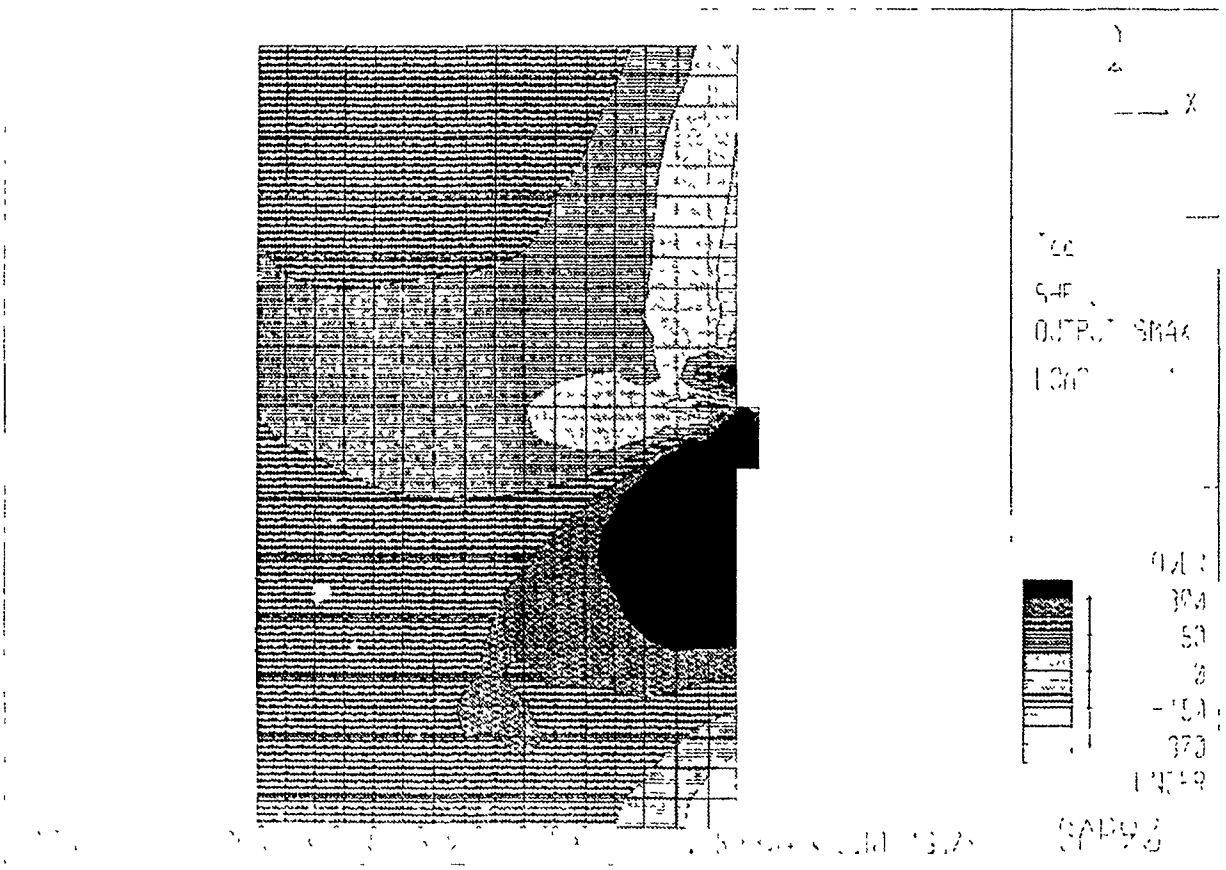

Figure 2.9 Distribution of principal stresses around the middle connection of the partial flange

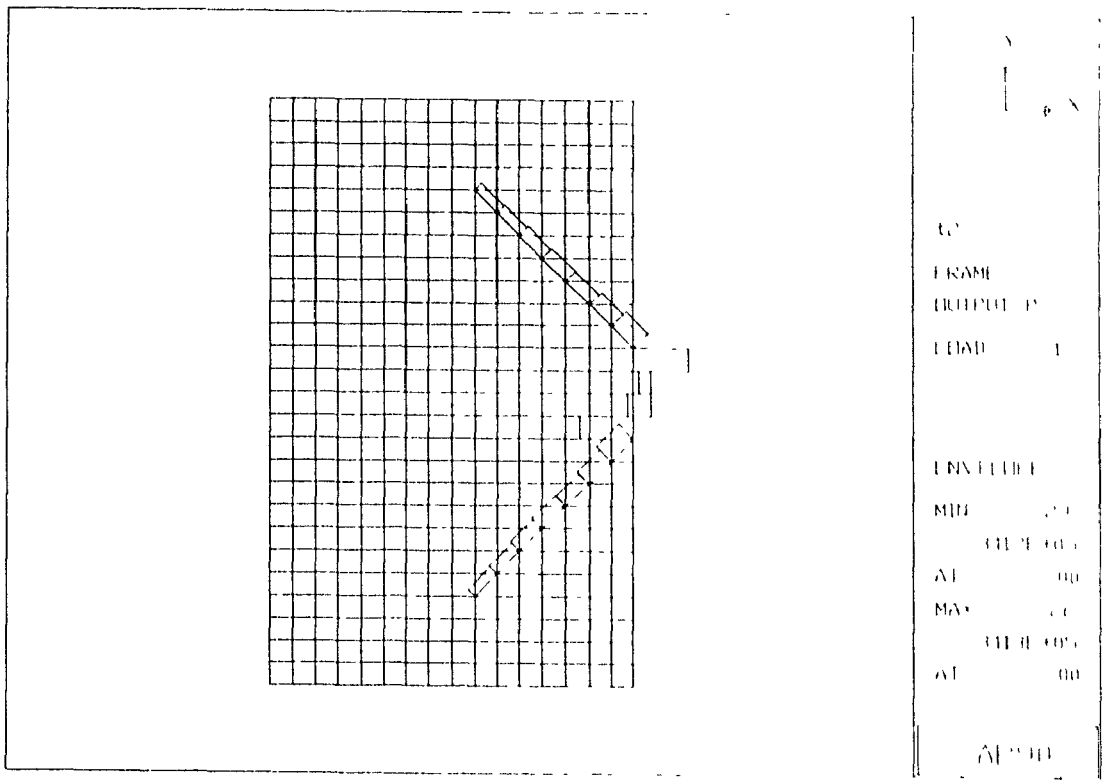

Figure 2.10 Force distribution along the middle connection anchor of the partial flange

2.3.2 Test Specimen and Boundary Conditions

The basic geometry of the test specimen was selected based on the zone of influence of the connection in the partial flange of the double-tee, namely, the region ABCD as shown in Figure 2.8, which is 1300 mm x 800 mm.

The concrete flange (refers to Test Specimen Panel) and the connection steel plate were modelled using 416 and 2 membrane shell elements, respectively. The reinforcing steel bars were idealized using 18 beam elements. The finite element idealization for test specimen is shown in Figure 2.11.

The test specimen boundary conditions were selected to ensure that the stress

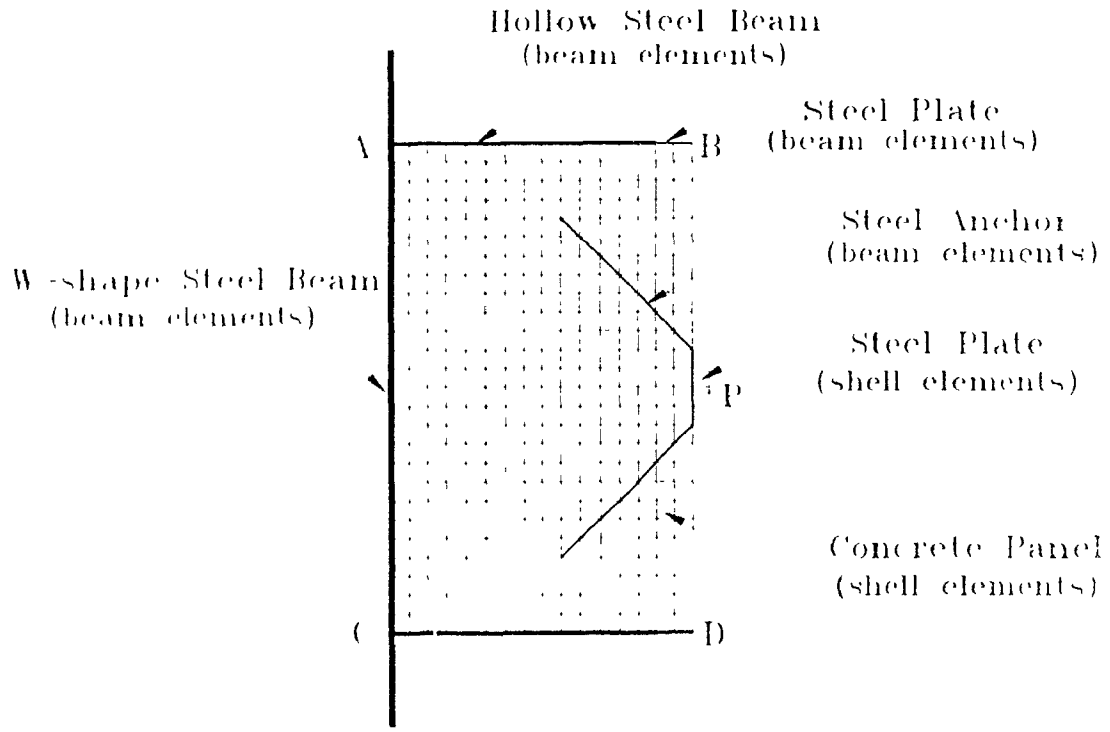

Figure 2.11 Finite element idealization for test specimen

analysis of partial double-tee flange with three connections. After some trials, it was decided to epoxy 100 mm by 8 mm steel plates to the specimen boundaries AB, CD and AC (Figure 2.11). Hollow steel section (203 x 102 x 8 mm) with a 100 mm by 8 mm plate welded on one face (102 mm face) were connected by spot welding to the epoxied plate on boundary AB and CD. The epoxied plate on boundary AC was similarly connected by spot-welding to a heavy wide flange steel beam (W 310 x 118), which was in turn anchored (post-tensioned) to the laboratory strong floor. These boundary elements were modelled using 16 beam elements for each of the faces AB and CD, and 28 beam elements for the boundary AC.

and CD, and 28 beam elements for the boundary AC.

The details of the finite element model are shown in Figure 2.11, which was analyzed using the SAP90 program. A load of 200 kN was applied to the connection as shown. The resulting distribution of the principal stresses in the concrete panel and the forces in the steel anchor are shown in Figures 2.12 and 2.13, respectively. Comparison of these principal stresses and steel forces with those in Figures 2.9 and 2.10 shows an excellent agreement between the two sets of results. Therefore, the above boundary conditions were selected for the subsequent experimental work. Practical requirements and procedure of construction of test specimen in the laboratory are presented in Sections 2.5 (Construction Sequence) and 2.7 (Test Set-up).

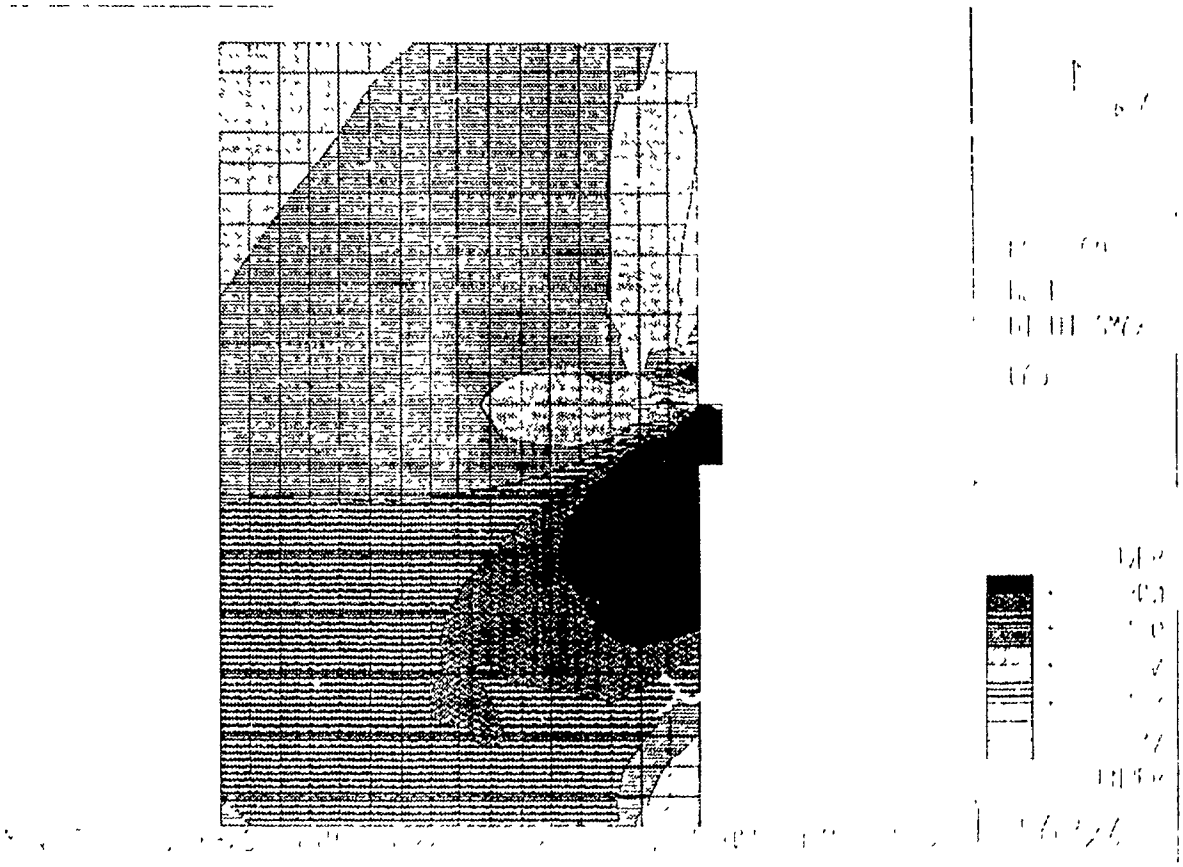

Figure 2.12 Distribution of principal stresses in the test specimen

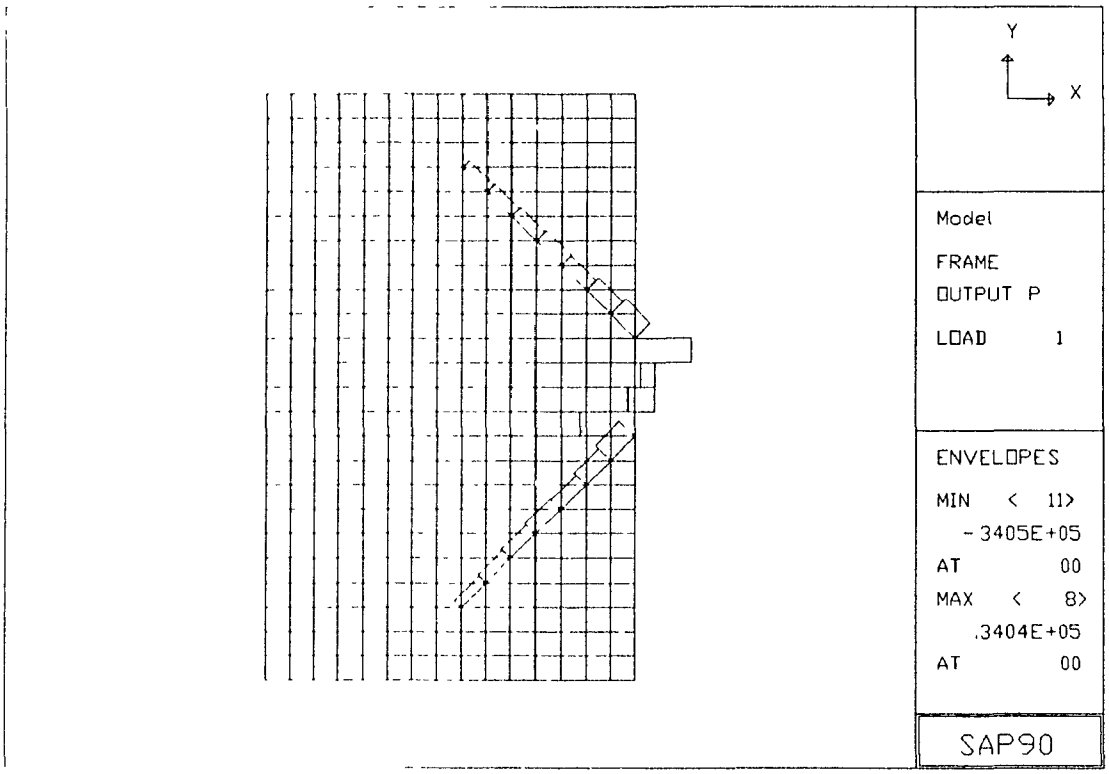

Figure 2.13 Force distribution along the connection anchor in the test specimen

2.4 Design and Description of Test Specimens

The experimental program consisted of tests on five typical connections commonly used in the industry, presented in Figure 2.1. Each specimen was 1300 mm by 800 mm in size, as modelled for analysis. The thickness of the concrete panel was 50 mm and it was increased to 75 mm for a distance of 150 mm from the free edge. These connections were detailed and tested to evaluate their response to low-cyclic loading, aimed at determining their ultimate strength , level of ductility and energy absorbing capability, etc.

For connections using deformed reinforcing bar under cyclic loads, most of load is carried by bond between the reinforcing steel and the concrete . The tensile and compressive strengths of the concrete, cover thickness and the amount of

transverse reinforcement play a dominant role in controlling the connection behaviour. Bond failure modes under low cyclic loading are very similar to those under monotonic loading. Under low - cycle loading, two types of bond failure are typical. The first is a direct pullout of the bar, which occurs when ample confinement is provided to the bar. The second type of failure is a splitting of the concrete where the cover or confinement is insufficient. In this case the failure is due primarily to the radial tensile stresses caused by the bearing of the bar lugs. In this study, since the cover thickness is not adequate, a splitting tensile failure will limit the bond capacity for a given anchorage length to a value lower than that for failure by pullout action. This effect is more important for cyclic than for monotonic loading, because of the increased severity of cracking and a more rapid deterioration of bond under cyclic loading. To compensate for the smaller cover thickness and the resulting splitting concrete, the anchorage length is increased to 480 mm instead of the normally required length of 300 mm With the increased embedment length, it is expected that the bar will yield in tension before it pulls out or splits the surrounding concrete. In this respect, the results of the investigations of the anchorage lengths of reinforcing bars subjected to cyclic loads at the University of Texas at Austin and Cornell University [20] are used. The ultimate capacity of the connection under monotonically increasing load (referred to as "monotonic strength") is calculated based on these development lengths. Concerning small concrete cover thickness, determination of the ultimate strength under monotonic load is based partially on the work of Jimenez et al[24] which is in turn dependant on the concrete cover thickness The specimens were designed initially using the simple truss analogy and the "shear friction" concept described in the CPCI Metric Design Manual[18] All test specimens were initially designed using the material resistance factors ϕ_c 0.60 and ϕ 0.85 and assuming a concrete compressive strength of f'_c = 35 MPa, a reinforcing bar yield strength, f_y = 400 MPa, and ultimate strength of steel headed stud, f_u 400 MPa The dowel action of the anchor bar was considered. The influence of the wire fabric mesh was not included. It should be noted that the final ultimate strength of the connections used for comparison with the test results were calculated using the theoretical calculations, CPCI method and the NONLACS program based on the

measured material properties. Design calculations are presented in Appendix A.

2.4.1 Test Specimen S1

Specimen S1 contained No. 15 weldable deformed reinforcing bars used as the anchorage in the connection, bent at 45 degrees, with an inside bend diameter of 95 mm. The length of each inclined leg was 480 mm. The straight part was 200 mm long and was welded to a 200 mm x 75 mm x 10 mm thick inclined steel plate with a fillet weld length of 100 mm. As can be seen form Figure 2.14, the test specimen contained uniform wire fabric mesh, 100 x 100 MW 13.3/ MW 13.3, with a steel ratio of ρ=0.0027 in each direction. The mesh was placed in the central plane of the 50 mm thick slab. The specimen had clear concrete covers varying from 29.5 mm to 17 mm with an average calculated cover thicknesses of 23 mm. The ultimate strength was determined using the "truss analogy" including the effect of dowel action, while the ultimate capacity of each truss leg depends on the concrete cover thickness. The details of calculation are presented in Appendix A.

2.4.2 Test Specimen S2

Specimen S2 contained a No. 15 weldable deformed reinforcing bar anchor which was bent at 45 degrees. A right angled hook was provided at the end of the straight lead of the bar as shown in Figure 2.15. The length of the straight part of each leg was 400 mm plus twelve bar diameter for the hook. The 200 mm straight part was welded to a 200 x 75 x 10 mm thick steel plate. The use of 90° hook enables the connection to remain in the inelastic range for a larger number of cycles before failure. The welded wire mesh used to reinforce the panel was identical to that for Specimen S1 with the same steel ratio of ρ=0.0027. The concrete clear covers were similar to those for Specimen S1. The details of Specimen S2 are shown in Figure 2.15.

The specimen was designed with special consideration for hooked reinforcing bars subjected to cyclic loading. Detailed calculations are presented in Appendix A.

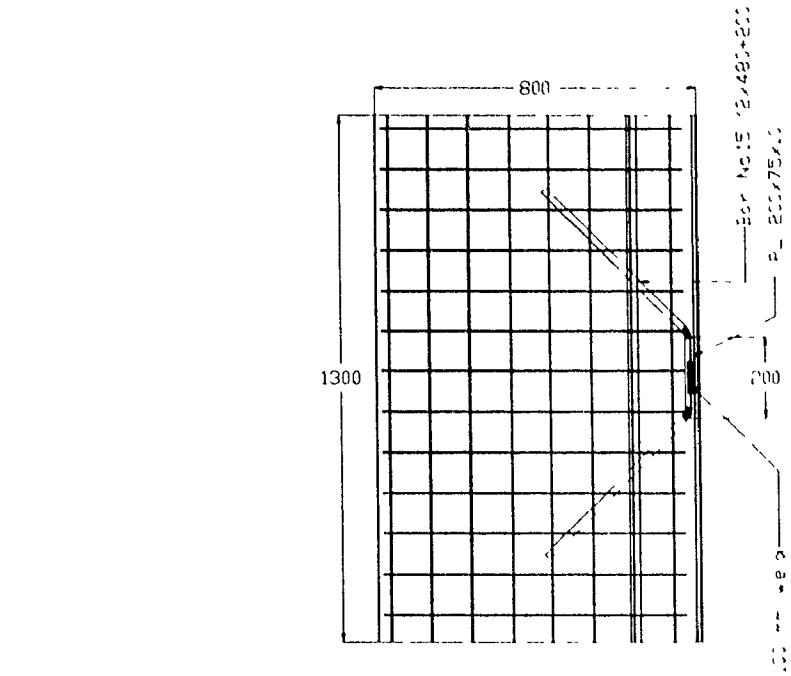

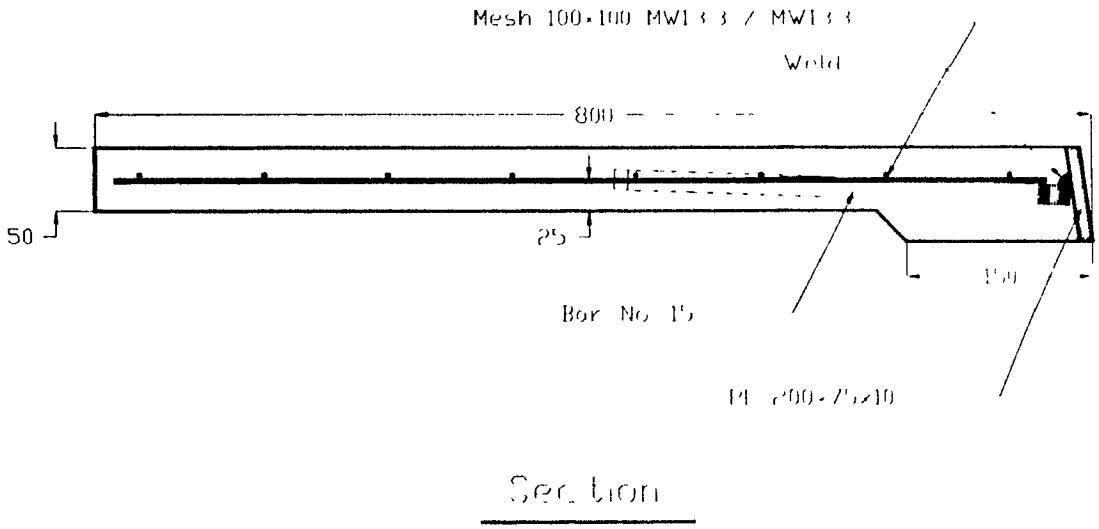

Figure 2.14 Details of Specimen S1

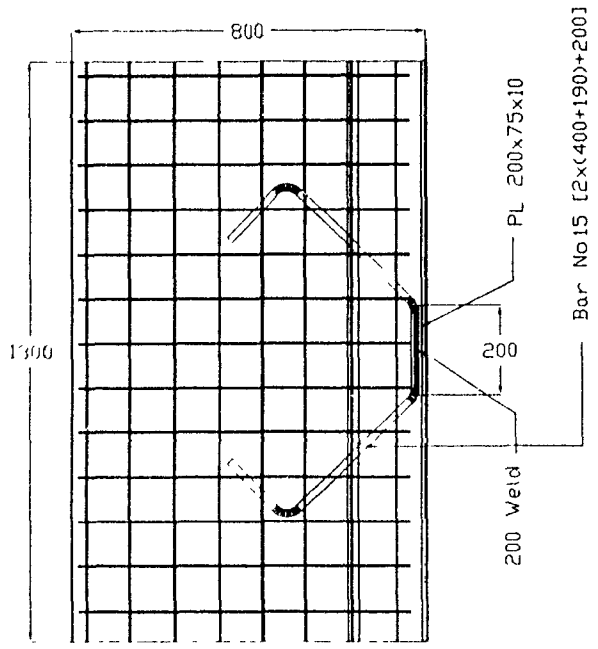

Plan View

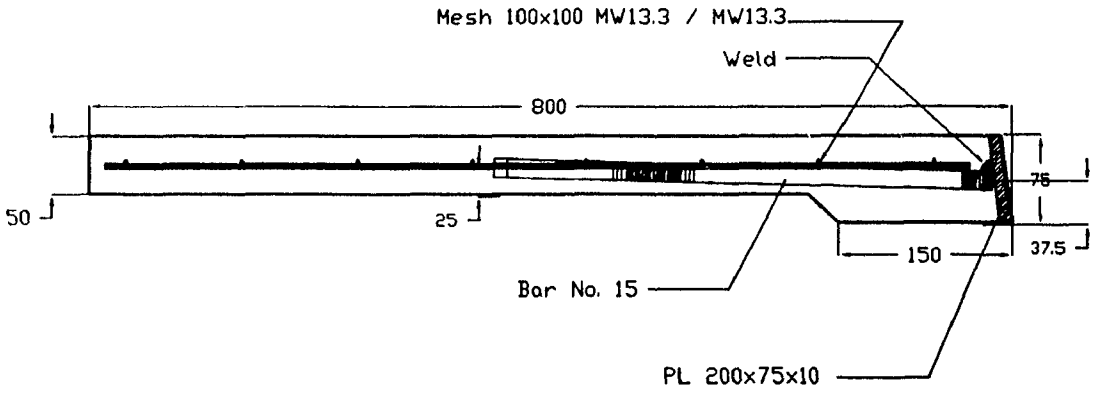

Section

Figure 2.15 Details of Specimen S2

2.4.3 Test Specimen S3

The Specimen S3 was reinforced with 2 No 15 weldable deformed bars oriented at 90 degrees to the direction of the shear force and welded to the flange of an embedded angle, 75 x 50 x 8 mm, 200 mm long, as shown in Figure 2.16. The panel reinforcement was similar to that for Specimen S1 and S2. The cover thickness of deformed reinforcing bar anchor varies from 29.5 to 17 mm with the average calculated cover thickness of 23 mm. The ultimate design capacity of the connection was calculated using the shear-fraction method in the CPCI Metric Design Manual[1.1]. Detailed calculations are presented in Appendix A.

2.4.4 Test Specimen S4

The test specimen was reinforced with 2 - ½ in. diameter Nelson studs, 2 in long fusion welded to a 12 mm thick steel plate. The assembly of the headed studs and steel plate was inclined to achieve a maximum concrete cover thickness around the studs and a maximum effective shear cone, which would result in a maximum ultimate capacity for the connection. The centres of the headed studs were coincident with the central plane of the 75 mm thick part of the panel. The wire mesh used to reinforce the specimen S4 was similar to that used in other specimens. The specimen details are shown in Figure 2.17. Detailed computations for the specimen are presented in Appendix A.

2.4.5 Test Specimen S5

Specimen S5 was reinforced with 2 No.15 weldable deformed reinforcing bars oriented at 45 degrees to the direction of the shear force and 2 - ½ in diameter Nelson studs, 2 in. long. Both the bars and the studs were welded to the flange of a 75 mm x 75 mm x 10 mm by 250 mm long steel angle (see Figure 2.18). It was expected that the headed studs would help to secure the connection under twisting and out of plane panel forces caused by the load being eccentric to the angle of the flange. The wire mesh used to reinforced Specimen S4 was identical to that for the other specimens with the steel ratio of ρ=0.0027 in both directions. The average clear cover thickness was 23 mm. nalysis of Specimen is presented in Appendix A

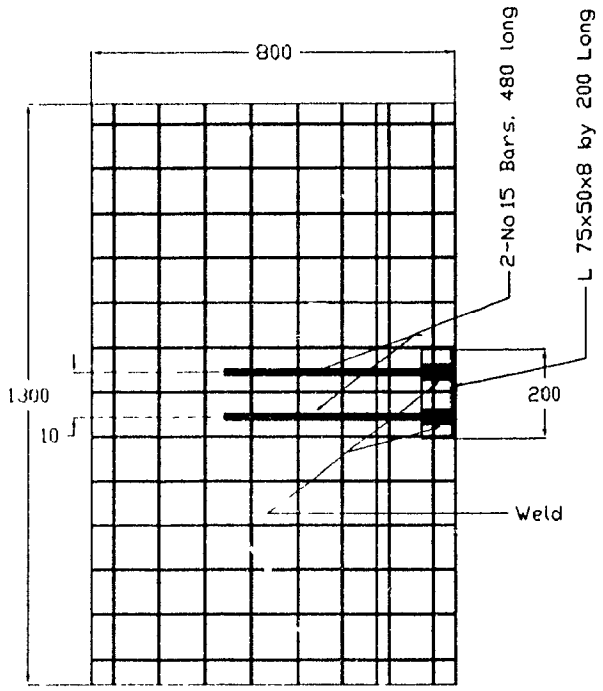

Plan View

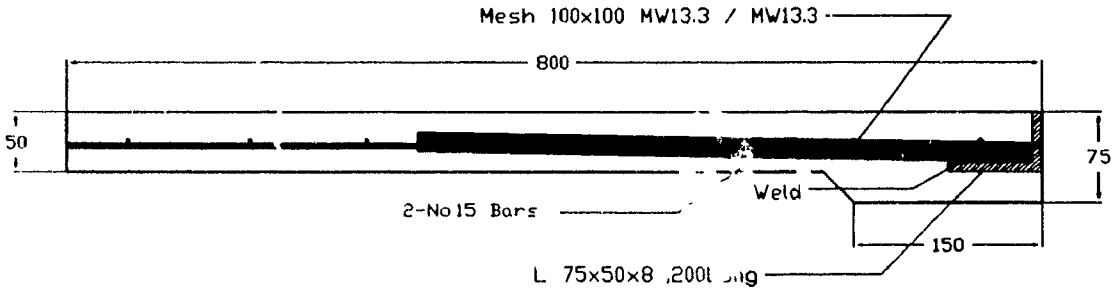

Section

Figure 2.16 Details of Specimen S3

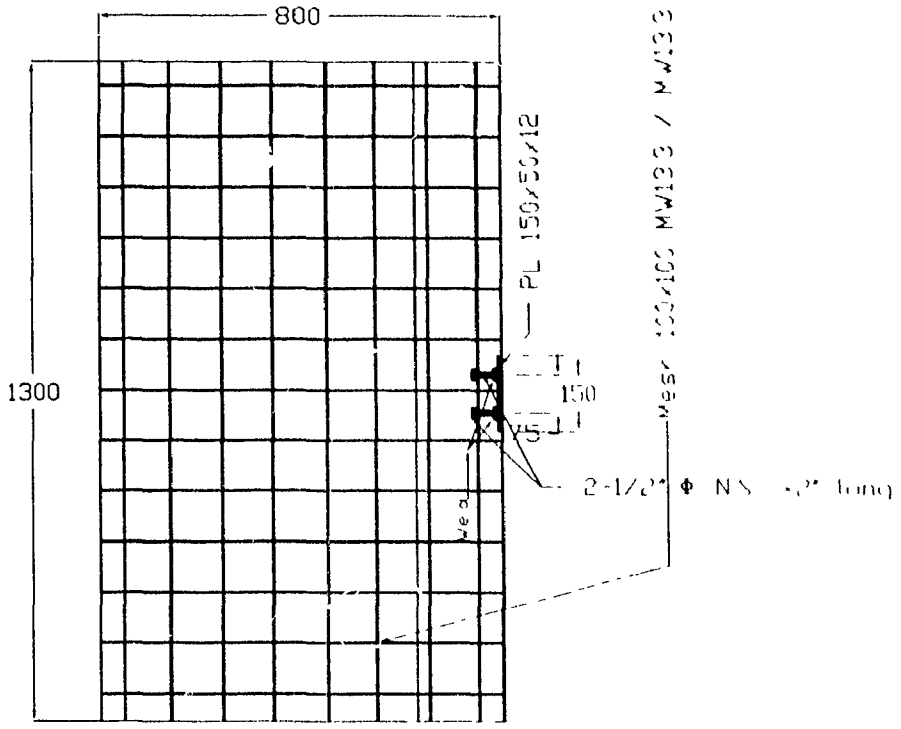

Plan View

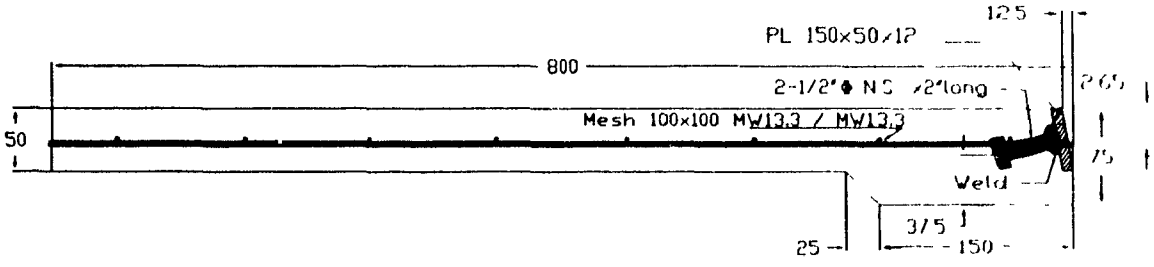

Section

Figure 2.17 Details of Specimen S4

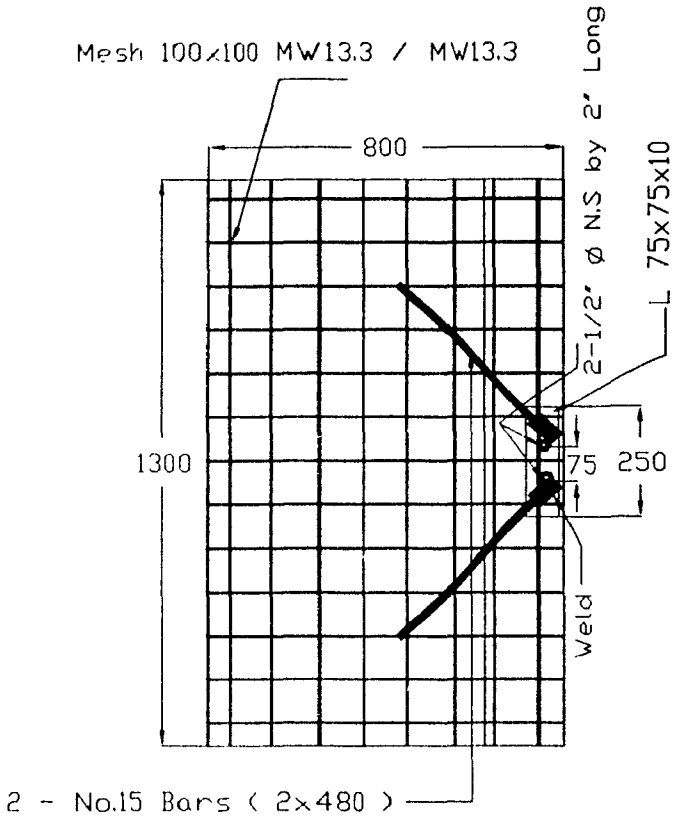

Plan View

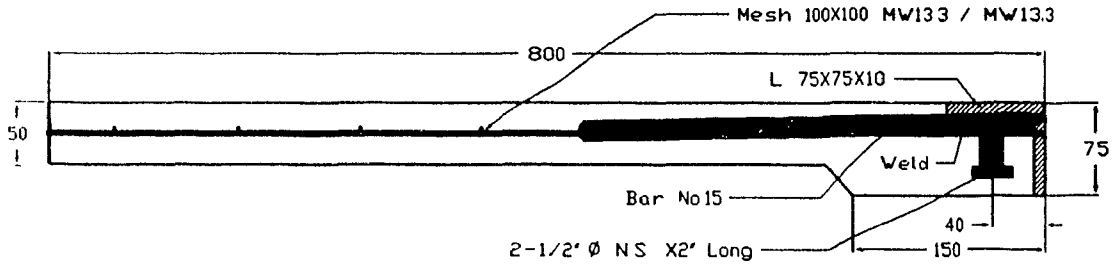

Section

Figure 2.18 Details of Specimen S5

2.5 Construction Sequence

Connections for Specimen S1, Specimen S2, and Specimen S3

The deformed reinforcing bar was first cut and bent. Strain gauges were installed on steel bars as shown in Figures 2.23a to 2.27a. The reinforcing bar was set at the centre of the inclined steel plate and was fillet welded. The assembly of the reinforcing bar and steel plate, and wire fabric mesh were placed in the plywood formwork so that these bars and the wire mesh would be in the middle plane of the concrete panel, see Figure 2.19. Additional lifting steel loops were provided at the face of the panel for handling. During the concreting, standard concrete cylinders were cast, and the specimen and the concrete cylinders were cured in wet burlap and plastic sheets. The specimens were cast in a horizontal position. The formwork was removed after 2 days, and moist curing was continued for an additional three days.

Three small steel channel sections were prepared by drilling a hole at the centre of their webs, and their flanges were welded to the bottom flange of W-shape heavy steel beam (refered to as the W-beam). A number of holes were drilled in the top flange of the W-beam for the connection to the two hollow structural section beams (refered to as the H.S.S. beam). Four strong angles were welded to each side of the H.S.S. beams, besides bolting to the flange of the W-beam.

Seven days after casting, the edges of the concrete panel were sand-blasted. A steel plate (100 mm by 8 mm) was bent to the outside dimensions of the panel and was sand-blasted to a white-metal finish, and it was epoxied to the panel edges. The epoxy bond was cured for at least 14 days.

The erection of each test specimen took place in 4 steps. The W-beam was first lifted in the loading frame and was post-tensioned to the strong floor of the Structures Laboratory. The specimen was then hoisted in the holding frame and was positioned vertically on the top flange of the W-beam, and adjusted such that the central plane of concrete panel was aligned with the web of W-beam. Then two H.S.S. beams were adjusted to have complete contact with the epoxied steel plate and bolted to the top of the flange of W-beam. Finally, the epoxied steel plate was tack welded all around to the W-beam and the two hollow section beams.

Connections for Specimen S4 and Specimen S5

The construction sequences for Specimens S4 and S5 were similar to those for Specimen S1, S2 and S3. The headed studs were fusion-welded to a steel plate and the assembly was positioned at the thicker edge of the concrete panel in Specimen S4, such that the centre of the heads of studs was coincident with the central plane of the 75 mm thick part of concrete slab.

For Specimen S5, the headed studs were first fusion-welded to the flange of the angle and then the deformed reinforcing bar was welded to the flange. All other steps and the erection sequence were identical to those for the specimens S1, S2 and S3.

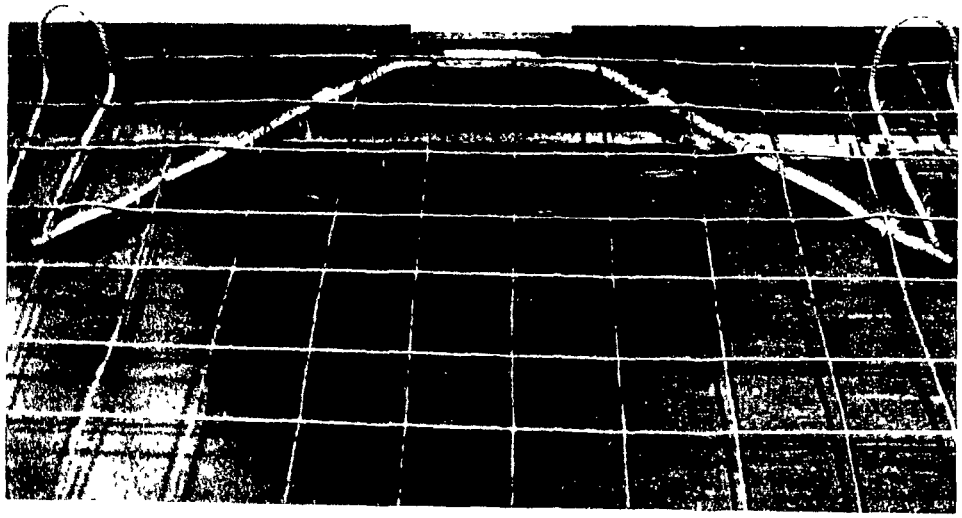

(a) Specimen S1

Figure 2.19 Formwork for casting test Specimens

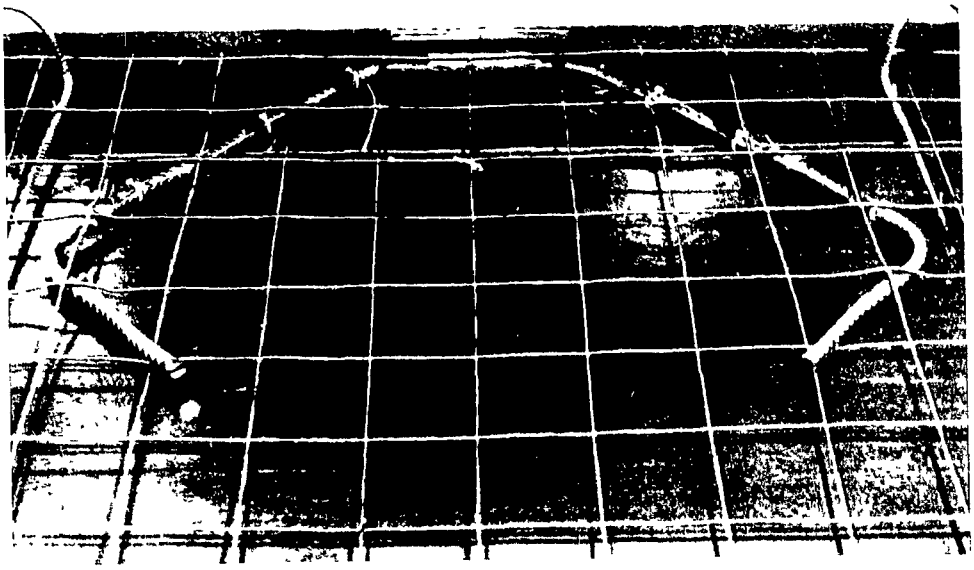

(b) Specimen S2

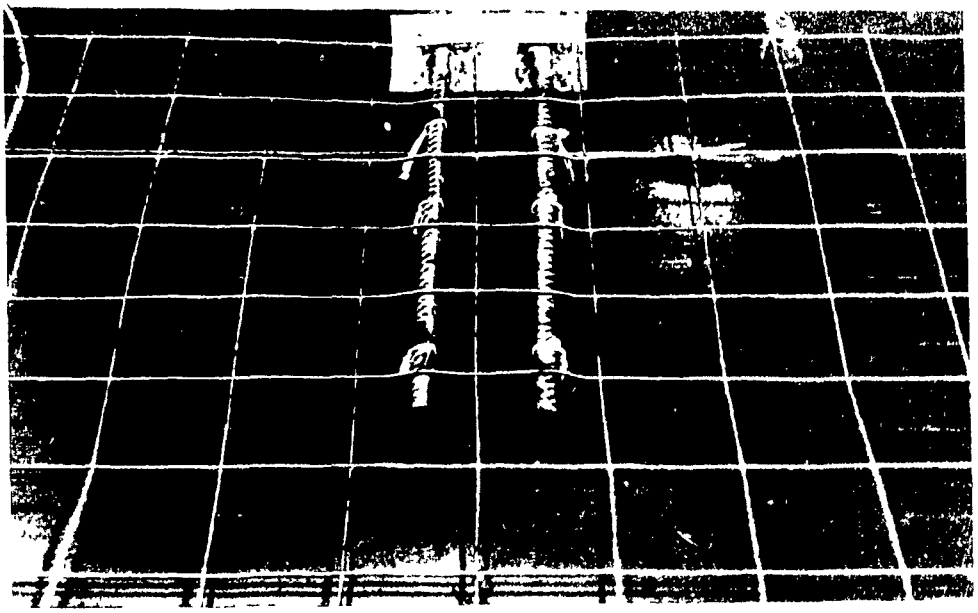

(c) Specimen S3

Figure 2.19 (Continued) Formwork for casting Specimens

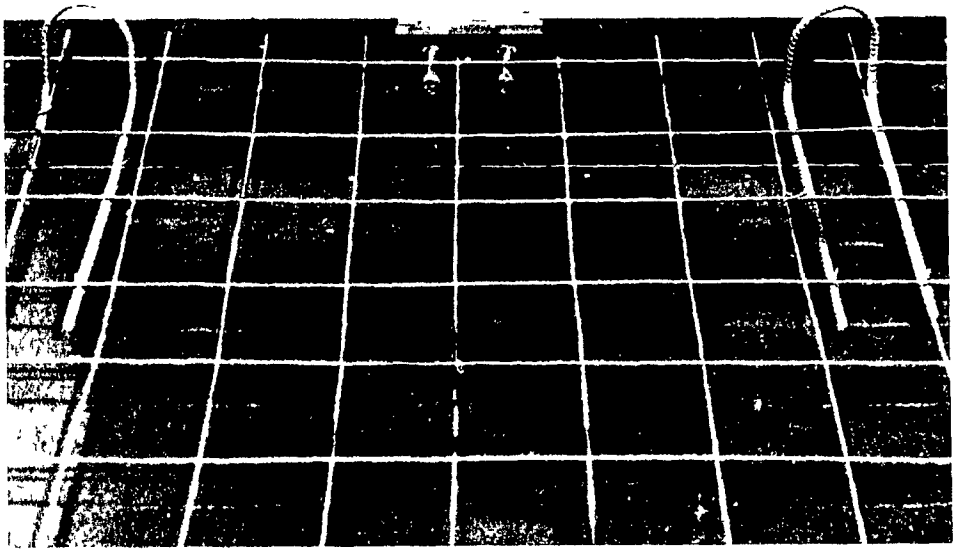

(d) Specimen S4

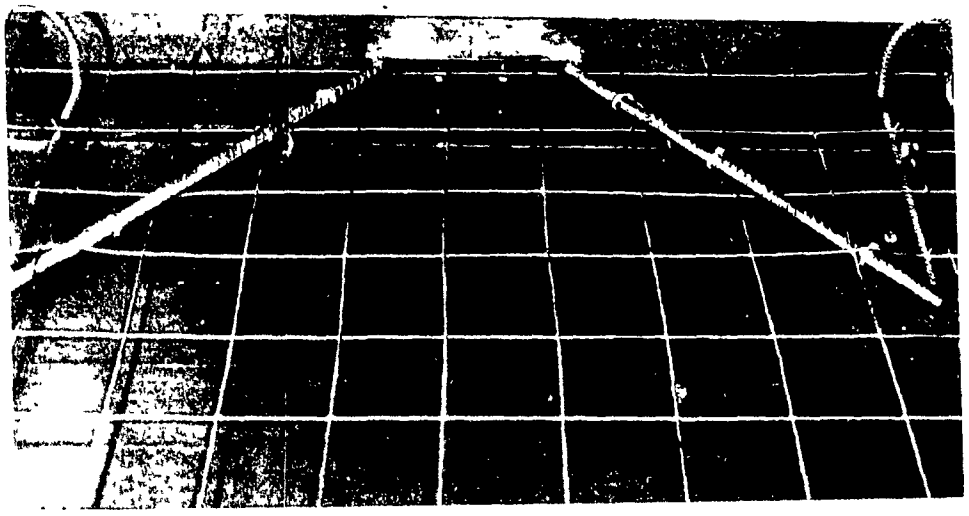

(e) Specimen S5

Figure 2.19 (continued) Formwork for casting Specimens

2.6 Material Properties

Concrete

The concrete mix was designed for a 28 - day compressive strength of 35 MPa using Type 30 cement (high early strength), two types of coarse aggregates with maximum sizes of 12.5 mm and 7 mm , and silica (size passing 0.5 mm) sand as fine aggregates and a slump of 75-100 mm. The mix details for the concrete are given in Table 2.1. At least three 150 x 300 mm cylinders were tested for each batch of concrete used to cast a test specimen to determine the average compressive strength f'_c, and the splitting tensile strength, f'_t. The concrete properties are summarized in Table 2.2. Typical stress-strain curve for concrete is presented in Figure 2.20a. The average tangent modulus, E_c, the compressive strain at the maximum compressive concrete stress, ε'_c, and the tensile strain at the maximum tensile stress, ε_t, are also summarized in Table 2.2. The average values were obtained at the time of testing the specimens which varied from an age of 40 to 65 days.

Table 2.1 Mix Design for 35 MPa Concrete

Ingredients	Quantity (kg/m^3)
Cement Type 30	520
Fine Aggregates (silica sand)	960
Coarse Aggregates (12.5 mm)	220
Coarse Aggregates (7 mm)	760
Water	270
Total	2730
Slump	80 ± 10 mm

Table 2.2 Summary of Concrete Properties

Test Specimen	f'_c (MPa)	ε'_c (x 10^{-3})	E_c (MPa)	f'_t (MPa)	ε_t (x 10^{-4})
Specimen S1	43	2.6	32200	4.1	1.08
Specimen S2	47	2.6	29400	4.2	1.09
Specimen S3	49	2.9	31200	4.3	1.10
Specimen S4	42	2.5	30376	4.0	1.07
Specimen S5	48	2.7	30400	4.2	1.09

Steel

The steel reinforcing used for the specimens consisted of No. 15 weldable bars with a minimum specified yield strength of 400 MPa. The weldable steel complied with the requirements of the CSA G30.16[22]. Samples from deformed reinforcing bars were tested using the standard tension test to establishing their properties. A 50 mm extensometer was used to determine the steel strains. Table 2.3 presents a summary of the steel properties. A typical stress-strain curve is shown in Figure 2.20b.

The ultimate strength for headed studs was assumed to be 400 MPa for design and analysis.

Table 2.3 Summary of Reinforcing Steel Properties

Property	No. 15
Yield Stress, f_y (MPa)	495
Young's Modulus, E_s (GPa)	220
Yield Strain, ε_y (%)	0.225
Ultimate Strain, ε_{ult} (%)	11.5
Strain-hardening Modulus, E^*_s (MPa)	1370

E^*_s is used in NONLACS program

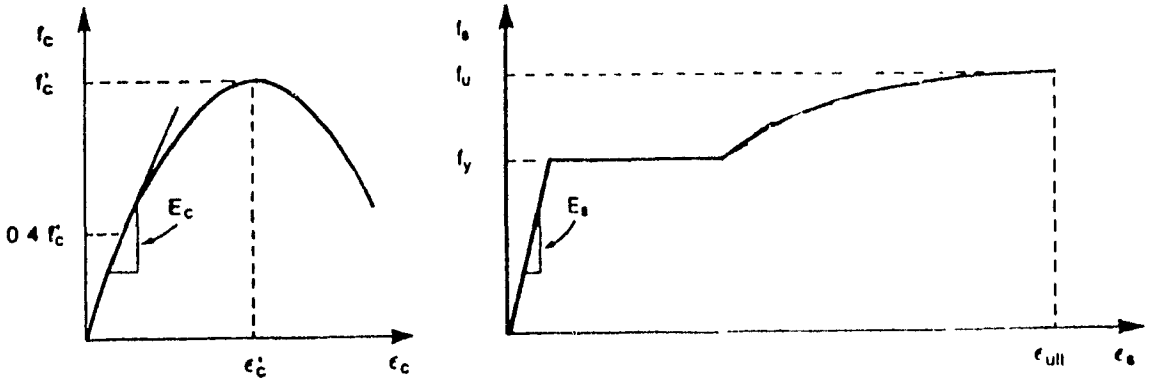

(a) Concrete in compression

(b) Steel in tension

Figure 2.20 Stress-strain curves for concrete and steel

2.7 Test Set-Up

Figure 2.21 presents the details of the test set-up and the loading frame. Shear force reversals were imposed on the test specimen by two sets of hydraulic jacks. One set of jacks was used to apply the shear force in the positive direction whereas the other set was used in the negative direction. The loading frame facilitated application of lateral loads (shear forces) and consisted of a braced frame post-tensioned (clamped) to the strong floor of the Structures Laboratory. The lateral displacement of the loading frame was measured during the test and found to be negligible.

As shown in Figure 2.21, the shear forces were applied to the connection by high strength threaded rods, pin-connected to a hollow steel section, which was welded to a steel plate to transfer pure shear to the connection. The specimen was painted, followed by mounting of the strain targets on the surface of the panel at selected locations.

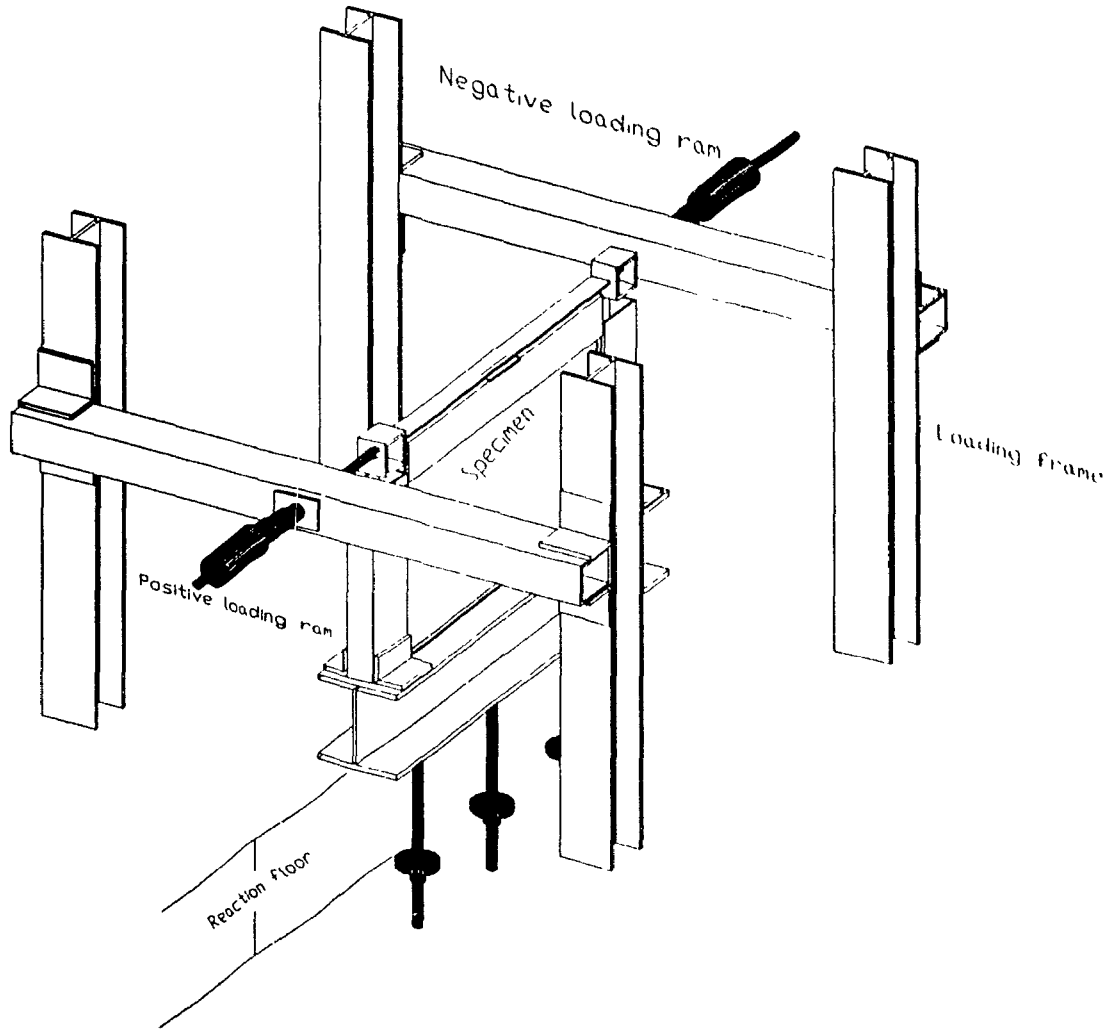

(a) Reaction frame

Figure 2.21 Test Set-Up

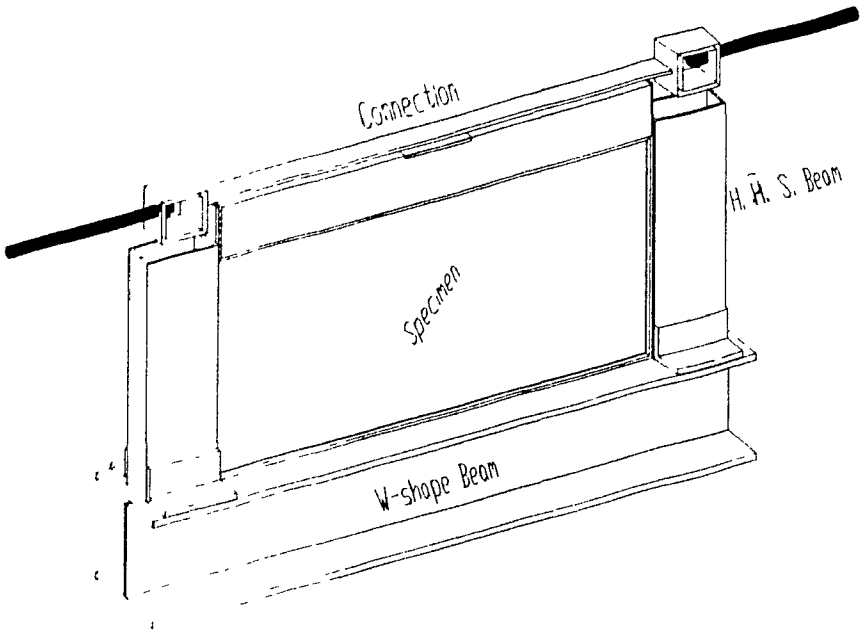

(b) Boundary of Condition for Test Specimen

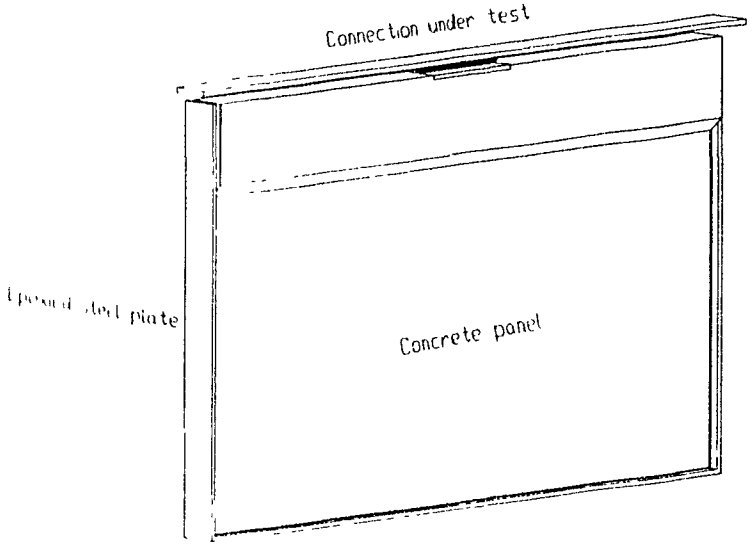

(c) Specimen Details (top)

Figure 2.21 (Continued) Test Set-Up

2.8 Loading History

The general loading history presented in Figure 2.22 was employed for the connection specimens. Most of the load cycles were "load-controlled" and consisted of three cycles at constant load levels (load stages). In most of the specimens, the first three load cycles were in the elastic range of response followed by three cycles beyond the cracking load of the test specimens.

The deflection at yielding, Δy, was defined as the horizontal displacement at which the steel at Location 1 or 4 yielded, accompanied by a reduction in stiffness which was displayed appeared in the load - deflection curves. In some cases, the tests were continued using "displacement-control". The exact loading history and level of loading for each specimen, along with the hysteresis response are presented in Figures 3.1, 3.9, 3.17, 3.25 and 3.32 and Tables 3.1 to 3.5.

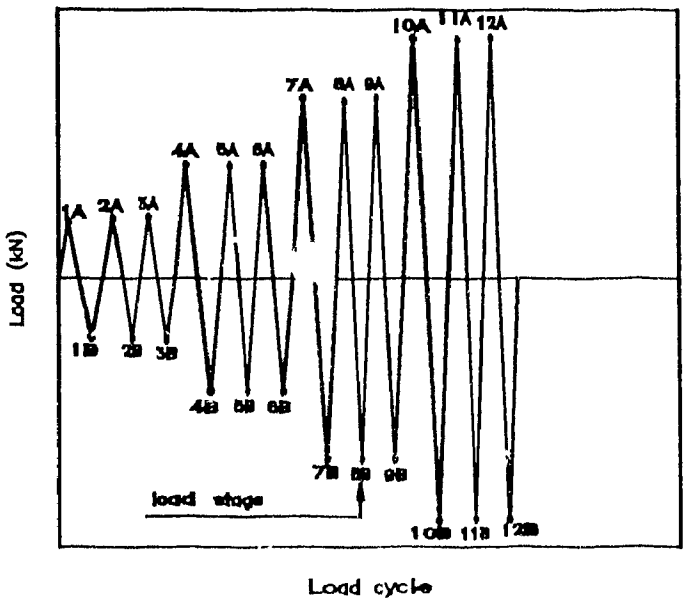

Figure 2.21 Typical Loading History

2.9 Instrumentation

Two 330 kN load cells were used to measure the shear forces applied to the specimen in the positive and the negative directions. Six electrical resistance strain gauges were used to measure the strains along the length of the outermost No 15 anchor bar in each specimen, as shown in Figures 2.23 throughout 2.27.

Steel strain targets (demec gauges) were attached to the concrete surface at 2 and 4 inch spacings along the direction of the reinforcing bar anchor and the area around the headed studs. The centre of each demec set was coincident with the location of strain gauges on the steel reinforcing bar, as shown Figures 2.23b to 2.27b. Two mechanical gauges were used to measure the displacements between the targets, determing the average strain on the surface of the concrete which was followed by an evaluation of principal strains at these locations.

Linear variable differential transformers (LVDT's) were used to measure horizontal and vertical deformations of the connection and horizontal deformation of the concrete panel specimen as shown in Figure 2.23a to 2.27a. A data acquisition system (Doric 245) was used to monitor the steel strain gauges, the LVDT's and the load cells. A reduction system which converted the voltages into loads, displacements and strains was used.

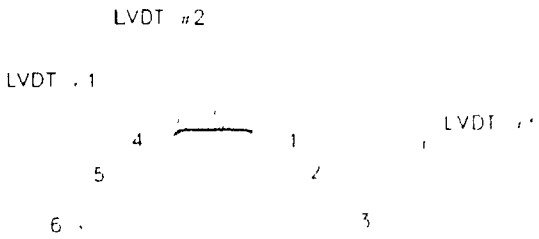

(e) Location of strain gauges

Figure 2.23 Instrumentation for Specimen S1

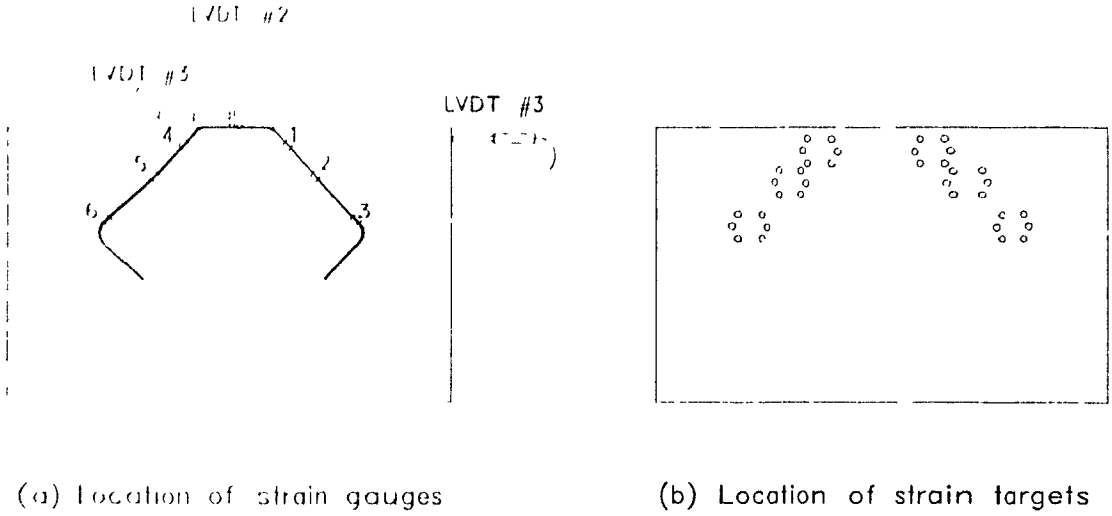

(a) Location of strain gauges (b) Location of strain targets

Figure 2.24 Instrumentation for Specimen S2

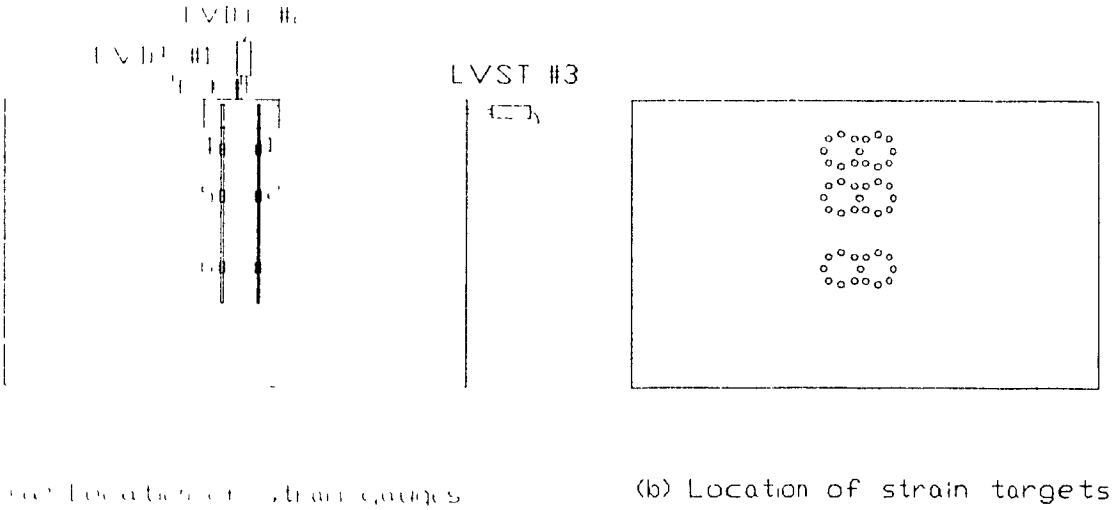

Figure 2.25 Instrumentation for Specimen S3

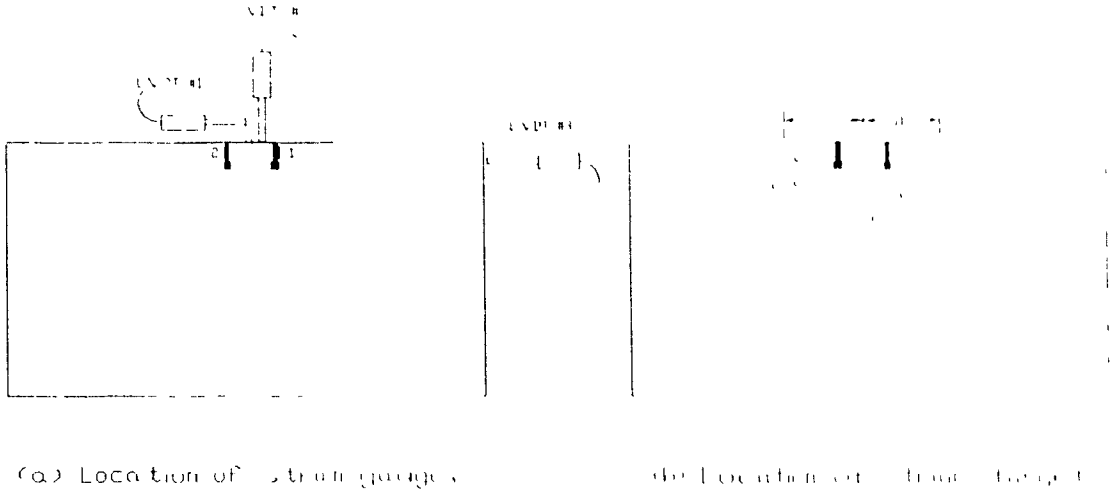

Figure 2.26 Instrumentation for Specimen S4

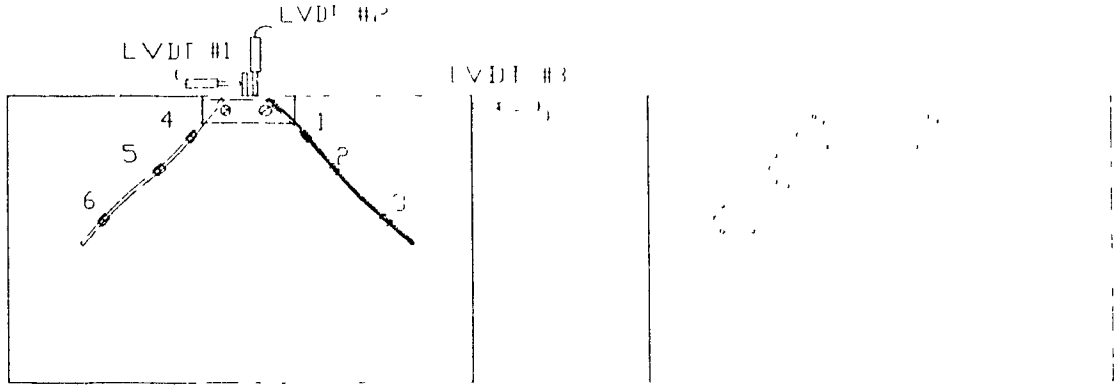

Figure 2.27 Instrumentation for Specimen S5

Chapter 3

NONlinear Analysis of Connection Responses

This chapter presents briefly the method of analysis used in this study along with the predicted responses of the five connections subjected to monotonically increasing loads, calculated using the NONLACS program [27,28]. It should be noted that at present the NONLACS program does not have the ability to subject steel or concrete structures to reversed cyclic loads, therefore no attempt was made to analyze the experimental results, which are compared qualitatively with selected experimental data in Chapter 5.

3.1 Finite element program - NONLACS program[27,28]

The NONLACS computer program[27,28] (NON-Linear Analysis of Concrete and Steel structures) analyzes and traces the non-linear behaviour, cracking and failure modes of reinforced and prestressed concrete beams, shear panels, slabs folded plates, shells of revolution, box girder bridges, and any other spatial structure normally considered to be an assemblage of "thin" plates subjected to bending and in plane forces.

3.1.1 Finite Element Modelling

The NONLACS program employs three types of finite elements: **(a)** A quadrilateral thin shell elements or quadrilateral facet shell elements (QFSE), Figure 3.1(c), which is composed of **i)** quadrilateral in-plane action elements (membranes) with four nodes, and two in-plane displacements,u and v ,and one rotation normal to plane,w, at each node, see Figure 3.1(a), and **ii)** Element with out of plane action elements (bending elements) , with four nodes and three degrees of freedom per node, namely, lateral displacement,w and normal rotations θ_x and θ_y as shown in

Figure 3.1(b). The program, provides the option of using a cubic displacement field in both directions, representing the general behaviour, or linear field in one direction and a cubic displacement in the other direction which best represents the beam behaviour problem.(b) One-dimensional uniaxial member, bar elements, with a linear displacement field, which are useful for truss members, prestressing tendons and reinforcing bars.(c) A spring element (boundary element) used to model prescribed displacements, elastic supports, and skewed boundary conditions. The element is also used to calculate the reactions at the supports.

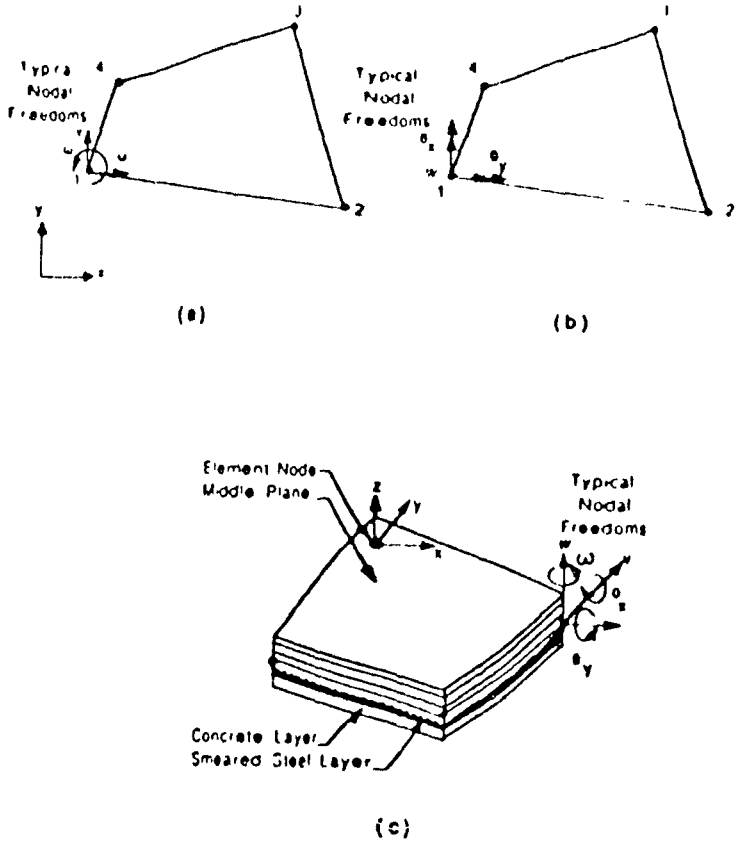

Figure 3.1 Some typical finite elements available in NONLACS program[27,28]: (a) membrane element; (b) bending element; (c) facet shell element

The structure is divided into an assemblage of some or all of the above element types. A reinforced concrete member is modelled using the layered technique. Each shell or plate bending element is divided into a number of imaginary concrete layers and equivalent "smeared" reinforcing steel layers, see Figure. 3.2. Each layer may have different properties and thickness corresponding to its state of stress or strain. The stiffness matrix is calculated by using the numerical integration procedure.

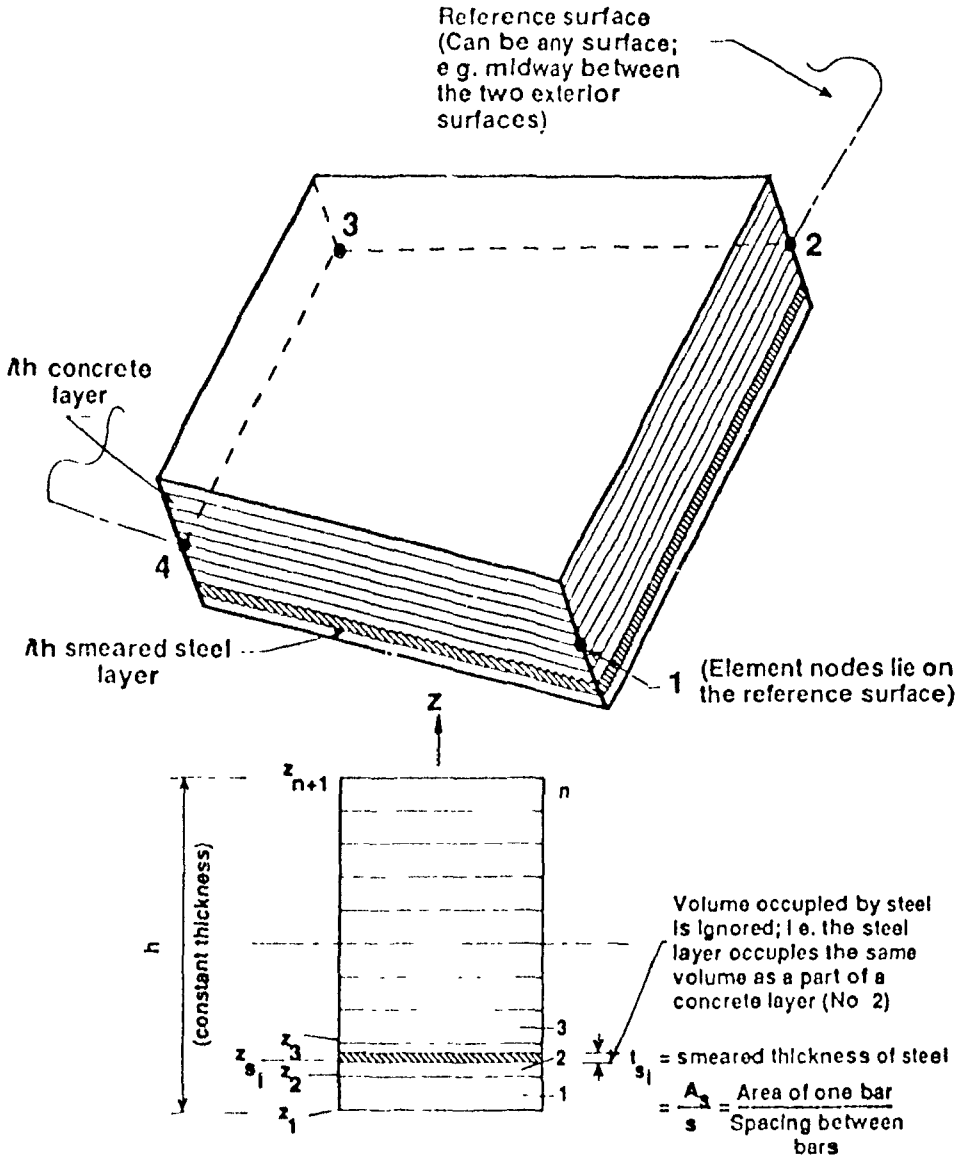

Figure 3.2 Layered element used in the analysis[27,28]

The 3 by 3 ... ss integration points is used. The layer material properties could be chang... ...e Gauss integration point to another. The contributions to the elem... ...s matrix at the integration points for composite concrete - steel and different elem... ...re obtained by the superposition of layer stiffnesses.

Modelling ... distributed steel such as reinforcing mesh as equivalent smeared layers is only suitabl... when steel is fairly distributed over the area of the elements. Concentrated re... ...or prestressing steel bars are, therefore, modelled as bar elements. ... ... bond between the reinforcing steel and the surrounding concrete ... ... is should be located on the reference surface.

3.1.2 Nonlin... Anal... ...ethod

The NONL... ...computer program has the capability of analyzing a linear problem by imposing a one load stage iteration assuming a linear stress - strain relationship.

For material constitutive modelling, concrete is idealized as a nonlinear material in compression including strain - softening after attaining the maximum stress and as a linear material in tension with linear unloading characteristics after cracking. In this respect, the NONLACS program uses a uniaxial compressive stress - strain curve. The intrinsic shape consists of two parts, see Figure 3.3(a). Part 1 up to a maximum compressive stress is based on Saenz's equation (1961), represented by the equation:

$$\sigma = \frac{E_o \epsilon}{1 + (\frac{E_o}{E_{sc}} - 2)\frac{\epsilon}{\epsilon_{cu}} + (\frac{\epsilon}{\epsilon_{cu}})^2} \qquad (1.1)$$

where, as shown in Figure 3.3,

E_{sc} = secant modulus of elasticity at peak stress

E_o = initial tangent modulus

σ = stress

ε = strain

ϵ_{cu} strain at peak stress.

Part II representing the inelastic strain softening follows the Smith - Young model according to the expression

$$\sigma = f_c'(\frac{\epsilon}{\epsilon_{cu}})e^{[1-(\frac{\epsilon}{\epsilon_{cu}})]} \qquad (4.2)$$

where f_c' = compressive strength

e - base of natural logarithm.

For uniaxial tensile stress - strain behaviour, the model proposed by Kabir (1976) is used. A linear descending branch for the unloading of concrete in tension is considered to account for the tension - stiffening after cracking, see Figure 3.3(a).

The concrete strength under biaxial compression and combined compression and tension is determined from the failure envelope of Kupfer and Gerstle (1973). Furthermore the equivalent strain concept due to Darwin and Pecknold (1977) is utilized to relate the increments of stress and strain in the principal directions. Therefore if σ_1 and σ_2 (major and minor principal stresses) exceed the concrete strength calculated using the envelope due to Kupfer and Gerstle, the concrete is assumed to fail along that principal direction. On the other hand, if the equivalent compressive strain in one direction exceeds the maximum concrete strain, $\epsilon_{cm,N}$, Figure 3.3(a), the concrete gets crushed. Cracking is revealed by checking the magnitudes of σ_1 and σ_2. When the principal tensile stress at a point (usually at Gauss integration point) equals or exceeds the tensile strength of concrete, cracking is assumed perpendicular to the principal tensile stress direction. The effect of the crack is smeared within the element by modifying the constitutive matrix. After cracking, β, the shear retention factor, with a value less than unity, is used to account for the shear stiffness due to aggregate interlock and dowel action, see Figure 3.4.

Ordinary reinforcing bars and prestressing tendons and bars are modeled as an elasto-plastic strain hardening material. The bilinear stress - strain relationship in Figure 3.3(b) is used. As can be seen from Figure 3.3(b), in the case of loading,

reloading, the Bauchinger effect, or load reversal which reduces the yield strength of steel, is also considered. The material parameters, f_y, E_s, E_s^*, and ε_{su}, which are respectively, the yield stress, the modulus of elasticity, the strain hardening modulus and the ultimate strain need to be input to define the stress-strain relationship. For shell plate elements, the model adopted in this program is based on the so-called incremental theory of plasticity in which the total plastic strain is obtained by scanning the plastic strain increments.

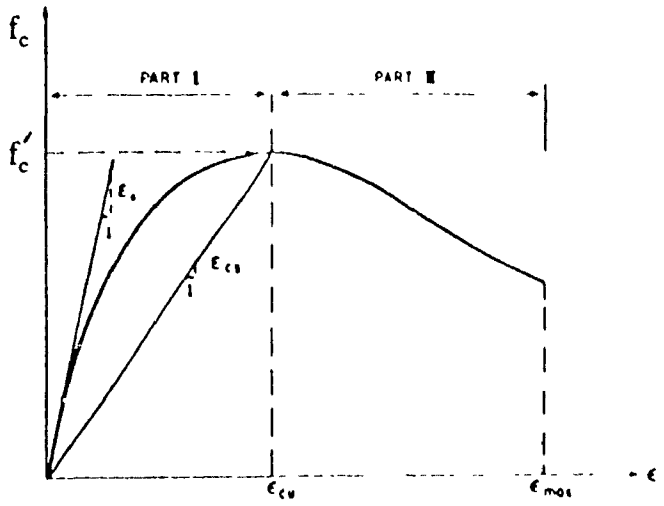

Concrete compressive stress-strain curve

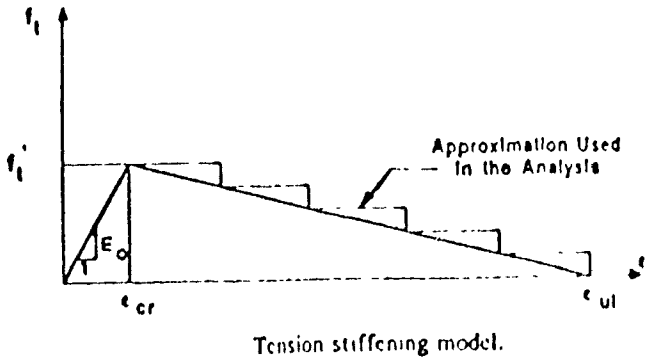

Tension stiffening model.

Figure 3.3 (a) Compressive and tensile stress-strain relationship for concrete[27,28]

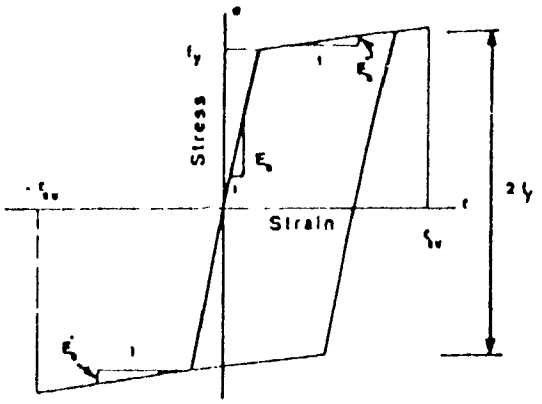

Figure 3.3 (b) Stress-strain relationship for steel[27,28]

Crack Configuration

- Uncracked Concrete

  Tangent moduli E_1 and E_2 coincide with principal stress directions $\sigma_{1\ major}$ and $\sigma_{2\ minor}$

Uncracked Concrete

- Cracked Concrete – Tension Stiffening Model
  - Principal directions – Normal and parallel to cracks
  - Zero stiffness perpendicular to crack
  - Conditions σ_1 or $\sigma_2 \geq f_t'$ — Cracked

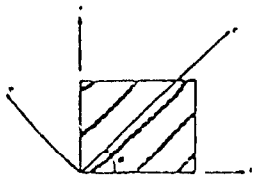

- ONE Crack $\sigma_1 \geq f_t'$ — $E_1 = 0$

$$[D] = \begin{bmatrix} 0 & 0 & 0 \\ 0 & E_2 & 0 \\ 0 & 0 & \beta G \end{bmatrix}$$

One 'Crack'

First 'Crack' Closed

- SECOND Crack perpendicular to σ_1. $\sigma_2 \geq f_t'$ — $E_2 = 0$

$$[D] = \begin{bmatrix} 0 & 0 & 0 \\ 0 & 0 & 0 \\ 0 & 0 & \beta G \end{bmatrix}$$

First 'Crack' Closed
Second 'Crack' Open

- Smeared Cracking Technique – replace G by βG

  To account for shear stiffness due to aggregate interlock and dowel action

  β = shear retention factor = 0.1 – 1.0 Lin (1973)

Both 'Cracks' Closed

Both 'Cracks' Open

Figure 3.4 Material constitutive model for concrete[26]

3.1.3 Procedure of Analysis

For nonlinear analysis, an incremental iterative tangent stiffness technique, with the load applied in appropriate increments, is used to trace the nonlinear response of the structure. During the first iteration after the application of a load increment, the incremental displacements are calculated using the tangent stiffness evaluated at the end of the previous load increment. The incremental stresses and strains in the concrete and the steel are calculated and added to the previous total stresses and strains to obtain the current approximated total stresses and strains. This is traced for each integration point for all of the elements. Use of the nonlinear constitutive relations gives, the real stresses related to the "current" strains. Any unbalanced stresses due to the difference between the "true" and the "approximated" stresses are calculated which are used to compute the equivalent nodal forces. These forces are imposed at the beginning of the second iteration. The procedure is continued until convergence is achieved, or the maximum number of iterations specified by the user in the data is reached. The solution is stopped when the divergence criterion, identified by large unbalanced forces or displacement increments, occurs. This is considered as failure or instability of the structure.

Program Limitations

The NONLACS program does not consider the following:

1. Large displacements or geometrical nonlinearities;
2. Fatigue effects due to cyclic loading;
3. Shear deformation normal to the surface, i.e. punching shear;
4. Bond slip at the interface of the concrete and the steel reinforcement,
5. Beam elements

Also, the program does not include a graphics module to plot the stresses and deformations in the structure.

3.2 NONLACS program- Application and Results

3.2.1 Finite Element Idealization

Each connection specimen was modelled using quadrilateral shell elements with cubic displacement fields in both directions. Figure 3.5 represents the finite element idealization used for the computer model, with 252 shell elements and 6 boundary elements (to calculate the reactions). These reactions were used to post-tension the W-shape steel beam at specimen boundary to the strong floor of the laboratory. The 232 nodes were numbered in an efficient way to get an optimum stiffness matrix with a minimum band width.

Each node had three degrees of freedom - normal rotation Θ_z, horizontal displacement Δ_x, and vertical translation Δ_y. A fine mesh was used to model the critical area with stress concentration close to the connection, while a coarse mesh was used in the zone farther away from the connection. A trapezoidal transition elements were used to connect the fine elements to the coarse elements. The aspect ratio for the concrete panel elements was maintained at value of 1, except for the concrete element adjacent to the H.S.S section, where the W-shape steel beam and the H.S.S had aspect ratios varying between 1 and 3.

The thickness of the concrete panel was divided into two layers. Since the thickness of the concrete panel varied, the concrete elements in the 75 mm thickness were divided in 25 mm and 50 mm thick layers, while in 50 mm thick panel, two 25 mm thickness layers were used, resulting in the same reference surface (Z=0). The steel beams (W-shape and H.S.S) at the specimen boundary were modelled by steel elements divided into two layers. The thicknesses of these elements were determined based on the moment inertia of the steel beams. The two dimensional steel anchors were idealized using the embedded reinforcement concept, while the steel wire mesh was idealized as a smeared steel layer.

To determine the reactions in the boundary elements, the spring concept (for each support; one horizontal and one vertical spring with high stiffness) was used.

The faceplate was modelled by steel plate elements. For Specimen S3 with an embedded angle, the anchored flange was idealized with a smeared steel layer,

while for Specimen S5 the steel angle was modelled with steel plate elements.

Loading was applied in 30 load steps, and the shear force was applied at three nodes, Node 135, Node 150, and Node 159 in the ratio of 50% of the total load for node 150 and 25% of the load at each of the nodes 135 and 159 (Figure 3.5). The total weight of the specimen was imposed in the first load step. Equilibrium was achieved using 15 iterations in each load step. The load steps for the shear forces had large increments at the start and much smaller increments towards the end to evaluate the "real" behaviour of the structure by taking into account the material non-linearity effects. The applied load was increased monotonically and shrinkage, creep and temperature effects were not considered.

The 3 by 3 Gauss integration points for analysis, and the result of the 5th integration point (middle, average point) were used to evaluate the stress and strain in the concrete (cracking pattern) and the overall deflection at Node 15.

It should be mentioned that Specimen S4 could not be modelled as the NONLACS program version at McGill University, does not have the ability to model the shear stud connector element.

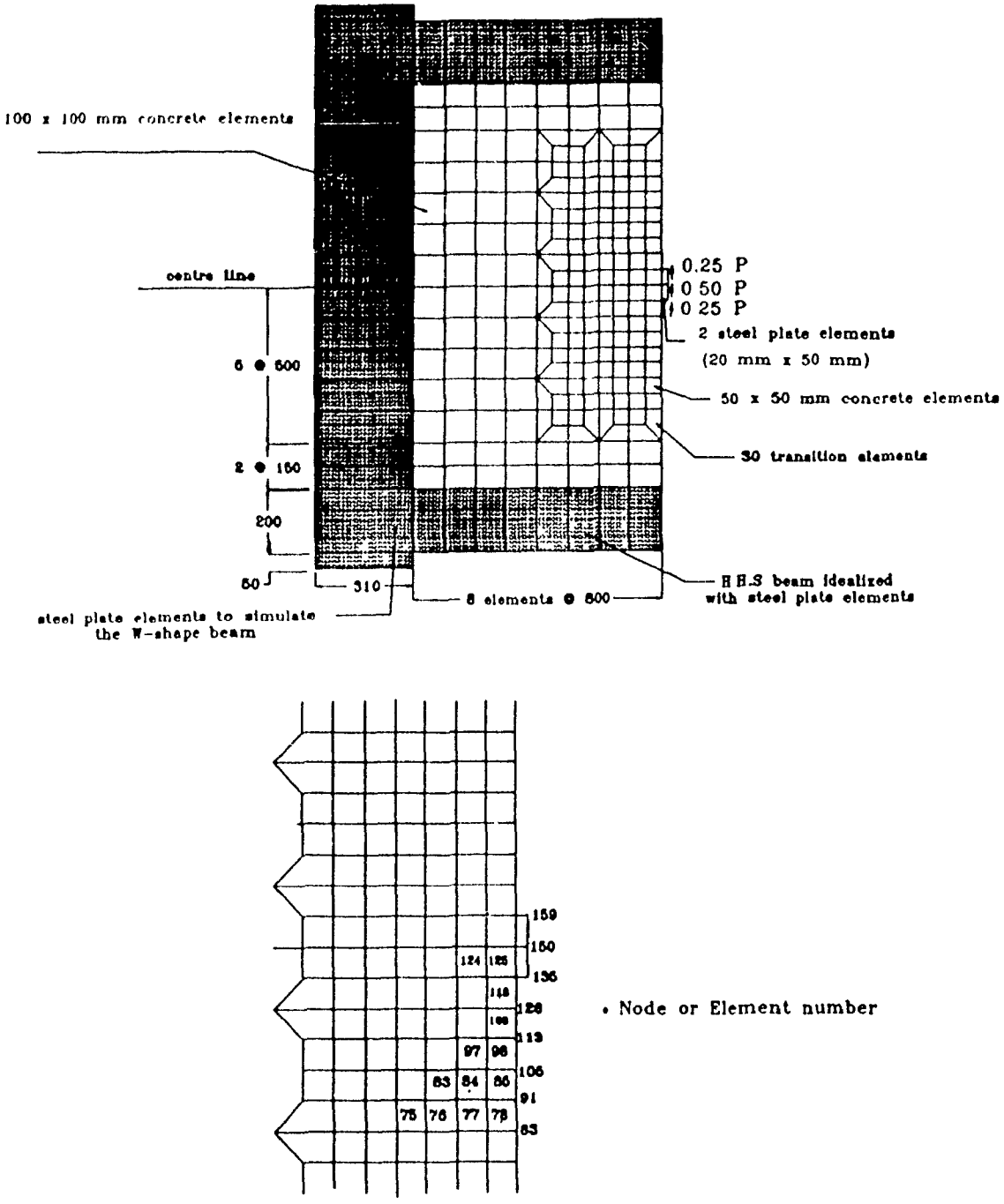

Figure 3.5 Finite element idealization for specimens

3.2.2 Discussion of analytical results

Selected results from the analysis are reviewed in the following sections. Because of the importance of the ultimate strength, displacement, response of steel anchor, and the cracking patterns for each connection, the discussion focuses on the load-deflection characteristic, ultimate capacity,load-steel strain response curves, and cracking and cracking propagation.

3.2.2.1 Load-deflection characteristics and ultimate strength

Connection S1

Figure 3.6 shows the analytical load-deflection curve (at Node 150) for Connection S1. As seen from Figure 3.6, the slope of the load-deflection curve (stiffness) decreases gradually after the initiation of the first cracks, which diminishes more rapidly as the number of cracks increased along the reinforcing bar in the connection. Since the NONLACS program is based on the continuous modification of the stiffness matrix to account for the progression of cracking in the connection and yielding of the steel reinforcement, a small increment in the applied load, when the number of cracks has increased significantly, would lead to a significant increase in displacements, strains and stresses. At a load of 125 kN, 48 elements had cracked while at the previous load stage, load of 120 kN, only 25 elements had cracked. Due to this increase in the number of cracked elements, the displacement increased from 0.38 mm to 0.51 mm , which is quite noticeable.

After the commencement of yielding of the reinforcing bar, the strain at Location 1 in tensile region increased very rapidly. An examination of the stresses obtained from the computer output, revealed that the reinforcing steel bar in the compression region had not yielded.

At a load value of about 176 kN, the tensile reinforcing bar started to yield. In the next load step (load of 177.5 kN), the connection underwent a significant increase in displacement at Node 150 due to the general yielding of reinforcing bar in the tension zone. A displacement of 2.68 mm was obtained at applied load of 177.5 kN. This rapid increase in displacement forced the concrete elements in

compression to fail by crushing of the concrete along the reinforcing bar and near the edge, although in the previous load step the compression steel was far from yielding (ε_s=840x10^{-6}), and the tension bar had just yielded (ε_s=2250x10^{-6}). As the applied load was increased and the connection reached its ultimate strength (180 kN), all of the concrete elements around the tension bar had entirely deteriorated and, finally, as the applied load was increased by a very small increment, reinforcing steel leg in the tensile zone pulled out, and the connection failed.

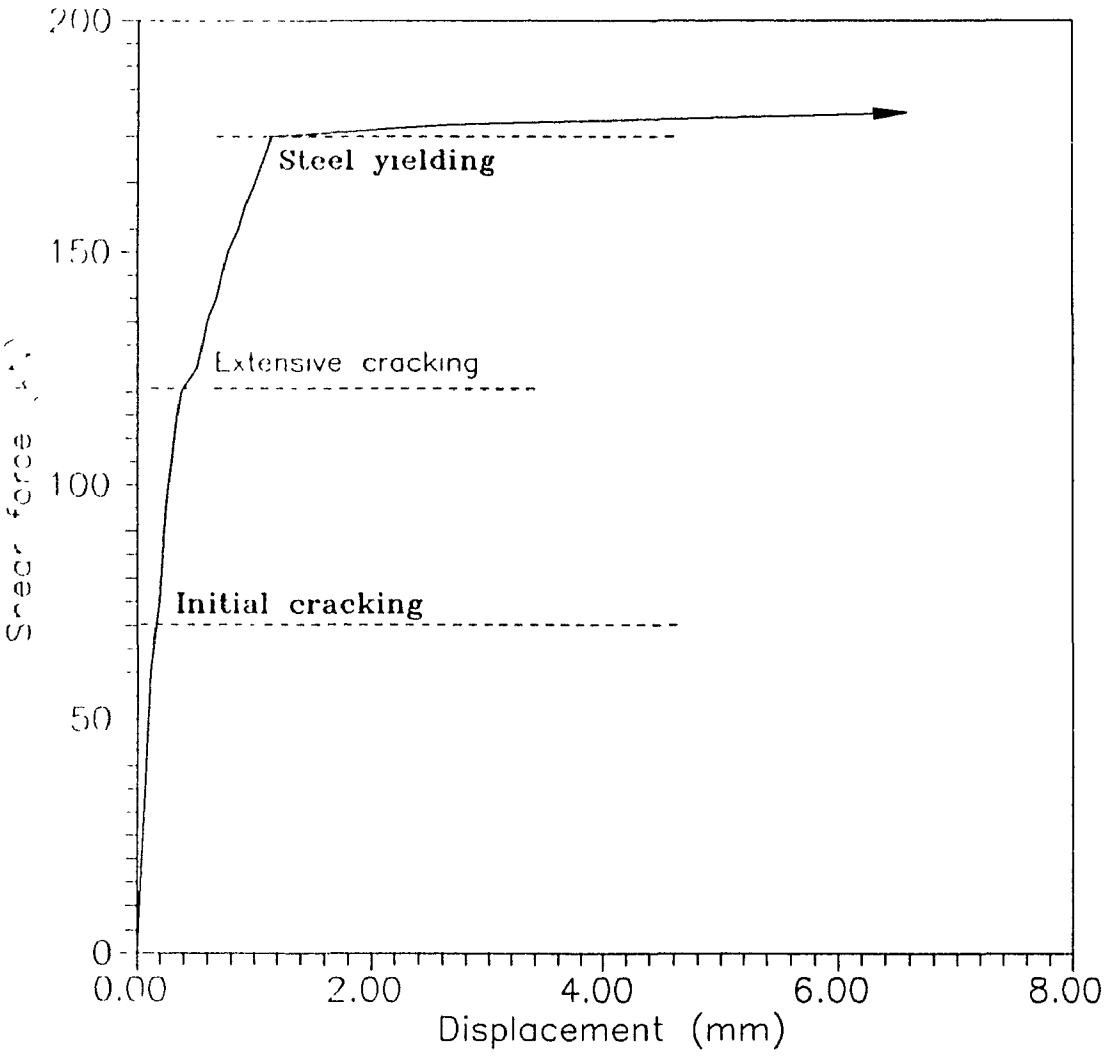

Figure 3.6 Load-deflection response for Connection S1

Connection S2

Figure 3.7 presents the load-deflection curve for Connection S2. As for Connection S1, the slope of the load-deflection curve (connection stiffness) continued to decrease after the appearance of the first crack, which a further decrease as more elements cracked. The load-deflection for Connection S1 and S2 show a good agreement in their load-deflection curves up to load of 120 kN. Therefore, up to this stage, the contribution of right angled hook to the specimen behaviour was not notable. Hence, the Connection S2 behaved identically to Connection S1. As the applied load increased up to 150 kN , a rapid change of slope occurred in the load-deflection curve , which was due to a significant increase in the number of cracked elements in comparison with the previous load step. It should be noted that the sharp change of stiffness in Connection S2 appeared at a load greater than that for Connection S1, which was due to the contribution of the 90 degree hook to the strength and stiffness of Connection S2. A review of the stresses in the output show that at a load value of 172.5 kN, the tensile reinforcing bar started to yield, whereas the strains in the compression leg were still well below the yield strain. In the next load step (load of 180 kN), the reinforcing bar in the compression zone had also yielded which was accompanied by crushing of the concrete elements around the yielded part. The connection underwent significant deflection due to the increase in the lengths of the reinforcing bars which had yielded in both compression and tension. This depended in turn on the increasing number of crushed and cracked concrete elements around the connection. A displacement of 2.22 mm was obtained at a load of 180 kN, while the displacement at an applied load of 177.5 kN (previous load step) was 0.87 mm, and the strain in the compression part (ε_s = 840x10^{-6}) was far from the yield strain and the tension part of the bar (ε_s=2250x10^{-6}) had just yielded. It indicates that after the yielding of the reinforcing bar, a small load increment (2.5 kN) resulted in a large deflection increase at Node 150. At the ultimate load value of 182.5 kN, all concrete elements around the steel leg in the tension zone were completely cracked, resulting in pull out of the leg and failure of the connection. Connection S2 failed at a slightly higher load than Connection S1, whereas the overall analytical response of Connection S2 was stiffer than the response of Connection S1

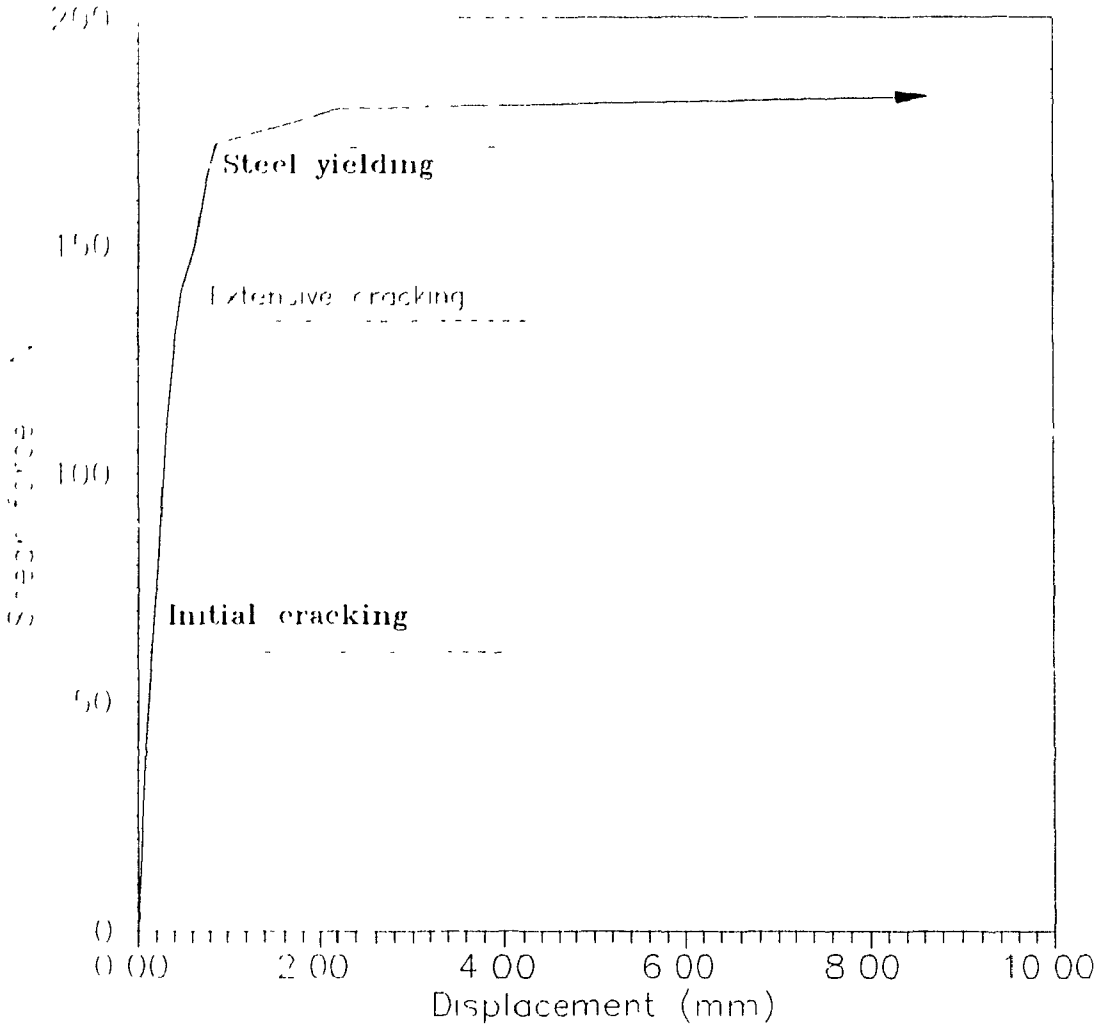

Figure 3.7 Load-deflection response for Connection S2

Connection S3

The variation of displacement at Node 150 with the applied load is shown in Figure 3.8. A decrease in the specimen stiffness (slope of the load-deflection curve can be noted at a load value of 40 kN , when the first cracks appeared in the specimen. The slope of the load-deflection curve remained almost constant up to a load of 115 kN. As the applied load was increased further, a rapid change was noted in the slope at a load of 120 kN. This was due to a significant increase in the number of cracked element from 12 to 20 along with two elements in which the

concrete had crushed at loads of 120 kN and 125 kN, respectively. This resulted in an increase of displacement from 0.61 mm to 1.20 mm. Since the program NONLACS uses an incremental-iterative approach, based on continuous modification of the tangent stiffness to take into account the progression of "cracked" and "crushed" elements, a small increment in the load at a stage when a significant number of elements have cracked or crushed, would result in a large increase in the displacement at Node 150.

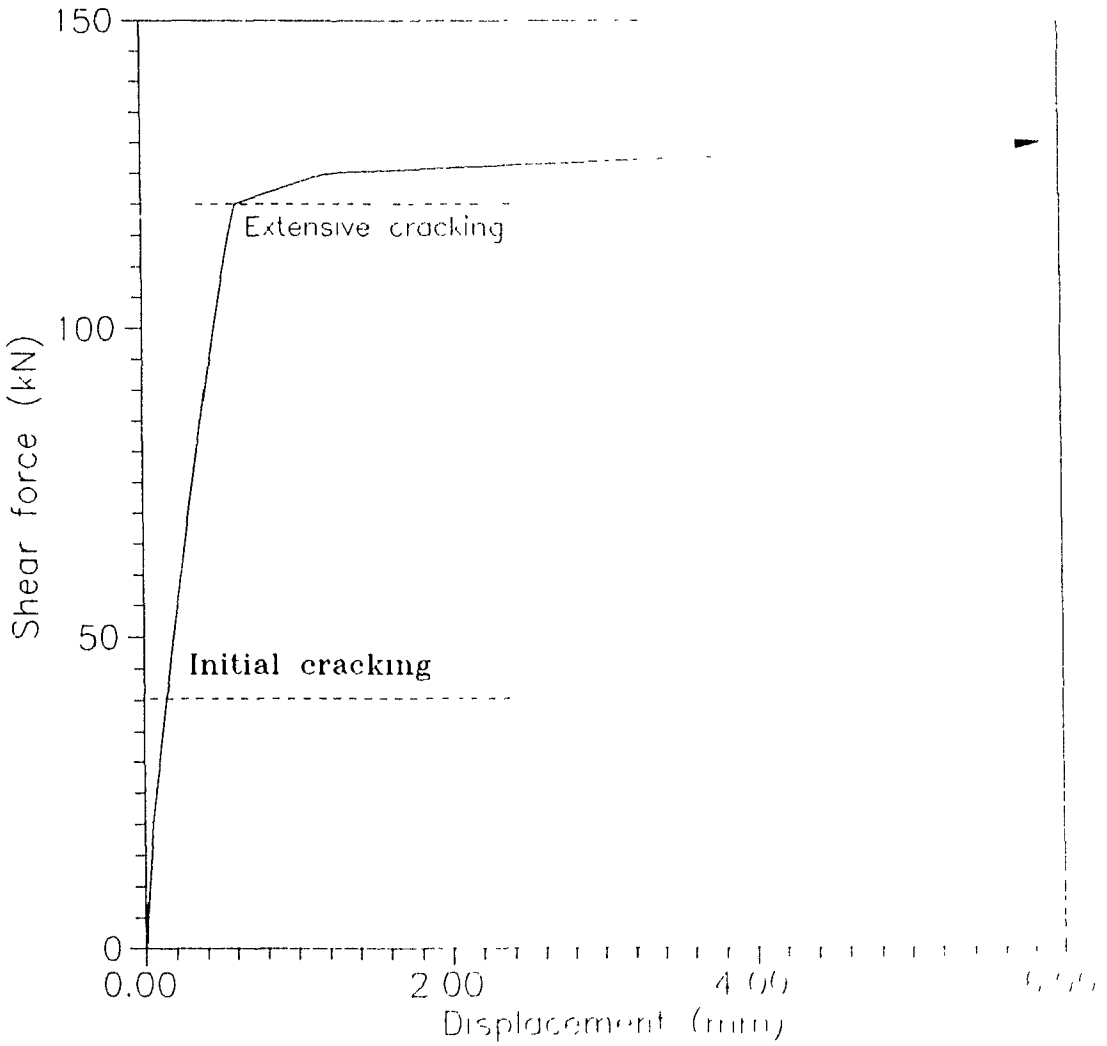

Figure 3.8 Load-deflection response for Connection S3

The connection failed at an ultimate load of 130 kN, at which stage the connection had undergone a large displacement. The concrete mode of failure consisted of total deterioration of the concrete around the reinforcing bar in the tension region in addition to the crushing of the concrete near the free edge which was subjected to dowel action. This behaviour indicates clearly that although the connection can be designed conventionally to resist the shear force based on the shear-friction hypothesis, proper detailing of the critical regions ("crushed" and "cracked" elements) should be given proper attention, especially when the connection is subjected to reversed cyclic loads due to earthquakes. It should be noted that the maximum strain in the tensile reinforcing bar at the ultimate load was 1800×10^{-6} which is less than the steel yield strain.

Specimen S5

The complete load-deflection response for Node 150 is depicted in Figure 3.9. The curve shows a linear response up to the first cracking, and it is clear that the specimen stiffness decreases after the concrete cracks. The slope of the load-deflection curve decreased gradually with an increase in the applied load, and this stiffness decrease was more pronounced as the number of "cracked" elements along and perpendicular to the steel anc' or increased. There are notable changes in the slope of the load-deflection curve at loads of 140 kN and 190 kN, which are due to a significant increase in the number of the cracked elements compared with that in the previous load steps. A more significant change in the slope was observed at a load value of 210 kN, which is due to yielding of the tension reinforcing bar (Figures 3.9 and 3.13). The displacement at which the first tensile reinforcing bar element yielded was approximately 1.34 mm. An examination of the stresses obtained from the output at this stage showed that the reinforcing bar in the tensile zone had just yielded, and the concrete elements around the yield part had failed,i.e. the concrete elements were cracked in both principal directions. In the next load increment at a load 212.5 kN, the displacement at Node 150 was 1.9 mm and the stiffness had decreased considerably.

The load at which the connection failed was approximately 215 kN, as the

connection underwent large displacement due to an increasing length of the bar having yielded in the tension region (length of 283 mm) along with a complete failure of the local concrete elements. A review of the output results showed that the local failures took place in elements 77, 78, 83, 84, 85, 97 and 98 by crushing of the concrete, while all of the other elements in this region had deteriorated due to complete cracking. The reinforcing bar started to pull out and the node 91 showed large displacement at the failure of the connection.

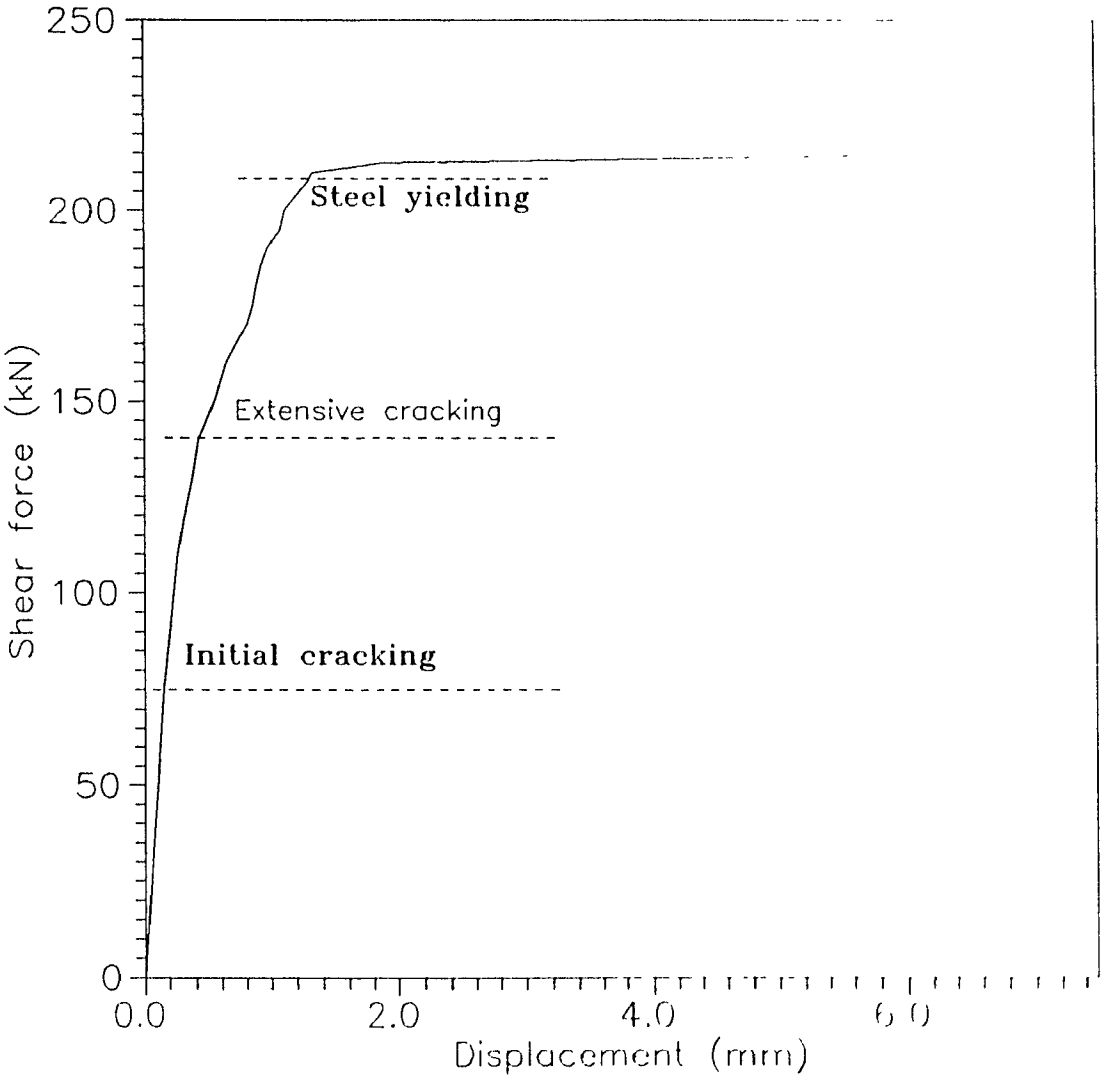

Figure 3.9 Load-deflection response for Connection S5

3.2.2.2 Response of Steel Bar Anchor in Connections

Connection S1

The variation of strains at Locations 1 and 4 in the steel reinforcing bar with load steps is depicted in Figure 3.10. The reinforcing bar at Location 1 started to yield at a load of 176 kN, while the bar at Location 2 yielded at a load of 178 kN. At this stage, strains, and therefore the stresses in all other reinforcing bar elements were still below the yield level.

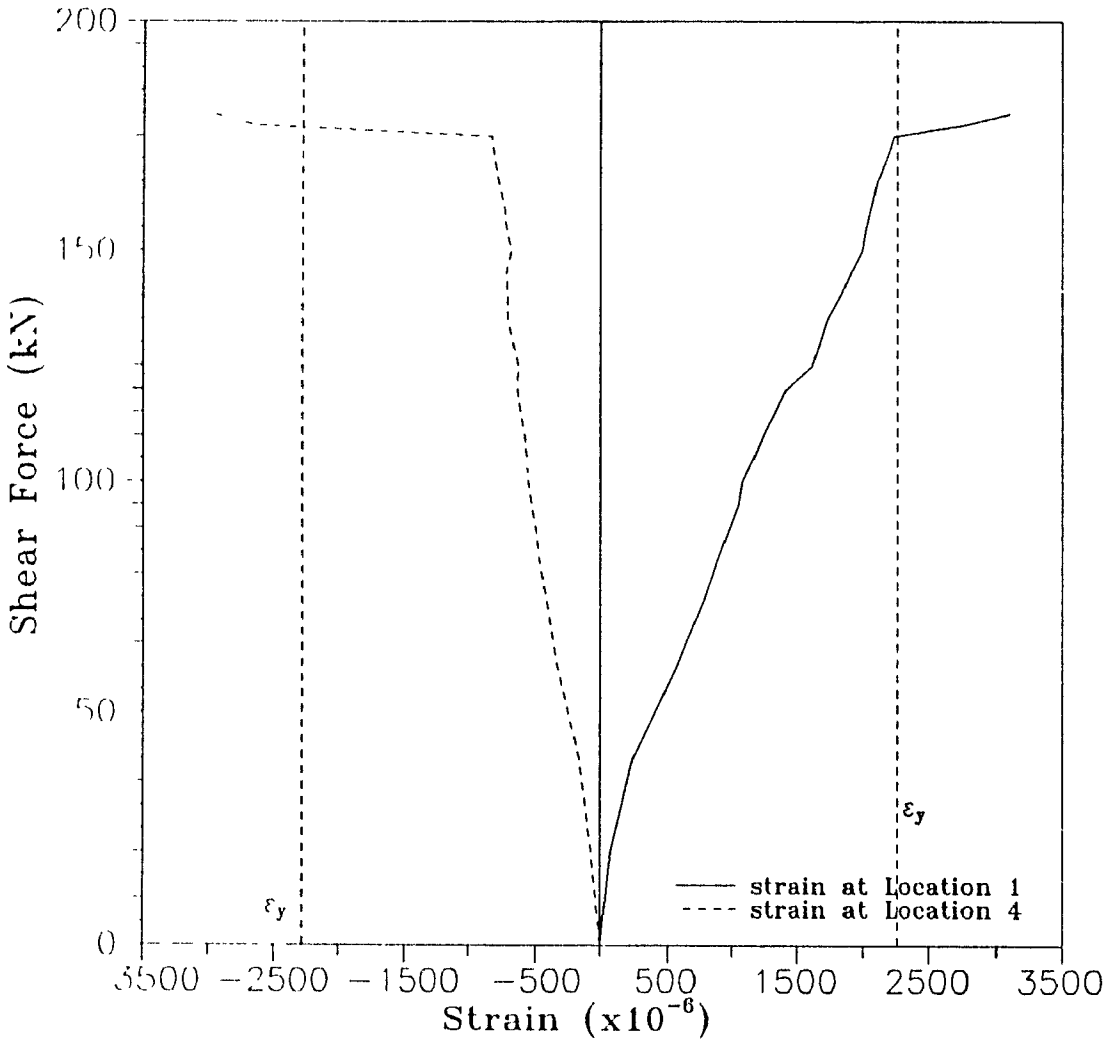

Figure 3.10 Load-steel strain curve for Connection S1

Increasing the load gradually to 177 kN caused further yielding of the steel bar, which resulted in a rapid increase in the displacement at Node 150. As the imposed load was increased beyond 177 kN, the reinforcing bar underwent much larger strains causing large deflection at the joint which resulted finally in failure of the connection.

It should be noted that up to a certain load level, when the concrete elements did not crack, the variation of strains for both the compression and tension steel legs were almost identical. After cracking, the strains in the tension leg increased more rapidly than that in the compression leg. This is basically because under the applied load, the connection must be in equilibrium, therefore the load resisted by the tensile leg must be equal to that for the compression zone. The bond resistance at the interface of the steel bar and the uncracked concrete along the compression leg is much better than that along the tensile leg.

Connection S2

The strain response of the reinforcing bar for Connection S2 is shown in Figure 3.11, where the variations of strains at both Locations 1 and 2 due to the monotonically increasing load are illustrated. The reinforcing steel began to yield in tensile region at Location 1 at an applied load of 172.5 kN, whereas the bar in the compression part at Location 2 yielded at a load of 177 kN. At this level of loading, the strains, and therefore the stresses at all other locations on the reinforcing bar elements were below the yield level.

Increasing the load to 180 kN forced the steel bar to yield along its length, which resulted in a rapid increase in the displacement of the connection. The rapidly increasing deflection after yielding of bar indicates inelastic response of the connection beyond the yield point. As the load was increased to the ultimate strength of the connection (180 kN), the reinforcing bar in the tensile part ruptured which caused very large displacements in the connection and led failure of the connection.

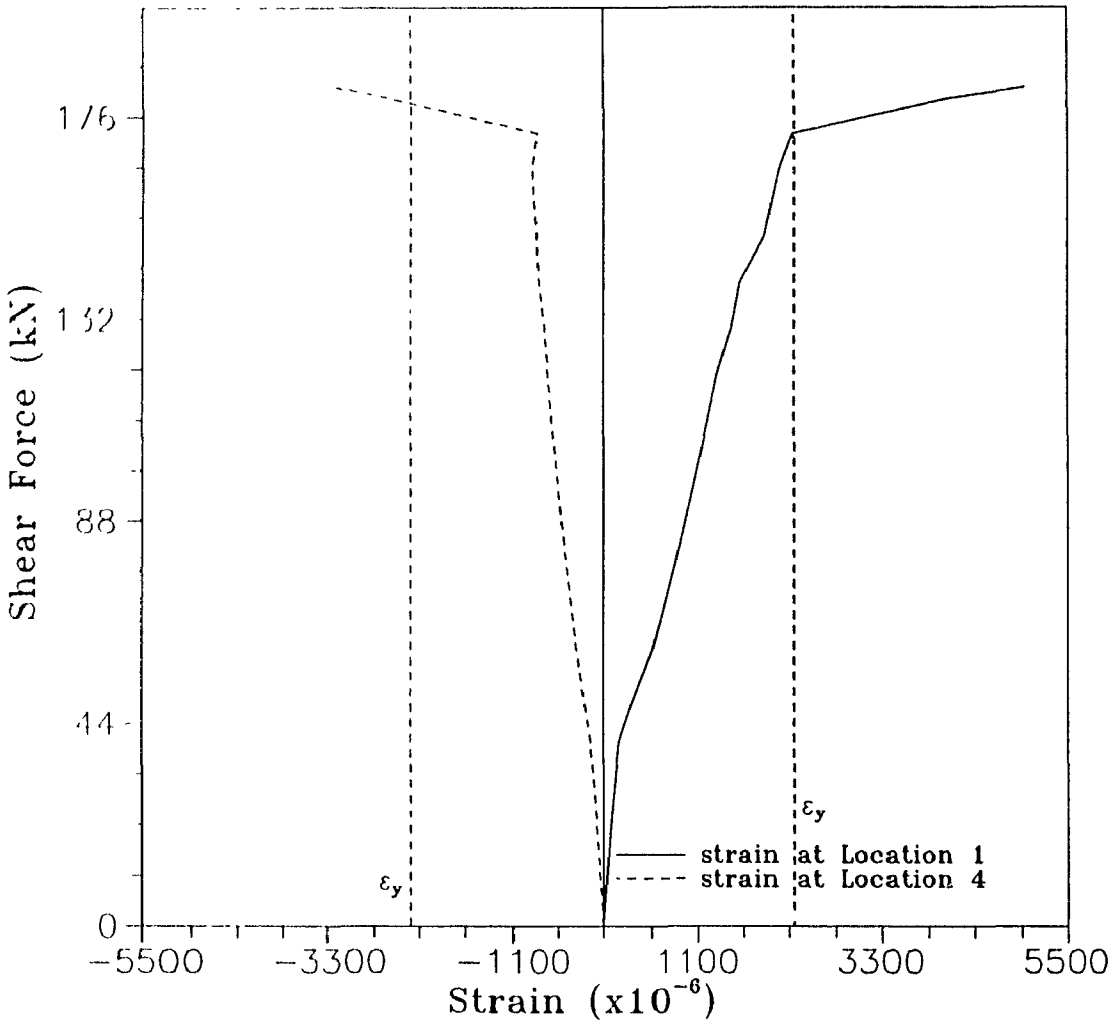

Figure 3.11 Load-steel strain curve for Connection S2

Connection S3

Figure 3.12 presents the variation of strains at Locations 1 and 4 of the reinforcing bar anchors. A large increase can be observed in the steel strains after the initiation of cracks in the concrete elements, which is due to transfer of more stresses to steel bar around the cracks. As the applied load was increased up to 120 kN, the slope of the load-steel strain curve remained almost constant. As load was increased to 125 kN, a significant change occurred in the slope of the load-strain curve, which was more due to crushing and complete cracking of the concrete elements near the free edge.

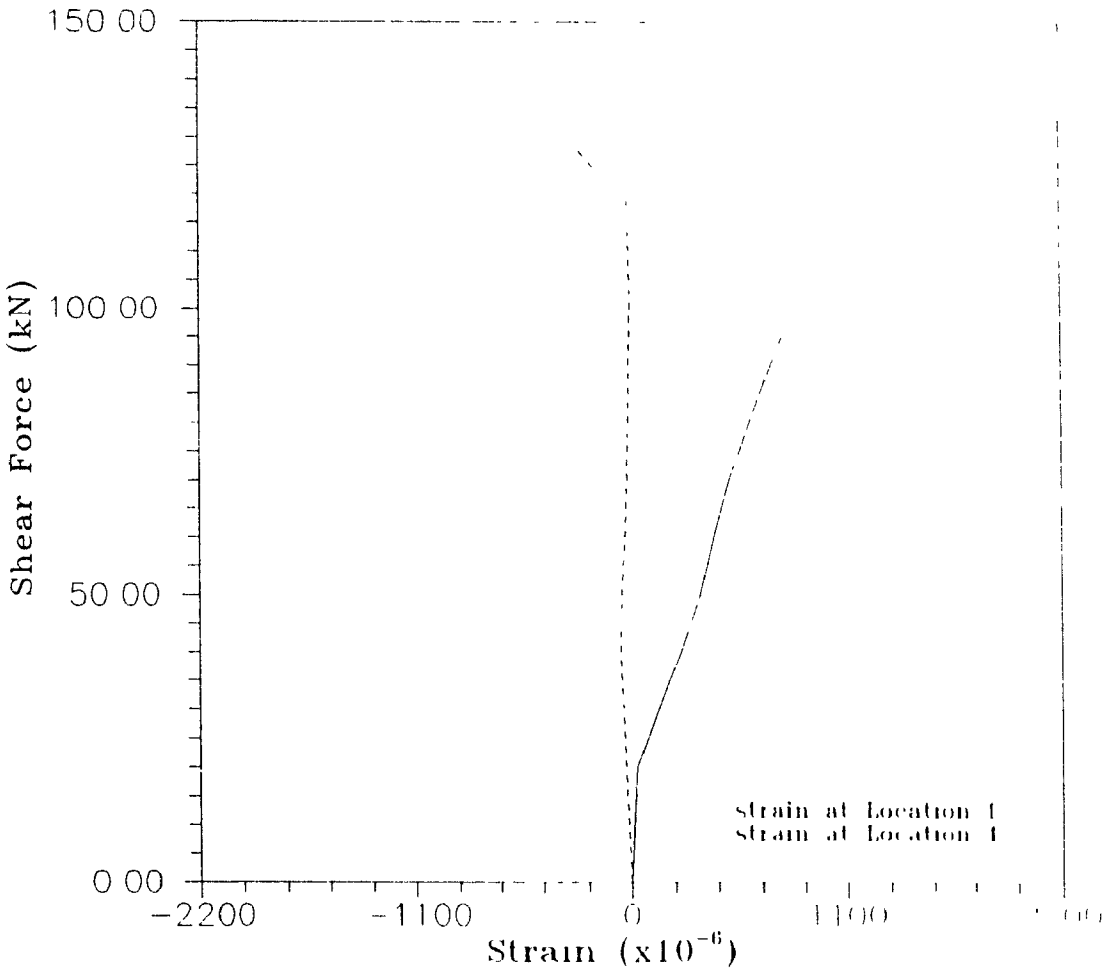

Figure 3.12 Load-steel strain curve for Connection S3

After cracking, the tensile stresses in the concrete were transferred to the steel bar through the uncracked concrete resulting in a significant increase in the steel stresses and strains near the cracks.

As can be seen from Figure 3.12, the strain at Location 4 remained almost linear up to a load value of 120 kN and the stresses in this reinforcing bar were extremely small. An examination of the NONLACS output revealed that none of the concrete elements had cracked in this region. In the next load step, when some element were cracked around this steel bar, the strain changed rapidly due to the

transfer of longitudinal stresses to the steel bar.

As the failure load was approached, the steel stresses were almost evenly distributed with higher values in the cracked zone and with slightly lower value towards the uncracked region. It should be mentioned that the reinforcing bar did not yield during the analysis as the specimen was loaded incrementally to failure.

Connection S5

Figure 3.13 shows the variation of strains at Locations 1 and 4 of the reinforcing bar in the tension and compression zone, respectively. During loading, the stresses in the tensile reinforcing bar of the connection increased locally at Location 1 where cracking occurred. It is clear from Figure 3.13, that when initial cracks occurred at a load of 75 kN, the slope of the load-steel strain curve changed rapidly. It is interesting to note that the steel strain response curves for both tensile (Location 1) and compression (Location 4) legs are linear, similar, and with almost the same rate of change up to a load of 75 kN. Beyond this stage, the curve for Location 4 (compression strain) remained almost linear due to uncracked concrete elements around the compression steel leg. As the load was increased, some change was observed in the slope of tensile strain response curve, due to further cracking.

The reinforcing bar in the tension zone started to yield at a load value of 207 kN, whereas the compression reinforcing bar did not yield. By increasing the load beyond the 207 kN, yielding continued along the remaining length of the steel bar, which forced more concrete elements to crack. When the applied load was increased to 112.5 kN, the reinforcing bar in elements 61, 75, 83 and 97 (about the 213 mm length of the bar) had yielded. A rapid change in the steel strain curve response was observed which marked the yielding of the reinforcing bar.

Examination of the stresses obtained from the computer output for Specimens S1, S2 and S5 showed a gradual variation of the steel stresses along the reinforcing bar, from the end of steel bar (minimum) to the load point (maximum).

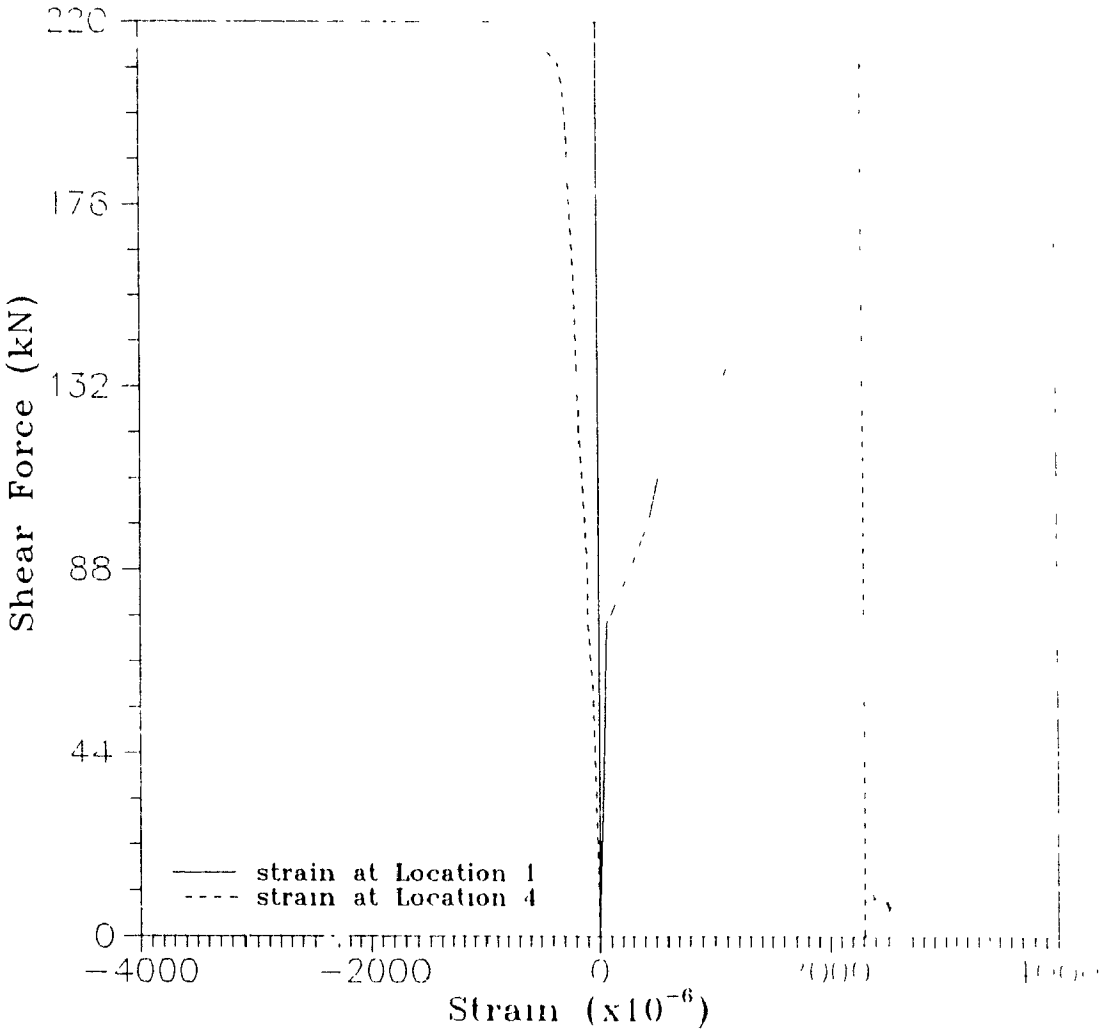

Figure 4.13 Load- steel strain curve for Connection S5

3.2.2.3 Cracking and Crack Propagation

A more clear understanding of the behaviour of the connection is obtained by investigating the cracking formation and crack pattern induced at different load stages. After the failure of a concrete element, the strain energy of the element is redistributed into the surrounding concrete elements. Thus, the surrounding elements will have a bigger share in the load sharing, and often even under the same applied load some new elements may fail.

The crack propagation in the connections was studied and the crack patterns were obtained at four critical stages: initial cracking (Stage I), two-third of the ultimate load (Stage II), yielding of the reinforcing bar (Stage III), and at the failure level (Stage IV)

Connection S1

The cracking patterns for Connection S1 at the different load stages are shown in Figure 3.14. Initial cracking occurred at a load value of 70 kN. Few concrete elements (4 elements) cracked in the tension zone near the free edge as shown in Figure 3.14(a). As the load was increased, cracking propagated toward the centre of concrete panel and along the reinforcing bar. At a load value of 120 kN (2/3 of failure load), in all 24 elements had cracked as shown in Figure 3.14(b). More elements had cracked along the line where the thickness of the concrete panel changed. At the next incremental loading (load of 125 kN), crack propagation was more rapid, and the number of cracked elements increased to 48, almost twice the number at the previous load step. This caused significant increases in the displacements. In the third stage of loading (yielding of reinforcing bar, stage III) with a load value of 175 kN, all of the concrete panel elements in the region around the tension bar had cracked. In total more than one-half of the concrete elements had cracked, see Figure 3.14(c)).

Increasing the load up to failure caused much slower crack propagation, although all concrete elements around the tension part had failed due to cracking. The complete failure of concrete elements surrounding the tension leg resulted in pull-out of the bar which was accompanied by crushing of the concrete in 11 elements. At this stage, the connection had failed.

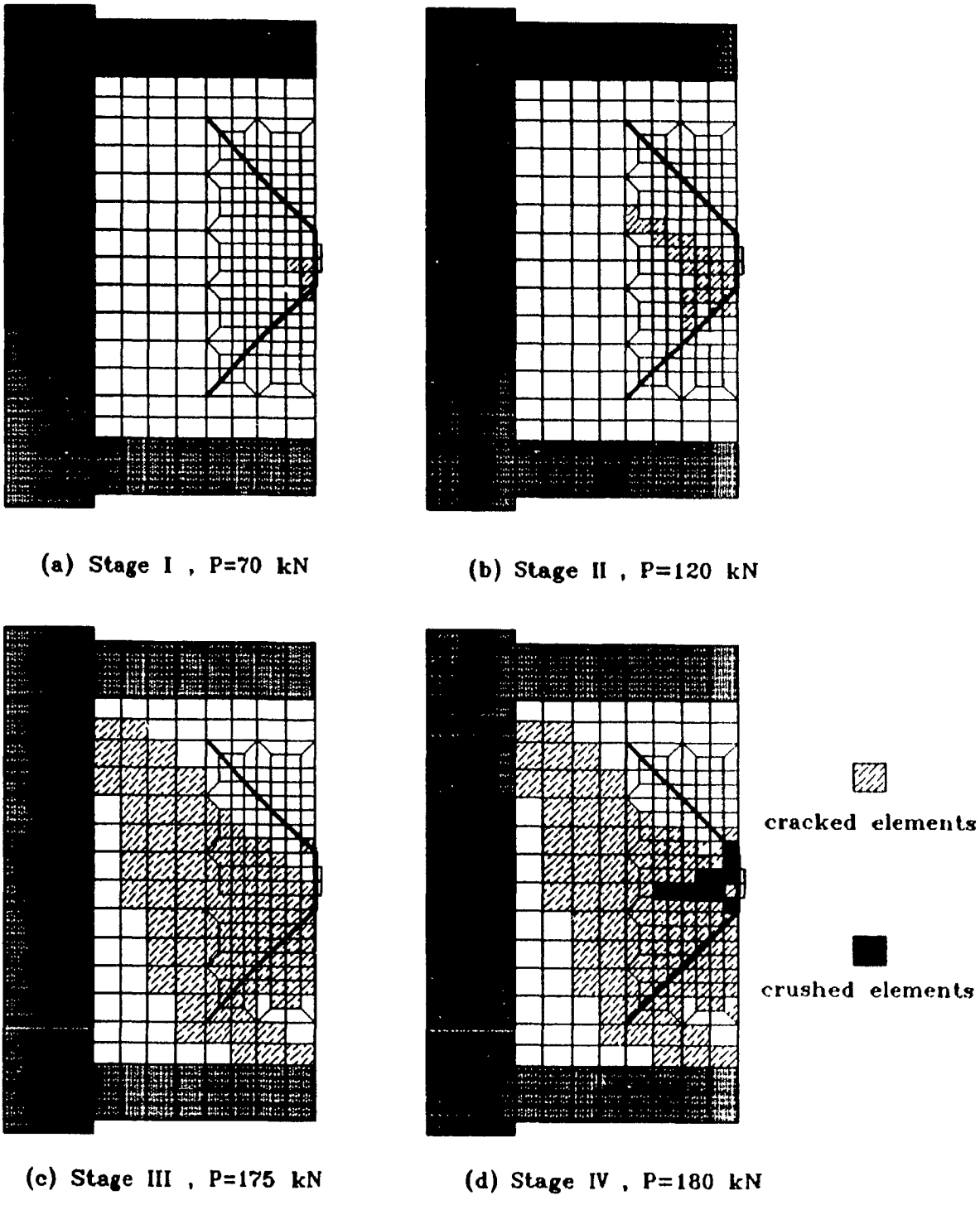

Figure 3.14 Cracked and crushed elements for Connection S1

Connection S2

The cracking patterns at the four selected load stages for Connection S2 are presented in Figure 3.15. Initial cracks formed in three elements near the free edge at a load of 60 kN as shown in Figure 3.15(a), and the principal tensile stress in one element near the edge was very close to the modulus of rupture of the concrete. The tensile stresses previously taken by the uncracked concrete elements were transferred to the reinforcing steel, resulting in a significant increase in the steel stresses, therefore, in the steel strain level around the cracks. This increase was over 240% with respect to the values at the previous load step. As the load was increased gradually, cracks propagated slowly in the tension zone. At a load of 120 kN (2/3 of the failure load, stage II), the number of cracked elements was 15 as shown in Figure 3.15(b). An examination of the results of the computer output at a load value of 140 kN revealed a more rapid propagation of cracks, resulting in a sharp change in both the load-strain and the load-deflection response curves. In the third load stage with load value of 172.5 kN (first yielding of tensile reinforcing bar, stage III), almost all concrete elements along the tensile leg and normal to it had cracked, see Figure 3.15(c). None of the elements approached the compressive failure stage, however, the compression stresses were rather significant.

As the applied load was increased and the specimen approached failure, some concrete elements under the hook part of the steel bar cracked due to biaxial tension, whereas the concrete elements in front of the hook part failed by combined tensile and compression stresses, as shown in Figure 3.15(d). The number of cracked elements increased significantly compared to the value for the stage at which the reinforcing bar had yielded. At the failure load of 182.5 kN, all concrete elements surrounding the reinforcing steel in tension zone had failed completely, indicating the total failure of connection. In this regard, the tension bar started to pull out from the concrete panel which caused several concrete elements (17 elements) to be subjected to biaxial compressive stresses resulting in the crushing of these elements.

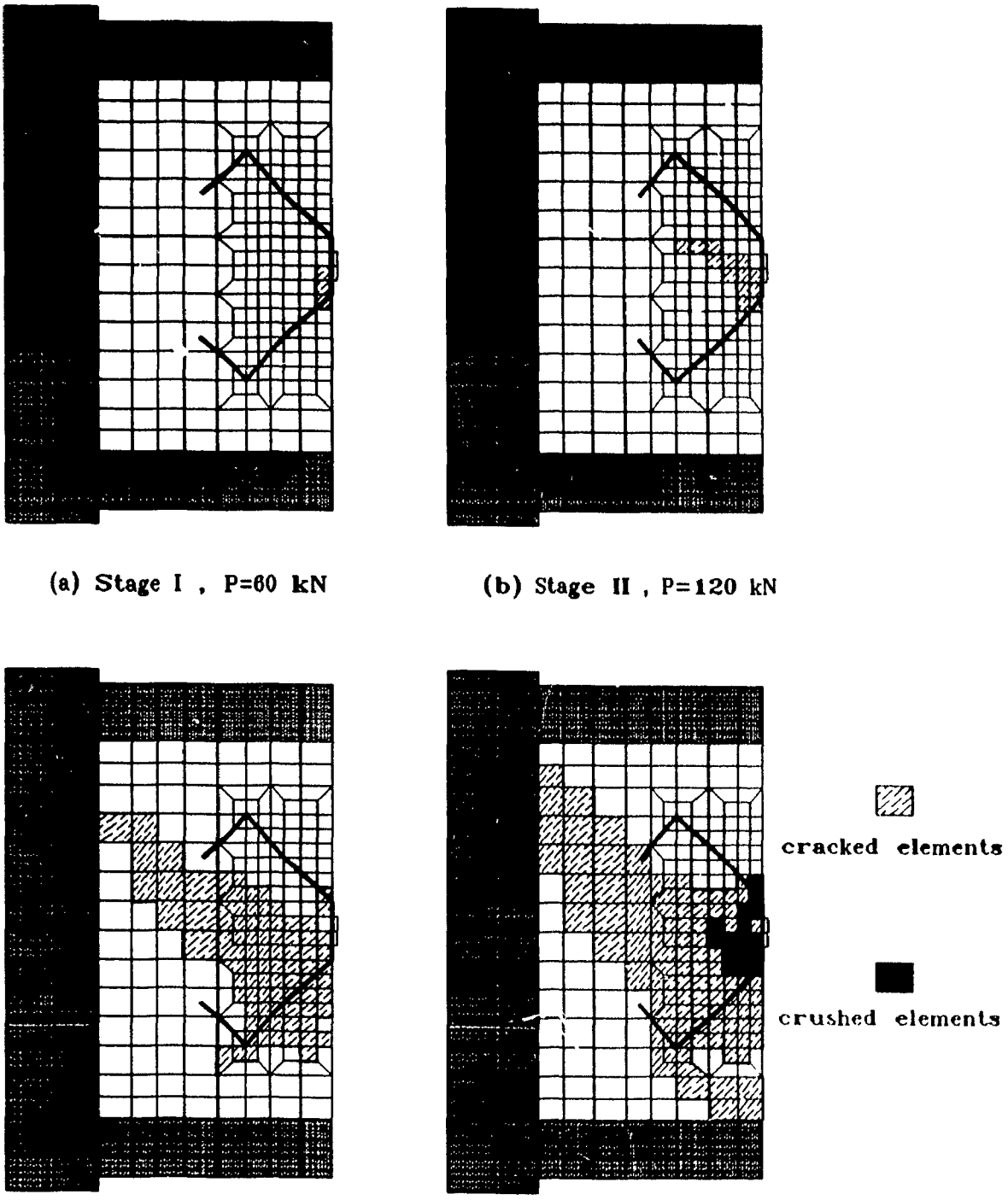

(a) Stage I , P=60 kN

(b) Stage II , P=120 kN

(c) Stage III , P=172.5 kN

(d) Stage IV , P=182.5 kN

Figure 3.15 Cracked and crushed elements for Connection S2

Connection S3

Figure 3.16 shows the crack patterns for Connection S3 during the incremental applied loading at the different load stages. The first cracks initiated at the outer-most face of the tension reinforcing bar at a load value of 40 kN are shown in Figure 3.16(a). Then as the load was increased monotonically, more concrete elements cracked along the reinforcing bar. In the following load steps, some concrete elements located between the two reinforcing bars were subjected to combined compression and tension stresses, resulting in cracking of these elements. At the second stage of loading (2/3 of failure load = 90 kN), 9 elements had cracked as shown in Figure 3.16(b). A review of the output results at a load of 120 kN showed that the number of cracked elements at any load stage increased proportionally with the applied load. None of the elements in the compression zone had failed. During the following load stage (load of 125 kN) two elements in the compression region had crushed due to the dowel action of the bars as shown in Figure 3.16(c). It should be noted that stage III was considered one load step before failure. The crushing of the concrete elements caused redistribution of the stresses in other elements which in turn resulted in more element to be cracked in the tension region. As more elements cracked around the tension steel bar, the tensile forces were transferred to the reinforcing bar. Therefore the steel strains changed rapidly, resulting in a significant increase in the displacement of the connection.

As the connection was loaded to failure (load of 130 kN), almost all the concrete elements around the tension reinforcing bar had failed completely, marking the failure of the connection as shown in Figure 3.16(d). The tension bar started to pull out from the concrete panel. This along with the dowel resistance of the concrete in front of the reinforcing bar near the edge, caused these elements to be subjected to very high biaxial compressive stresses resulting in crushing of these concrete elements.

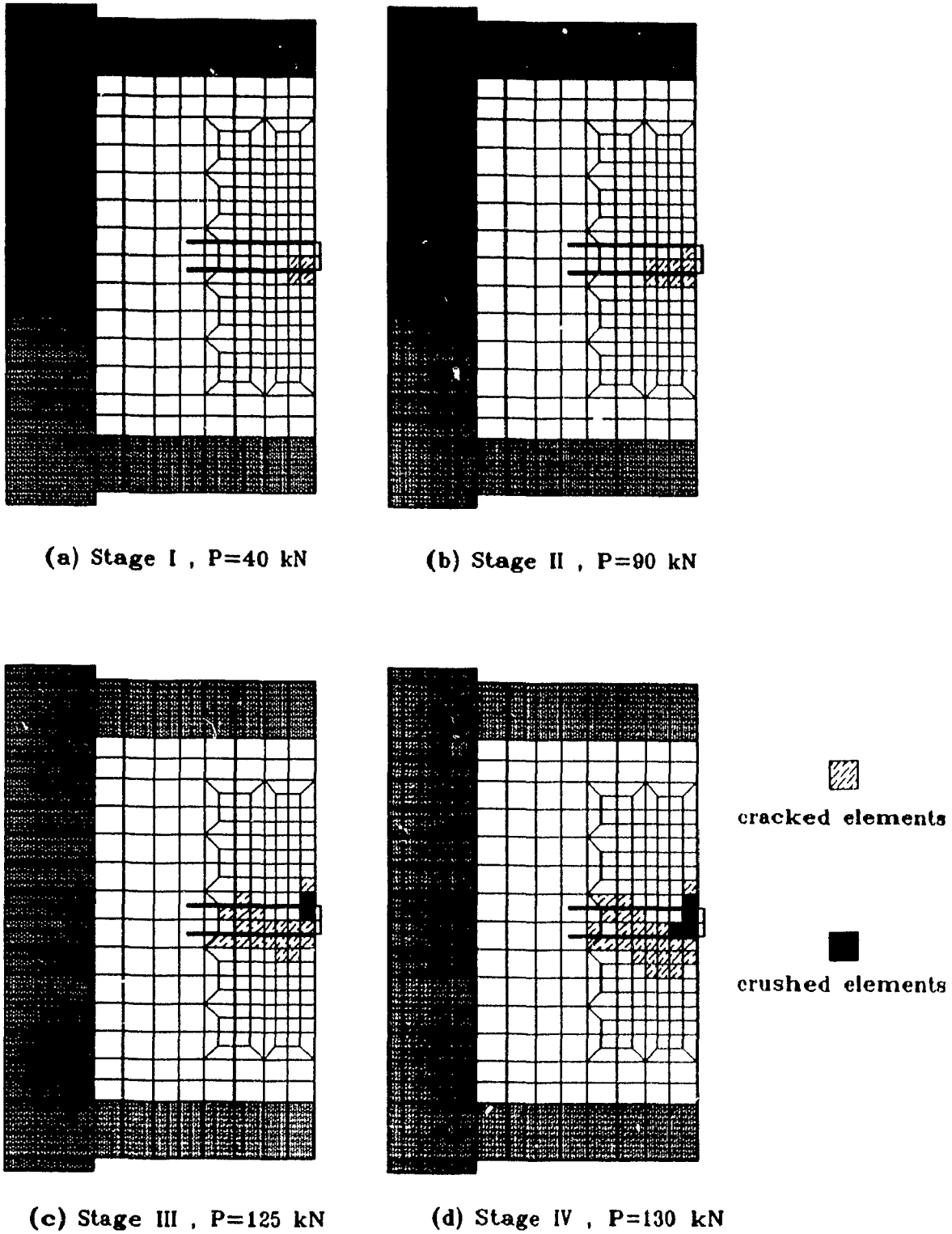

Figure 3.16 Cracked and crushed elements for Connection S3

Connection S5

The cracking patterns are shown for all four load stages. The cracked or crushed elements are shown in Figure 3.17. The load at which the first cracks initiated was approximately 75 kN as shown in Figure 3.17(a). As the load was increased monotonically, cracks propagated along and normal to the reinforcing bar. The area of cracked elements had gradually increased during the second stage of loading (load value of 140 kN). At a load of 140 kN (2/3 of the failure load), 34 elements had cracked. In the third load stage (yielding of the reinforcing bar, stage III), all concrete elements around the reinforcing bar in tensile zone had cracked. In total, more than half of the concrete panel had cracked as shown in Figure 3.17(c). None of the elements in the compression zone had failed. In the following loading steps, cracks propagated rather slowly. Finally, as the load was increased up to the failure load of 215 kN, all concrete elements around the tension steel bar had deteriorated, indicating the failure of the connection. The tension steel bar started to pull out from the concrete panel resulting in crushing of some concrete elements as shown in Figure 3.17(d). This is because the crack along the steel bar caused redistribution of the stresses to the adjacent elements, resulting in their crushing due to very high biaxial compressive stresses.

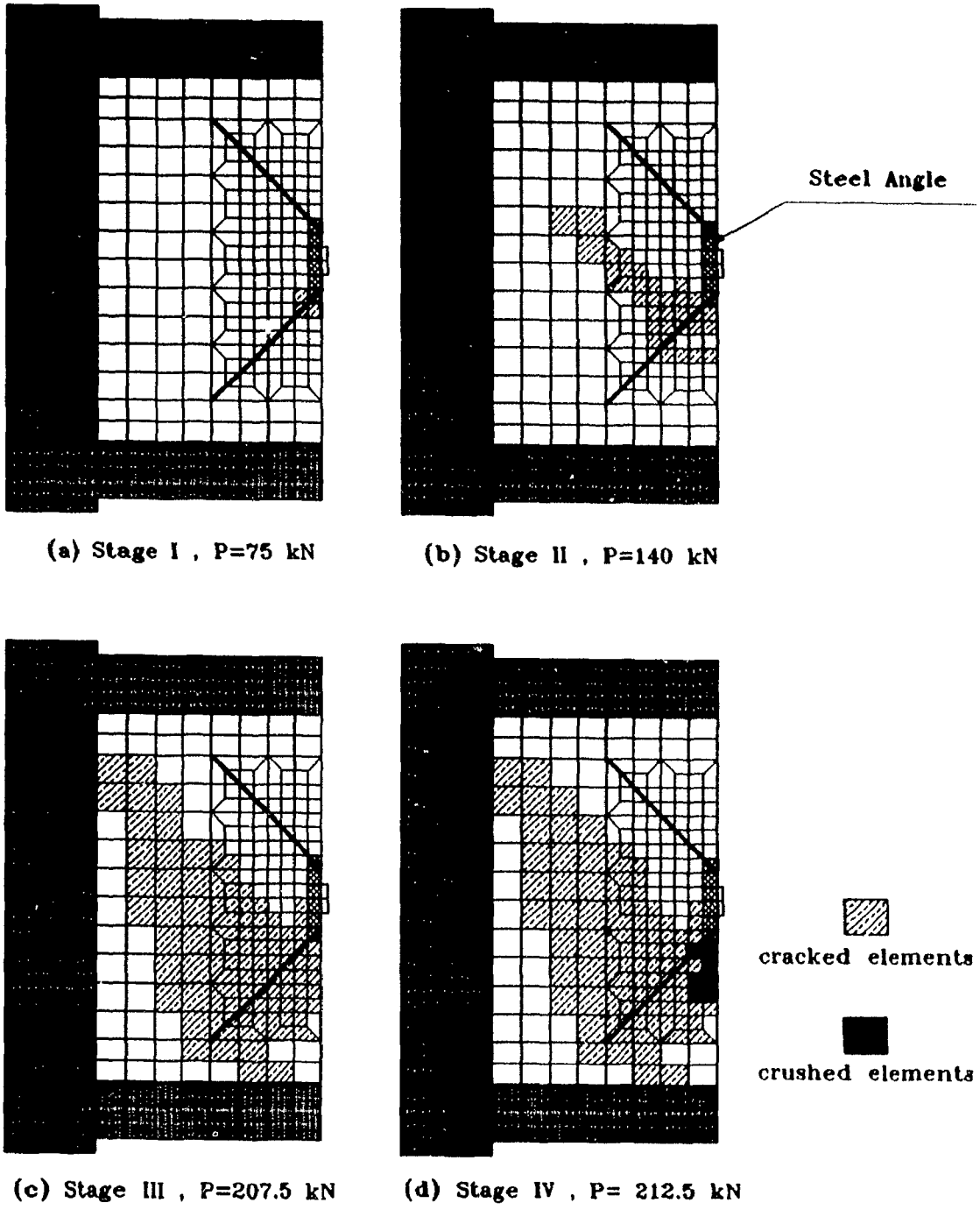

Figure 3.17 Cracked and crushed elements for Connection S5

Chapter 4

Experimental Results

4.1 Introduction

This chapter describes the complete response of each of the five specimens tested to destruction under reversed cyclic loading. Horizontal and vertical displacements of the connections, total displacement of the specimen and its accompanying boundaries steel frame, which had been modelled using the SAP90 analysis results, strains at six locations on the reinforcing bar anchor and at two locations on the welded headed studs were measured. The concrete surface strains were obtained using demec gauge readings at locations coincident with the bar strain gauges.

The following figures are presented for each of the five connection specimens:

1. Applied load vs. horizontal displacement response.

2. Applied load vs. vertical displacement response.

3. Applied load vs. measured strain in the reinforcing bar anchors and in the headed studs.

4. Peak load vs. maximum surface principal strain.

5. Measured strain vs. distance along the embedded anchors at ultimate load.

6. Peak load vs. measured maximum crack width.

7. Photographs of the specimen at different load stages.

4.2 Test Specimen S1

4.2.1 The Specimen

Specimen S1 was reinforced with a No. 15 deformed bar, bent at 45° welded to a 10 mm thick steel plate and a uniform wire fabric mesh, 100 x 100 MW13.3 / MW13.3 (see Figure 2.15). It was designed and detailed with special consideration for development length under low cycle loading[20].

Determination of the ultimate strength under monotonically increasing load (referred to as "monotonic" load) is based on the anchorage length for seismic loading , and the equations which in turn are dependent on the concrete cover thickness . All calculations were performed considering equilibrium of the joint using the truss analogy. The dowel action of the anchor was considered in the calculations; the wire fabric mesh was not included.

3.2.2 Loading History and Cycles 1 - 3

Table 4.1 summarizes the loading history for Specimen S1, along with the measured horizontal displacements at these load stages. As can be seen from Figures 4.1 and 4.2, and Table 4.1, the specimen was subjected to one elastic cycle (Cycle 1), followed by two cycles (Cycles 2 and 3) at a peak load of 36 kN causing a number of small cracks around the reinforcing bar in the concrete panel. The first splitting crack appeared at the free edge of the Specimen along the length of the reinforcing bar. It can be noted from Figure 4.4a that the maximum principal strain in the concrete panel is less than the concrete cracking tensile strain at Location 1. No crack was observed at this location. The measured crack width at this load stage was 0.08 mm. A symmetrical crack formed during the loading in the reverse direction (termed "negative" loading from here on). The maximum principal strain in the concrete panel measured at the demec gauges at Location 4, coincident with the strain gauge on the bar at the same location, is 124 x 10^{-6} where in the crack formed and extended throughout the demec gauge set. The load - deflection curves remained almost linear until the end of the third cycle, 3B

Table 4.1 Summary of Loading History for Specimen S1

Cycle	Load Stages	Horizontal Displacement (mm)**	Shear Force V (kN)
Elastic	1A - 1B	+0.16, -0.08	±35
Cracked	2A - 3B	+0.18, -0.10	±36
52% P_{ult}*	4A - 6B	+0.68, -0.71	±96
82% P_{ult}	7A - 8B	+3.80, -3.11	±150
Failure	9B	5.72	+145

* Calculated maximum strength under monotonically increasing loads (182 kN)

** Deflection at the peak load of last cycle of a given load stage

4.2.3. Load Cycles 4 - 6

The load was increased to a peak load 96 kN for this step (Load Step 4A), which is 50% of the monotonic ultimate design strength. The splitting crack extended along the reinforcing bar and widened to a width of 0.33 mm. The first diagonal crack was observed at the location of change in thickness of the panel, where due to a smaller cover thickness, there is a decrease in the local bond stress. Cracking occurred when the maximum tensile strain at that location exceeded the value of 110×10^{-6} (cracking strain of concrete). The "maximum principal strain vs distance along the bar" curves are presented in Figure 4.3. The first sign of concrete splitting at the end of the face plate was observed at its right corner. It showed slipping of the reinforcing bar and rotation of the face plate in the plane of the panel. Figure 4.4a presents a photograph of the specimen at Load Cycle 4A. These cracks caused a change in the slope of the load - displacement response (see Figure 4.1). The horizontal displacement at this load stage was 0.6 mm, which remained almost constant until the end of the Cycle 6B. The same behaviour was observed for the negative load cycles.

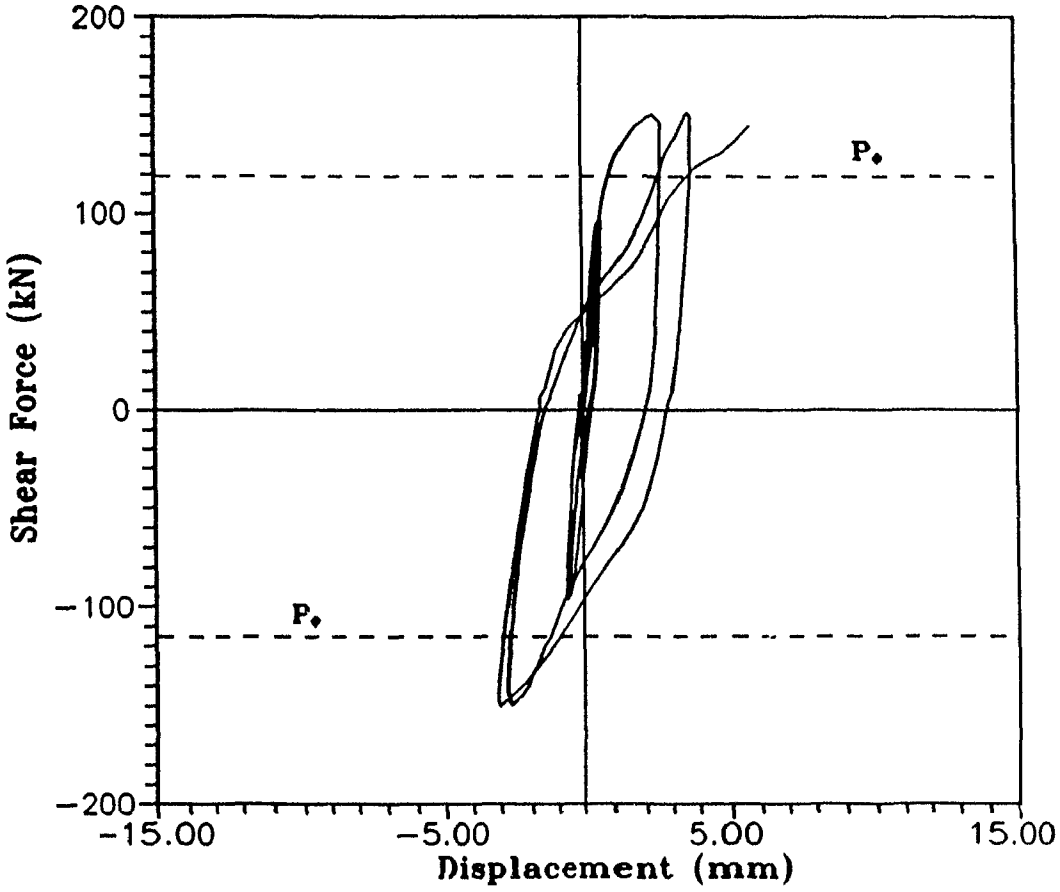

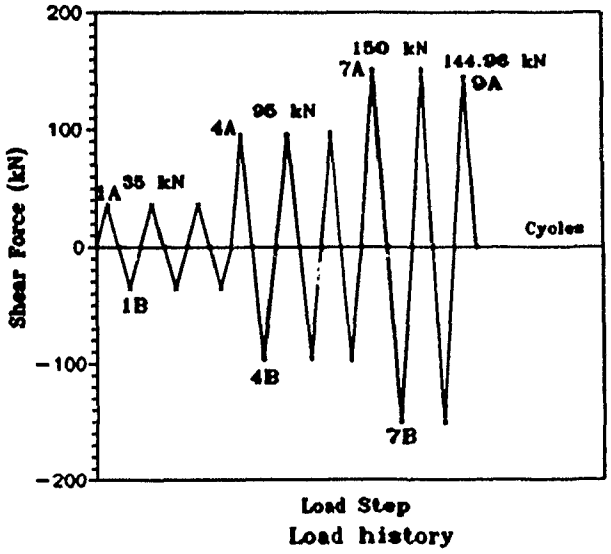

Figure 4.1 Hysteresis response of Specimen S1

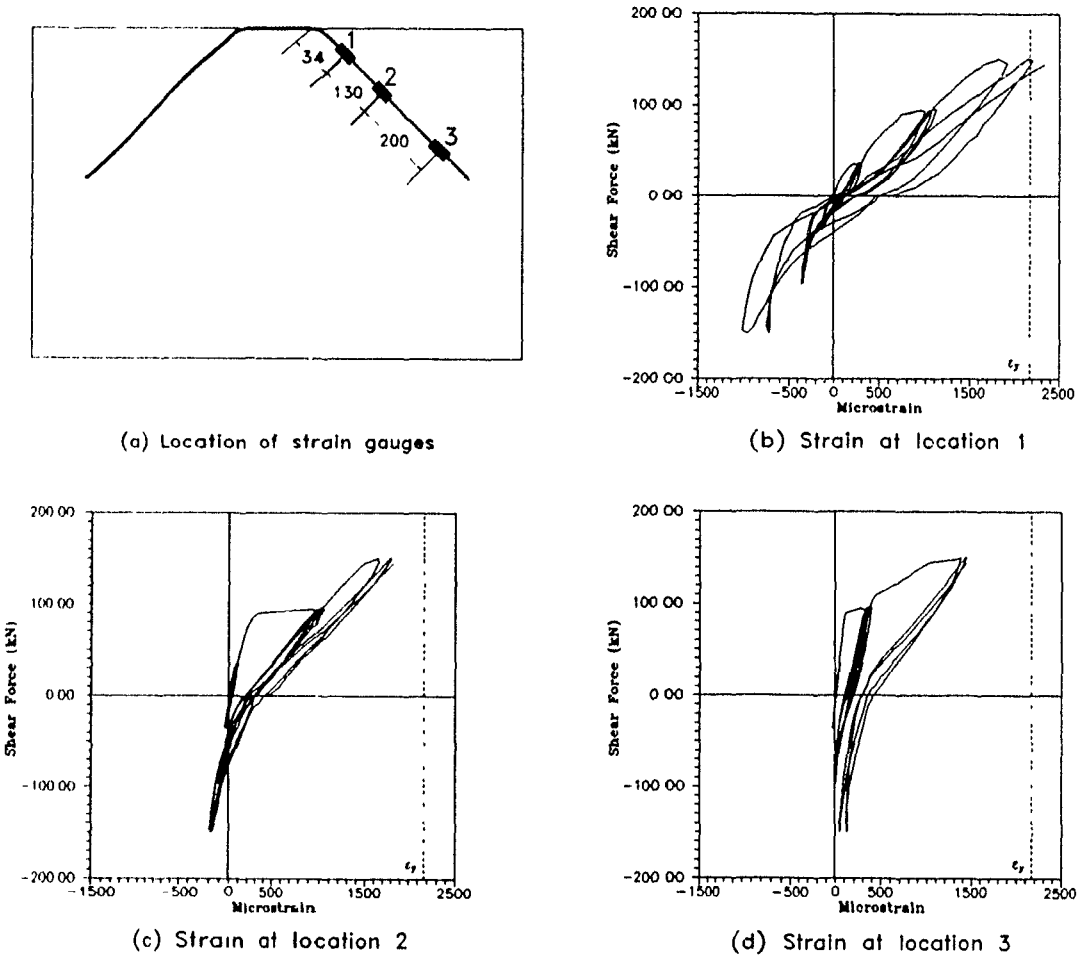

Figure 4.2 Measured strains along the length of reinforcing bar anchor Specimen S1

The previous crack along the length of the reinforcing bar had widened significantly and extended. The strain values at Locations 1 and 2 were very close, showing very little force transfer due to bond between Locations 1 and 2. The maximum strain was 980 x 10^{-6} which is 47% of the yield strain, see Figure 4.2.

4.2.4 Load Cycles 7 - 9

As the applied load was increased to 150 kN (Cycle 7A), the splitting crack along the reinforcing bar extended further, and more diagonal cracks appeared perpendicular to the splitting crack (Figure 4.4b). As seen in Figure 4.3, the

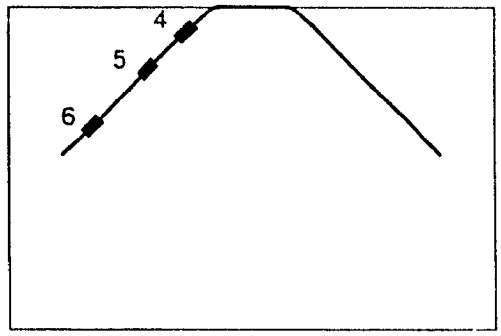

(e) Location of strain gauges

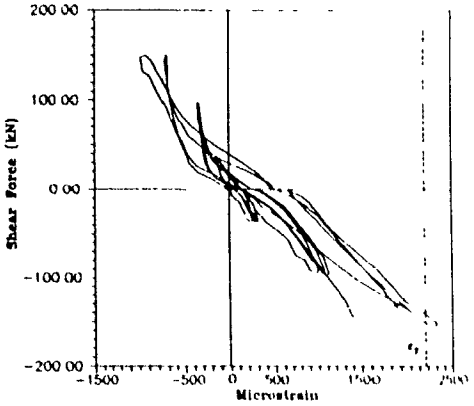

(f) Strains at location 4

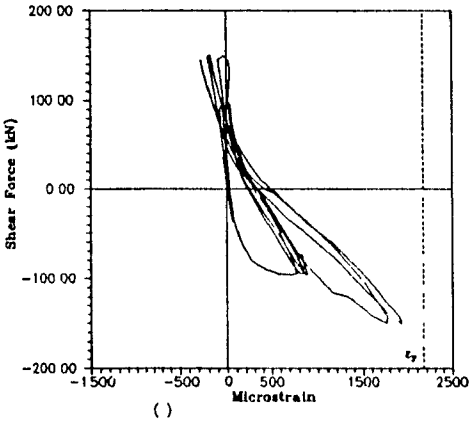

(g) Strains at location 5

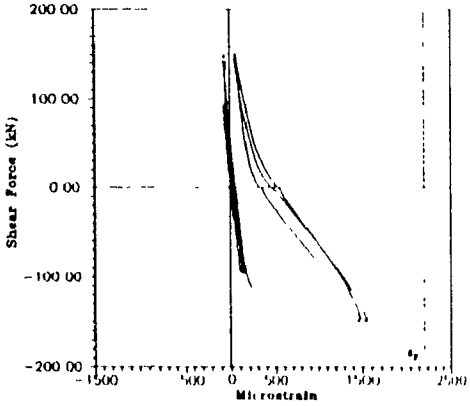

(h) Strains at location 6

Figure 4.2 (Continued) Measured strains along the length of reinforcing bar anchor Specimen S1

maximum principal strains at all three sets of demec gauges (Locations 1, 2 and 3) along the reinforcing bar were computed to be more than the cracking tensile strain of the concrete, which explains the appearance of the diagonal cracks along the anchor bar until its end. As can be seen in Figure 4.1, the displacement changed significantly by more than twice the displacement at the end of load stage 6A, indicating energy dissipation in the connection system. The maximum measured crack width was 0.8 mm. In the following cycle of this load stage 8, the reinforcing bar yielded and the measured horizontal displacement was 3.8 mm (Δ_y). Since the bar in the compression zone did not yield, there was no significant change in the load

- deflection curves. The same behaviour was observed with the loading in the reverse direction (see Figure 4.4b).

Failure occurred in the next cycle at a maximum load of 145 kN due to brittle fracture of the reinforcement close to the weld (see Figure 4.4c). At this load stage, the horizontal displacement was 5.72 mm, giving a displacement ductility of μ = 5.72/3.8 = 1.5. Figure 4.5 presents the Load - vertical displacement characteristics of the connection faceplate. This vertical displacement is due to the slipping of the bar on account of the cracks along and normal to the bar and the resulting rotation of the connection. In the prototype system, some of this displacement is prevented by the adjacent flange.

Figure 4.1 shows a change of stiffness and a significant increase in the displacement during Cycle 7A, which is due to diagonal and splitting cracks (see Figure 4.4b). It should be noted that the factored design capacity is calculated using ϕ_s = 0.85, this capacity is 0.85 V_{ult} = 0.85 x 140 = 119 kN. It shows that up to the factored design load, the behaviour under the cyclic loading is very close to that under monotonic static loading. The energy dissipated and the residual displacement are very small due to the elastic behaviour of the anchorage bar.

The variation of strains along the length of the reinforcing bar at ultimate load are presented in Figure 4.6 which indicates that approximately more than one third of the reinforcing bar has yielded when the bar was subjected to tension.

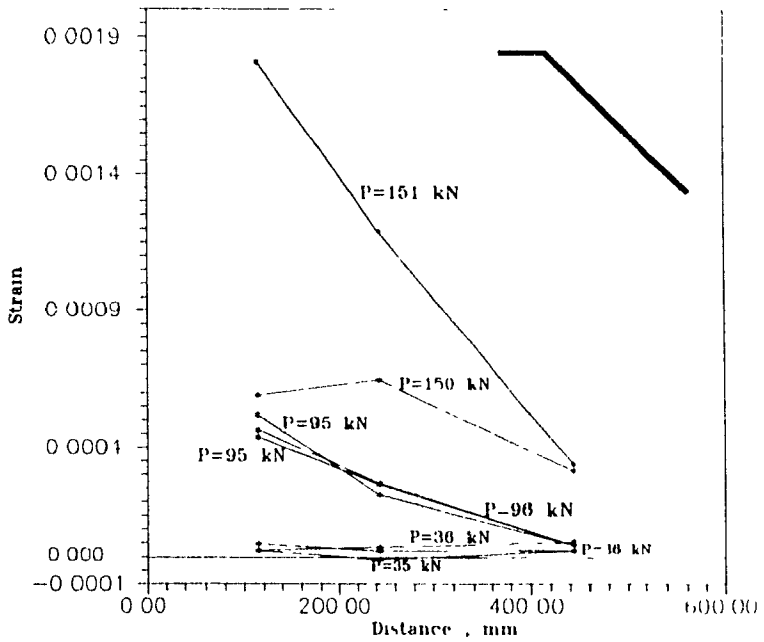

(a) Maximum principal strains, right side, positive load

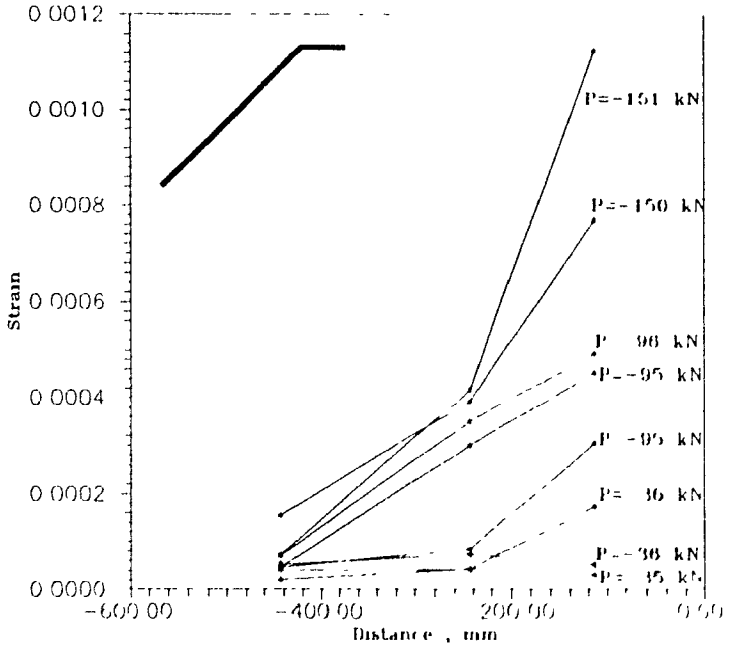

(b) Maximum principal strains, left side, negative load

Figure 4.3 Maximum principal strain distribution in the panel along the length of reinforcing bar, rosette measurements, Specimen S1

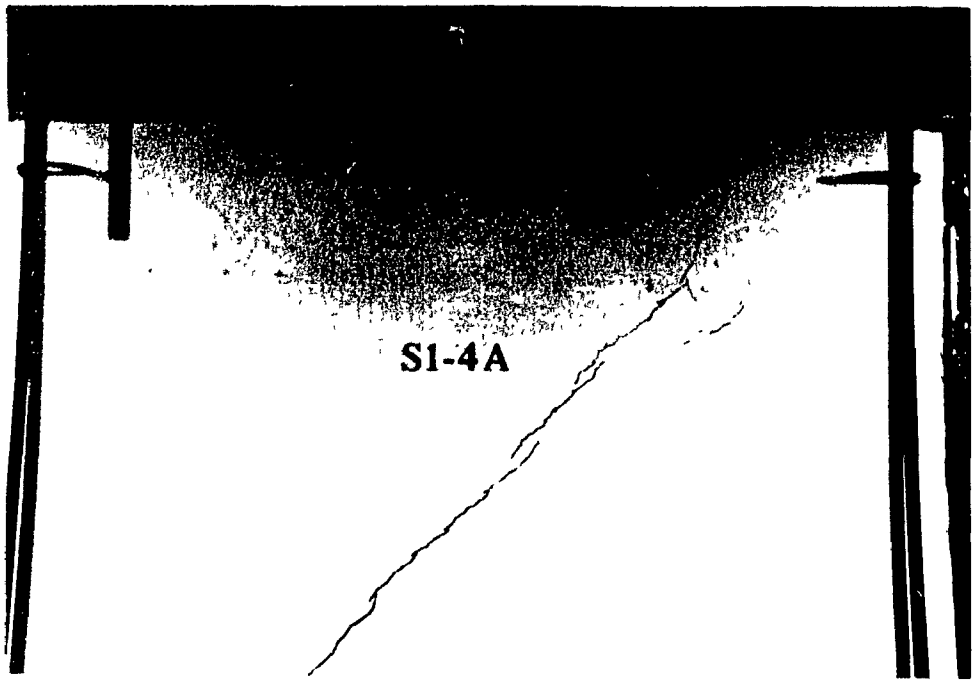

(a) Crack pattern of connection at 50% of P_{ULT}, P=96 kN

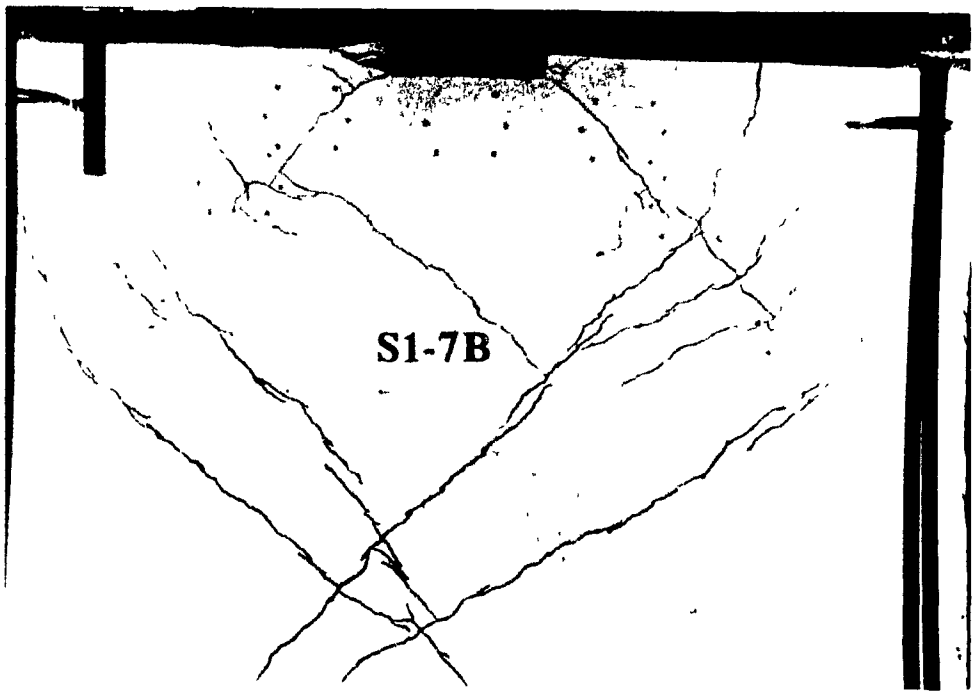

(b) Connection at $1\Delta_y$, P=150 kN

Figure 4.4 Photographs of Specimen S1

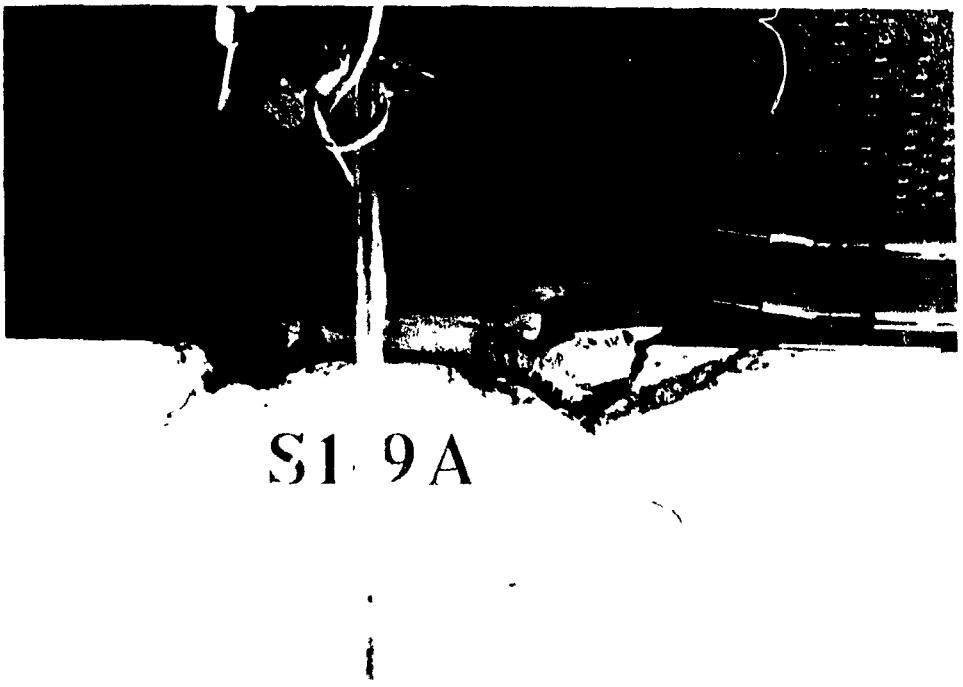

(c) Connection close-up at failure

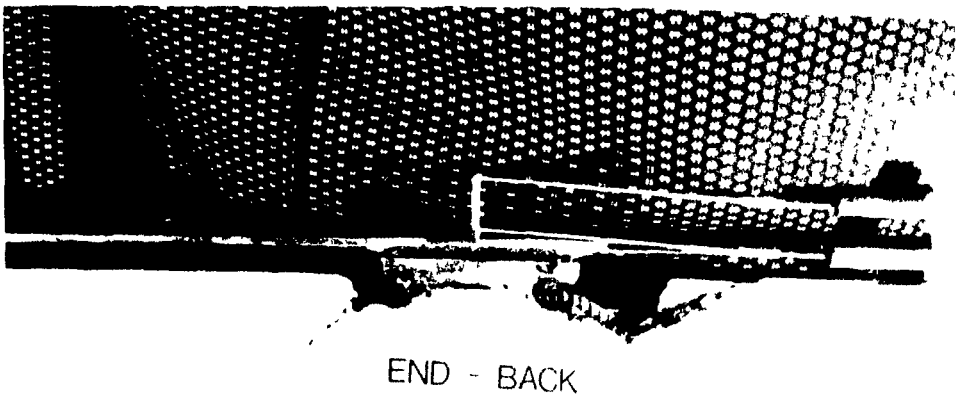

(d) Connection close-up at the end of test

Figure 4.4 (Continued) Photographs of Specimen S1

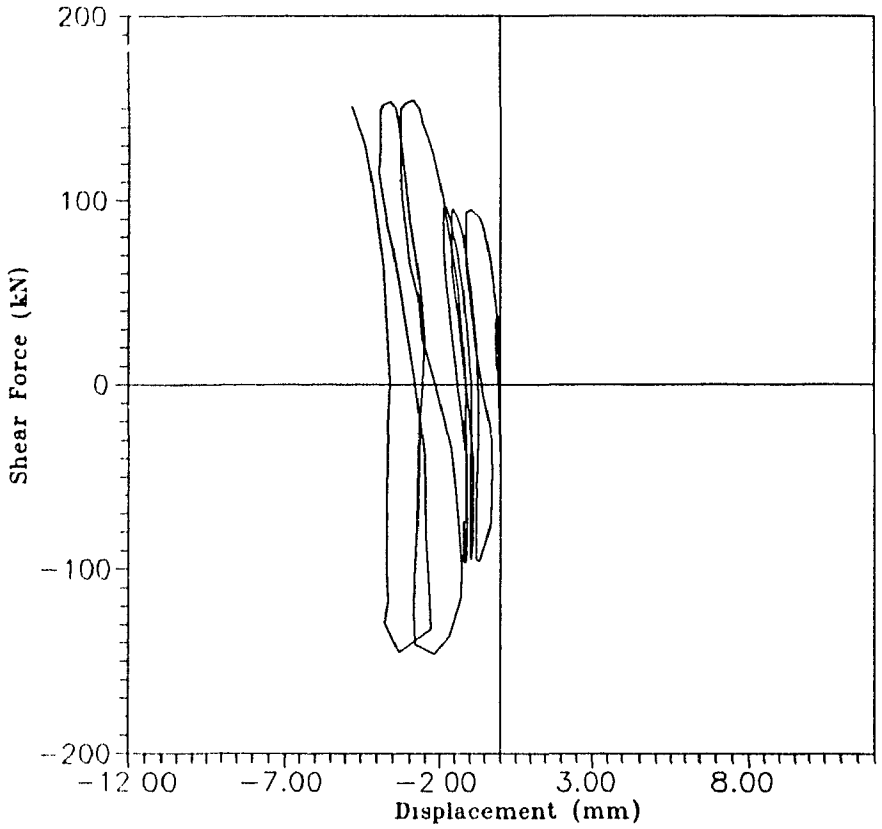

Figure 4.5 Load vs. vertical displacement Specimen S1

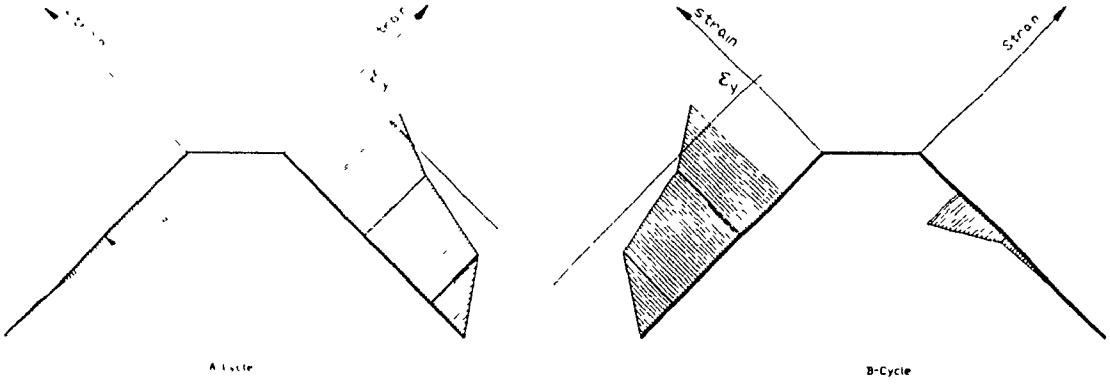

Figure 4.6 Strain vs. distance along the length of reinforcing bar prior to failure, Specimen S1

4.2.5 Crack Width at Peak Cycle Loads

The maximum crack width for the peak load in each load step is plotted in Figure 4.7 which also shows the best fit curve to the experimental results. The crack width, d_{max}, is related to the peak load, P, for positive loading by the following equation:

$$P = +666\, d_{max} - 1943\, d_{max}^2 + 2726\, d_{max}^3 - 1307\, d_{max}^4 \qquad (4\text{-}1)$$

and for negative loading,

$$P = -761\, d_{max} + 2423\, d_{max}^2 - 3435\, d_{max}^3 + 1625\, d_{max}^4 \qquad (4\text{-}2)$$

The area under this curve is an indicator of the fracture energy absorption characteristic of the connection.

4.2.6 Bond Between Steel Plates and Concrete Panel

The bond between the steel plate epoxied to the perimeter of the concrete panel was examined at different stages of the experiment and it was found to be intact everywhere. A plot of the measured deflection of the epoxied steel plate with the load variation is shown in Figure 4.8 which illustrates a basic linear response.

4.2.7 Summary- Specimen S1 was subjected to the loading history outlined in Table 4.1 and Figure 4.1, with six load cycles beyond the factored design load of 110 kN As can be seen in Figure 4.1, most of the deflection occurred after the development of diagonal cracks and significant extension of the splitting cracks along the length of the bar. Well rounded hysteresis loop were observed after the sixth cycle
A displacement ductility of 1.5 was achieved. The maximum load applied was 150 kN which is 82% of predicted monotonic ultimate capacity, while the failure occurred due to fracture of the reinforcing bar close to the weld. The importance of fully welding all of the straight part of the bar to the face plate was apparent. Also the steel plate epoxied to the panel remained intact during the reversed cyclic loading (see Section 4.2.6).

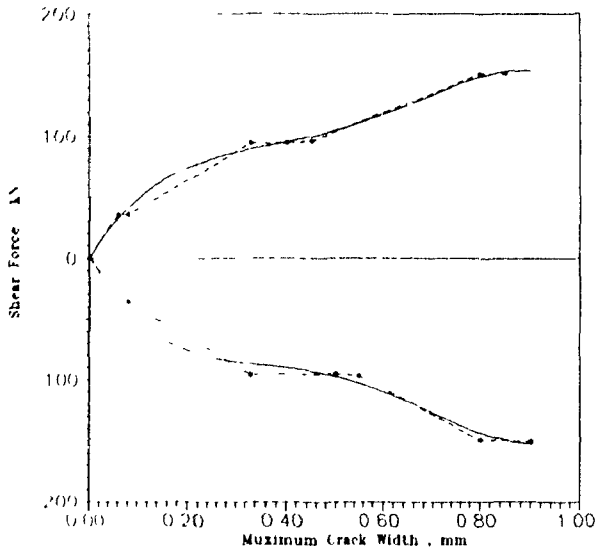

Figure 4.7 Peak loads vs. maximum crack width Specimen S1

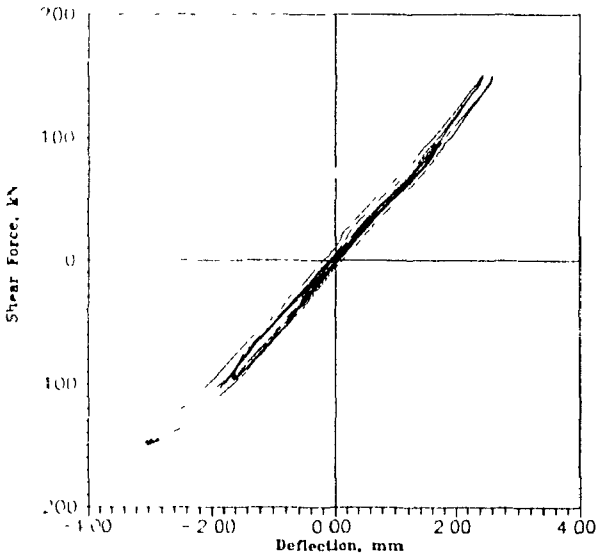

Figure 4.8 Load vs. deflection of steel frame as modelled, Specimen S1

4.3 Test Specimen S2

4.3.1 The Specimen

Specimen S2 was reinforced with a No.15 bar,bent at 45°and with a right angled hook as shown in Figure 2.16. A 75 mm x 200 mm x 12 mm thick plate was welded to the reinforcing bar anchor and a uniform wire fabric mesh identical to that of Specimen S1. It must be noted that the full horizontal straight part of the reinforcing bar, 200 mm, was welded to the plate. As for Specimen S1, this specimen was designed and detailed with special consideration for development length under low - cycle loading[20].

4.3.2 Loading History and Cycles 1 - 6

Table 4.2 summarizes the loading history for Specimen S2. As can be seen from Figures 4.9 and 4.10, and Table 4.2, the specimen was loaded through three elastic cycles at a peak load of 26 kN (Load Cycles 1 - 3), followed by three cycles at a peak load of 55 kN (Load Cycles 4 - 6). Figure 4.11a reveals that the maximum principal strains at the end of the third elastic cycle (3B) were smaller than the concrete failure tensile strain. The first crack appeared on the concrete surface coincident with the starting point of the inclined reinforcement, at a load of 42 kN in Cycle 4A, see Figure 4.11a. The crack was directed along the line of the reinforcing bar. This caused a change in the stiffness, as can be seen from Figure 4.9.The same crack pattern occurred at the opposite side of the joint when the connection was subjected to a negative load of 32 kN (see Figure 4.11b). The crack on the back side of the Specimen was noticed during Cycle 6.

4.3.3 Load Cycles 7 - 9

When the load was increased to 85 kN, a diagonal crack appeared at 175 mm below the top concrete surface, where the thickness of the panel changes, while the splitting crack extended along the bar. A symmetric crack pattern formed when the specimen was loaded in the opposite direction. Figures 4.11a and 4.11b show that at a distance of 247 mm along the bar, the location at which the crack occurred had

Table 4.2 Summary of Loading History for Specimen S2

Cycle	Load Stages	Horizontal Displacement (mm) **	Shear Force V (kN)
Elastic	1A - 3B	+0.13, -0.07	±26
Cracked	4A - 6B	+0.33, -0.27	±56
40% P_{ult}*	7A - 9B	+0.83, -1.51	±85
50% P_{ult}	10A - 12B	+2.02, -2.55	±112
60% P_{ult}	13A - 15B	+3.05, -4.69	±133
70% P_{ult}	16A - 18B	+4.47, -7.48	±155
80% P_{ult}	19A	+6.61	+170
82% P_{ult}	19B	-8.92	-175
75% P_{ult}	20A	+7.15	+160
82% P_{ult}	20B	-9.78	-175
80% P_{ult}	21A	+7.78	-170
82% P_{ult}	21B	-10.51	-170
Failure	22A	+8.36	+151
Failure	22B	-13.00	-146

* Calculated maximum strength under monotonically increasing loads (182 kN)

** Maximum displacement at the peak load of the last cycle

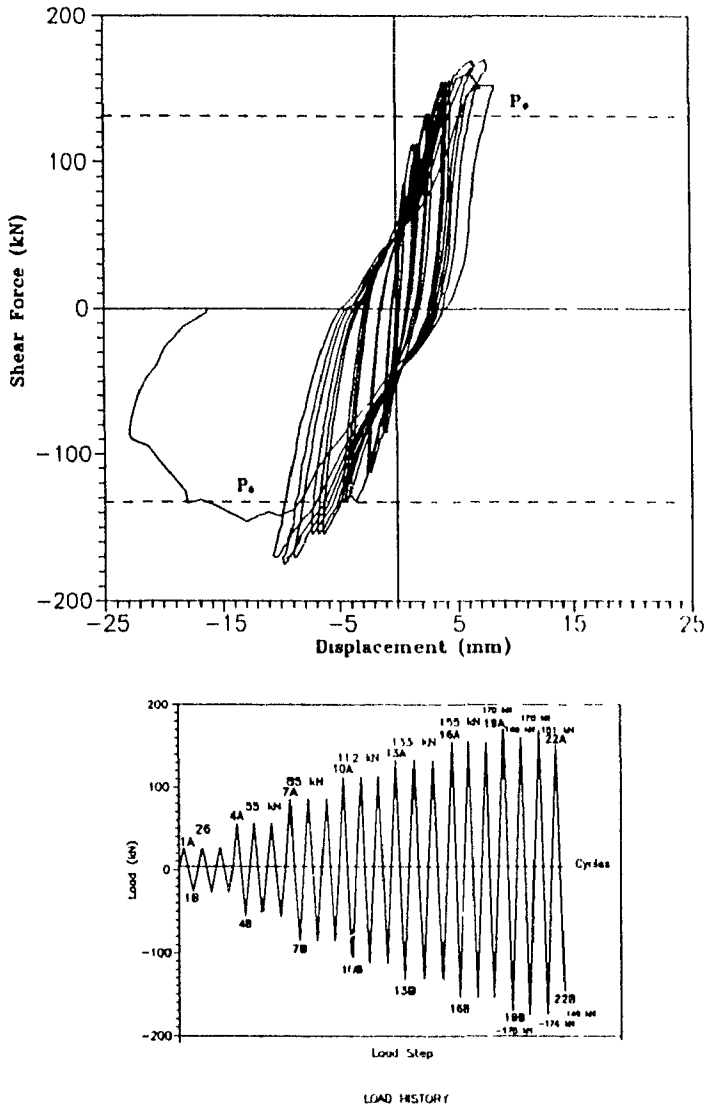

Figure 4.9 Hysteresis response of Specimen S2

maximum principal strains greater than the tensile cracking strain of the concrete. During the following two cycles at the same load, the diagonal crack and the splitting crack propagated, especially due to the reversed cyclic loadings. The maximum crack width was 0.30 mm. The maximum strain at Location 1 of the reinforcing bar was 850 x 10^{-6} which indicates that the steel bar was still in the elastic range (see Figure 4.10b).

4.3.4 Load Cycles 10 - 12

The maximum load for the next load stage (Cycle 10A) was chosen to be 112 kN based on the observation of two more significant diagonal cracks around the hook part of reinforcing bar. For loading in the positive direction, the tensile strain in the bar around the end part of straight embedded part in tension zone increased because of dowel action and tension force in steel bar. Consequently, one crack appeared approximately 30 mm before the beginning of the hook while the other appeared at the end of the bend. It should be noted that the maximum principal strains computed using the strain data from demec gauges were considerably larger than the concrete cracking strain (Figures 4.11a and 4.11b). As seen in Figures. 4.11a and 4.11b, the principal strains at Locations 1 and 3 are larger than that at Location 2 in the higher cycles. This is due to dowel action and the bearing stresses around the hook part at Locations 1 and 3, respectively. The maximum measured anchorage strain at Location 1 was 1620×10^{-6}, which is about 73% of the steel yield strain. The maximum width of the crack observed was 0.6 mm. No significant changes in the displacements and bar strains were observed during the following two cycles at this load stage. The load - deflection curves remained relatively linear up to the end of these load steps (Cycle 12), indicating that the stiffness and strength degradation is insignificant.

4.3.5 Load Cycles 13 - 15

The specimen was then subjected to three load cycles (Cycles 13 - 15) at a load of 133 kN, to investigate the cyclic response of the connection about factored design capacity . The first diagonal crack extended to the edge of the specimen, while the maximum strain in the steel bar was 1985×10^{-6}. It shows that up to the designed factored capacity, the reinforcing bar remained in the elastic range. The maximum measured crack width at the peak of cycle 15A was about 0.95 mm. The maximum displacements at the first cycle(13A) and the last cycle of this load stage (15A) were 2.38 mm and 2.60 mm, respectively. Consequently, by reversing load at a peak load stage of 133 kN, there was not a significant increase in the displacement. A symmetrical crack pattern formed on the other side of the connection during the

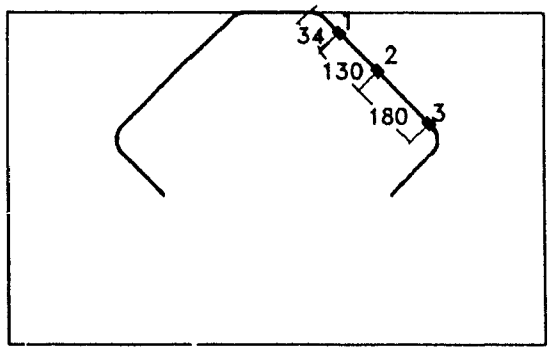

(a) Location of strain gauges

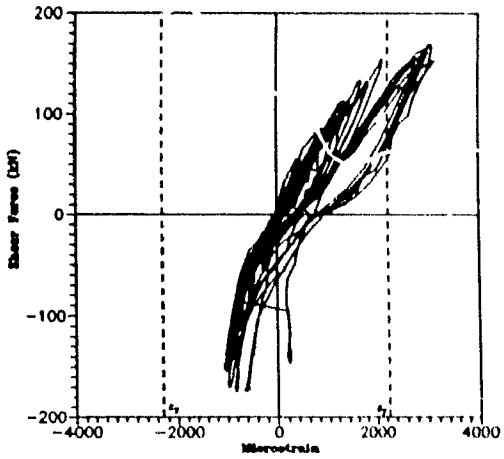

(b) Strains at location 1

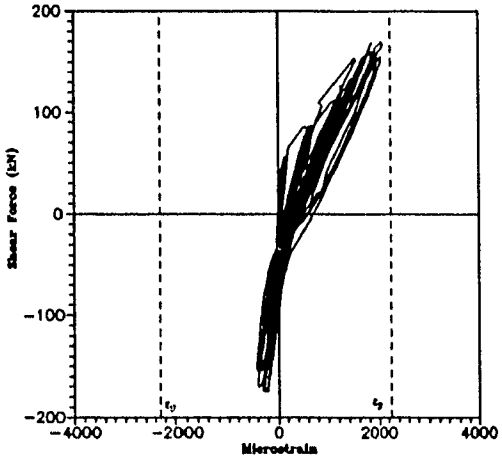

(c) Strains at location 2

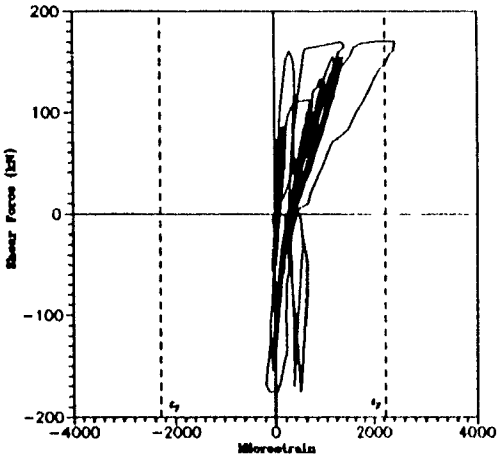

(d) Strains at location 3

Figure 4.10 Measured strains along the length of reinforcing bar anchor Specimen S2

negative loading.

4.3.6 Load Cycles 16 - 18

The specimen was then subjected to three cycles with a peak load of 155 kN (Cycles 16 - 18), which is about 70% of the monotonic ultimate load. The first yielding was expected to occur at a load between 150 and 160 kN. It should be mentioned that based on the hand method of analysis (truss analogy), the reinforcing

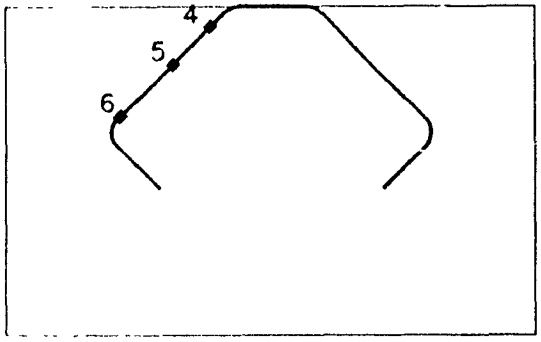

(e) Location of strain gauges

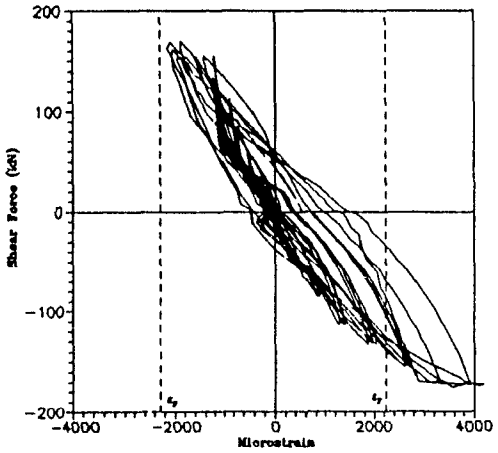

(f) Strains at location 4

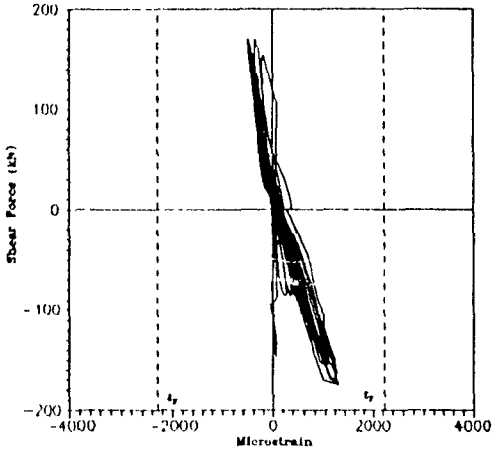

(g) Strains at location 5

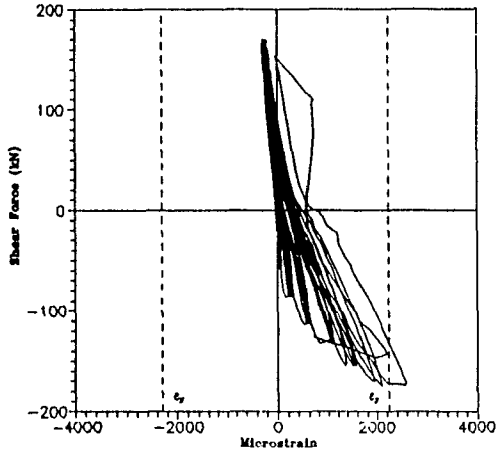

(h) Starins at iocation 6

Figure 4.10 (continued) Measured strains along the length of reinforcing bar Specimen S2

bar should have yielded at a load of 140 kN, but the yielding was delayed since the surrounding concrete was resisting some of the tension. The maximum displacement at the first cycle was 3.8 mm. The measured strain at Location 1 was 2170 x 10^{-6} which is close to the yield strain of the steel bar (see Figure 4.10a). Upon load reversal, the reinforcing bar yielded at Location 4 at a load of 135 kN, while the measured displacement at yield was -5.2 mm. In the next load cycle (Cycle 17), the strain at Location 1 exceeded the yield strain.

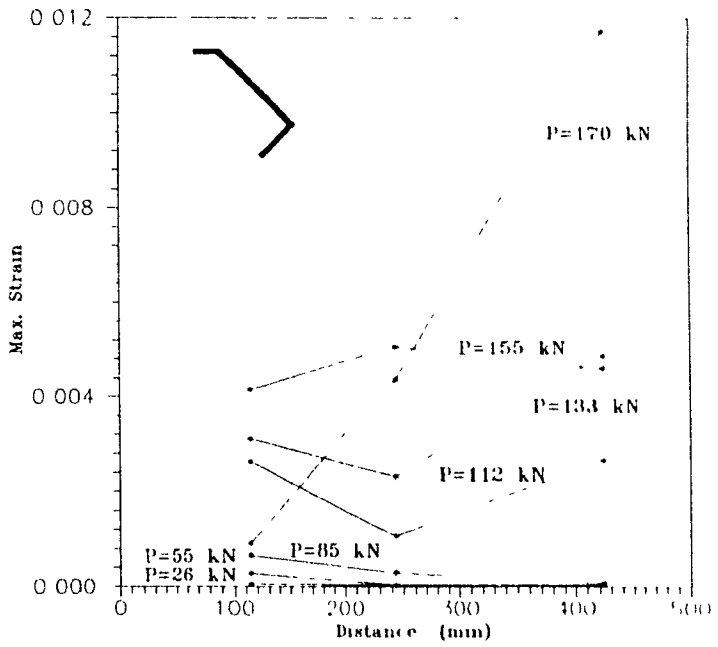

(a) Maximum principal strains, right side, positive load

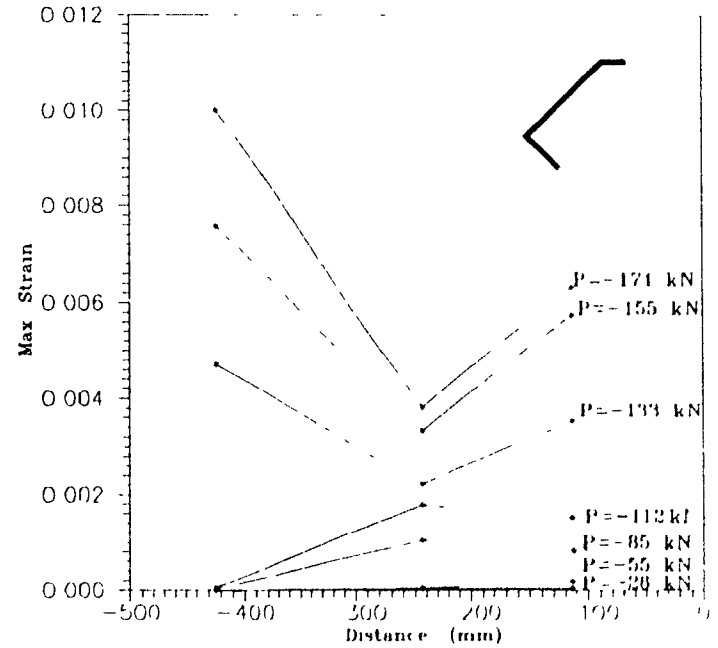

b) Maximum principal strains, left side, negative load

Figure 4.11 Maximum principal strain distribution of panel along the length of reinforcing bar, rosette measurements, Specimen S2

The displacement at yield during the positive load cycle was measured to be 3.3 mm (Δ_y). In the next cycle, the strains at both Locations 1 and 4 did not change considerably. The photograph of the connection region at the first yield in Figure 4.12a shows these features.

4.3.7. Load Cycles 19 - 21

As the load was increased to 170 kN (Cycle 19A), which is about 80% of the ultimate design load, the measured displacement was 6.6 mm ($2\Delta_y$). When a load of 175 kN was imposed during the negative cycle, the measured displacement was -8.9 mm. An additional splitting crack was observed under the hook in compression basically due to compression under the hook and dowel action in the bar resulting in the splitting crack. In the next cycle, at a load of 160 kN (Cycle 20A), the first diagonal crack at the location of change in panel thickness was completely open, and the wire fabric mesh across that crack was fractured. Also, the second diagonal crack near the end of the straight part opened significantly on both faces of the specimen. This caused a reduction of 13 kN in the peak load, as presented in Table 4.2. This effect can be seen in the hysteresis loop in Figures 4.9 and 4.10b. In addition the maximum principal strains at Locations 1 and 2 decreased considerably (see Figure 4.11a). It was noted that the splitting crack in the compression zone extended to the end of the straight part of anchorage because of the high compressive force in the reinforcing bar. During the following cycle (21), the specimen was loaded to 170 kN and the measured displacement was 7.6 mm. The maximum crack width was 11 mm. The stiffness for the cycles of this load stage (Cycles 19 - 21) decreased significantly in comparison with previous load stages which were due to more yielding of a part of the reinforcing bar. A photograph in Figure 4.12b shows the crack pattern at a lateral deflection of 6.6 mm ($-2\Delta_y$).

4.3.8 Load Cycle 22

Finally, one cycle at maximum loads 150 kN (22A) and -146 kN (22B) for its positive and negative peaks, respectively, was imposed. During positive loading (Cycle 22A), the cover around the hook bend spalled off more on the backside of the

specimen and a gap of 4 mm formed between the anchor bar and the concrete, indicating complete movement of the hook bend in the plane of the concrete panel. The measured displacement was 8.36 mm giving a displacement ductility of 2.5. Figure 4.12c presents a close up photograph of the hook region at this stage ($2.5\Delta_y$). Upon load reversal, the cover spalled off and the splitting crack along the bar length extended below the hook part (see Fig 4.13d), resulting in an increase in the displacement (see Figure 4.9). The gap between the reinforcing bar and the concrete was measured to be about 3.5 mm. The test was stopped because both hooks rotated out of the plane of the concrete panel. The load was gradually decreased to zero. This was accompanied by a rapid increase in the displacement. The measured displacements were 8.4 mm and -13 mm at the peaks of Cycles 22A and 22B, respectively.

Figure 4.13 shows the load - vertical displacement characteristics of the specimen. This displacement is due to the splitting of the concrete along reinforcing bar as a result of cracking along and perpendicular to the bar causing rotation of the connection. The flange of the adjacent tee in an actual structure prevents some of this displacement.

The profile of strains along the length of the reinforcing bar is shown in Figure 4.14. The entire inclined straight part of the reinforcing bar with the exception of the middle part had yielded.

The mode of failure observed was the splitting of the concrete along the length of the bar and crushing of the concrete in front of the hook bend. It must be mentioned that after splitting of the crack along the full length of the straight part of the bar, all of the load resistance got concentrated in the hook part which failed in turn. Consequently, the residual displacements were significant. Also the hysteretic load - deflection response loops were more well-rounded, resulting in large areas within the loops and more energy dissipated than in Specimen S1. A photograph of Specimen S2 after testing is presented in Figure 4.12(e).

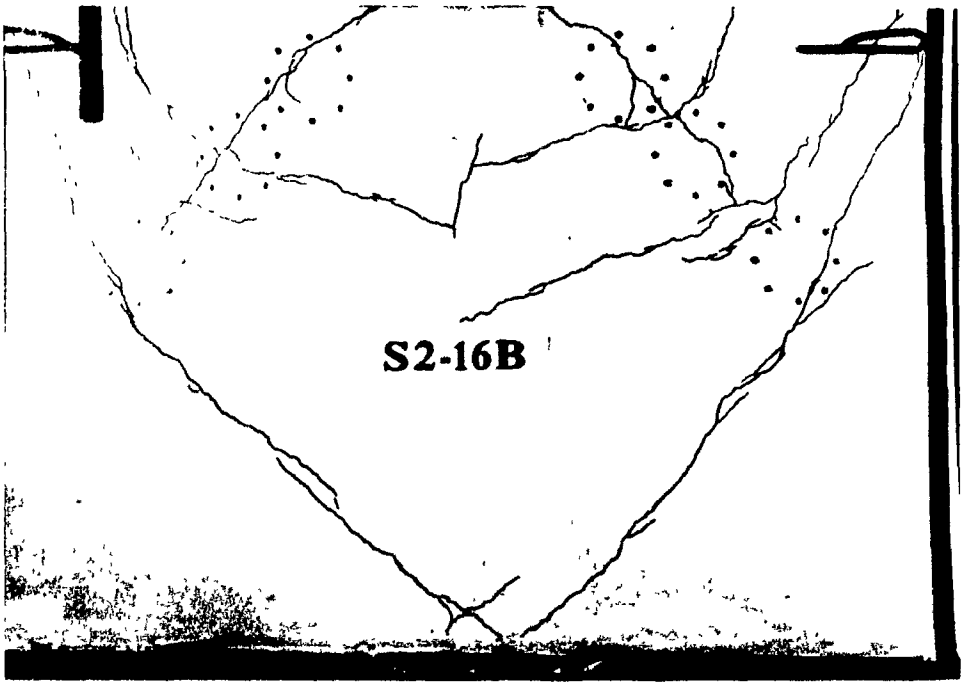

(a) Connection at first yield, Δ_y , P=155 kN

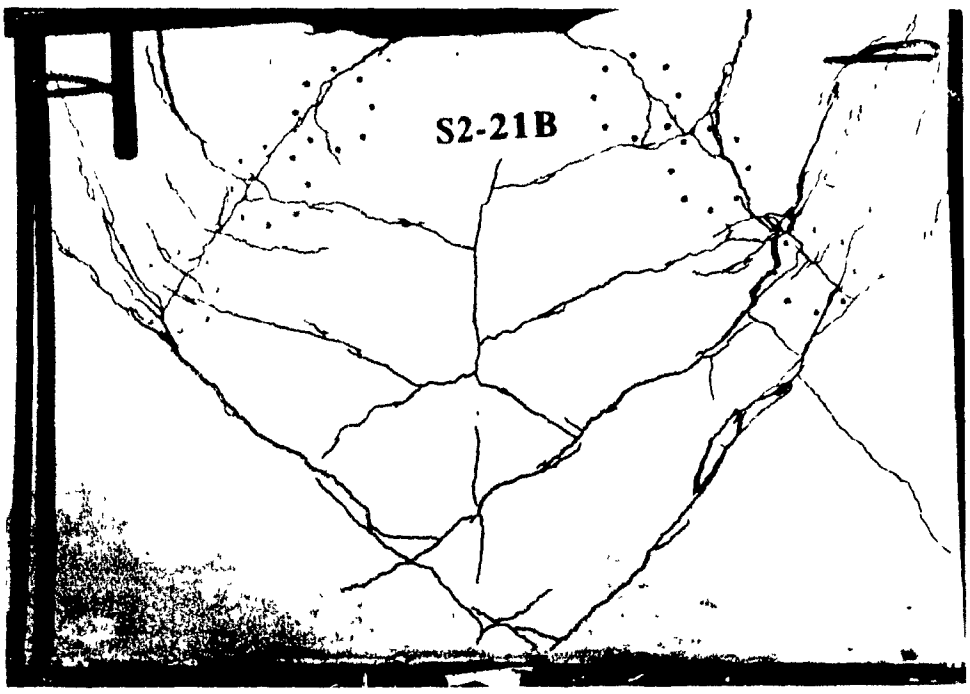

(b) Connection at $-2\Delta_y$, P=170 kN

Figure 4.12 Photographs of Specimen S2

(c) Connection close-up at $2.5\Delta_y$, hook region, back side

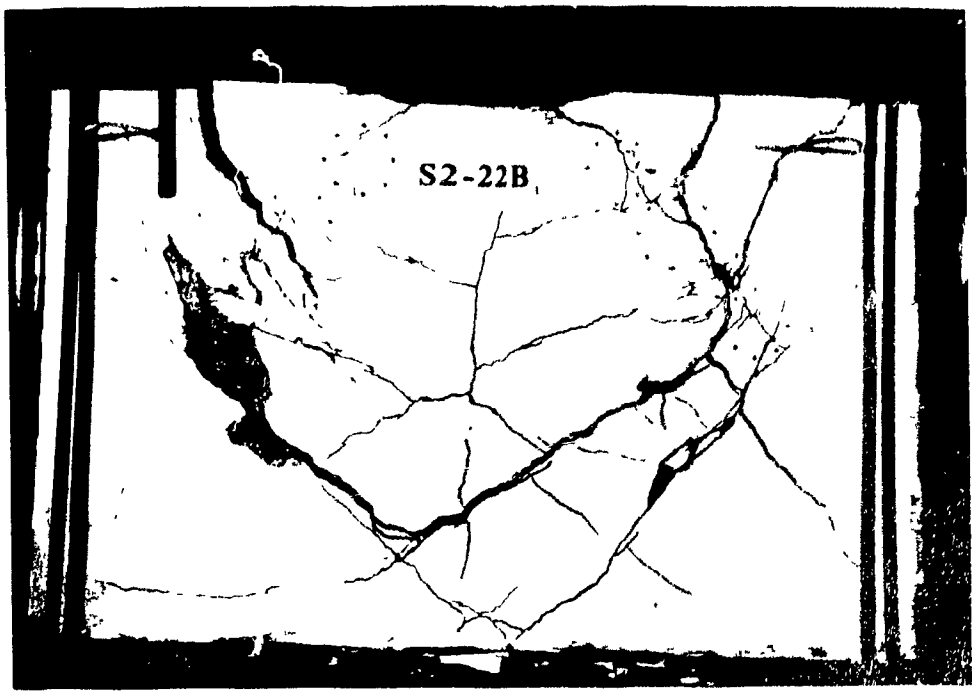

(d) Connection at $-2.5\Delta_y$

Figure 4.12 (Continued) Photographs of Specimen S2

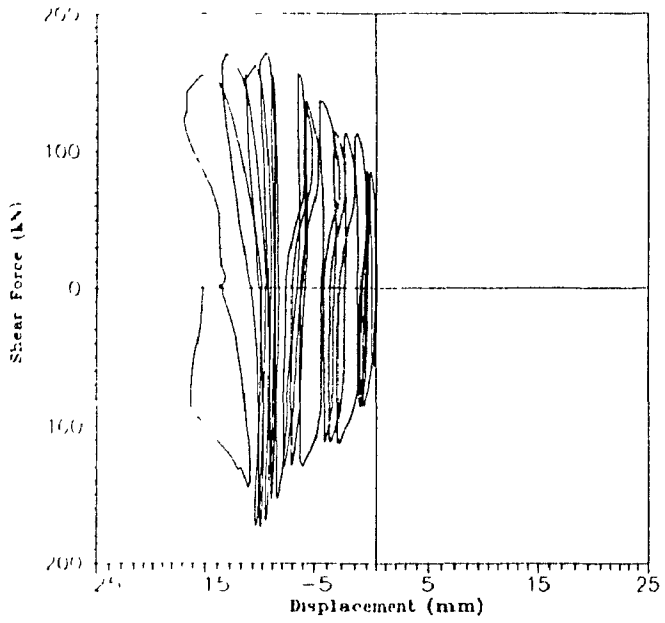

Figure 4.13 Load vs. vertical displacement Specimen S2

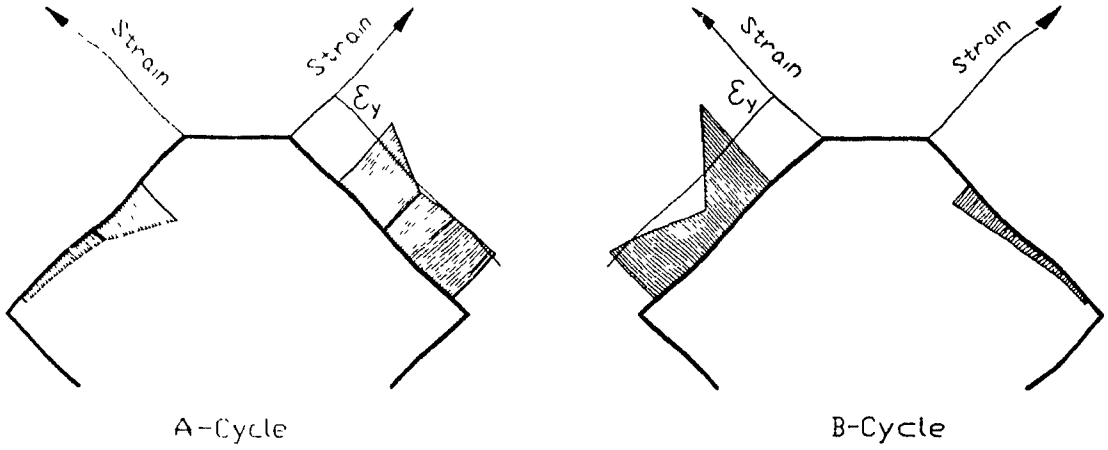

Figure 4.14 Strain vs. distance along the length of reinforcing bar prior to failure, Specimen S2

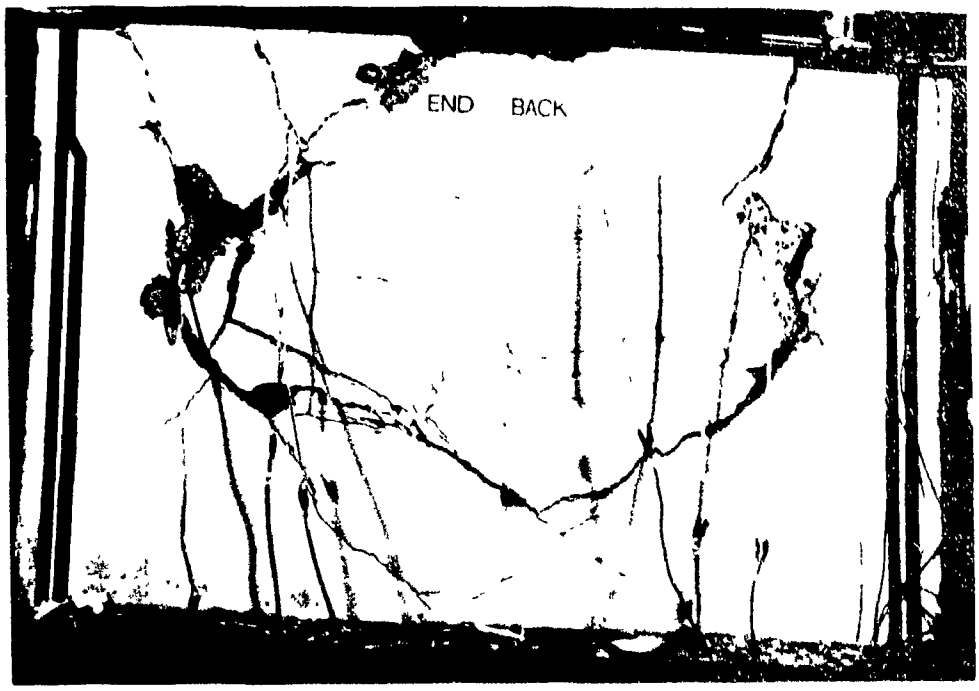

(e) Specimen after testing

Figure 4.12 (Continued) Photographs of Specimen S2

4.3.9 Crack Width at Peak Cycle Loads

The maximum crack width variation in the tensile zone for this type of load history at peak load of each stage is presented in Figure 4.7 which also shows the "best fit" curves to the experimental results. These curves are expressed by the following equations: For positive loading,

$$P = + 658.5\, d_{max} - 1893\, d_{max}^2 + 2697\, d_{max}^3 - 1692\, d_{max}^4 + 382.5\, d_{max}^5, \qquad (4.3$$

and for negative loading,

$$P = - 641.5\, d_{max} + 1546\, d_{max}^2 - 1822\, d_{max}^3 + 960\, d_{max}^4 - 183.5\, d_{max}^5 \qquad (4.4)$$

The area under such a curve is an indicator of the fracture energy dissipation

characteristic of the connection of the specimen.

4.3.10 Bond between Steel Plate and Concrete Panel

The bond between the concrete panel and the steel plate as modeled was tested during the experiment and it was founded to be intact everywhere. Figure 4.16 presents the variation of measured vertical displacement with load which exhibited basically a linear behaviour.

4.3.11 Summary Specimen S2 was subjected to the loading history summarized in Table 4.2 and Figure 4.9, in which the factored design capacity was achieved before yielding of the reinforcing steel at any location. A displacement ductility of 2.5 was achieved. The reinforcing bar did not yield at Locations 2 and 5 (see Figures. 4.10 and 4.14). However, due to stress concentration around the hook, yielding occurred at Locations 3 and 6 only in the last cycle. The specimen failed because of the propagation of the splitting and diagonal cracks along with the cracking of the concrete in front of the hooks, while the applied loads were 170 kN and -175 kN for positive and negative loading, respectively. The load - deflection curves were quite well rounded and the enclosed area within the loops became larger, therefore the energy dissipated increased with an increase in the applied load. The maximum measured load resisted by the specimen was 170 kN which is about 120% and 82% of the predicted ultimate monotonic capacity using the CPCI and the Nonlacs program, respectively.

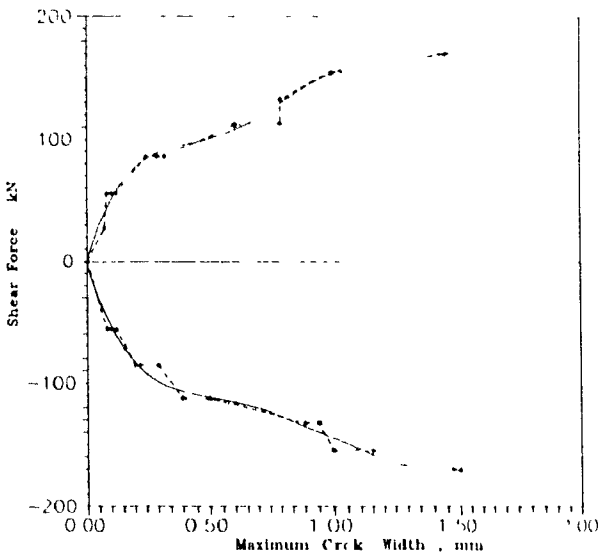

Figure 4.15 Peak loads vs. maximum crack width Specimen S2

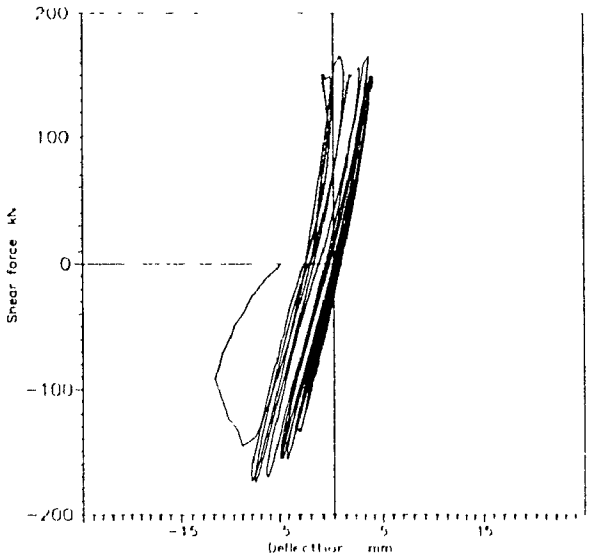

Figure 4.16 Load vs. deflection of steel frame as modelled, Specimen S2

4.4 Test Specimen S3

4.4.1 Test Specimen

Specimen S3 was reinforced with No. 15 deformed bars welded to an angle flange at 90° and a uniform wire fabric mesh, 100 x 100 MW13.3 / MW13.3 (see Figure 2.17). It was designed and detailed with special consideration for the bar development length under low cyclic loading.[20]

4.4.2 Loading History and Cycle 1 - 6

Table 4.3 summarizes the loading history for Specimen S3. As can be seen from Figures 4.17, 4.18 and 4.19 and Table 4.3, the specimen was subjected to three elastic cycles (Cycles 1 -3) with a peak load of 25 kN. The load-deflection response remained quite linear (see Figure 4.17). Figure 4.19 shows that the principal strains related to load P = ±26 kN are all below the cracking strain of concrete, 110 x 10^{-6}. The first crack appeared at the top edge along the reinforcing bar in the following cycle (Peak load = 50 kN) at a load of 35 kN. The maximum crack width was 0.2 mm. The splitting crack along the reinforcing bar was due to dowel action. The load- principal strain curves in Figure 4.19 show that the maximum principal strain is higher than concrete cracking strain 110 x 10^{-6}, causing extension of the crack up to a distance of about 200 mm along the reinforcing bar.

4.4.3 Load Cycle 7 - 9

A peak load of 80 kN (Cycle 7A), 65% of P_{ult}, was chosen based on splitting crack extension to the location coincident with the second strain gauge on the reinforcing bar, 255 mm below the top edge (see Figure 4.18a). The maximum strain was measured to be 1000 x 10^{-6} which is slightly less than half of the yield strain. A horizontal crack was observed between the two reinforcing bars, which shows the tensile - flexural behaviour of the concrete between the bars. The load - deflection curves are almost straight although several cracks had appeared.

Table 4.3 Summary of Loading History of Specimen S3

Cycle	Load Stages	Horizontal Displacement (mm)**	Shear Force V (kN)
Elastic	1A - 3B	0.09, - 0.07	± 25
Cracked	4A - 6B	0.20, - 0.22	± 50
65% P_{ult}*	7A - 9B	0.42, - 0.53	+ 85, - 80
85% P_{ult}	10A - 13B	- 1.40, - 1.80	+ 113, - 107
95% P_{ult}	14A - 15B	4.25, - 5.34	+ 127, - 121
Failure	16A - 16B	5.52, - 6.14	+ 120, - 117

* Calculated maximum strength under monotonically increasing loads (130 kN)

** Maximum displacement at the peak load of last cycle

4.4.4 Load Cycles 10 - 13

As the peak load was increased to 107 kN (Cycle 10A, factored shear resistance, 85% of P_{ult}), diagonal cracks appeared at three locations along the reinforcing bar with the upper one extending close to the edge. It is should be noted that the factored shear strength is governed by the shear-friction principles , and using the reinforcing bar resistance factor, ϕ_s = 0.85, gives the capacity of 0.85 V_{ult} = 0.85 x 130 = 110 kN. Figure 4.20a presents a photograph of the test specimen at the factored capacity of 110 kN. As can be seen from Figure 4.19, the principal strains in the concrete at the load step, P = ± 107 kN, are all higher than the concrete cracking strain of 110 x 10^{-6}. These cracks affect the hysteresis loop, as can be seen in Figure 4.17. The test then continued for another 3 cycles at the same load stage. The splitting cracks continued to open along the reinforcing bar and reached a maximum width of 1.2 mm. It was noted that last load - deflection loop (Cycle 13) in Figure 4.17 was fatter than the preceding loops of this load stage Upon load reversal, the displacement was -1.8 mm.

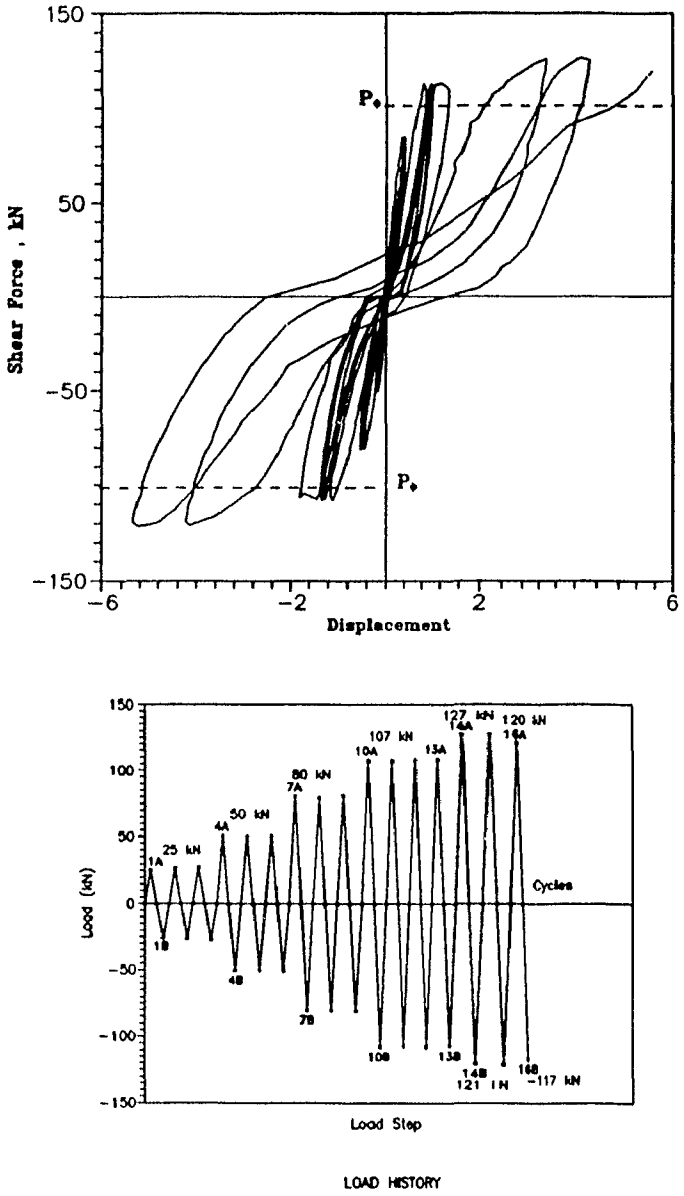

Figure 4.17 Hysteresis response of Specimen S3

4.4.5 Load Cycles 14 - 16

As the load was increased to 127 kN, the reinforcing bar yielded at a displacement of 125 mm below the top edge. This effect is shown on the hysteresis loop, causing an increase in the displacement from 1.3 mm to the yield displacement, Δy, of 3.2 mm (see Figures. 4.17 and 4.18a).

A photograph of the joint region at the first yield is presented in Figure 4.20b. Upon load reversal, the reinforcing bar yielded at a load of 110 kN. At this stage,

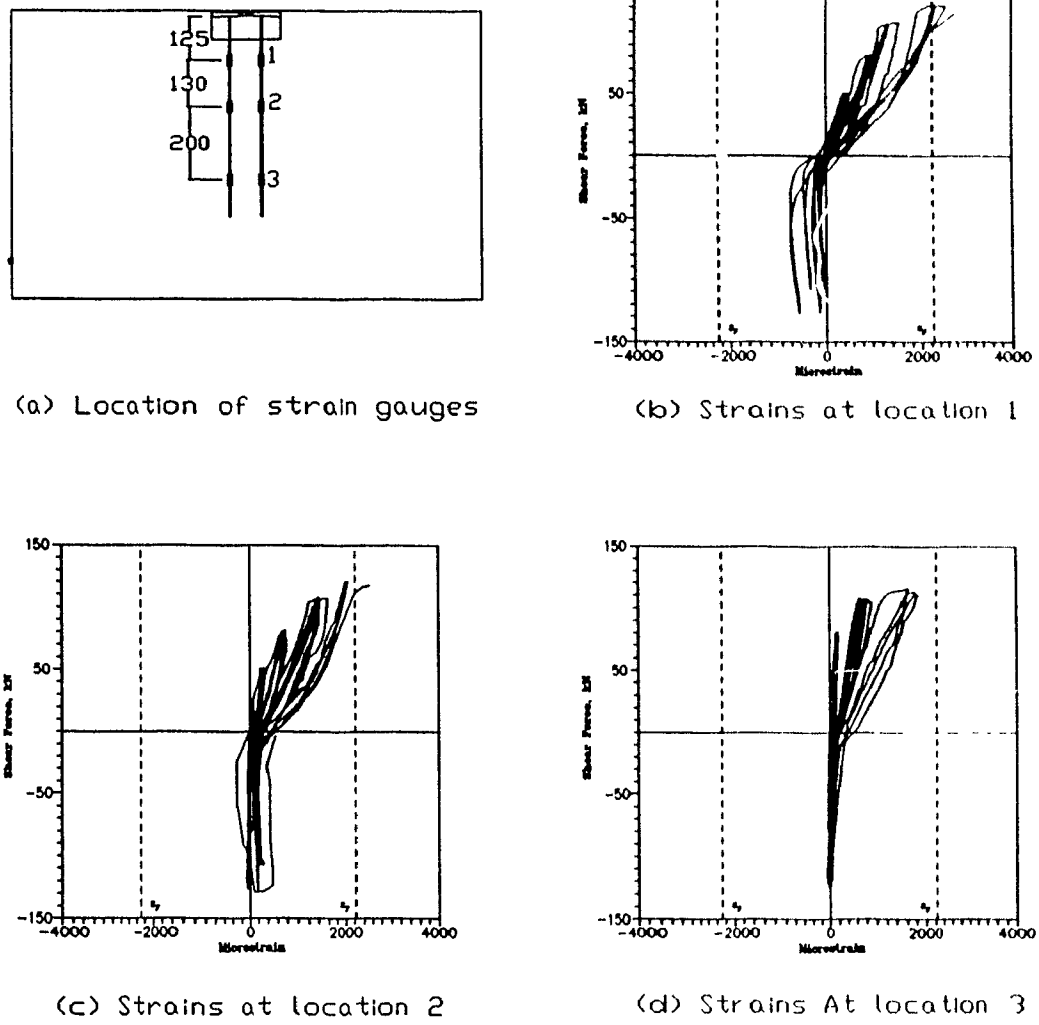

Figure 4.18 Measured strains along the length of reinforcing bar anchor Specimen S3

the lateral displacement was 3.9 mm. The maximum displacement at the peak of the negative load cycle, -121 kN, was -4.2 mm. The test was continued for one more cycle at this load stage. The strain at Location 2 was very close to yield and the maximum width of splitting crack along the reinforcing bar increased to 1.75 mm Figure 4.17 reveals the significant increase in the width of the loops due to yield and several cracks around the embedded flange angle at the specimen back side. The area under the loop increased significantly resulting in more energy dissipation after

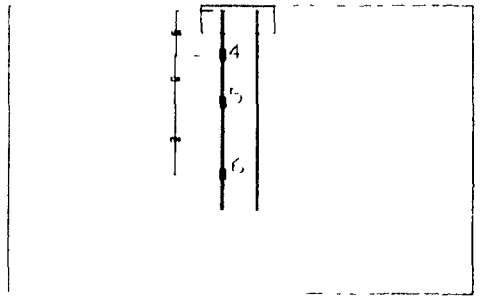

(e) Location of straingauges

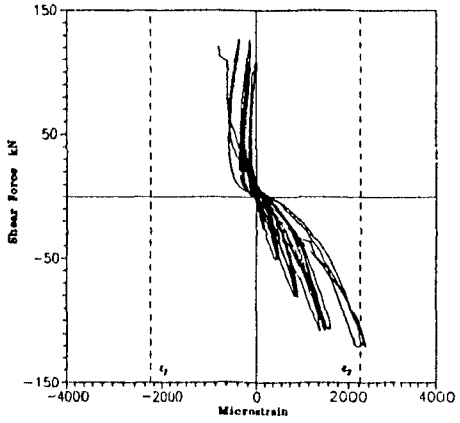

(f) Strains at location 4

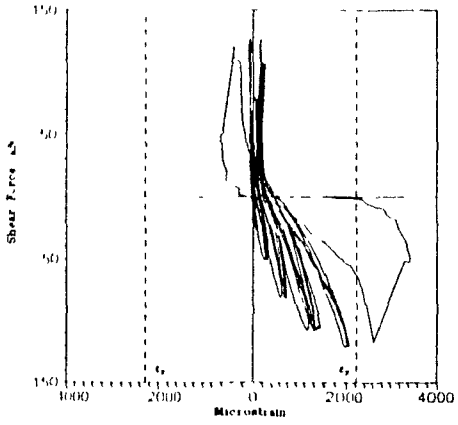

(g) Strains at location 5

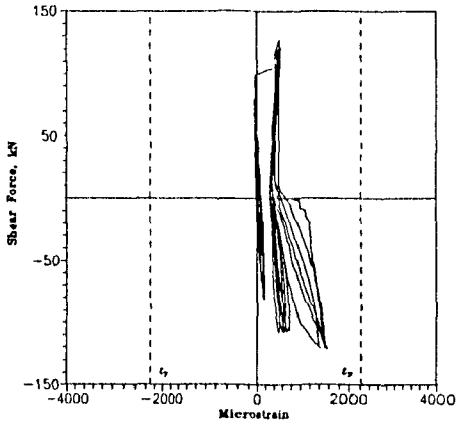

(h) Strains at location 6

Figure 4.18 (Continued) Measured strains along the length of reinforcing bar Specimen S3

yielding of the connection. Finally, the test specimen was subjected to a 120 kN peak load (Cycle 16), when the specimen failed. The concrete cover under the angle had spalled off and the splitting crack extended along the entire length of the bar. Due to full extension of the splitting crack along the bar, the specimen could not carry any more load (see Figure 4.20c).

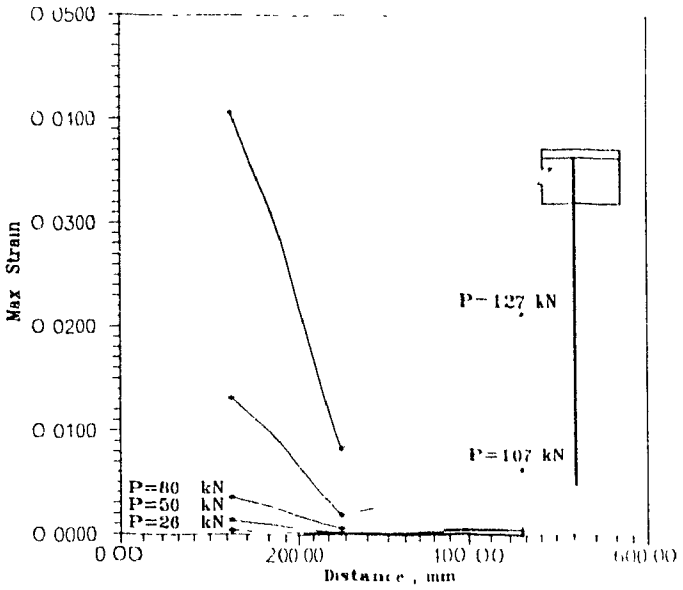

(a) Maximum principal strains, right side, positive load

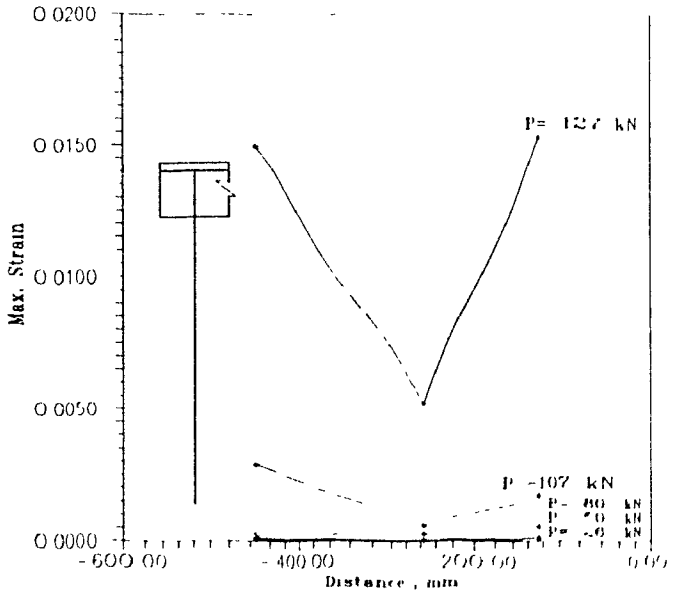

b) Maximum principal strains, left side, negative load

Figure 4.19 Maximum principal strain distribution of panel along the length of reinforcing bar, rosette measurements, Specimen S3

The maximum displacement prior to failure was measured to be 5.52 mm, and the maximum crack width was 2 mm, giving a displacement ductility of μ = 5.5 / 3.2 = 1.7. The specimen was then subjected to a load of 117 kN in the negative direction when the concrete cover under the angle spalled off completely, and the load decreased to 50 kN. The maximum displacement was measured to be 6.14 mm, and the maximum crack width was 2 mm during the reversed loading cycle, the specimen was able to resist a peak load of 117 kN, at which time the load dropped again to about 30 kN. The specimen was unable to resist any further loads and the test was stopped. This cycle was not included in the dissipated energy calculations. Failure of the connection was preceded by progressive crushing and spalling off of the concrete below the angle (concrete cover under the angle flange) and widening of the splitting crack along the bars due to dowel action. The load - vertical displacement characteristics of the connection faceplate are presented in Figure 4.21. The vertical displacement is due to slipping of the reinforcing bar influenced by the diagonal cracks and cracks along the bar and the resulting rotation of the connection. This vertical displacement is somewhat smaller in the actual structure because of the restraint from the adjacent flange.

Figure 4.22 presents the variation of the strain in the steel bar along its length at ultimate load. As can be seen, half of the reinforcing bar had yielded. The strains around the middle third are the largest, which is due to the local effect of dowel action. A photograph of the joint region after failure is presented in Figure 4.20d.

4.4.6 Crack Width at Peak of Load Cycle

Figure 4.23 shows a plot of the maximum crack width for the peak loads of each load step and the "best fit" curve to these experimental results. The curves are represented by the following expressions for positive and negative loadings, respectively:

$$P = + 224\ d_{max} - 156.8\ d_{max}^2 + 39.4\ d_{max}^3; \quad (4\text{-}5)$$

$$P = - 239.8\ d_{max} + 173.4\ d_{max}^2 - 41.6\ d_{max}^3. \quad (4\text{-}6)$$

The area under the curve is indicative of the energy dissipation characteristic of the connection.

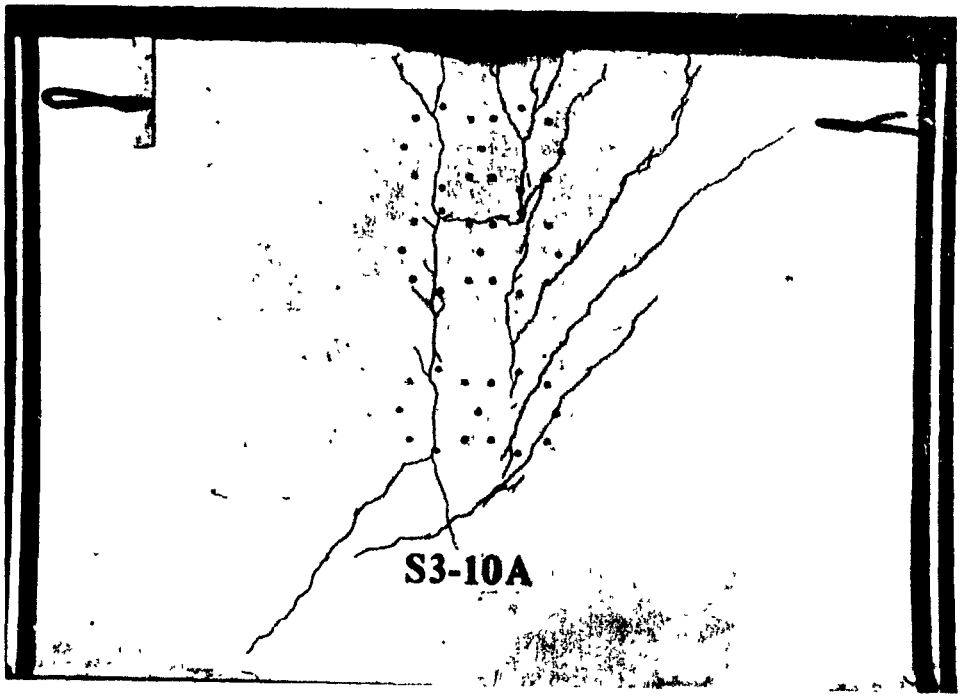

(a) Connection at factor design strength , P=113 kN

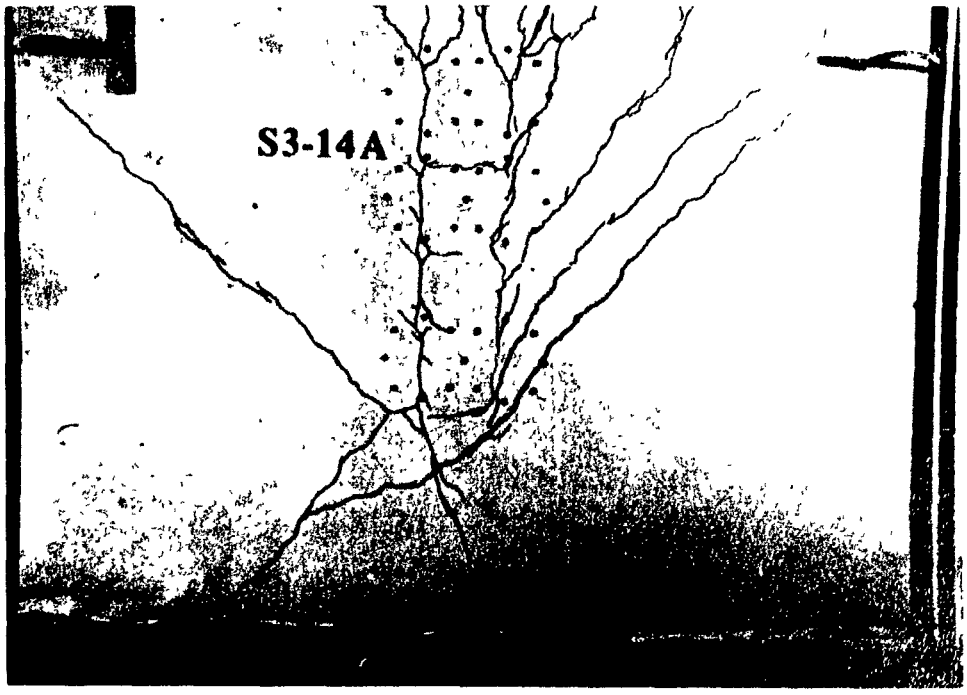

(b) Connection at $1\Delta_y$, P=127 kN

Figure 4.20 Photographs of Specimen S3

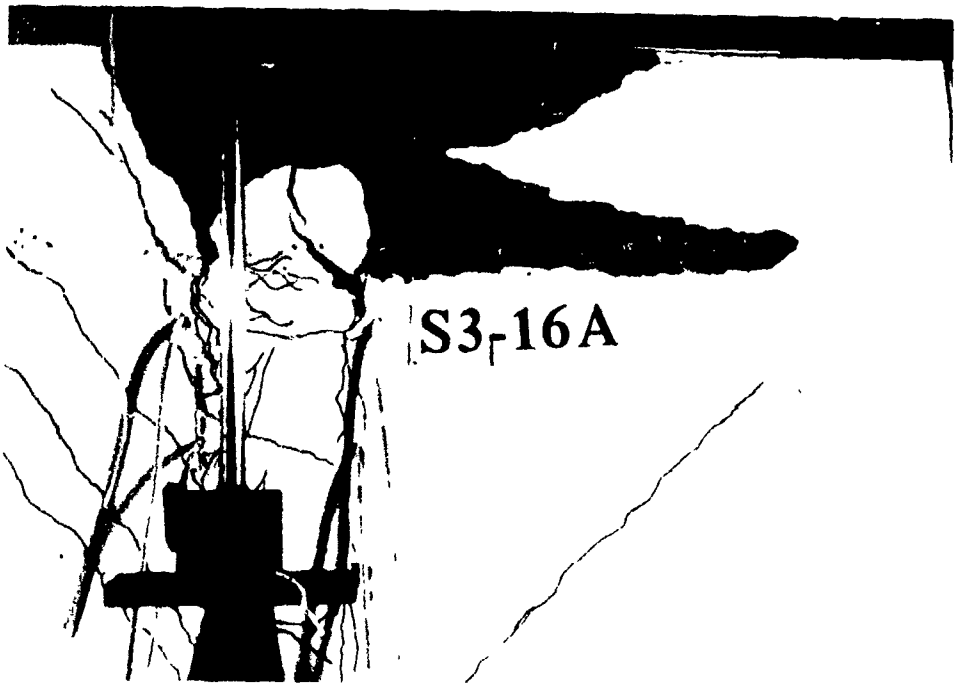

(c) Close-up of Connection at $1.7\Delta_y$, failure, back side

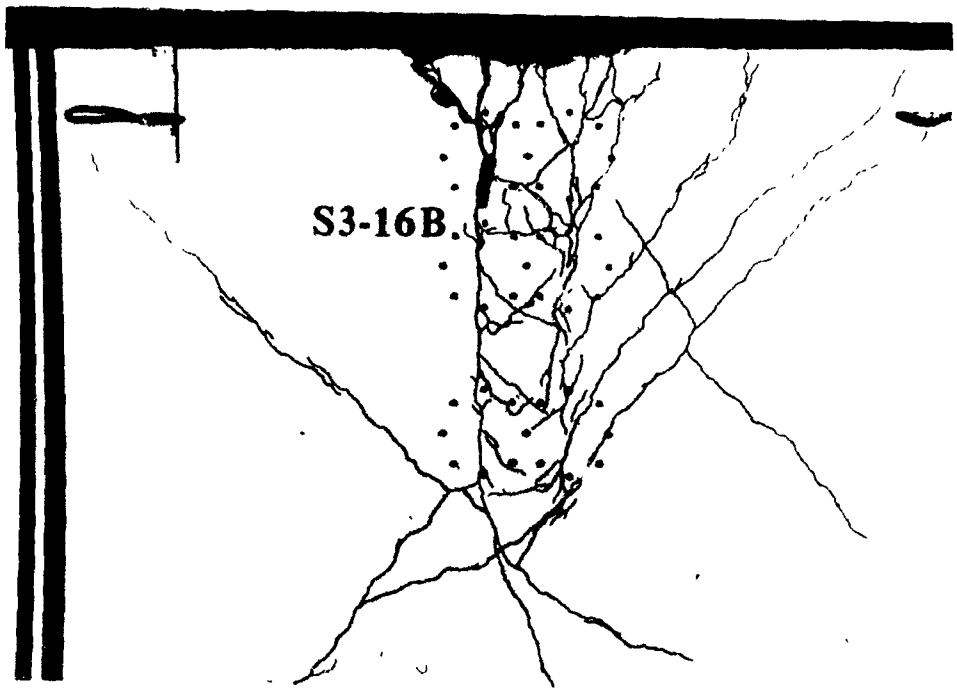

(d) Close-up of Connection at $-1.7\Delta_y$

Figure 4.20 (Continued) Photographs of Specimen S3

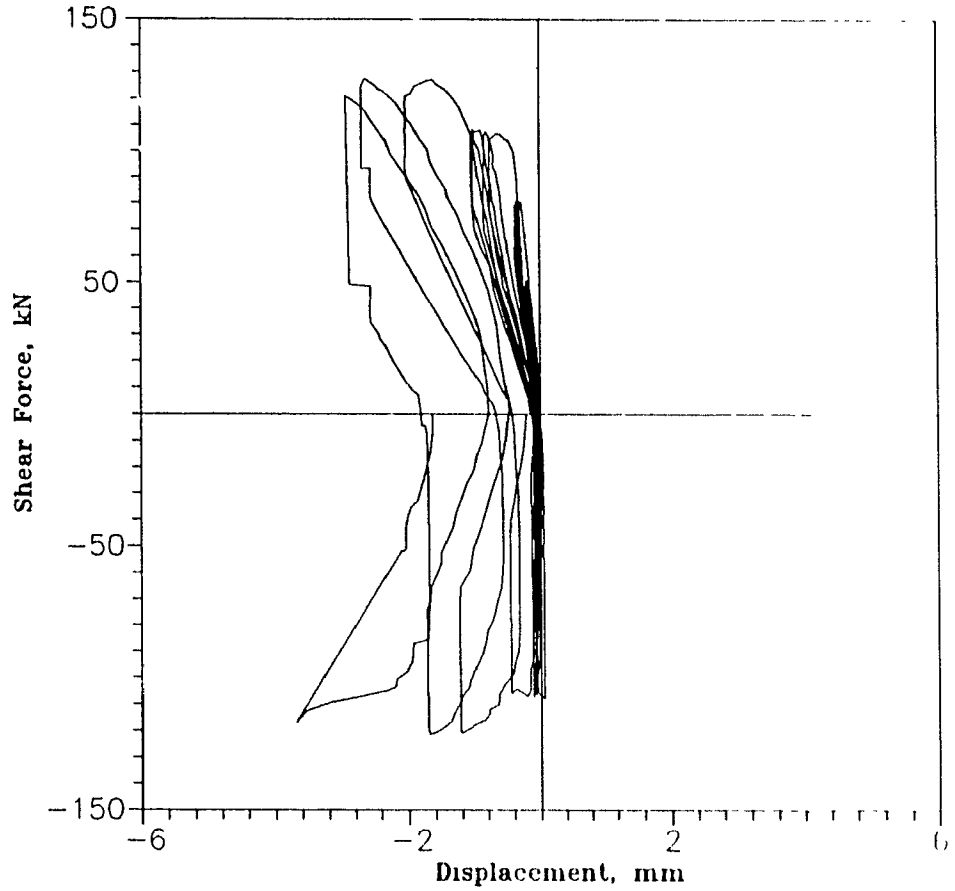

Figure 4.21 Load vs. vertical displacement Specimen S3

4.4.7 Bond between Steel Plates and Concrete Panel

The bond between the concrete panel which was epoxied to the steel plate welded to the box and W-shaped beams (as modelled by SAP90 results) was studied at various steps during the experiment and it was found to be intact everywhere. Figure 4.24 presents a plot of measured deflections of the epoxied steel plate with the load variation, which indicates the basic linear response as expected.

4.4.8 Summary According to the loading history summarized in Table 4.3 and Figure 4.17, Specimen S3 was loaded to 9 cycles beyond the factored design load of P_ϕ = 110 kN. The hysteresis loop area is relatively very small up to the factored

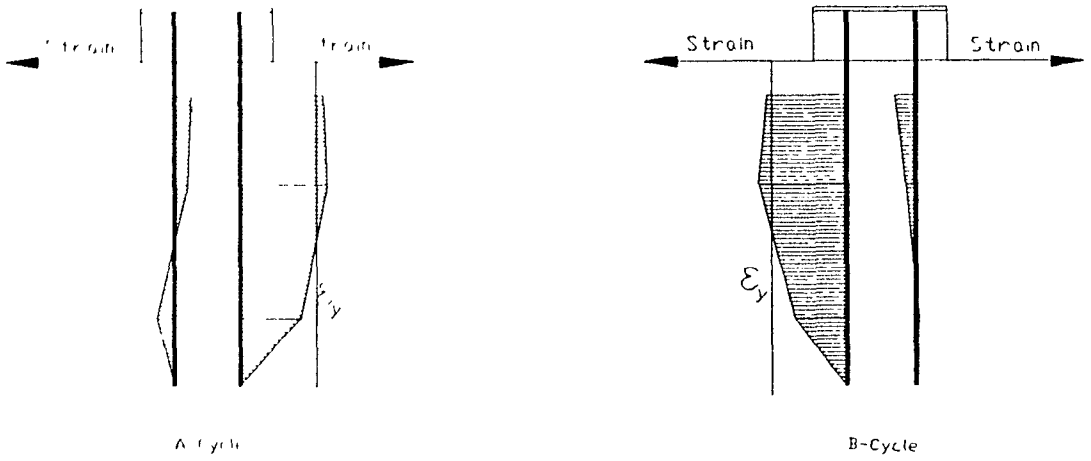

Figure 4.22 Strain vs. distance along the length of reinforcing bar prior to failure, Specimen S3

design load (85% of failure load) and decreases with cycling at the same load. The pinching effect was pronounced and consequently the loop area which represents hysteretic damping was small. Inelastic deformations were concentrated at the three last cycles after the yielding of the reinforcing bar and the occurrence of a number of diagonal cracks and significant extensions of the longitudinal splitting cracks. A displacement ductility of 1.7 was achieved. The reinforcing bar yielded at Locations 1 and 4 during Cycles 13 to 16, while at Locations 2 and 5 yielding occurred only during the last cycle. The reinforcing bar did not yield at Locations 3 and 6.

As can be seen from Figure 4.17 and Table 4.3, the maximum load imposed during testing was 127 kN which gives 95% of the predicted monotonic ultimate strength of the specimen. The mode of failure observed was by progressive crushing and spalling of the concrete cover below the angle flange and the longitudinal splitting of the concrete surrounding the reinforcing bars due to dowel action.

In using this specimen, the importance of preventing spalling of the concrete below the angle flange (cover) due to shear at the interface of the flange angle and the surrounding concrete was apparent. It can be improved by confining the surrounding concrete and welding small headed studs to the flange. To improve the joint capacity, the angle can be placed in a manner similar to that in Specimen S5, with the full flange thickness below the concrete surface.

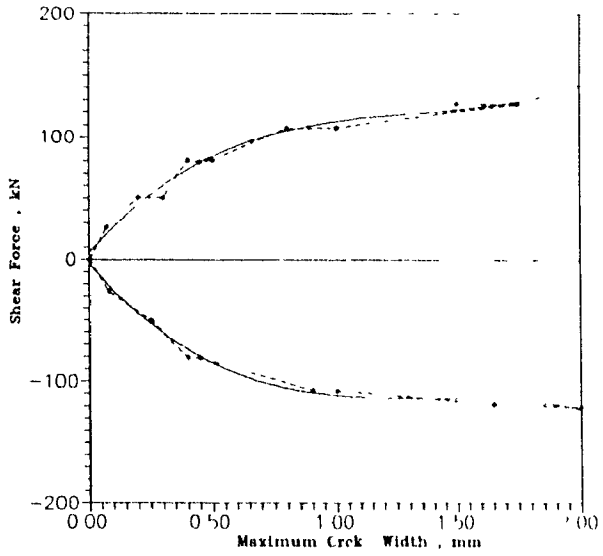

Figure 4.23 Peak loads vs. maximum crack width Specimen S3

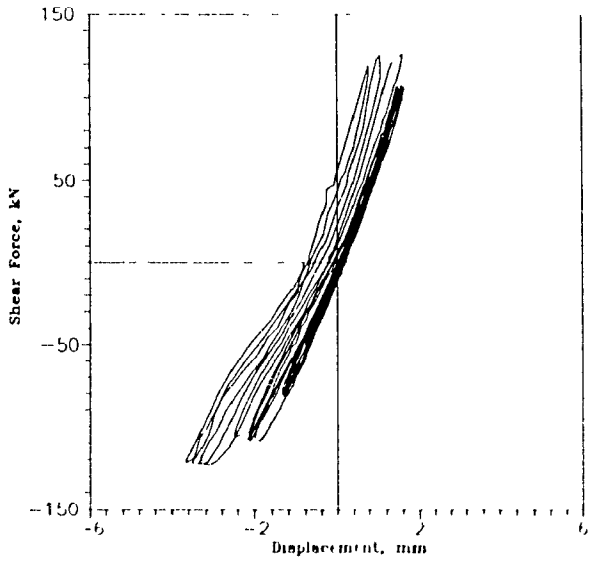

Figure 4.24 Load vs. deflection of steel frame as modelled, Specimen S3

4.5 Test Specimen S4

4.5.1 The Specimen

The specimen was reinforced with 2 - ½ in.(12.5 mm) diameter Nelson studs 2 in. (50 mm) long, welded to a plate inclined as shown in Figure 2.18 to achieve the maximum bearing resistance. A 100 x 100 MW13.3/MW13.3 standard wire fabric mesh was placed in the central plane of the 50 mm thick panel. Specimen S4 was designed according to the current strength method suggested in the CPCI Metric Design Manual[18]. No special provisions for seismic performance were considered.

4.5.2 Loading History and Load Cycles 1 - 6

Table 4.4 summarizes the loading history for Specimen S4. As shown in Table 4.4 and Figure 4.25, the specimen was subjected to three elastic cycles at a peak load of 20 kN (Cycles 1A - 3B), followed by three cycles (Cycles 4 - 6) at a peak load of 35 kN. The first crack appeared below the interface of the concrete and the face plate at a load of 31 kN. This crack extended along the stud and ended within an additional diagonal shear crack,forming a partial conical crack which at a later steps led to a "shear-cone" failure. Another crack appeared at the corner of the face plate in the concrete. Upon load reversal (Cycle 4B), a symmetrical crack pattern formed at a load of -28 kN, causing a change in stiffness as shown in Figure 4.25. The maximum crack width was 0.08 mm. A photograph of the connection at Cycle 4B is presented in Figure 4.27a. At the second cycle of this load stage (Cycle 5A) the diagonal shear crack extended toward the free edge at an angle of 30 degrees with respect to the direction of loading. Figure 4.28 demonstrates that the principal strain along the line with an inclination of 30° is greater than concrete cracking strain of 110×10^{-6}. Similar behaviour was observed during the negative load cycle. At the last cycle of this load stage (Cycle 6), the shear-cone crack at the right side extended to the free edge of the test specimen. The maximum steel strain at Location 1 of headed studs was 670×10^{-6} (see Figure 4.26). The width of "shear-cone" crack was about 0.2 mm. The rapid opening of this crack suggested that failure was imminent.

The loops in the load-deflection response clearly show the degradation of stiffness

Table 4.4 Summary of Loading History of Specimen S4

Cycle	Load Stages	Horizontal Displacement** (mm)	Shear Force V (kN)
Elastic	1A - 3B	+0.05, -0.10	+20
Cracked	4A - 4B	+0.12, -0.23	+35
50% P_{ult}*	5A - 6B	+0.20, -0.32	+35
65% P_{ult}	7A	+0.39	+48
Failure	7B	-0.80	-30

* Calculated maximum strength based on monotonically increasing load (73 kN)

** Displacement at peak of last cycle of the load stage

4.5.6 Load Cycle 7

As the applied Load was increased to 48 kN (65% of P_{ult}), the cone shear-cone crack, representing the effective stress area, continued to open. The tensile strain at the stud at Location 1 decreased to about 500 x 10^{-6}, while at Location 2 the compression zone, the strain remained constant. The reduction of strain at Location 1 was due to the significant propagation of the shear crack through the thickness of the concrete panel. The maximum measured displacement was 0.40 mm. The factored design capacity, P_{ϕ}= 43 kN, calculated using the provisions in the CPCI Metric Design Manual[18], was reached during Cycle 7A. A photograph of the connection region is presented in Figure 4.27b. Finally, the test specimen was subjected to a negative load of 30 kN. The horizontal displacement was 0.8 mm and it increased to 1.15 mm as the applied load was maintained on the specimen. After

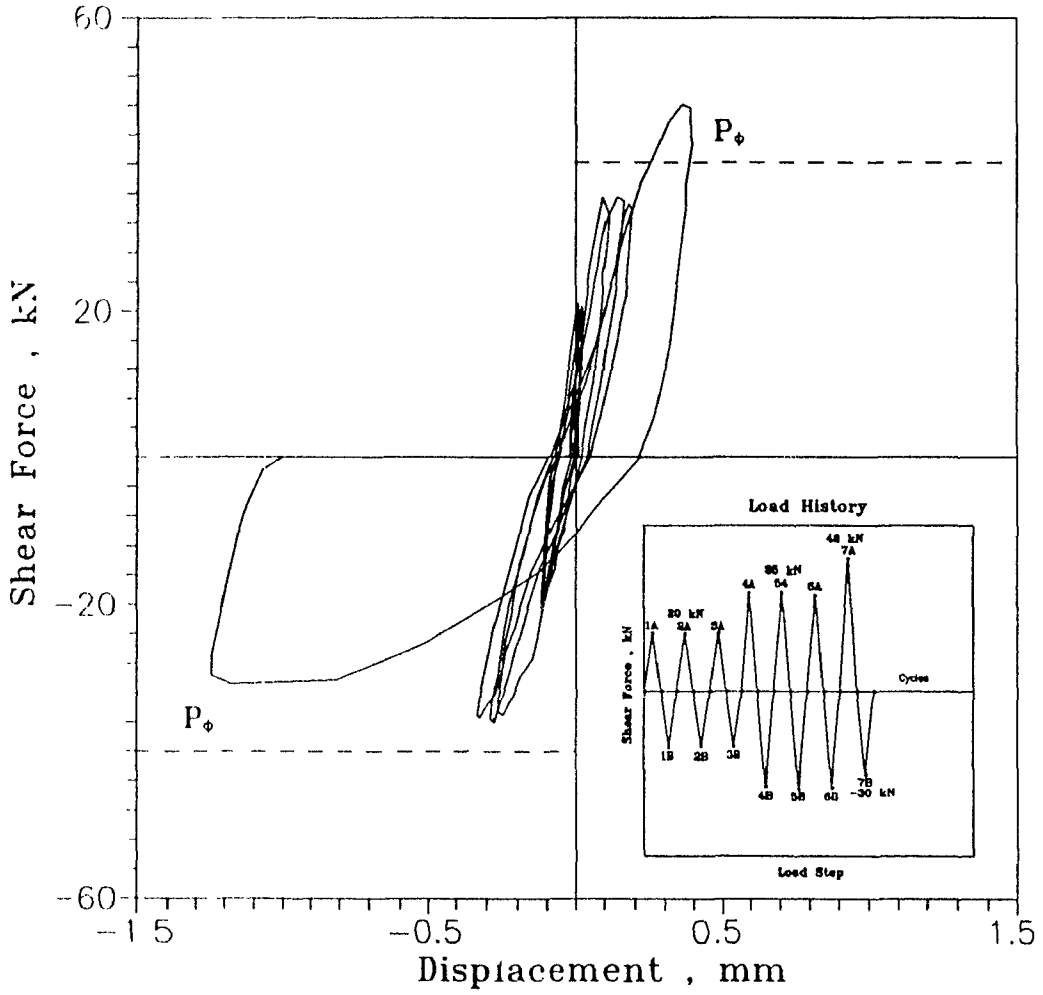

Figure 4.25 Hysteresis response of Specimen S4

surrounding the connection. Figures. 4.27c and 4.27d show the photographs of the specimen after failure.

Figure 4.29 presents the Load versus vertical displacement of the connection. The vertical displacement is due to the upward movement of the connection on account of splitting and diagonal cracking and the resulting rotation of the connection, while in the prototype some of this displacement is prevented by the adjacent flange.

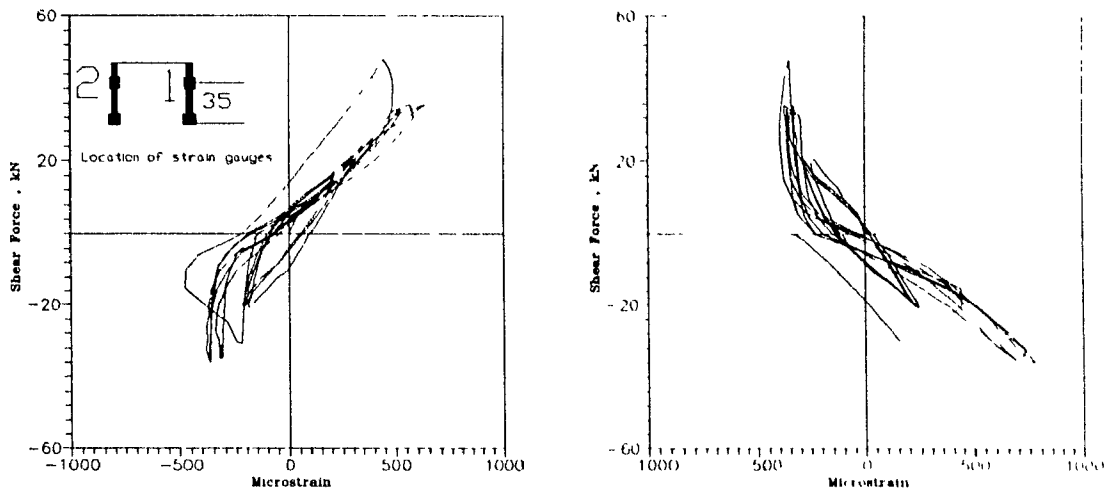

Figure 4.26 Measured strains in headed studs, Specimen S4

4.5.7 Crack Width at Peak of Load Cycle

The variation of maximum crack width in the tensile region with the peak Load is plotted in Figure 4.30. The area under this curve is an indication of the fracture energy dissipation characteristic of the connection.

The internal horizontal crack formed in the plane between the studs propagated vertically, representing the occurrence of the in-plane splitting crack due to cyclic loading. This crack reduced the stiffness and strength of the joint significantly at the early load stages.

4.5.8. Bond between the Steel Plate and Concrete

The bond between the steel plate and the concrete panel edges was examined at different load cycles of the experiment and was observed to be intact everywhere. The deflection of the steel plate at different load levels was measured and is plotted in Figure 4.31 which exhibits linear behaviour.

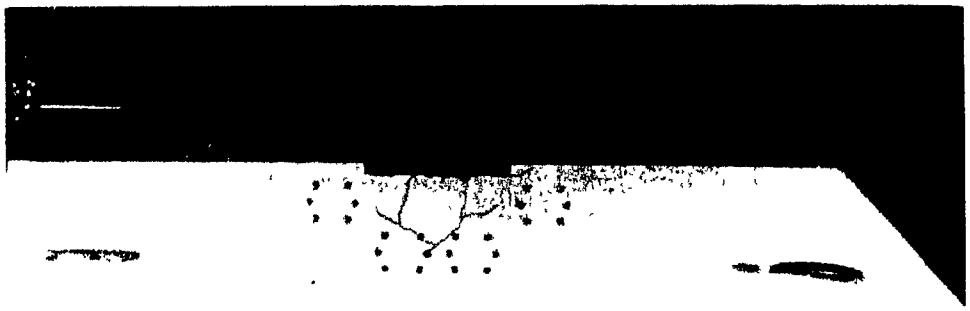

S4-4B

(a) Connection at first symmetrical crack , P=-35 kN

S4-7A

(b) Connection at design factored capacity

Figure 4.27 Photographs of Specimen S4

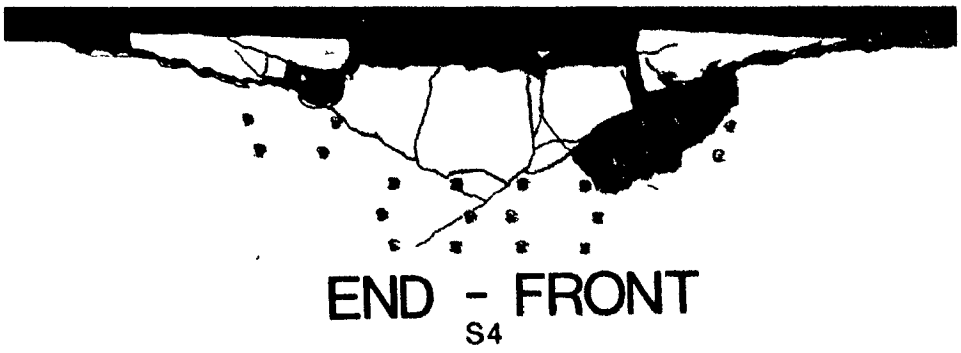

(c) Connection after testing, front

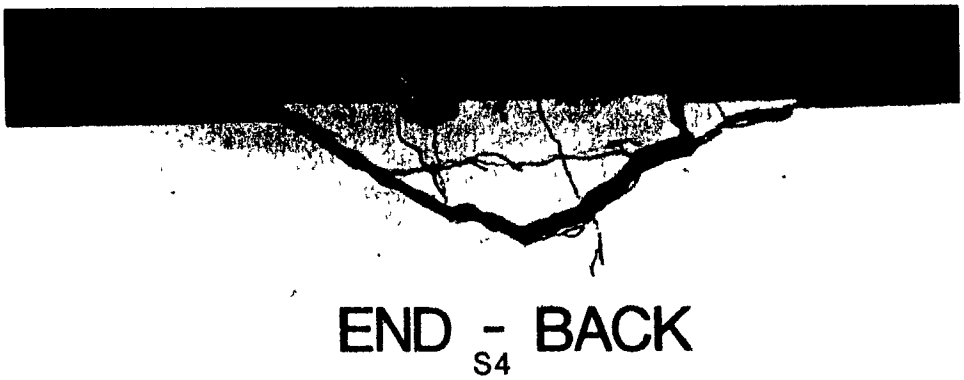

(d) Connection after testing, back

Figure 4.27 (Continued) Photographs of Specimen S4

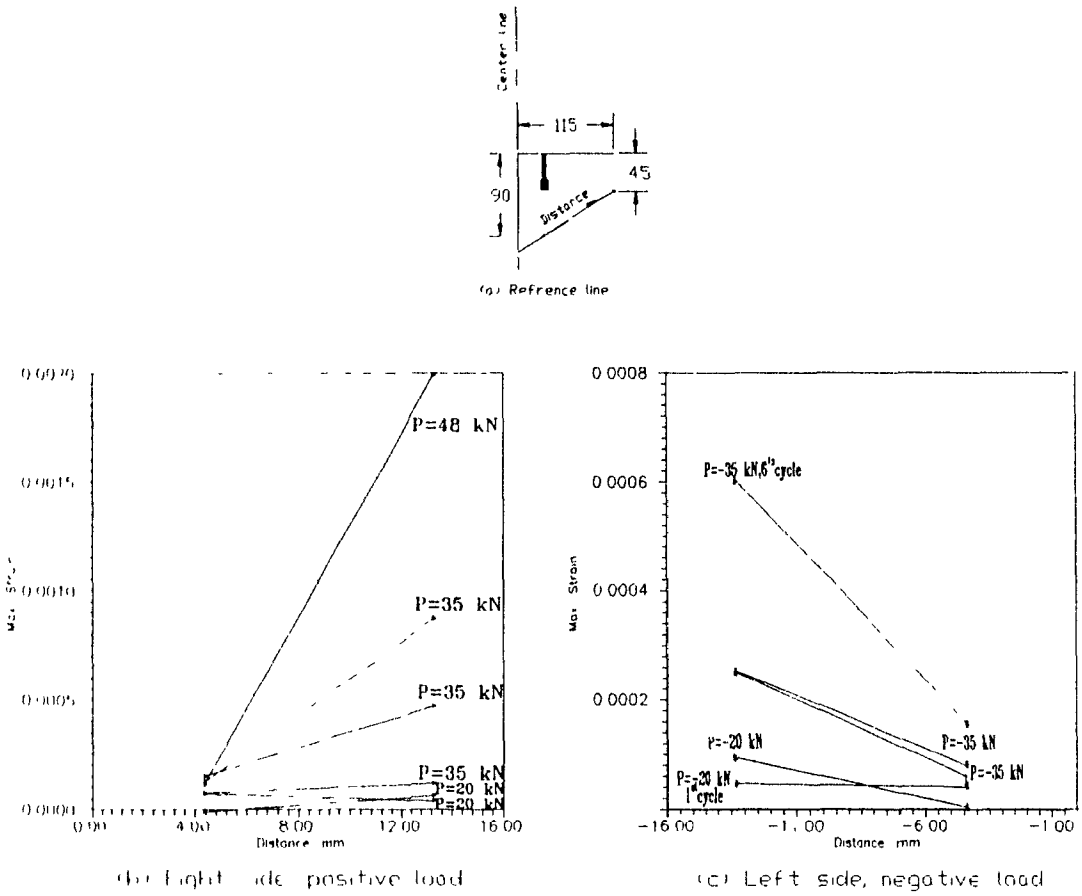

Figure 4.28 Maximum principal strain distribution of slab along the reference line, rosette measurements, Specimen S4

4.5.9 Summary Specimen S4 was subjected to the loading history summarized in Table 4.4 and exceeded the design factored strength only at the last cycle in one direction (7A), but not in the other direction (7B). The loops were very narrow indicating small energy dissipation. The maximum load applied during the last cycle (Cycle 7) was 48 kN representing 65% of the calculated monotonic ultimate capacity. The angle of inclination of the "shear-cone" crack, used to determine the effective stress area, was observed to be 30-degrees, which increases the effective stress area in comparison with 45-degrees angle recommended in the CPCI Metric Design Manual[18]. The test specimen failed when a block of concrete surrounding the studs broke away ("shear-cone" failure) due to depletion of tensile capacity.

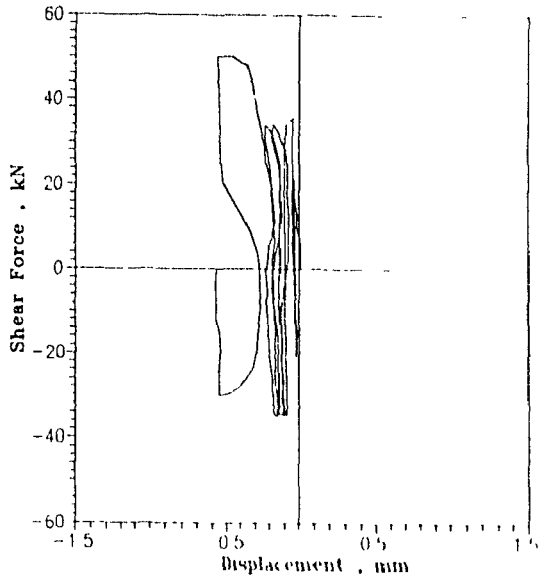

Figure 4.29 Load vs. vertical displacement, Specimen S4

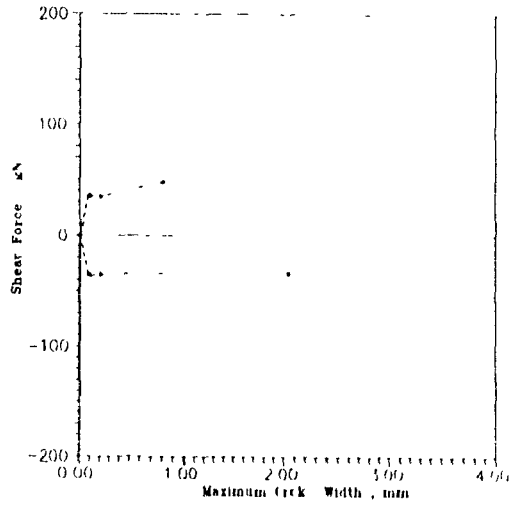

Figure 4.30 Peak loads vs. maximum crack width Specimen S4

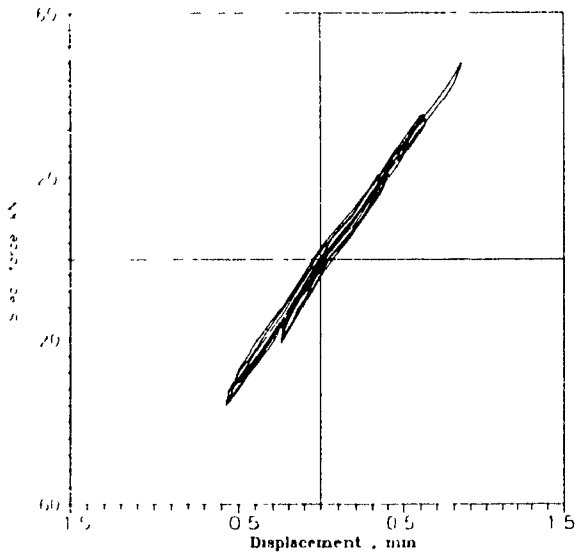

Figure 4.31 Load vs. deflection of steel frame as modelled, Specimen S4

4.6 Test Specimen S5

4.6.1 The Specimen

Specimen S5 was reinforced with two No. 15 deformed steel bar, oriented at an angle of 45- degrees and 2 - ½ in. diameter Nelson studs, 1/2 in. (12 mm) long, welded to a flange of 75 x 75 x 10 mm by 250 mm l g angle, and a uniform 100 x 100 MW 13.5/ MW 13 3 wire fabric mesh. The s · · nen design was based on the contribution of the anchor reinforcing bar and heade tuds, separately. The ultimate strength of the connection was the summation of these cont' ibutions; influence of the wire fabric mesh was not included. Special consideration for the development length based on the bond response to low cyclic, earthquake simulation, was considered to calculate the reinforcing bar contribution to the strength of the connection[20]. No special seismic considerations were made to determine the contribution of the headed studs to the ultimate strength. Determination of the monotonic ultimate strength was based on the anchorage length for seismic loading and the formulas which in turn

are dependent on the concrete cover thickness (see Appendix A), whereas for design of studs, the current CPCI provisions were used.

4.6.2 Loading History and Load Cycles 1 - 6

Table 4.5 summarizes the loading history for Specimen S5. As can be seen from Figures 4.32 and 4.33 and Table 4.5, the specimen was subjected to three cycles at a peak load of 36 kN causing the first crack to appear at the angle flange corner, on the surface of the concrete during Cycle 2A. The loops were very narrow due to near elastic behaviour.

Table 4.5 Summary of Loading History for Specimen S5

Cycle	Load Stages	Horizontal Displacement (mm)**	Shear Force V (kN)
Elastic	1A - 1B	+0.128, -0.139	± 36
Cracked	2A - 3B	+0.134, -0.155	± 36
30% P_{ult}*	4A - 6B	+0.454, -0.674	+ 75
40% P_{ult}	7A - 9B	+0.716, -1.301	+ 105
50% P_{ult}	10A - 12B	+0.952, -1.701	± 130
63% P_{ult}	13A - 15B	+2.010, -2.541	± 160
70% P_{ult}	16A - 18B	+2.419, -3.601	± 180
80% P_{ult}	19A - 19B	+3.570, -6.83	+ 200
73% P_{ult}	20A	+ 6.248	+ 185
Failure	20B	-6.34	-173

* Calculated maximum strength based on monotonically increasing load (247 kN)

** Maximum deflections at the peak of last cycle of load stage

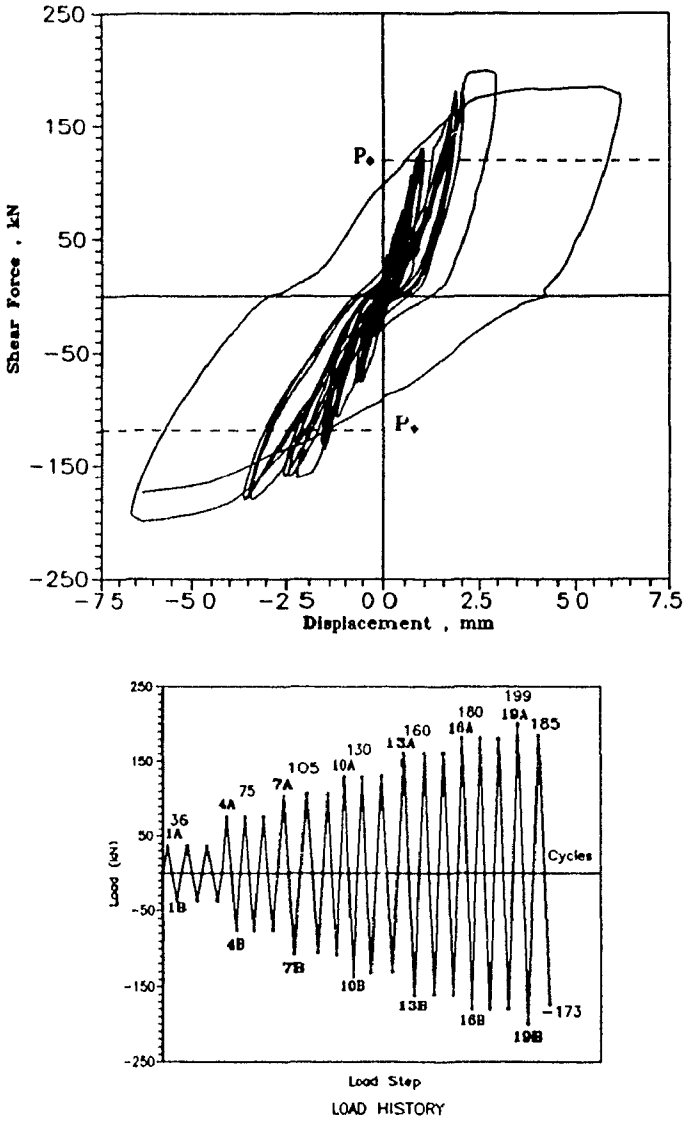

Figure 4.32 Hysteresis response of Specimen S5

In the second cycle of the load stage with a peak load value of 75 kN (30% of P_{ult}) (Cycle 5A), the first sign of concrete crushing at the top corner of the angle was observed. The splitting crack extended along the anchor bar and a small diagonal crack appeared about 100 mm below the top concrete surface. The maximum displacement recorded was 1 mm. The maximum principal strain in the concrete determined from the measurements using the demec gauge set at this location was 340 X 10^{-6} which is greater than the cracking strain of concrete (110 X 10^{-6}) (see Figure 4.34).

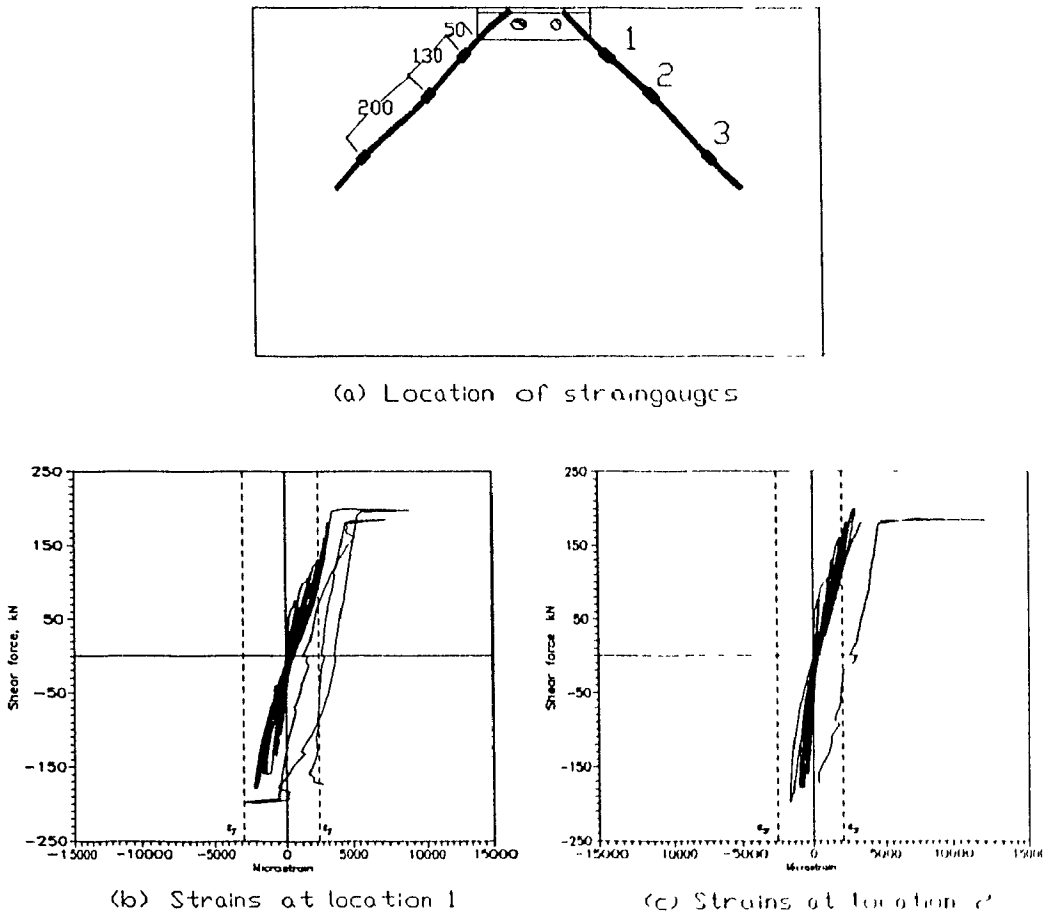

Figure 4.33 Measured strains along the length of reinforcing bar anchor Specimen S5

4.6.3. Load Cycles 7 - 9

The specimen was then subjected to three cycles (7A - 7B) at peak loads of 105 kN (40% of P_{ult}). During Cycle 7A, a diagonal crack appeared at a distance of about 125 mm from the end of the bar (Location 3) where the maximum principal strain in the concrete was 400×10^{-6}, which is greater than the ultimate tensile strain of the concrete. Two more diagonal cracks formed at the location where the panel

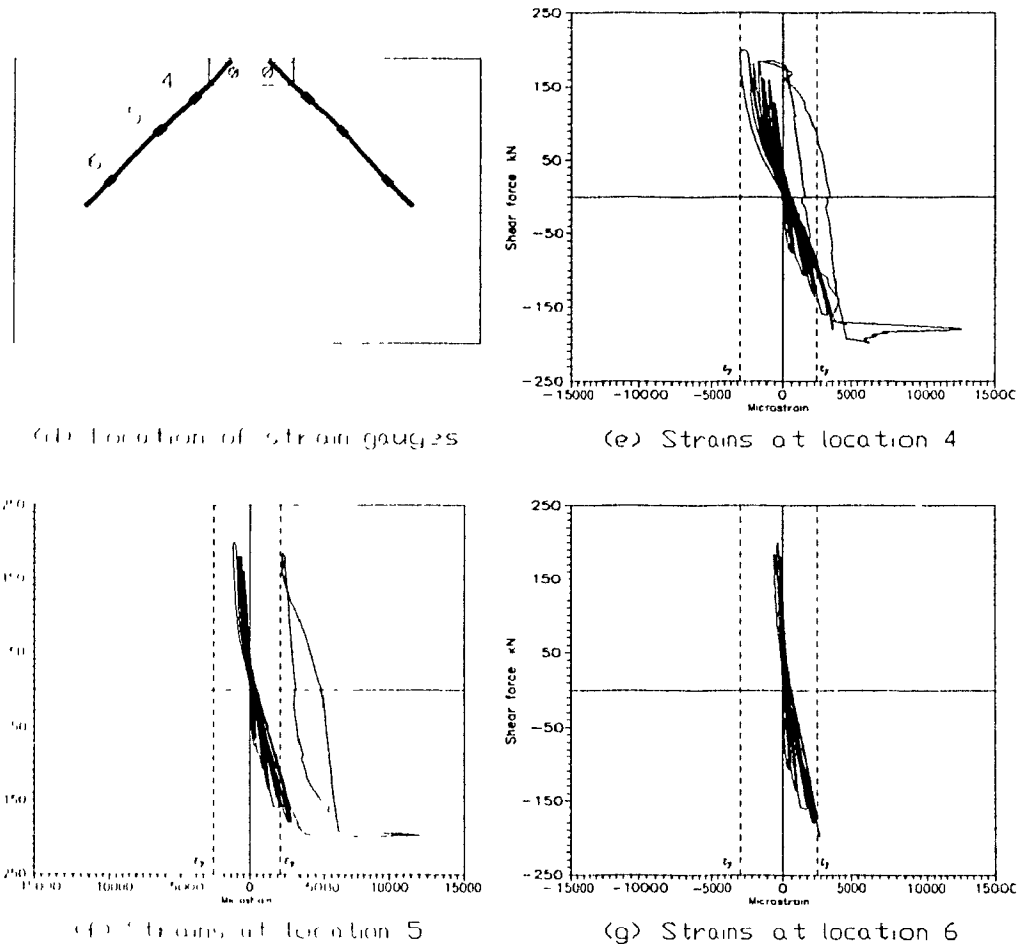

Figure 4.33 (Continued) Measured strains along the length of reinforcing bar

Specimen S5

thickness changes, and the splitting crack extended along the length of the bar. The maximum horizontal deflection was 1.35 mm, and the maximum width of the splitting crack along the bar was 0.33 mm.

4.6.4. Load Cycles 10 - 12

The next step was to increase the shear force to a peak load of 130 kN, (50% of P_{ult}). There is a change in the stiffness (see Figure 4.32) at a shear force of 120 kN, which related to a significant additional diagonal crack at the end of the

reinforcing bar and extension of the splitting crack along the bar. The maximum principal strain at this location was 840 x 10^{-6} which confirms the presence of the crack. The maximum measured strain in the steel bar was 2050 x 10^{-6} which was close to the yield of the reinforcing steel. On the back side, two vertical cracks were observed at the corners of the angle. It should be mentioned that at this load cycle the factored design capacity of the specimen was reached. This factored design capacity was determined by multiplying the calculated monotonic ultimate capacity (suggested in the CPCI method) of 140 kN by ϕ_s (0.85) which is the reinforcing bar resistance factored. This gives factored design capacity of P_ϕ = 0.85 x 140 = 119 kN.

4.6.5 Load Cycles 13 - 15

As the applied shear force was increased to 160 kN (63% of P_{ult}), the maximum measured displacement was 1.85 mm. Figure 4.32 illustrates a sharp change in stiffness at a shear force of about 132 kN . This corresponds to yielding of the reinforcing bar in the tension part The displacement, Δ_y= 1.85, was chosen based on the yielding of the reinforcing bar and the shape of the hysteresis curve (see Figure 4.32, Cycle 13A). Figures 4.32 and 4.33 display some pinching in the load - deflection response. This behaviour occurs due to the closing of the cracks along and normal to the reinforcing bar in the compression zone The maximum crack width was measured to be 1.2 mm. Upon load reversal, the reinforcing bar on the other part of the connection exhibited the same phenomenon. The deflection at yield (Δy) was measured to be -2.21 during the negative load cycle (Cycle 13B) There were no appreciable changes in the measured deflection and the steel strains during the following cycles (Cycles 14 - 15). A photograph of the joint region is presented in Figure 4.35a.

4.6.6. Load Cycles 16 - 18

The test specimen was then subjected to three cycles (Cycle 16 to 18) with a maximum applied load of 180 kN. In Cycle 16A, a strain of 2514 x 10^{-6} was recorded at Location 2, which indicated that the reinforcing bar had yielded. There was no strain recorded for Location 3 since the strain gauge was lost during the casting.

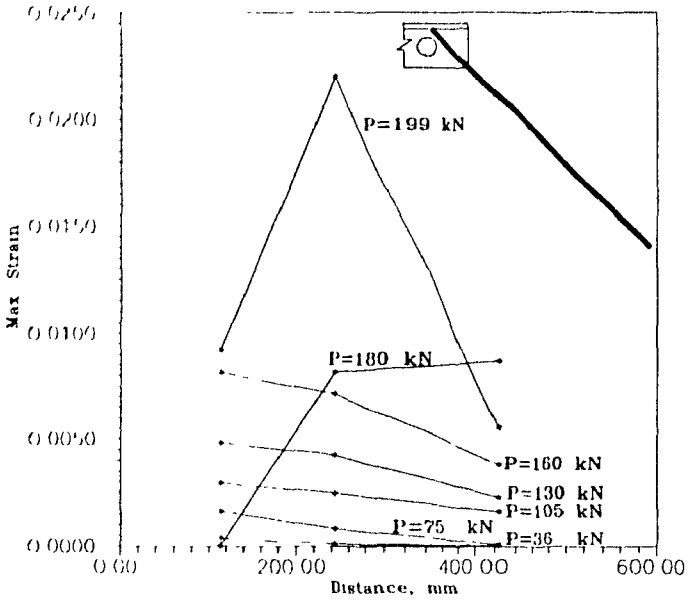

(a) Maximum principal strains, right side, positive load

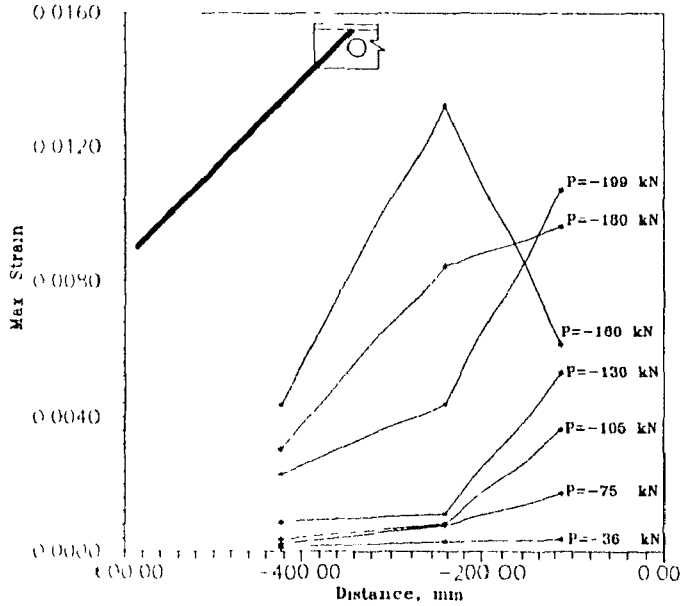

b) Maximum principal strains, left side, negative load

Figure 4.34 Maximum principal strain distribution of panel along the length of reinforcing bar, rosette measurements, Specimen S5

The larger area under the hysteresis loop is due to the increasing yielding in reinforcing bar. Not much change was observed in the following two cycles at the same load stage (Cycles 17 - 18). The strains at Locations 4, 5, and 6 were measured to be 3596 x 10^{-6}, 2665 x 10^{-6}, and 2044 x 10^{-6}, respectively (see Figures 4.33d to 4.33g). The maximum displacement in the last cycle of this load step was 2.97 mm (1.6 Δy). Two cracks extended vertically from the two ends of the angle and extended to the horizontal crack which had formed during the previous cycle 100 mm below the free edge. These cracks, the two vertical and the horizontal, formed an approximately "W" shaped pattern (see Figure 4.35e).

4.6.7. Load Cycles 19 - 20

As the load was increased to 200 kN (Cycle 19A), the maximum displacement was 3.57 mm (1.8 Δy). Figure 4.35b presents a photograph of the joint region. This deflection increase can be noted in Figure 4.32, and it is due to yielding of almost the entire reinforcing bar along its embedment length in the tension zone and the yielding of the reinforcing bar at Location 4 in the compression zone. Figures 4.33b and 4.33e indicate a significant increase in the strains at Locations 1 and 4, respectively. Upon load reversal, the measured strains at Locations 4, 5, 6 were measured to be 6320 x 10^{-6}, 12096 x 10^{-6} and 2389 x 10^{-6}, respectively (see Figures 4.33e to 4.33g). The yielding of the entire length of the bar in tension and a partial bar length in compression (Figure 4.33) are reflected in the increase in the measured displacement of -6.83 mm (approximately 3Δy) and the relatively wider loop in the load- deflection response and the accompanying stiffness deterioration. The maximum crack width at 100 mm from the free edge along the reinforcing bars was measured to be 2mm. The cover on the specimen front face along the 100 mm length of reinforcing bars had spalled off. The "W" shaped crack at the back side had opened significantly, and the splitting crack extended along the entire length of the reinforcing bar. The specimen was then subjected to a maximum horizontal displacement of 3Δy, (Cycle 19A) when the maximum measured load was 185 kN. The measured strains at Locations 1 and 2 are measured to be 7388 x 10^{-6} and 7159 x 10^{-6} which were about 3 times the yield strain, while in Locations 4, 5, and 6 the measured strains were -664 x 10^{-6}, 2360 x 10^{-6}, and -540 x 10^{-6}, respectively

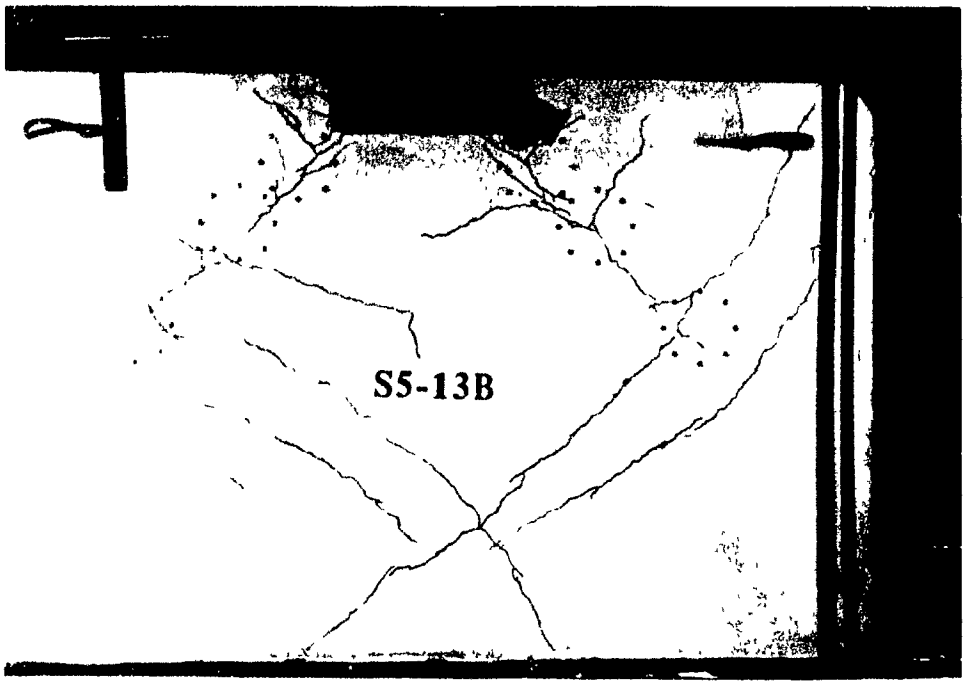

(a) Connection at $-1\Delta_y$, first yield, P=160 kN

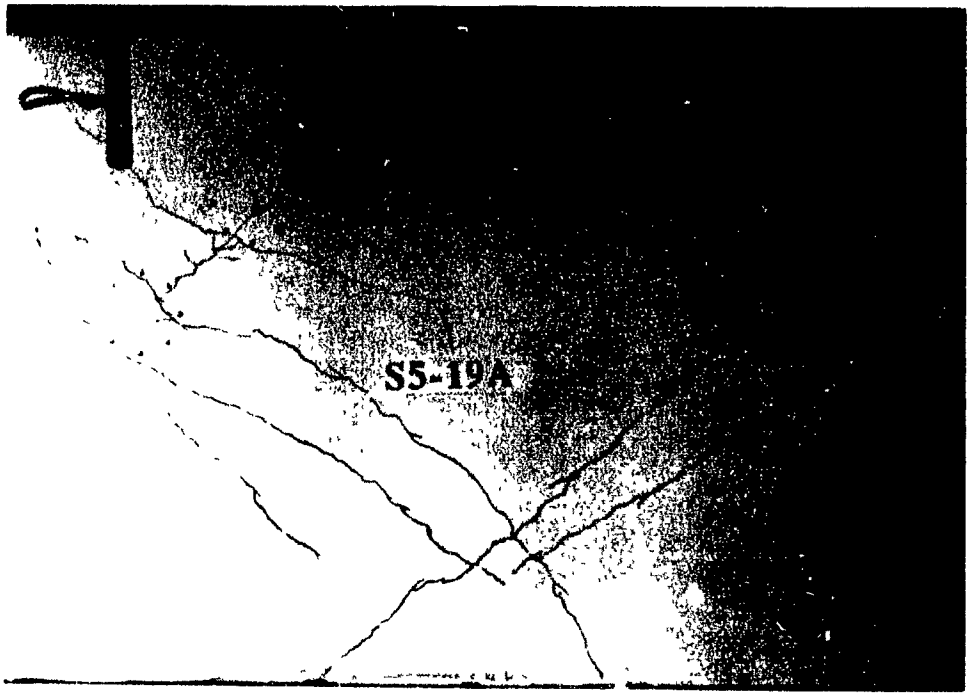

(b) Connection at $1.8\Delta_y$, $P=P_{max}=200$ kN

Figure 4.35 Photographs of Specimen S5

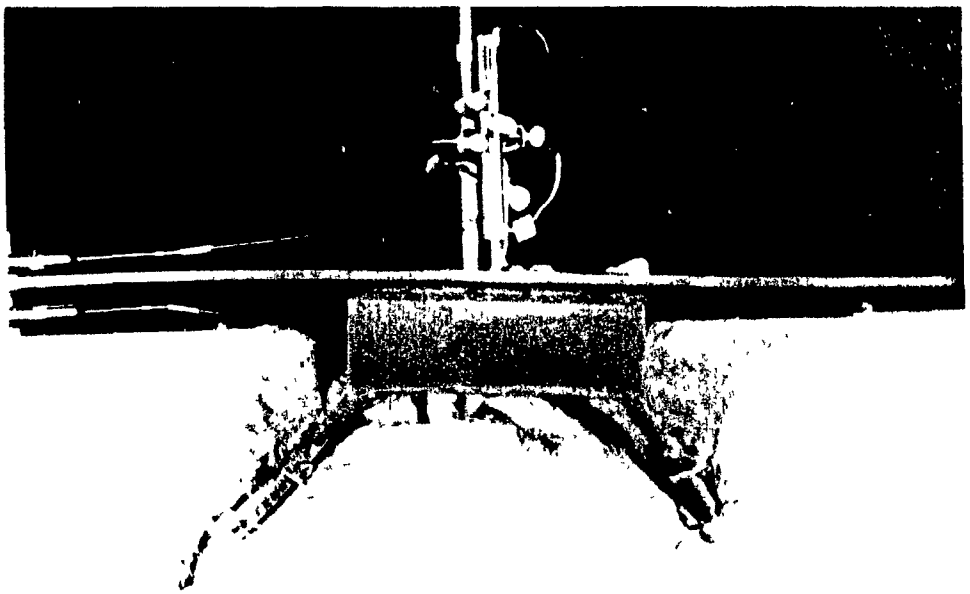

(c) Connection close-up at $-3\Delta_y$

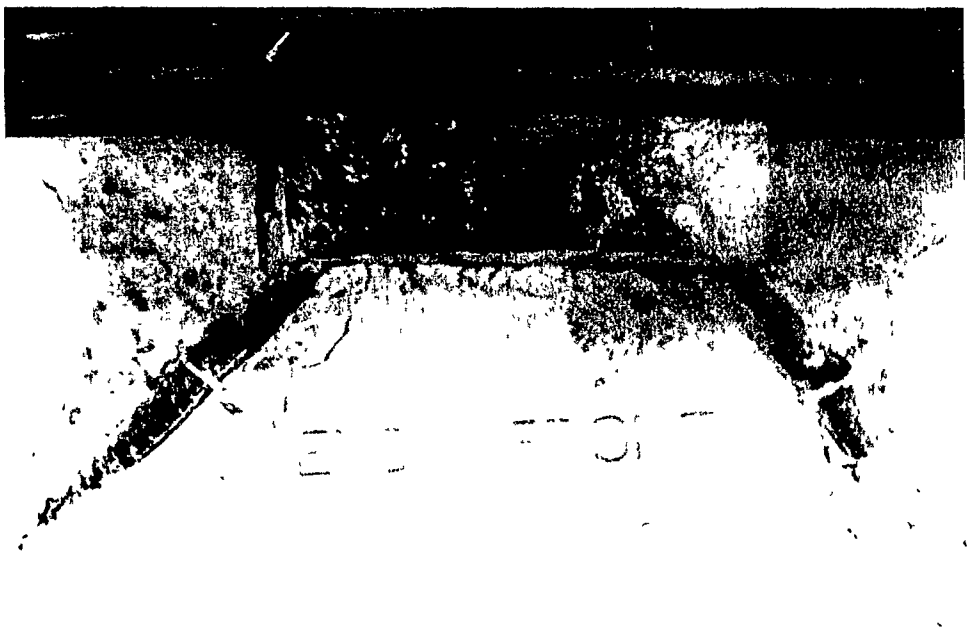

(d) Connection close-up (front side) after testing

Figure 4.35 (Continued) Photographs of Specimen S5

Finally, the specimen was subjected to negative loading up to a maximum load of 173 kN (Cycle 20B), when failure occurred (see Figure 4.35c). The maximum displacement prior to failure was recorded to be -6.34 mm which gave a displacement ductility of μ = 6.34 / 2.21 = 2.9. The strains at Locations 4, 5, and 6 were measured to be -4632 x 10^{-6}, 17415 x 10^{-6}, and 2314 x 10^{-6} respectively, which reveals the yielding of the entire length of the reinforcing bar. Splitting failure was accompanied by pull-out of the end part of the reinforcing bar and "cone - shear" failure of the concrete surrounding the stud were observed. Figures 4.35d and 4.35e are photographs of the connection after the test.

(e) Connection close-up (back side) after testing

Figure 4.35 (Continued) Photographs of Specimen S5

Along the embedment length, the measured strain at Locations 1 and 2 were recorded to be +2523 x 10^{-6} and +480 x 10^{-6} which suggests that a part of the reinforcing bar in the compression zone was in tension. This was basically due to bending of the reinforcing bar in the compression zone after the loss of the concrete cover in the vicinity of the connection.

Figure 4.36 presents the load - vertical displacement characteristic for the specimen. This vertical displacement is caused by slipping of the bar on account of cracks along and normal to the bar and the resulting rotation of connection. With the presence of an adjacent panel in the actual structure, some of this displacement is prevented which may result in a slight increase the connection ultimate capacity.

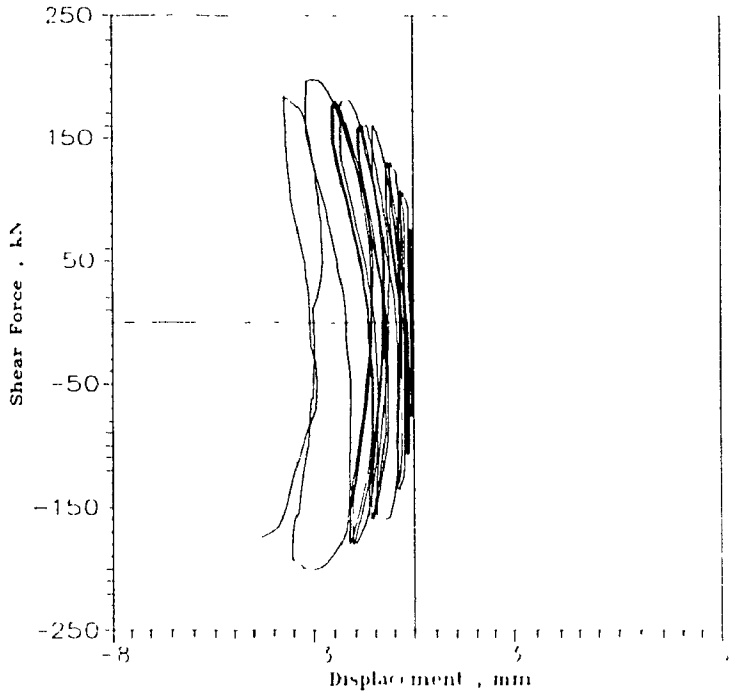

Figure 4.36 Load vs. vertical displacement Specimen S5

Figure 4.37 illustrates the strain variation along the length of the reinforcing bar at maximum load, indicating that almost all of the length of the bar in the tension zone had yielded during the reversed loading cycle while about one fifth of the bar in compression zone yielded.

4.6.8 Crack Width at Peak of Load Cycles

The maximum crack width for the peaks of the various load cycles in each step is shown in Figure 4.38 which also shows the best fit curve to the experimental load. The crack opening, d_{max} is related to the peak load with the following expressions: For positive loading :

$$P = + 826.5\, d_{max} - 2397\, d_{max}^2 + 3393\, d_{max}^3 - 2338\, d_{max}^4 + 763\, d_{max}^5 - 93.8\, d_{max}^6 \quad (4\text{-}7)$$

and for negative loading:

$$P = -799\, d_{max} + 2561\, d_{max}^2 - 4379.5\, d_{max}^3 + 1513\, d_{max}^4 - 1513\, d_{max}^5 + 235.3\, d_{max}^6 \quad (4\text{-}8)$$

The area under the curve is an indication of the fracture energy dissipation characteristic of the connection.

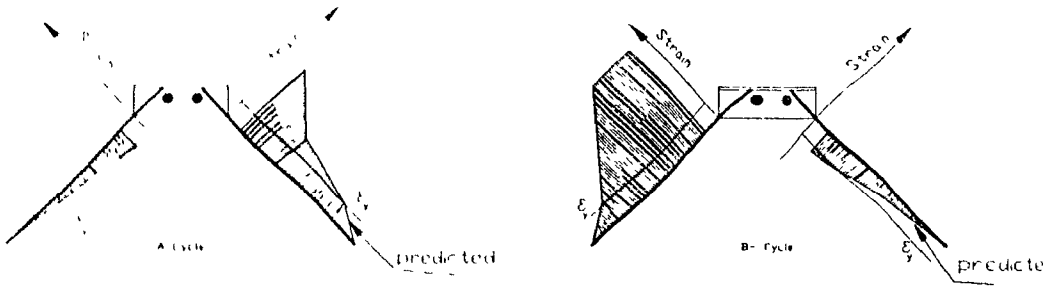

Figure 4.37 Strain vs. distance along the length of reinforcing bar prior to failure, Specimen S5

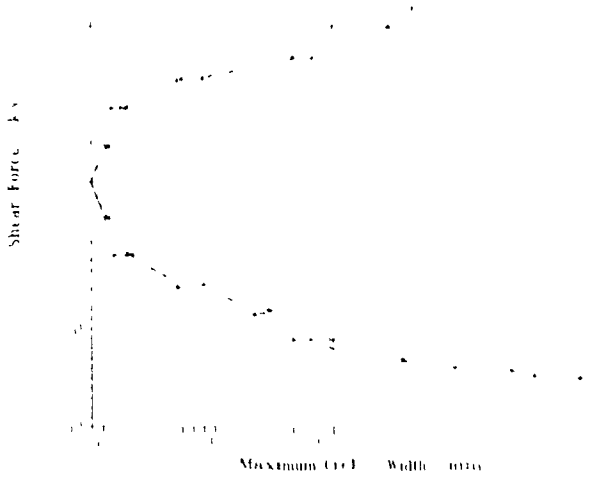

Figure 4.38 Peak shear force vs. maximum crack crack width Specimen S5

4.6.9 Bond between the Steel Plates and Concrete Panel

The bond between the steel plate epoxied to the concrete panel was found to be intact along entire length during the reversed cyclic loading. As can be seen in Figure 4.39, the variation of the epoxied steel plate deflection with the shear force illustrate a basic linear response.

4.6.10 Summary Specimen S5 was subjected to the loading history outlined in Table 4.5 and Figure 4.32 with 9 load cycles beyond the factored design strength of 119 kN. Considerable inelastic deformations occurred after yielding of the reinforcing bar, and eventually the entire steel bar yielded in tension. A displacement ductility of 3 was achieved. The mode of failure was splitting of the concrete along the reinforcing bar, with the exception of the pull-out of its end part, and concrete "cone shear" off near the headed studs. The headed studs helped increase the connection strength and stiffness compared with the other specimens, however after the cracking of the concrete surrounding the studs, the stiffness degradation was quite rapid resulting in large inelastic displacements. The maximum loads resisted by the specimen were 200

kN and - 200 kN, while the failure occurred at one cycle later at loads of 185 kN and -173 kN for positive and negative loadings, respectively.

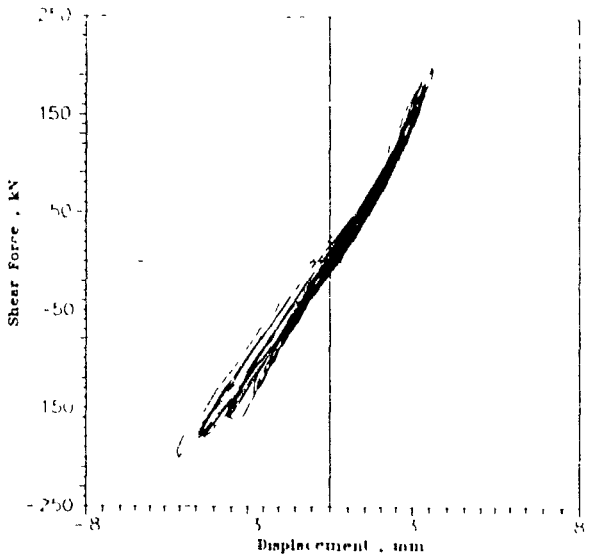

Figure 4.39 Load vs. deflection of steel frame as modelled, Specimen S5

4.7 Discussion and Comparison of Experimental Results

Comparison of the response of the test specimens subjected to reversed cyclic loads are based on their overall responses and the ability to dissipate energy. The load-horizontal displacement envelopes of the responses of the connections are presented in Figure 4.40. In addition, the cumulative energy dissipated (summation of the energy absorbed in each cycle) during the test versus the cumulative ductility are compared in Figure 4.41. The cumulative ductility index is calculated for each specimen by the summation of the displacement ductility ratio (Δ_i/Δ_y) for each load cycle. The energy dissipated by each test specimen was computed based on the area under the load-deflection response curves.

As can be seen from Fig 4.41, the energy dissipated was greater in Specimen S2 than in the other specimens, although , the displacement ductility of Specimen S5 (μ = 3) was greater than the ductility of Specimen S2 (μ = 2.5). The displacement ductility of 3 was attained for Specimen S5, but a lot of pinching was observed in the load - deflection response, accounting for the great reduction in cumulative energy dissipated. The cumulative energy dissipated by Specimen S5 up to a load of 180 kN is almost 27% of the total energy dissipated. This was due to the contribution of the headed studs in the connection, causing the connection to be stiff, before significant "cone - shear" cracking in the concrete surrounding the studs and prior to complete yielding of the reinforcing bar anchor (see Figure 4.32). Specimens S2 and S5 presented almost similar envelopes, although different failure modes were observed. Specimen S5 exhibited the greatest ultimate strength (200 kN), in comparison to the other specimens, while the energy dissipated in Specimen S2 was the greatest, see Figures. 4.40 and 4.41. Specimen S1 failed by a brittle fracture mechanism because of lack of full welding along the straight part of the reinforcing bar. A contributing mechanism to bar fracture near the weld was rotating and slipping of the bar within its plane. As the reinforcing bar slipped, the resulting additional shear concentrated in the bar near the weld led to fracture of the bar at this point.

Figure 4.41 shows that Specimens S1 and S2 dissipated the same amounts of

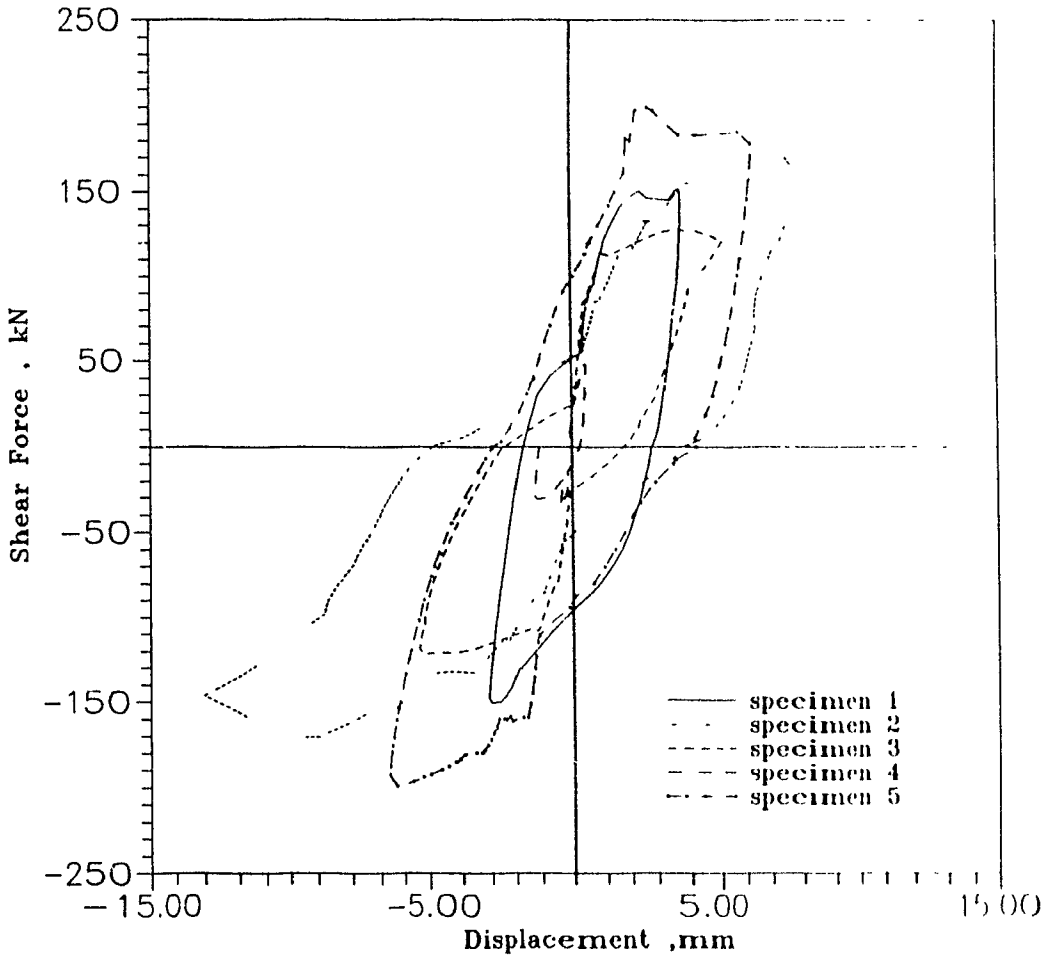

Figure 4.40 Envelopes of responses

energy corresponding to the same level of cumulative ductility in the lower cumulative ductility range. Although Specimen S2 showed a more flexible response (see Figure 4.40) due to the provision of the hook, it caused a considerable improvement in its energy dissipation ability, after splitting bond failure occurred along the straight part of anchor bar. Although the Specimen S5 showed an improved response as seen in the load-deflection envelope in Figure 4.40, the energy dissipation capability was not significantly improved when compared to Specimen S2 (see Figure 4.41).

Specimen S3 which failed by spalling of the concrete block below the angle (cover of angle), displayed a small displacement ductility of 1.7 and low energy dissipated (see Figure 4.41). The pinching behaviour up to the 13th cycle accounted

for a significant reduction in the cumulative energy dissipated. Figure 4.41 shows clearly that Specimen S3 remained elastic up to Cycle 9 (P=80 kN).The cumulative energy dissipated up to the 13th cycle was computed to be about 20% of the total energy dissipated during the test (see Figure 4.41). About 80% of the energy was dissipated in the last three cycles after a lot of cracking and crushing of the concrete around the embedded angle as well as yielding of a significant part of the reinforcing bar anchor. Energy dissipated by Specimen S1 is greater than that in Specimen S3 (see Figure 4.41), although Figure 4.40 shows that the envelope for Specimen S3 is more flexible than that for Specimen S1. It should be noted that in general a more flexible envelope of the load-deflection response (see Figure 4.40) is an indicator of an increased stiffness degradation of the connection under cyclic loading.

Specimen S4 had the smallest energy dissipation as well as the smallest area under the envelop response. As it was observed, the mode of concrete failure occurred by "shear-cone" failure of the concrete surrounding the studs. This type of response is not associated with displacement ductility or energy dissipation ability. Since in Specimen S4 the headed studs did not yield , the definition of cumulative ductility is meaningless. Therefore, it is not presented in Figure 4.41. The cumulative energy was calculated to be 60 J.

During the initial cycling in all specimens, stiffness degradation are not noticeable and the load-deflection curve remains quite linear.

Failure occurred at about 110%, 120%, 97%, 59% and 140% of the predicted monotonic ultimate capacity using the CPCI method for Specimens 1, 2, 3, 4 and 5, respectively. It should be noted that serious cracking of the anchorage zone was observed before noticeable yielding along the length of reinforcing anchor bar. The failure modes are presented in the Summaries for each specimen.

It should be noted that with the exception of Specimen S4, which was reinforced with headed studs,each specimen was able to sustain load even after yielding of a considerable length of the reinforcing steel bar anchor. However, the

strength increases at this load steps are relatively small, and therefore the need to conduct future experiments using "displacement-controlled" rather than "load controlled" tests would be more useful in obtaining a complete picture of the response of these connections.

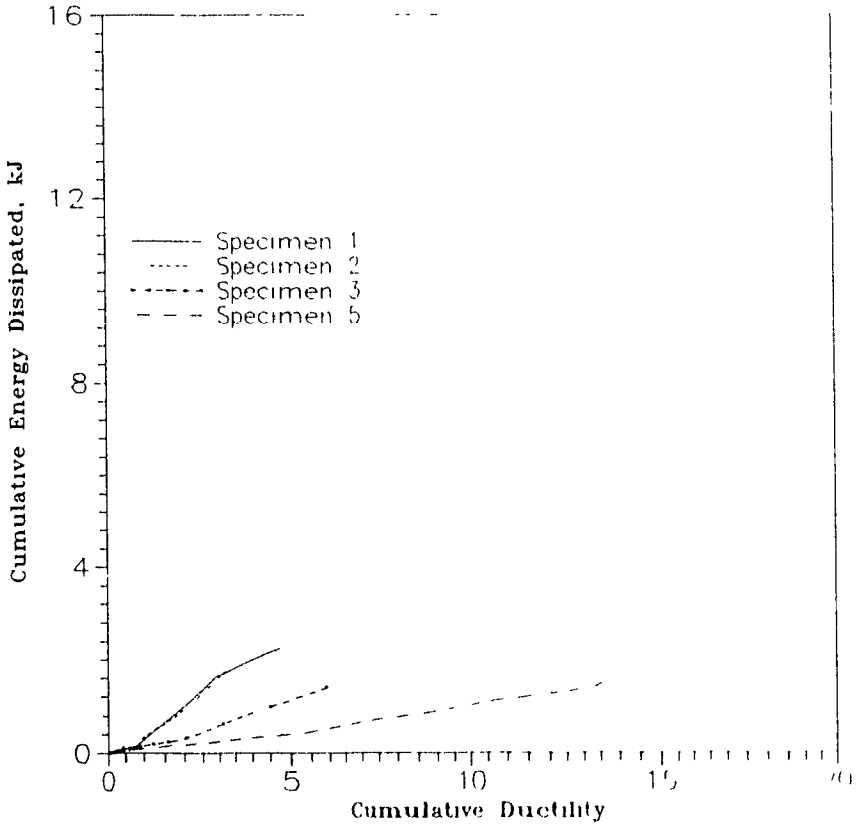

Figure 4.41 Energy dissipated by specimens reinforced with bar anchors

Chapter 5

Evaluation of Analytical and Experimental Results

As mentioned in Chapter 4, the NONLACS finite element analysis program was used to study the non-linear responses of Connections S1, S2, S3 and S5 (between double-tees), subjected to monotonically increasing loads until failure. Again, as mentioned previously, the NONLACS program can be used to study the response of structural reinforced concrete subjected to monotonically increasing loads only. The output from NONLACS analysis presented in this chapter is referred to as "analytical" results. As noted in Chapter 4, the experimental specimens were subjected to reversed cyclic loads to study their complete responses; the experimental results are labelled as "experimental" results. Strictly speaking, the "experimental" results can not be compared with the "analytical" predictions because the loading imposed on the analytical and experimental specimens are different- being monotonically increasing loads for the analytical study and reversed cyclic loads for the experimental investigation. Therefore, some differences are expected between the analytical and experimental results. The following evaluations are based on analytical predictions, conventional methods of design and the experimental data.

The analytical load - deflection characteristics and the ultimate strength of a connection provide key information necessary to understand the connection response. In predicting the load - deflection response of the structure, complete stress - strain relationship for steel including strain hardening and non-linear stress - strain relationship for concrete including the tension stiffening effects should be considered. The constitutive material models used in the NONLACS program were presented in Section 4.2. The "analytical" and "experimental" results for load-deflection characteristics, ultimate strength, and response of reinforcing steel anchors are compared in this chapter. For each element, the stress and the strain at the 5th (middle point) Gauss integration point were selected to evaluate the crack propagation, while the displacement of Node 150 coincident with the location where

displacement of the specimens was measured (see Figure 4.5), and the strains at Location 1 [illegible] ne (Figure 5.2) for the steel anchor were also compared with the experimen[illegible]

5.1 Specimen S1

The analytical lo[illegible]ection curve for Node 150 is compared in Figure 5.1 with the experimen[illegible]nt response for Specimen S1. The analytical initial stiffness, and th[illegible] first cracks initiated, correlate well with the test results. Thi[illegible] elastic responses of the analytical and the experimental spec[illegible] seen from Figure 5.1, the slope of experimental load-deflection curve decr[illegible]gnificantly after the early cycles in the elastic range (Table 4.1), while the "analytical" slope is not affected significantly. The analytical ultimate strength is 180 kN, which is 15% larger than the experimental value. The analytical ultimate displacement predicted to meet the last convergence criterion (0.0005 of the norm of the displacement vector was used as convergence criterion in the NONLACS program) is 2.7 mm, which is 50% smaller than the experimental results. The lower strength and the larger experimental displacement are due to the fact that the cyclic loading causes degradation of bond strength and stiffness at the interface of the concrete and the reinforcing bar, which in turn reduces the stiffness and the ultimate capacity of the connections.

Comparison of the results from the NONLACS analysis and conventional methods of design show that the ultimate strength of the connection calculated using the "truss analogy" are in good agreement with the NONLACS results. It is interesting to note that the ultimate strength according to the modified CPCI method is 183.5 kN which is just 3% larger than analytical prediction value, and the value calculated using the alternate method (see Appendix A), is 170 kN which is 9% smaller than the analytical predicted value (Table 5.1), showing very close agreement between the value obtained using modified CPCI method and the NONLACS program. The ultimate strength according to the CPCI method is 140 kN which is 22% smaller than the analytical predicted value (Table 5.1).

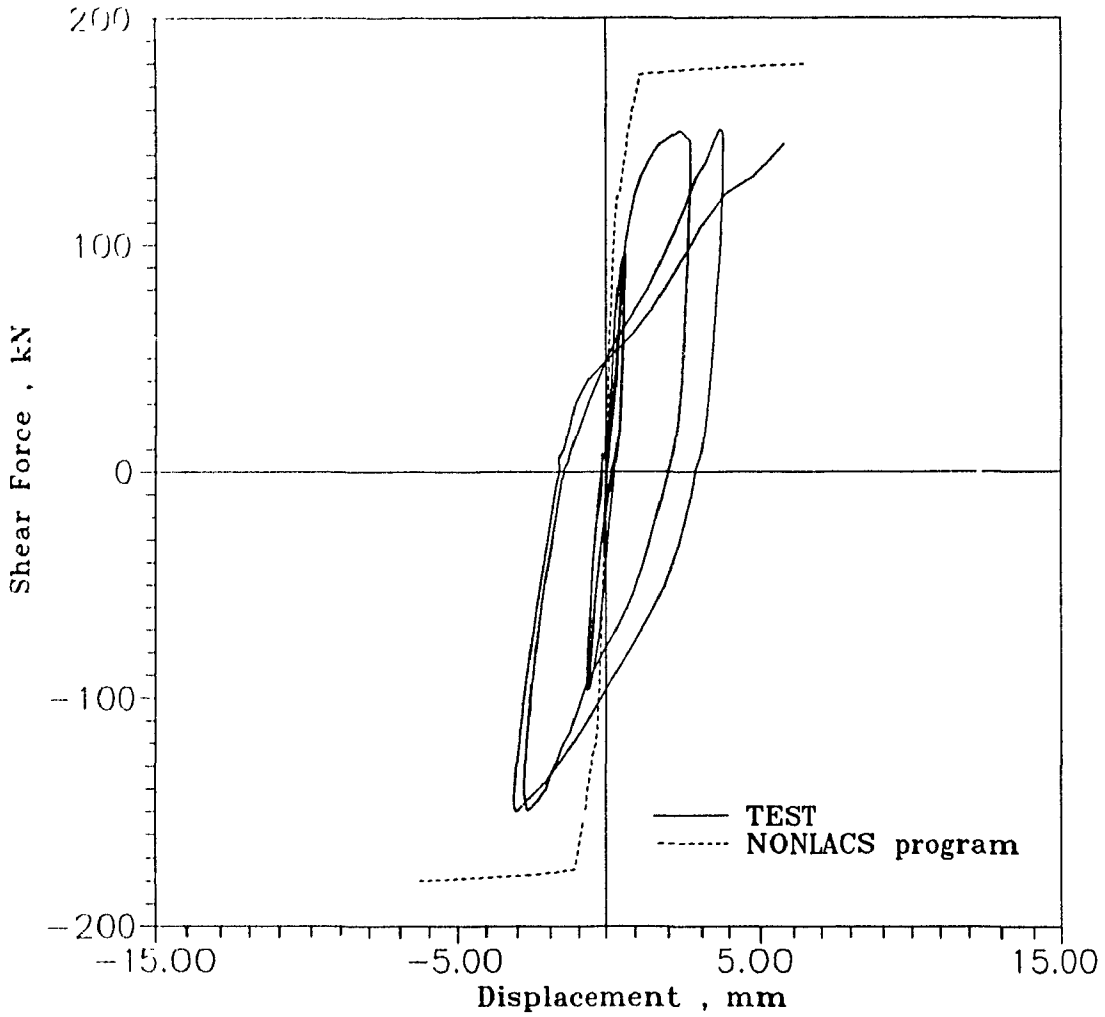

Figure 5.1 Comparison of analytical and experimental load-deflection responses for Specimen S1

Analytical load-steel strain curves for the connection are compared with the experimental results in Figure 5.2. It is seen that the strain plot corresponds well with the envelope of the load-strain test results. It can be noted that the analytical load at which the tensile steel reinforcing bar element yielded was close to 176 kN, which is about 14% higher than the corresponding "experimental" value. This difference is again due to the effect of the cyclic loading of the experimental specimen.

The cracking pattern, at the commencement of cracking correlated well for the "analytical" and "experimental" models. However, the extent of cracking of the

concrete in the analytical model was smaller than that for experimental models (at loads higher than 50 kN). This is due to the cyclic loading, which affects both the cracked and uncracked elements in both compression and tension regions, and also because perfect bond is assumed between the concrete and the steel for both the reinforcing bar anchor and the reinforcing mesh in the "analytical" specimen.

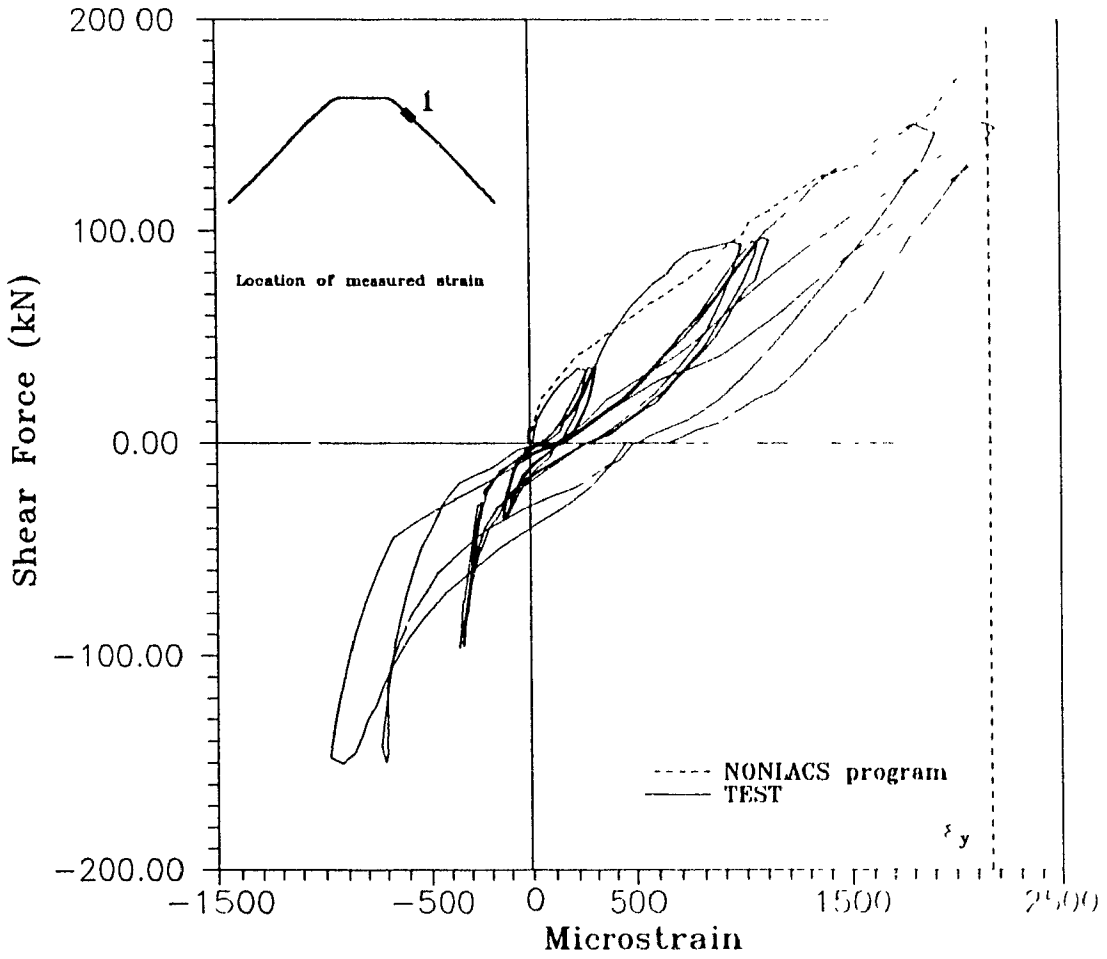

Figure 5.2 Comparison of analytical and experimental load-steel strain responses at location 1 for Specimen S1

5.2 Specimen S2

The experimental and analytical plots of the applied load P versus the Node 150 displacement are compared in the Figure 5.3. The initial stiffness and the load

at initiation of the first cracks correspond well with the experimental results. This correlation is due to the fact that both specimens were basically in the elastic range before crack initiation. The slope of the load-deflection plot diminishes significantly after the initial cracking (few cycles after the elastic range, see Table 4.2), whereas the "analytical" stiffness is not influenced considerably (see Figure 5.3). The analytical ultimate load is 183.5 kN, which is about 7% higher than the experimental value. The maximum "analytical" displacement predicted to achieve the specified convergence criterion is 2.22 mm, about 27% of experimental result. The lower strength and the larger experimental displacement can be attributed to the effects of the cyclic loading, which tends to deteriorate the bond strength and stiffness and the ultimate strength of the connection.

Comparison of the results from the NONLACS analysis and the conventional design method show that the ultimate strength calculated according to the modified CPCI method and the value calculated using the alternate method (see Appendix A) are 183.5 kN and 187 kN, which are only 0.5% and 2.5% higher than the analytical value, respectively (see Table 5.1). This indicates excellent agreement between the NONLACS results and the values calculated using the modified CPCI and the alternate method of design. The ultimate strength according to the CPCI method of design is 140 kN which exhibits 23% smaller than the analytical predicted value (see Table 5.1)

The analytical and experimental results are compared for the applied load versus the strain at Location 1 of the reinforcing steel in Figure 5.4. It can be seen that the analytical strain curve correlates well with the envelope of experimental load-strain results. It should be noted that the analytical load corresponding to yielding of the tensile steel bar was approximately 172 kN, which is about 11% higher than the value obtained experimentally.

The analytical and experimental cracking patterns, at the initiation of first cracks show good agreement. However, the extent of propagation of cracks in the "analytical" model was smaller than that in the experimental results, at loads higher than 60 kN, basically because of the deterioration of bond at the steel-concrete interface and the resulting deterioration of the specimen under reversed cyclic

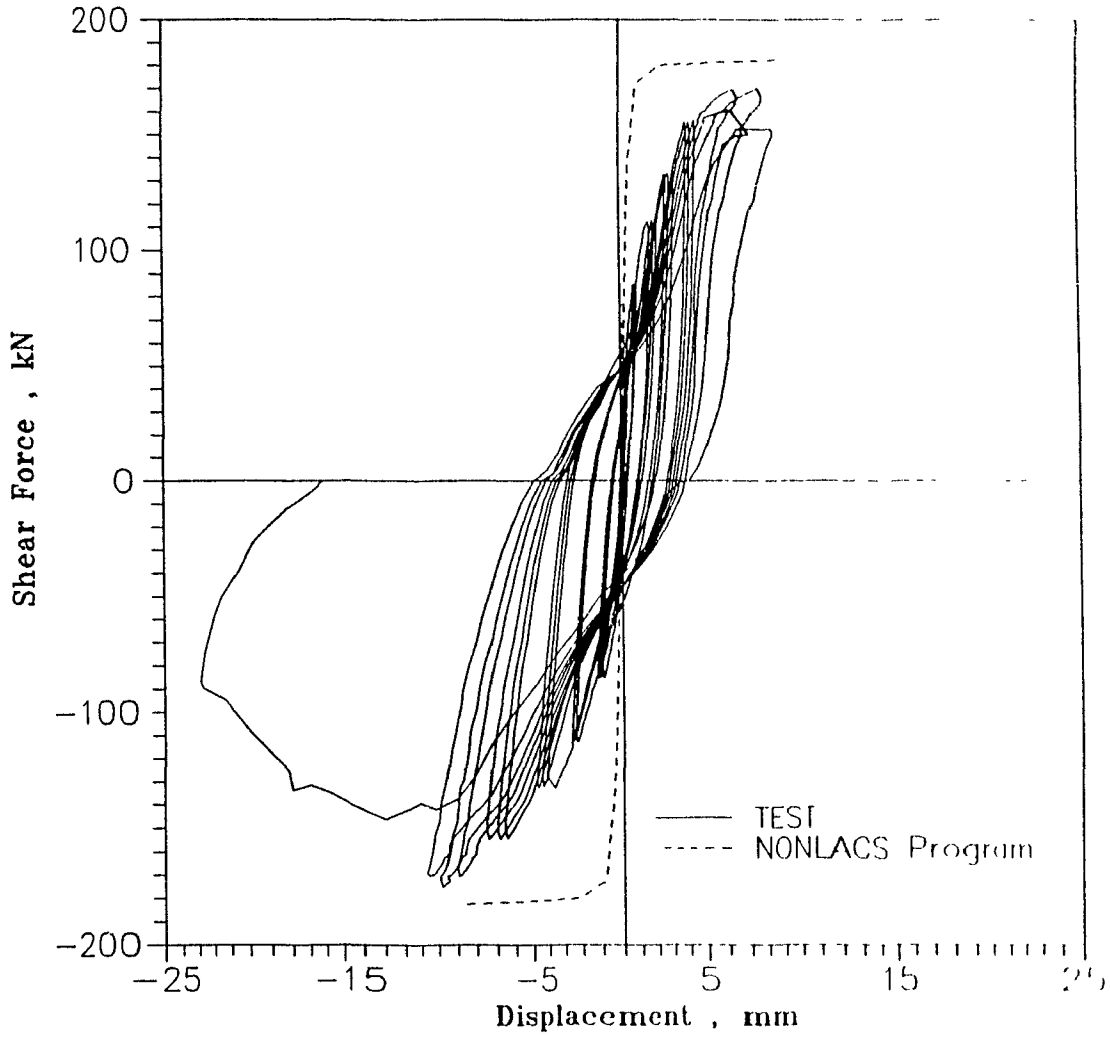

Figure 5.3 Comparison of analytical and experimental load-deflection response for Specimen S2

loading, and the assumption of "perfect" bond between the concrete and the steel in the analytical model

The failure in the "experimental" and "analytical" models occurred in the tensile zone due to complete deterioration of concrete along the straight part of the bar and in front of the 90 degree hook.

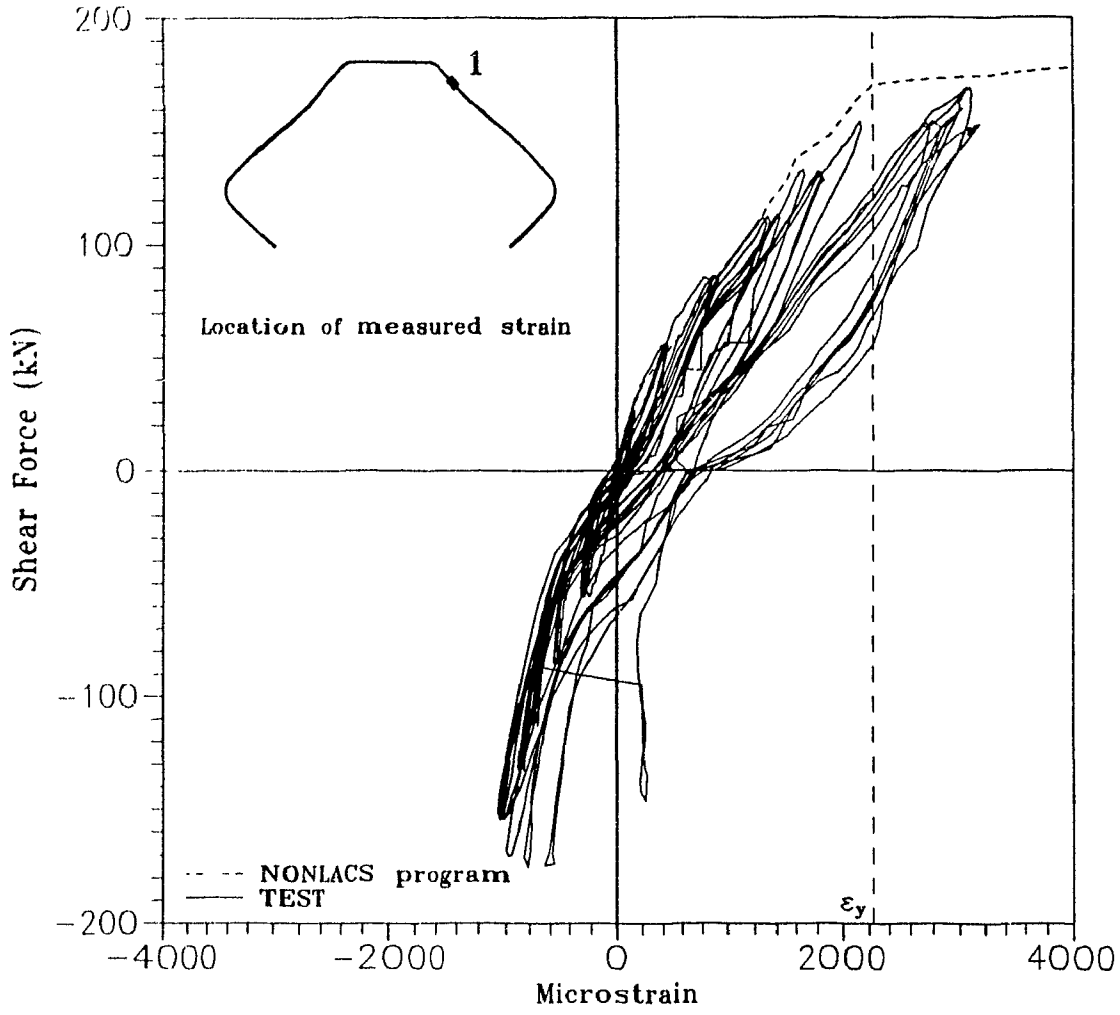

Figure 5.4 Comparison of analytical and experimental load-steel strain responses at Location 1 for Specimen S2

5.3 Specimen S3

The "analytical" and "experimental" load-deflection curves at Node 150 for Specimen S3 are compared in Figure 5.5. It can be noted that the correlation is generally good. The difference between the "analytical" and "experimental" ultimate strength values is about 4%. In addition to the load-deflection curve, Table 5.1 compares the "experimental" and "analytical" strength values.

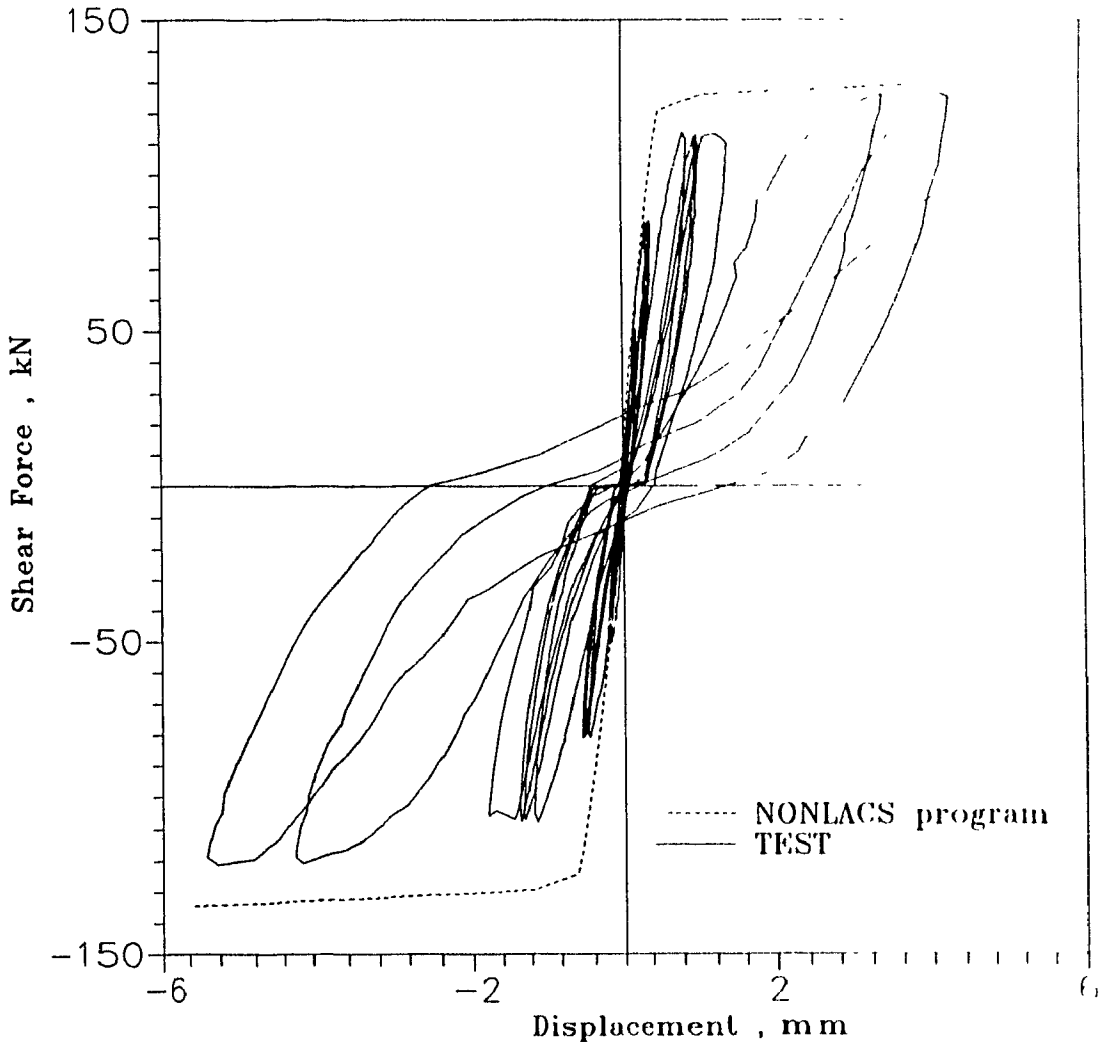

Figure 5.5 Comparison of analytical and experimental load-deflection responses for Specimen S3

The slope of the experimental load-deflection curve decreases significantly at load higher than 80 kN, whereas the slope of the analytical load-deflection curve is not significantly affected. The maximum analytical displacement at the last convergence is 1.2 mm which is 78% smaller than the experimental value. Here again, there are differences between the two sets of results, basically due to the influence of the reversed cyclic loads, resulting in a greater degradation of the strength and stiffness of the connection compared with the response under monotonically increasing loads. When compared with the calculated capacity using the shear friction design method,

the calculated ultimate strength is about 2% higher than the NONLACS value.

Figure 5.6 compares the "analytical" and "experimental" load-steel strain results. The overall analytical response is stiffer than the envelope of the experimental response. It can be seen that the reinforcing bar did not yield in the "analytical" model.

The initiation and propagation of cracks, during the early load steps (up to 40 kN) corresponds well for the "analytical" and "experimental" models. However, for loads higher than the 50 kN, the extent of the "experimental" crack distribution was larger than the corresponding "analytical" results.

Both "analytical" and "experimental" results show that the failure was governed by deterioration of the concrete surrounding the steel angle, particularly the concrete cover over the angle flange.

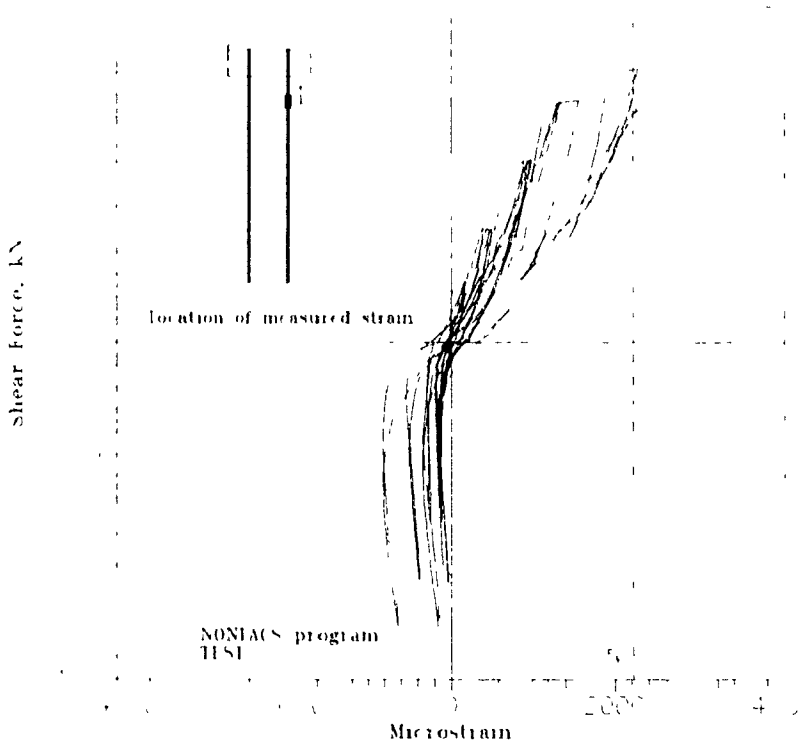

Figure 5.6 Comparison of analytical and experimental load-steel strain responses at Location 1 for Specimen S3

5.4 Specimen S4

As mentioned earlier, the specimen was not analyzed using the NONLACS program, because of the inability of the program to model shear connectors. As a consequence, the comparison is made between the "experimental" results and the "analytical" values. The specimen strength calculated using the CPCI method is compared with the corresponding experimental value in Table 5.1.

The "analytical" ultimate strength is 73 kN, which is about 1.7 times the "experimental" value. The lower strength is mostly due to degradation caused by the reversed cyclic loading. As it was observed experimentally, the behaviour of the connection under the in-plane loading was governed essentially by cracking of the concrete surrounding the headed studs, which caused "cone-type" failure of the connection. The critical stress state of the concrete resulting in cracking was mostly biaxial tension . It was also noted that the opening and closing of the cracks in the concrete due to cyclic load contributed most significantly to the reduction in the ultimate strength of the connection.

5.5 Specimen S5

The "analytical" and "experimental" load-deflection curves for Node 150 are compared in Figure 5.7. The analytical initial stiffness corresponds well with the experimental results, which is basically due to the near elastic behaviour of both specimens up to the initial cracking load. As the applied load was increased the "experimental" stiffness (slope of the load-displacement plot) decreased significantly, while the "analytical" stiffness did not change appreciably The load-deflection curves showed that the "analytical" ultimate strength is about 7.5% higher than the "experimental" value. The "analytical" displacement corresponding to last convergence is 1.9 mm, about 70% smaller than the experimental value. The overall analytical load-deflection response is stiffer than the envelope of experimental response. These differences are mostly due to the "experimental" reversed cyclic loads, resulting in deterioration of bond strength and stiffness at the interface of steel bar and concrete and significant concrete cracking in the vicinity of the headed studs. These effects reduce the stiffness and the ultimate strength of the connection.

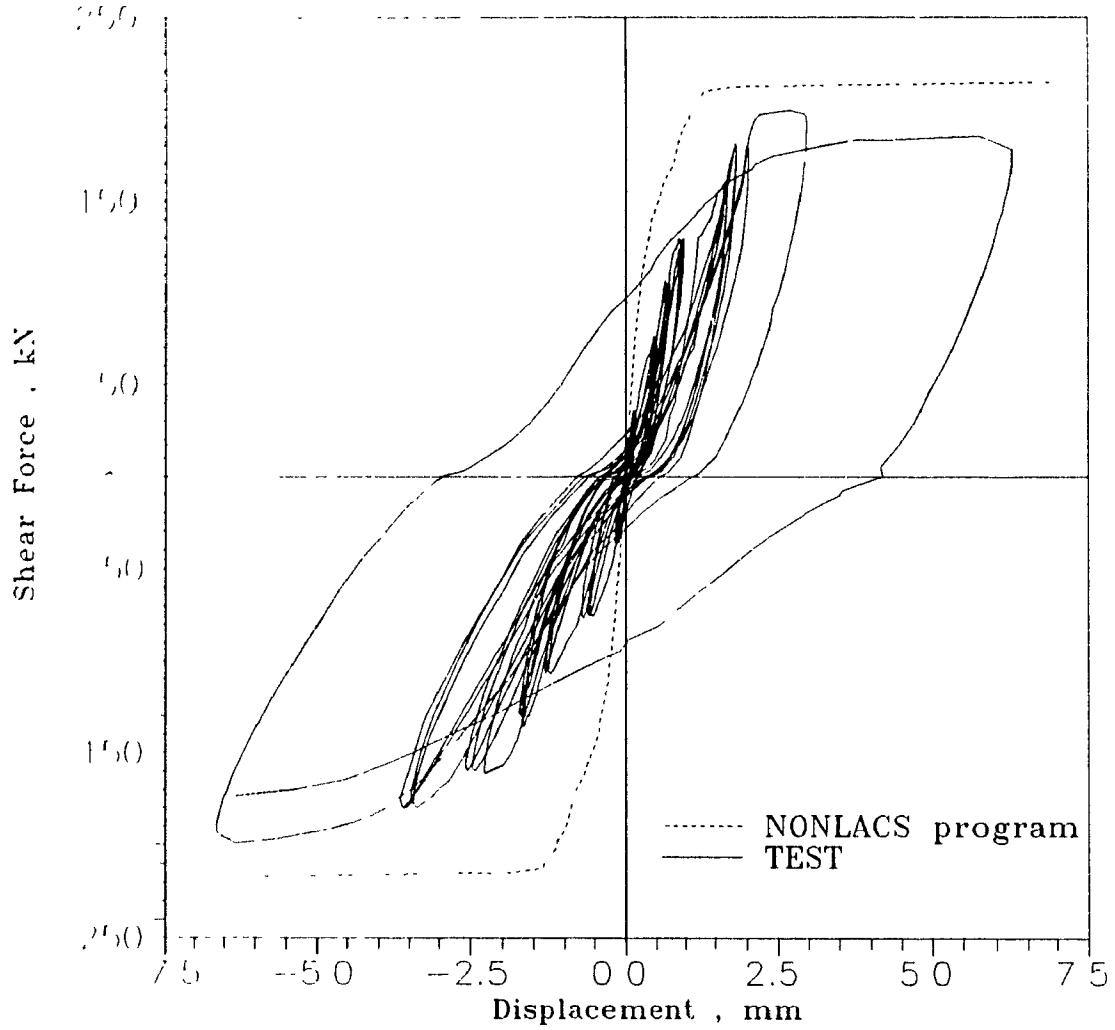

Figure 5.7 Comparison of analytical and experimental load-deflection responses for Specimen S5

Comparison of the results of the NONLACS program and the conventional design methods show that the CPCI and the modified CPCI methods are conservative by about 14% and 35%, respectively, while the strength calculated using the alternate method (see Appendix A) is about 15% higher than the corresponding values obtained from the NONLACS program (see Table 5.1).

Figure 5.8 compares the analytical and experimental load-steel strain curves for Specimen S5. As can be seen, the general envelope of the experimental load-strain curve is more flexible (softer) than the analytical response. It is should be

noted that the "analytical" load at which the tensile steel bar yielded was approximately 207 kN, about 1.3 times the "experimental" value. These differences, again, are mostly due to the cyclic loading used for testing the "experimental" specimen.

The cracking pattern, at the commencement of cracking for the "experimental" and "analytical" models are in good agreement. However, the extent and propagation of the cracking (at loads higher than 75 kN) in the experimental specimen were larger than those for the analytical model. The mechanism of failure obtained from the NONLACS results for the "analytical" model subjected to monotonically increasing loads was similar to that for the "experimental" model, subjected to reversed cyclic loads.The mode of failure in the "analytical" model was due to extensive deterioration of the concrete along the entire length of the reinforcing bar accompanied by complete cracking in the vicinity of the headed studs.

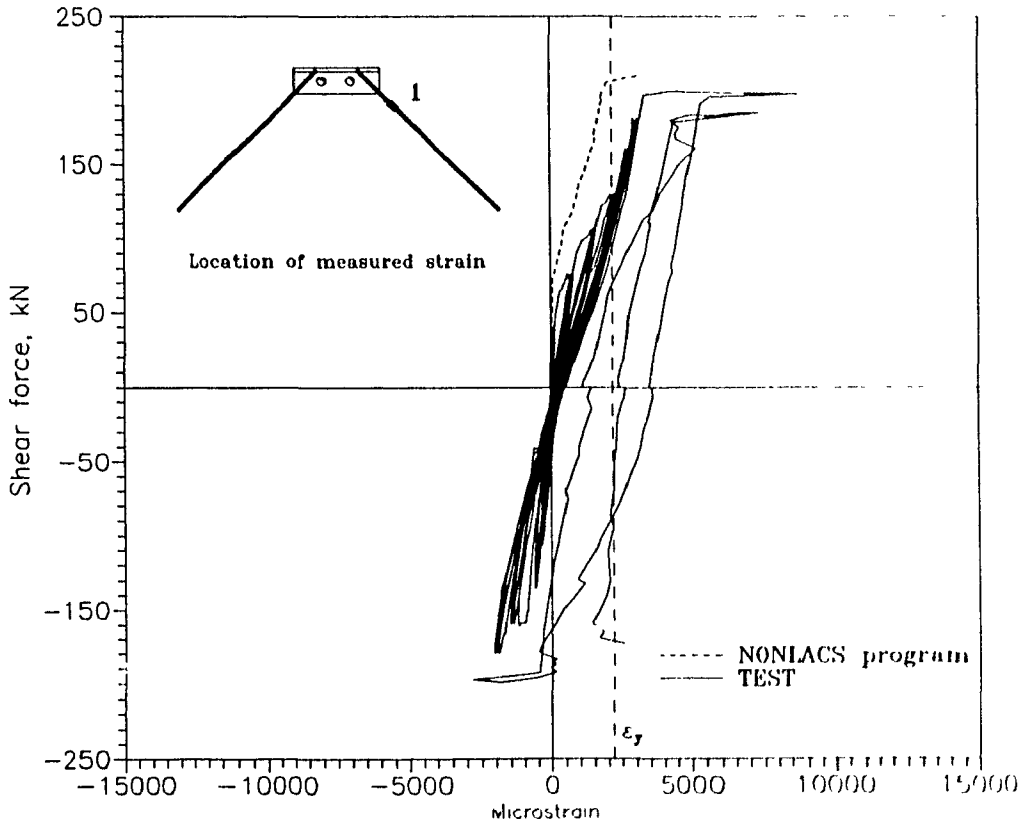

Figure 5.8 Comparison of analytical and experimental load-steel strain responses at Location 1 for Specimen S5

Table 5.1 Comparison of "Analytical" and "Experimental" Strengths

Connection	Analytical Strength (kN)				Experimental Strength (kN)
	CPCI Method	Modified CPCI Method	Alternate Method	NONLACS Results	
S1	140	183.5	170	180	150
S2	140	183.5	187	182.5	170
S3	128	-	-	130	125
S4	73	-	-	-	43
S5	140	183.5	247	215	200

Chapter 6

Design Recommendations and Conclusions

The experimental part of this research program consisted of tests on five full scale specimens representing the connections between precast double tee flanges or between a double-tee flange and lateral resisting elements. Although there are empirical methods available for design of these connections, these are unable to predict the complete response of connection. The Precast/Prestressed Concrete Institute design method provides a model only for elastic design of connection, however, this method cannot predict the inelastic response under monotonically increasing loads or for the inelastic response under reversed cyclic loads. The embedment length requirement for the reinforcing bar anchor as suggested by the current design method, is based on the bond response of the steel reinforcement under monotonically increasing loading when the concrete cover thickness is sufficient (thick panel). However this research program involved a thin panel (50 mm thickness) for investigation of the complete response of the connections under reversed cyclic loads. The design recommendations and conclusions are based on the experimental results, analytical response predictions and the results of the non-linear analyses of the response of these specimens when subjected to monotonically increasing loads. Table 6.1 summarizes the values of the ratio, β, the "analytical" ultimate strength to the "experimental" ultimate strength ratio, calculated using the CPCI method, together with the design and detailing requirements for this kind of connections The design recommendations and conclusions are summarized below:

1. The boundary conditions for the experimental specimens were selected from the results of elastic analyses (SAP90) of double-tee flanges subjected to static shearing forces. Steel plates were epoxied to the concrete panel and the entire assembly was then welded to a steel frame (Chapter 2). The experimental response at the

specimen boundary was noted to be linear with the load and satisfactory.

2. The panel (flange) thickness and concrete quality can have a marked effect on the behaviour of the connection. In calculating the static ultimate design load, the effect of average concrete cover thickness along the reinforcing bar of the connection is taken into account.

3. Serious cracking of the anchorage zone was observed before noticeable yielding along the length of reinforcing anchor bar. Any such damage reduces the likelihood of a good response in a subsequent earthquake.

4. (a) Preliminary values of β, the ratio of the ultimate static strength calculated using the CPCI method to the values obtained experimentally are shown in Table 6.1 along with the other relevant recommendations for the embedment length of the anchors and thicknesses of the steel plate or the angle . It should be noted that these recommendations are based on the results of only one specimen in each category, and therefore more experimental and analytical research is needed.
(b) It must be ensured that the anchor bar is welded completely along its length to the steel plate or the angle comprising the joint.

5. (a) Specimen S5 exhibited the largest ultimate strength and displacement ductility (3.0), however, its response in the intermediate cycles, before significant concrete cracking around the studs, showed some pinching, which is reflected in the low energy absorption characteristics. Specimen S2 exhibited the best energy absorption characteristics and had a displacement ductility ratio of 2.5. Therefore, the use of a 90° hook can improve the overall response of the connection, especially in Specimen S5 with headed studs.

(b) Specimen S4 displayed the lowest ultimate strength and the worst energy absorption characteristics compared with all other specimens tested. This specimen failed with a 30°concrete cone being sheared off, compared with the 45° angle

suggested by the CPCI method. Therefore, new mechanisms for dissipating energy should be explored. One suggestion is to investigate whether it is possible to design the connection S4 such that the energy is dissipated in the steel headed studs

6. The design approach of the CPCI gives a conservative prediction for the ultimate strengths of Specimens S2 and S5, while the ultimate strengths of Specimens S1 and S3 are close to the experimental results. The experimental ultimate strength of Specimen S4 is only 0.59 of the ultimate strength given by the CPCI method The CPCI method overestimates the ultimate strength of the connection and the reduction factor of 0.6 is recommended. It should be noted that this value has been calculated using the unfactored concrete strength. Therefore, for design purposes, this value should be multiplied by ϕ_c (0.6), the resistance factor for concrete.

7. The experimental strength for Specimens S1, S2, S4 and S5 were 0.83, 0.93, 0.96 and 0.93 of the analytical strength predicted by the NONLACS program

Suggestions for Future Studies

Very little experimental data is available on the behaviour of thin flange connections subjected to reversed cyclic loading. More experimental work should be undertaken to study the influence of different parameters such as the reinforcing bar diameter and yield strength, concrete strength and cover thickness, stud size (including length and diameter), and the type of loading (monotonically increasing or reversed cyclic involving shear, tension or combined shear and tensile loads) to improve the understanding of the seismic response of these connections. Also, large numbers of similar connections should be tested to establish a strength distribution for these connections.

Table 6.1 Design requirements and values of β

Connection	β	Design Requirements
Connection 1	1.10	a) Provide reinforcing bar embedment length $l_d = 154.5\ d_b/\sqrt{f'_c} > 30\ d_b$ b) Completely weld all of the straight part of the bar to the face plate. c) Use a face plate of thickness, $t \geq 4/5\ d_b$
Connection 2	1.21	a) Provide reinforcing bar embedment length based on: $l_{hd} \geq 149.5\ d_b/\sqrt{f'_c}$ (with hook at the end) b) Completely weld all of the straight part of the reinforcing bar to the face plate. c) Use a plate of thickness, $t \geq 4/5\ d_b$
Connection 3	0.97	a) The embedment length must be $l_d = 154.5\ d_b/\sqrt{f'_c} > 30\ d_b$ b) Use an angle with $t \geq 3/4\ d_b$ c) Provide confining reinforcing bar (smaller size), or use the headed studs welded perpendicularly to the angle to counteract the spalling of the concrete below the angle.
Connection 4	0.59	a) Detail the joint in which stud failure is predicted b) Provide longer headed studs welded to the plate at larger centre to centre distances c) Use plate thickness, $t \geq 3/4\ d_b$
Connection 5	1.43	a) Provide reinforcing bar embedment length $l_d = 154.5\ d_b/\sqrt{f'_c} > 30\ d_b$ b) Use an angle with $t \geq 4/5\ d_b$

References

[1] Kunze, W. E., Sbarounis, J. A., Amerhein, J.E. "*The March 27 Alaskan Earthquake - Effeson Structures in Anchorage.*" ACI Journal, Vol 62, No 6, June 1965, pp. 635 - 648.

[2] Hawkins Neil M. "Seismic resistance of prestressed and precast concrete" structures. Part 1 - Prestressed Concrete. *Prestressed Concrete Institute Journal*, 22(61): November-December 1977, pp 80-110.

[3] Hawkins Neil M. "Seismic resistance of prestressed and precast concrete" structures. Part 2 - Prestressed Concrete. *Prestressed Concrete Institute Journal*, 23(1): January-February 1978, pp 40-58.

[4] Becker James M. and Sheppard David A Connection for seismic resistant precast concrete connection. *In Design of Prefabricated Concrete Buildings for Earthquake Loads* , Applied Technology Council, April 1981 ATC-8, pp 657-683

[5] Stanton J.F., Anderson R.G., Donal C.W., and McCleary D E. *Design of Connections for Precast Prestressed Concrete Building for the Effect of Earthquake* Prestressed Concrete Institute, Chicago, U S A. 1986 TR-5-86, 184 PP

[6] Aswad, A., "Selected Precast Connections Low - Cycle Behaviour and strength", *Proceedings of the Third Canadian Conference on Earthquake Engineering*, Vol 2, Montreal, 1979, pp 1201-1224.

[7] Neille, D. S., "*Behaviour of Headed Stud Connections for Precast Concrete Panels under Monotonic and Cycled Shear Loading.*" , PhD. Thesis, University of British Columbia, May 1977

[8] Karsan, I. D., and Jirsa, J. O., "Behaviour of Concrete under Compressive Loadings", *Journal of the Structural Division, ASCE*, Dec. 1969.

[9] Schicker, V., Powell, G. H., "*Inelastic seismic analysis of large panel buildings*" Report No. UCB/EERC-80/38, Earthquake Engineering Research Centre, College of Engineering, University of California, Berkeley, Sept 1980

[10] Spencer, R. A. and Neille, P. S., "Cyclic Tests of Welded Headed Stud Connections", *PCI Journal*, Vol. 21, No. 3, May - June, 1976, pp 70 - 83

[11] Precast/Prestressed Concrete Institute, *PCI Design Hand book - Precast and Prestressed Concrete* Prestressed Concrete Institute, Chicago, U.S.A Second Edition, 1985.

[12] Precast/Prestressed Concrete Institute, *PCI Design Handbook - Precast and Prestressed Concrete.* Prestressed Concrete Institute, Chicago, U. S. A., first edition, 1971.

[13] Spencer, R. A., "Earthquake Resistant Connections for Low Rise Precast Concrete Buildings", *Seminars on Precast Concrete Construction in Seismic Zones.* Tokyo, October 27 - 31, 1986, pp 61 - 81.

[14] Kallros, M., *An Experimental Investigation of Behaviour of Connections in Thin Precast Concrete Panels under Earthquake Loading.* M.A.Sc Thesis, University of British Columbia, April 1987.

[15] Associate Committee on the National Building Code. "*National Building Code of Canada 1990*" National Research Council of Canada, Ottawa, Canada, 1990.

[16] Canadian Standard Association, CSA, "*Design of Concrete Structure for Buildings. CAN3 - A23.3-M84*", Rexdale, Canada, 1984.

[17] Precast/Prestressed Concrete Institute, *Design and Typical Details of Connection for Precast and Prestressed Concrete,* Chicago, U.S.A, Second Edition, 1988.

[18] Canadian Prestressed Concrete Institute, CPCI, *Metric Design Manual - Precast and Prestressed Concrete.*, Ottawa, Canada, Second Edition, 1987.

[19] ACI Committee 318, "*Building Code Requirements for Reinforcing Concrete (ACI 318 - 89) and Commentary - ACI 318 R - 89*", American Concrete Institute, Detroit, 1989, 360 pp

[20] ACI Committee 408, "*Bond and Development Lengths*" Subcommittee on Repeated Loading State-of-The-Art Report on Bond Under Cyclic Loading, Final Draft, RTI-July 1989.

[21] ATC-3 (Applied Technology Council), "*Tentative Provisions for the Development of Seismic Regulations for Buildings*", National Bureau of Standards, U.S. Department of Commerce, Washington, DC, June, 1978.

[22] Canadian Standard Association, "*Weldable Low Alloy Steel Deformed Bars for Concrete Reinforcement, G30.16 - M.*" Canadian Standards Association, Rendale, Canada

[23] Wilson, E. W. and Habibullah A. "*SAP 90, A Series of Computer Programs for Static and Dynamic Finite Element Analysis of Structures.*" Computer Structures, Inc., 1918 University Avenue, Berkeley, California, U.S.A., July 1989.

[24] R. Jimenez, R.N. White, and P.Gergery. Bond and Dowel capacities of Reinforced Concrete. *ACI Journal, Symposium Paper, 76-4* January 1979, pp 73-93.

[25] Martin, L.D. and Korkosz, W. J. "*Connections for Precast Prestressed Concrete Buildings - Including Earthquake Resistance.*" Prestressed Concrete Institute, Chicago, U.S.A., 1982, TR - 2 - 82, 297 pp.

[26] *American Society of Civil Engineers, ASCE,* "State of -The- Art Report, Finite Element Analysis of Reinforced Concrete", New Yourk, 1982

[27] G. A. M. Ghoneim. "*Nonlinear Finite Element Analysis of Concrete Structures*" PhD. Eng. Thesis, Department of Civil Engineering, University of Calgary, Calgary, Canada, 1978.

[28] A. G. Razaqpur and M. E. Nofal. "*Transverse Load Distribution at Ultimate Limit States in Single Span Slab-on-Girder Bridges With Compact Steel Sections*" Technical Report MISC-88-01, The Research and Development Branch Ministry Of Transportation, Ontario, Canada, September 1988.

[29] Tong W. K. T. "*Non-Linear Seismic Analysis of a One-Storey Precast Concrete Building.*" M. A. Sc. Thesis, University of British Columbia., 1984, 240 pp

[30] Parmar S. S. "*2-D Non-Linear Seismic Analysis of One-Storey Eccentric Precast Concrete Building.*" M. A. Sc. Thesis, University of British Columbia , 1987, 167 pp.

[31] Canadian Standard Association, CSA, "*Steel Structures for Buildings - Limit States Design, CAN3-S16.1-M89.*", Rexdale, Canada, 1989.

Appendix A

Design and Analysis of Test Specimens

The ultimate strength of the specimens were calculated using the following three methods:

1. The CPCI method using a steel strength equal to its measured yield strength ($f_s = f_y$), reinforcing bar resistance factor, $\phi_s = 1$, and concrete resistance factor, $\phi_c = 1$, when the connection fails.

2. The modified CPCI method using a steel strength equal to its measured ultimate strength ($f_s = f_{ult}$), reinforcing bar resistance factor, $\phi_s = 1$, and concrete resistance factor, $\phi_c = 1$, when the connection fails.

3. An alternate method, using the equations due to Jimenez et al[24] to calculate the dowel and pullout forces in the bar legs, the length of reinforcing bars selected based on anchorage lengths required when the bars are subjected to reversed cyclic loading[20], and equations 1-12 and 1-14, was used to calculate the required anchorage lengths.

M15 weldable deformed reinforcing bar with a cross-section area, $A_s = 200$ mm^2, and measured material properties were used for all of the specimens.

It should be noted that the ultimate strength of Connections S3 and S4 were obtained only using the CPCI method.

A.1 Specimen S1

CPCI Method

Each reinforcing bar leg is assumed to reach its yield strength when the connection fails. Then the ultimate compressive strength, C_u, in the compression leg and the ultimate tensile strength, T_u, in the tensile leg are given by:

$$C_u = T_u = A_s \times f_y \qquad \text{(A-1)}$$

where A_s = 200 mm

f_y = measured ultimate stress for steel bar = 495 MPa

Substituting in equation A-1, gives:

$$C_u = T_u = 200 \times 495 \times 10^{-3} = 99 \text{ kN}$$

and, using truss analogy, the value of V_{ult} is given by:

$$V_{ult} = (C_u + T_u)\cos 45°$$

$$V_{ult} = 140 \text{ kN}$$

Modified CPCI Method

Each reinforcing bar leg is assumed to reach its ultimate strength when the connection fails. Then the ultimate compressive strength, C_u, in the compressive leg and the ultimate tensile strength, T_u, in tensile leg are given by:

$$C_u = T_u = A_s \times f_{ult} \qquad \text{(A-1)}$$

where A_s = 200 mm

f_{ult} = measured ultimate stress for steel bar = 649 MPa

Substituting in equation A-1, gives:

$$C_u = T_u = 200 \times 649 = 129.8 \text{ kN}$$

and, using truss analogy, the value of V_{ult} is given by:

$$V_{ult} = (C_u + T_u)\cos 45°$$

$$V_{ult} = 183.5 \text{ kN}$$

Alternate Method

The dowel strength of the M15 bar is calculated using the following equation:

$$V_{d_o} = 0.75 \frac{b_n}{n} d_b \quad \textbf{(in Imperial units)} \qquad \text{(A-2)}$$

$$V_{d_o}=0.0052\frac{b_n}{n}d_b \quad \textbf{(in S. I. units)} \qquad (A\text{-}3)$$

where d_b = diameter of steel bar = 16 mm

b_n = net thickness = total thickness - d_b = 75 -16 = 59 mm

n = number of bars in one layer of reinforcement = 1

Substituting these values in equation A-3 gives the value of V_{do} as

$$V_{do} = 4.9 \text{ kN}$$

This dowel force acts normal to the steel bar.

To determine the bond capacity of M15 corresponding to a splitting type of failure, the anchorage length used in the specimen was considered. This anchorage length was already designed based on specified material properties using equation 1-12 as:

$$l_d = \frac{154\ 5xd_b}{\sqrt{f_c'}} \geq 30d_b \qquad (1\text{-}12)$$

Substituting in equation 1-12 gives the value of l_d = 418 mm, which must be larger than $30d_b$ = 30x16 = 480 mm.

Therefore, the anchorage length is

$$l_d = 480 \text{ mm}$$

The ultimate tensile and compression strengths in the tensile and compressive legs are identical, and are calculated as follows:

$$T_u=\frac{d_b l_d C\sqrt{f_c'}}{35.4d_b+0.537l_d} \quad \textbf{(in Imperial units)} \qquad (A\text{-}4)$$

Substituting in equation A-4 gives the value of T_u as:

$$T_u = \frac{d_b l_d C\sqrt{f_c'}}{424.45 d_b + 6.87 l_d} \quad \textbf{(in S. I. units)} \qquad \text{(A-5)}$$

$$C_u = T_u = \frac{16 \times 480 \times 23 \times \sqrt{43}}{424.45 \times 16 + 6.87 \times 480} = 115 \ kN$$

Using the "truss analogy" and including the dowel strength, the value of the ultimate shear strength of the connection, V_{ult}, is given by

$$V_{ult} = 2 \text{ x } (4.9 + 115) \cos 45° = 170 \text{ kN}$$

A.2 Specimen S2

CPCI Method

Since the ultimate strength of the connection depends only on the reinforcing bar properties, the ultimate strength is identical to that of Specimen S1.

Therefore, $V_{ult} = 140$ kN

Modified CPCI Method

Since the ultimate strength of the connection depends only on the reinforcing bar properties, the ultimate strength is identical to that of Specimen S1.

Therefore, $V_{ult} = 183.5$ kN

Alternate Method

The dowel strength of Specimen S2 is identical to that for Specimen S1, therefore, the value of V_{do} is

$$V_{do} = 4.9 \text{ kN}$$

To calculate the bond strength corresponding to a splitting type of failure, the development length for hooked bar anchor used in test specimen was considered.

This anchorage length was designed using the equation 1-14 as:

$$l_{hd} = \frac{149.5 \times d_b}{\sqrt{f'_c}} \quad \textbf{(in S. I. units)} \qquad (1\text{-}14)$$

Substituting in equation 1-14 gives the value of straight part of hook anchorage, l_{hd} as:

$$l_{hd} = 400 \text{ mm}$$

The length of right angle hook part is taken 12 times the diameter of the steel bar, which is equal to 12 x16 =192 mm.

The ultimate tensile stress in the hooked bar is calculated using the following equation in Clause 12.5.2 of the CSA Standard CAN3-A23.3-M84[16]:

$$l_{hb} = \frac{100 d_b}{\sqrt{f'_c}} \frac{f_s}{400} \quad (S.I.) \qquad (A\text{-}6)$$

where $l_{hb} = l_{hd} + R_{ba} + d_b = 400+95/2+16 = 432.5$ mm

R_{ba} = the inside radius of the hook

f'_c = 47 MPa (concrete compressive strength for Specimen S2)

Substituting in equation A-6 gives the value of f_s = 741 MPa, which must be less than the ultimate strength of the reinforcing bar steel.

Therefore,

$$f_s = f_{ult} = 649 \text{ MPa}$$

The ultimate strength of the hooked steel bar, T_u , therefore, is

$$T_u = A_s \text{ x } f_{ult} = 200 \text{ x } 649 = 129.8 \text{ kN} \qquad (A\text{-}7)$$

Because of equilibrium in the truss analogy, the force in the compression leg must be equal to that for the tensile leg, which gives:

$$T_u = C_u = 129.8 \text{ kN}$$

Using the "truss analogy" and including the dowel strength, the ultimate strength of the Specimen S2, V_{ult}, is given by

$$V_{ult} = (V_{do} + C_u + T_u)\cos 45° = (4.9 + 129.8 + 129.8)\cos 45° = 187 \text{ kN}$$

A.3 Specimen S3

CPCI Method

The reinforcement bars welded to the embedded angle should be large enough to ensure that they do not yield even when the connecting plate (welded to the plate or angles on either side of the joint) is stressed to its ultimate strength. This minimizes cracking damage to the panel. It should be noted that the material resistance factors were considered to be equal to 1 to obtain the unfactored strength of the connection.

The connection works by a shear-friction mechanism, and the Clauses 11.7.4 to 11.7.10 from CSA Standard CAN3 - A23.3-M84[10] are used to calculate the ultimate strength of Specimen S3 as follows:

Since shear-friction reinforcement is perpendicular to the shear plane, the ultimate factored shear resistance, V_{ult}, is computed by:

$$V_{ult} = A_{vf} f_y \mu \qquad (A\text{-}8)$$

where A_{vf} = area of shear-friction reinforcing bar = 2 x 200 = 400 mm^2

$\mu = 0.8\lambda$ for concrete anchored to steel plate by reinforcing bar, and contact plane one full plate thickness below the concrete surface

$\lambda = 1$ for normal density concrete

f_y = yield strength of the reinforcing bar, but shall not be taken as greater than

400 MPa (Clause 11.7.6) = 400 MPa

Substituting values in equation A-8, gives

$$V_{ult} = A_{vf}\, f_y\, \mu = 400 \times 400 \times 0.8 \times 1 \times 10^{-3} = 128 \text{ kN}$$

The shear strength is checked using Clause 11.7.5, according to which the ultimate strength must not be greater than

$$V_{ult} = 0.25\, f'_c A_{cv} \qquad \text{(A-9)}$$

where f'_c = 49 MPa (compressive strength of the concrete)

A_{cv} = area of the concrete section resisting shear transfer

$= 200 \times (75 + 50) = 25{,}000\ mm^2$

Substituting in equation A-9 gives:

$$V_{ult} = 0.25 \times 49 \times 25000 \times 10^{-3} = 306.3\ kN$$

Also, the strength obtained from equation A-8 shall not be greater than value given by

$$V_{ult} = 6.5\, A_{cv} = 6.5 \times 25000 \times 10^{-3} = 162.5\ kN \qquad \text{(A-10)}$$

Consequently, the ultimate shear strength of Specimen S3, V_{ult}, is

$$V_{ult} = 128\ kN$$

A.4 Specimen S4

CPCI Method

When the studs are welded to the plate, the ultimate strength of the connection, V_{ult}, is calculated using the shear-friction principles.

If the connection fails because of exhaustion of the stud strength, the connection strength can be calculated as:

$$V_{ult} = A_{vf} f_{yst} \mu \qquad \text{(A-11)}$$

where A_{vf} = cross-sectional area of the studs = $2 \times 127 = 254\ mm^2$

$\mu = 0.8\lambda$ for the contact plane a full plate thickness below the concrete

surface.

$\lambda = 1$ for normal density concrete

f_{yst} = assumed yield strength of the studs ,but ≤ 400 MPa

Substituting values in the equation A-11 gives:

$$V_{ult} = 254 \times 400 \times 0.8 \times 1.0 = 81.3 \text{ kN}$$

The ultimate shear strength is checked using Section 4.5 of the CPCI Metric Design Manual[18] , according to which the strength should be less than

$$V_{ult} = 6.5\ A_{cv} \qquad \text{(A-12)}$$

where A_{cv} = area of concrete section resisting shear transfer which is given by:

$$A_{cv} = 150 \times 75 = 11250 \text{ mm}^2$$

Substituting in equation A-12 gives:

$$V_{ult} = 6.5 \times 11250 \times 10^{-3} = 73 \text{ kN}$$

which should be less than

$$V_{ult} = 0.25\ f'_c A_{cv} \qquad \text{(A-13)}$$

Substituting values in equation A-13 gives

$$V_{ult} = 0.25 \times 42 \times 11250 = 118 \text{ kN}$$

The smallest values of V_{ult} governs, therefore

$$V_{ult} = 73 \text{ kN}$$

A.5 Specimen S5

CPCI Method

The effect of the studs was not considered in evaluating the ultimate strength of the connection S5. Therefore the ultimate strength is identical to those for

Specimens S1 and S2.

Hence, $V_{ult} = 140$ kN

Modified CPCI Method

The effect of the studs was not considered to in evaluating the ultimate strength of Connection S5. Therefore, the ultimate strength is identical to those for the specimens S1 and S2.

Hence, $V_{ult} = 183.5$ kN

Alternate Method

The concrete surrounding the headed studs must shear off before the connection fails at load, $V_{ult(stud)}$. Therefore the ultimate shear strength of the connection subjected to monotonically increasing loads is equal to the sum of the ultimate strength of the reinforcing bar anchor and that of the headed studs as represented by equation A-14.

$$V_{ult} = V_{ult(stud)} + V_{ult(bar)} \qquad \text{(A-14)}$$

where $V_{ult(stud)}$ = ultimate shear strength of the connection with headed studs

$V_{ult(bar)}$ = ultimate shear strength of the connection with reinforcing bar anchor

The contribution of the studs to the strength of the connection is equal to the ultimate strength obtained for Specimen S4. Therefore,

$$V_{ult(stud)} = \underline{73} \text{ kN}$$

and, the shear strength of the steel bar, $V_{ult(bar)}$, is determined using equation A-5 as:

$$T_u = \frac{d_b l_d C \sqrt{f'_c}}{424.45 d_b + 6.87 l_d} \qquad \textbf{(in S. I units)} \qquad \text{(A-15)}$$

where f'_c = 47 MPa (compressive strength of concrete)

and, the other parameters are as defined for Specimen S1 with the same values. Substituting values in equation A-5, gives the maximum value of the forces in the compression and tension legs as:

$$C_u = T_u = \frac{16 \times 480 \times 23 \times \sqrt{47}}{424.45 \times 16 + 6.87 \times 480} = 120\ kN$$

The force resisted by dowel action is 4.9 kN, identical to that for Specimen S1. Using the "truss analogy", the ultimate strength of the reinforcing bars, $V_{ult(bar)}$, is given by:

$$V_{ult(bar)} = (4.9 + 120 + 120)\text{Cos}45^\circ = \underline{174}\ \text{kN}$$

The ultimate strength of the specimen S5, V_{ult}, is calculated by substituting values in equation A-14:

$$V_{ult} = V_{ult(stud)} + V_{ult(bar)} = 73 + 174 = 247\ \text{kN}$$